LIVING α-OLEFIN POLYMERIZATION BY CATIONIC ZIRCONIUM AND HAFNIUM COMPLEXES CONTAINING CHELATING DIAMIDOPYRIDINE LIGANDS

by

PARISA MEHRKHODAVANDI

B.Sc. (Honours) in Chemistry, University of British Columbia
(1998)

Submitted to the Department of Chemistry
In Partial Fulfillment of the Requirements
For the Degree of

DOCTOR OF PHILOSOPHY
at the

MASSACHUSETTS INSTITUTE OF TECHNOLOGY
September 2002

Signature of
Author _____
Department of Chemistry
August 5, 2002

Certified
by _____
Richard R. Schrock
Thesis Supervisor

Accepted
by _____
Robert W. Field
Chairman, Departmental Committee on Graduate Students

This doctoral thesis has been examined by a Committee of the Department of Chemistry as follows:

Professor Daniel G.
Nocera _____
Chairman

Professor Richard R.
Schrock _____
Thesis Supervisor

Professor Joseph P.
Sadighi_____

For Sohrab and Doulat, with love.

For Bamas Jahangir, my inspiration.

In memory of Memas Khorshid.

LIVING α-OLEFIN POLYMERIZATION BY CATIONIC ZIRCONIUM AND HAFNIUM COMPLEXES CONTAINING CHELATING DIAMIDOPYRIDINE LIGANDS

by

PARISA MEHRKHODAVANDI

Submitted to the Department of Chemistry, September 2002,
in Partial Fulfillment of the Requirements
for the Degree of Doctor of Philosophy in Chemistry

ABSTRACT

Chapter 1

Arylated diamidopyridine ligands $[H_3CC(2\text{-}C_5H_4N)(CH_2NAr)_2]^{2-}$ ($[ArNpy]^{2-}$) were synthesized *via* a Buchwald coupling between $H_3CC(2\text{-}C_5H_4N)(CH_2NH_2)_2$ and ArBr. Dimethyl complexes $[MesNpy]ZrMe_2$ (**1**) and $[TripNpy]ZrMe_2$ (**8**) were prepared. Synthesis of **1** was complicated by the formation of ether adducts such as $[MesNpy]Zr(THF)Me_2$ (**2**) and zirconates such as $[Li{\cdot}OEt_2][(MesNpy)ZrMe_3]$ (**3**). In all of these complexes, the ligand was coordinated with *fac* geometry, creating a face with open coordination geometry. Methyl group exchange between neutral dimethyl complexes **1** and **8** was observed. Activation of **1** or **8** with 1.0 or 0.5 equiv of $[Ph_3C][B(C_6F_5)_4]$ led to dinuclear monocations $\{[(MesNpy)Zr]_2Me_3\}\{B(C_6F_5)_4\}$ (**11**) and $\{[(TripNpy)Zr]_2Me_3\}\{B(C_6F_5)_4\}$ (**12**). These dinuclear complexes were unreactive towards dimethyl compounds, $[Ph_3C][B(C_6F_5)_4]$, or ethers at 25 ˚C, but showed limited reactivity at 40 ˚C. The J_{CH} values for all three methyl groups in **11** and **12** was 109 Hz, which suggests a structure with three bridging methyl groups for these complexes. The hafnium complex $[MesNpy]HfMe_2$ (**16**) was synthesized. Activation of **16** with $[Ph_3C][B(C_6F_5)_4]$ yielded $\{[(MesNpy)Hf]_2Me_3\}\{B(C_6F_5)_4\}$ (**17**), similarly to **11** and **12**. Activation of **16** with $B(C_6F_5)_3$ resulted in $\{[(MesNpy)Hf]_2Me_3\}\{MeB(C_6F_5)_3\}$ (**18**). No interaction between $[MeB(C_6F_5)_3]^-$ and the metal center was observed.

Chapter 2

Zirconium complexes $[MesNpy]ZrMe_2$ (**1**) and $[TripNpy]ZrMe_2$ (**8**) were activated with $[Ph_3C][B(C_6F_5)_4]$ and reaction of the resulting activated species with 1-hexene was examined by kinetics studies. In polymerization reactions with these species, unreacted $\{[(ArNpy)Zr]_2Me_3\}\{B(C_6F_5)_4\}$ was observed after complete consumption of the olefin. In reactions involving activated **1**, 2,1 insertion of 1-hexene was observed. 2,1-Insertion of olefin and unreacted dinuclear species led to low catalyst efficiency and high polymer M_n values. The dibenzyl, $[MesNpy]ZrBn_2$ (**20**), and dineopentyl, $[MesNpy]ZrNp_2$ (**22**), complexes were prepared and activated with $[Ph_3C][B(C_6F_5)_4]$ to yield $[(MesNpy)ZrBn][B(C_6F_5)_4]$ (**21**) and $[(MesNpy)ZrNp][B(C_6F_5)_4]$ (**23**), respectively. NMR studies of **21** show that the ligand pyridyl ring is not coordinated to zirconium. Complex **21** showed low reactivity towards 1-hexene. Complex **23** polymerized 1-hexene, but decomposed at 0 ˚C. Complexes $[MesNpy]Zr(i\text{-}Bu)_2$ (**24**) and $[TripNpy]Zr(i\text{-}Bu)_2$ (**26**) were prepared and activated with $[Ph_3C][B(C_6F_5)_4]$ to yield

[(MesNpy)Zr(i-Bu)][$B(C_6F_5)_4$] (**25**) and [(TripNpy)Zr(i-Bu)][$B(C_6F_5)_4$] (**27**), respectively. Polymerization reactions with **25** showed first order kinetics, but the catalyst decomposed at 0 ˚C in a first order manner. Polymer M_n values are higher than expected for polymerizations with both **25** and **27**.

Chapter 3

Dialkyl hafnium complexes [MesNpy]HfR_2 (R = Et (**28**), n-Pr (**31**), n-Bu (**32**), i-Pr (**37**)) and mixed alkyl complexes [MesNpy]Hf(i-Pr)R' (R' = Me (**35**), Cl (**36**)) were prepared. Activation of **28** with [Ph_3C][$B(C_6F_5)_4$] led to both alkyl and β-hydride abstraction, and formation of [(MesNpy)HfEt][$B(C_6F_5)_4$] (**29**) and [(MesNpy)Hf(n-Bu)][$B(C_6F_5)_4$] (**30**), the product of ethylene insertion into **29**. Activation of **31** and **32** with [Ph_3C][$B(C_6F_5)_4$] resulted in β-hydride abstraction. Activation of **35** with [Ph_3C][$B(C_6F_5)_4$] or [$HNMe_2Ph$][$B(C_6F_5)_4$] led to formation of methyl-bridged dinuclear species. Activation of **37** with [Ph_3C][$B(C_6F_5)_4$] led to β-hydride abstraction to yield [(MesNpy)Hf(i-Pr)][$B(C_6F_5)_4$] (**38**) and the product of propene insertion into **38**, [(MesNpy)Hf($CH_2CH(CH_3)$(i-Pr))][$B(C_6F_5)_4$] (**39**). The secondary alkyl cation, **38**, decomposes significantly faster the primary alkyl cation, **39**. Complex **38** was prepared independently by reaction of **37** with [$HNMe_2Ph$][$B(C_6F_5)_4$]. This complex decomposed by C-H activation of the NMe_2Ph by-product to yield [(MesNpy)Hf($C_6H_4NMe_2$)][$B(C_6F_5)_4$] (**40**). Reaction of **37** with $B(C_6F_5)_3$ yielded [(MesNpy)Hf($CH_2CH(CH_3)$(i-Pr))][$HB(C_6F_5)_3$] (**41**). Polymerization of 1-hexene with **41** followed first order kinetics.

Chapter 4

Hafnium complexes [MesNpy]$Hf(i\text{-}Bu)_2$ (**42**) and [TripNpy]$Hf(i\text{-}Bu)_2$ (**46**) were synthesized and activated with [Ph_3C][$B(C_6F_5)_4$] to yield the alkyl cations [(MesNpy)Hf(i-Bu)][$B(C_6F_5)_4$] (**43**) and [(TripNpy)Hf(i-Bu)][$B(C_6F_5)_4$] (**47**). Complex **43** catalyzed the living polymerization of 1-hexene, as shown by kinetics and bulk polymerization studies. Molecular weights of the polymers obtained with **47** are higher than expected. ^{13}C-labeling studies with these neutral and cationic complexes showed that there is alkyl exchange between cations, but that it is promoted by neutral dialkyl complexes. Activation of **42** with $B(C_6F_5)_3$ led to [(MesNpy)Hf(i-Bu)][$HB(C_6F_5)_3$] (**48**). The rate of polymerization with **48** was lower that that with **43**, demonstrating an anion effect. The effect of inhibitors on 1-hexene polymerization was studied. The NMe_2Ph inhibitor was prone to C-H activation of the aryl ring, and the C-H activation product, [(MesNpy)Hf($C_6H_4NMe_2$)][$HB(C_6F_5)_3$] (**50**), was independently prepared and characterized. Suitable inhibitors were bulky ethers and amines that did not contain aryl groups.

Appendix 1

Tantalum complexes [MesNpy]$TaMe_3$ (**51**) and [TripNpy]$TaMe_3$ (**52**) were synthesized by reaction of Li_2[ArNpy] with $TaMe_3Cl_2$. The synthesis was complicated by formation of a by-product (**53**) in which only one of the amido arms is coordinated and the ligand backbone is interacting with the metal center. Activation of **51** with [Ph_3C][$B(C_6F_5)_4$] led to the mononuclear cation [(MesNpy)$TaMe_2$][$B(C_6F_5)_4$] (**54**).

Thesis Supervisor: Dr. Richard R. Schrock
Title: Frederick G. Keyes Professor of Chemistry

TABLE OF CONTENTS

LIST OF ABBREVIATIONS

Anal.	Analysis
b	broad
BINAP	2,2'-bis(diphenylphosphino)-1,1'-binaphthyl
Bn	benzyl, -$CH_2(C_6H_5)$
i-Bu	*iso*-butyl, -$CH_2CH(CH_3)_2$
n-Bu	*n*-butyl, -$CH_2CH_2CH_2CH_3$
t-Bu	*tert*-butyl, -CMe_3
(t-Bu)NON	[((t-Bu)$NCH_2CH_2)_2O$]
BuLi	*n*-butyllithium
Calcd	calculated
Cp	$(C_5H_5)^-$
Cp"	$(1,2\text{-}Me_2C_5H_3)^-$
d	doublet
dba	dibenzylideneacetone
deg, (˚)	degree(s)
DEPT	Distortionless Enhancement by Polarization Transfer
dimethylaniline	N,N-dimethylaniline
equiv	equivalent(s)
eq	equation(s)
fac	*facial*
EI	Electron Impact
Et	ethyl
g	grams
GPC	Gel Permeation Chromatography
gCOSY	gradient field Correlation Spectroscopy
h	hour(s)
HRMS	High Resolution Mass Spectroscopy
Ind	Indenyl
J	coupling constant in Hertz
k_d	decomposition rate for polymerization reactions
k_{obs}	observed rate constant for polymerization reactions
k_p	propagation rate constant for polymerization propagation
K	equilibrium constant
m	multiplet(s)
M_n	number average molecular weight
M_w	weight average molecular weight
Me	methyl
MeLi	methyllithium
Mes	mesityl, 2,4,6-trimethylphenyl
$MesN_2NMe$	[$(MesNCH_2CH_2)_2NMe$]
MesNpy	[$H_3CC(2\text{-}C_5H_4N)(CH_2NAr)_2$], Ar = 2,4,6-$Me_3C_6H_2$
mer	*meridional*
MS	mass spectroscopy
NaO-t-Bu	sodium-*t*-butoxide

NMR	nuclear magnetic resonance
Np	neopentyl, -$CH_2C(CH_3)_3$
OTs	tosylate, *para*-toluenesulfonate, 4-$MeC_6H_4SO_3$
PDI	Polydispersity Index
Ph	phenyl
ppm	parts per million
i-Pr	*iso*-propyl, -$CHMe_2$
n-Pr	*n*-propyl, -$CH_2CH_2CH_3$
py	pyridine
q	quartet
rac	racemic
ROESY	Rotating Frame Overhauser Enhancement Spectroscopy
s	singlet
sep	septet
t	triplet
tmeda	tetramethylethylenediamine
THF	tetrahydrofuran
TMS	trimethylsilyl
TMSCl	trimethylsilylchloride
Trip	2,4,6-triisopropylphenyl
TripNpy	$[H_3CC(2\text{-}C_5H_4N)(CH_2NAr)_2]$, Ar = 2,4,6-$(i\text{-}Pr)_3C_6H_2$
δ	chemical shift downfield from tetramethylsilane in ppm

LIST OF COMPOUNDS

Chapter One

1 [MesNpy]$ZrMe_2$
2 [MesNpy]Zr(THF)Me_2
3 [Li·OEt_2][(MesNpy)$ZrMe_3$]
4 [MesNpy]Zr(NMe_2)$_2$
5 [MesNpy]$ZrCl_2$
6 [TripNpy]Zr(NMe_2)$_2$
7 [TripNpy]$ZrCl_2$
8 [TripNpy]$ZrMe_2$
9 [(MesNpy)ZrMe][B(C_6F_5)$_4$]
10 [(TripNpy)ZrMe][B(C_6F_5)$_4$]
11 {[(MesNpy)Zr]$_2$$Me_3$}{B($C_6F_5$)$_4$}
12 {[(TripNpy)Zr]$_2$$Me_3$}{B($C_6F_5$)$_4$}
13 [(TripNpy)Zr(DME)Me][B(C_6F_5)$_4$]
14 [MesNpy]Hf(NMe_2)$_2$
15 [MesNpy]$HfCl_2$
16 [MesNpy]$HfMe_2$
17 {[(MesNpy)Hf]$_2$$Me_3$}{B($C_6F_5$)$_4$}
18 {[(MesNpy)Hf]$_2$$Me_3$}{MeB($C_6F_5$)$_3$}
19 [(MesNpy)HfMe][MeB(C_6F_5)$_3$]

Chapter 2

20 [MesNpy]$ZrBn_2$
21 [(MesNpy)ZrBn][B(C_6F_5)$_4$]
22 [MesNpy]$ZrNp_2$
23 [(MesNpy)ZrNp][B(C_6F_5)$_4$]
24 [MesNpy]Zr(i-Bu)$_2$
25 [(MesNpy)Zr(i-Bu)][B(C_6F_5)$_4$]
26 [TripNpy]Zr(i-Bu)$_2$
27 [(TripNpy)Zr(i-Bu)][B(C_6F_5)$_4$]

Chapter 3

28 [MesNpy]$HfEt_2$
29 [(MesNpy)HfEt][B(C_6F_5)$_4$]
30 [(MesNpy)Hf(n-Bu)][B(C_6F_5)$_4$]
31 [MesNpy]Hf(n-Pr)$_2$
32 [MesNpy]Hf(n-Bu)$_2$
33 [(MesNpy)Hf(n-Pr)][B(C_6F_5)$_4$]
34 [(MesNpy)Hf($CH_2CH(CH_3)$(n-Pr))][B(C_6F_5)$_4$]

35 [MesNpy]Hf(i-Pr)(Me)
36 [MesNpy]Hf(i-Pr)(Cl)
37 [MesNpy]Hf(i-Pr)$_2$
38 [(MesNpy)Hf(i-Pr)][B(C_6F_5)$_4$]
39 [(MesNpy)Hf($CH_2CH(CH_3)$(i-Pr))][B(C_6F_5)$_4$]
40 [(MesNpy)Hf($C_6H_4NMe_2$)][B(C_6F_5)$_4$]
41 [(MesNpy)Hf($CH_2CH(CH_3)$(i-Pr))][HB(C_6F_5)$_3$]

Chapter 4

42 [MesNpy]Hf(i-Bu)$_2$
43 [(MesNpy)Hf(i-Bu)][B(C_6F_5)$_4$]
44 [TripNpy]Hf(NMe_2)$_2$
45 [TripNpy]$HfCl_2$
46 [TripNpy]Hf(i-Bu)$_2$
47 [(TripNpy)Hf(i-Bu)][B(C_6F_5)$_4$]
48 [(MesNpy)Hf(i-Bu)][HB(C_6F_5)$_3$]
49 [(n-Bu)$_4$N][MeB(C_6F_5)$_3$]
50 [(MesNpy)Hf($C_6H_4NMe_2$)][HB(C_6F_5)$_3$]

Appendix 1

51 [MesNpy]$TaMe_3$
52 [TripNpy]$TaMe_3$
53 tantalum decomposition by-product
54 [(MesNpy)$TaMe_2$][B(C_6F_5)$_4$]

LIST OF FIGURES

Chapter 1

Chapter 2

Chapter 3

Chapter 4

Appendix 1

LIST OF SCHEMES

Introduction

Chapter 1

Chapter 2

Chapter 3

Chapter 4

LIST OF TABLES

Chapter 1

Chapter 2

Chapter 3

Chapter 4

Appendices 1 and 2

General Introduction

Metal-catalyzed polymerization of olefins has been a topic of intense interest in the past few decades, and a wealth of information has been gained about various aspects of the field.[1] A subset of this field, living Ziegler-Natta polymerization of α-olefins, has been a topic of interest to a number groups in the past few years.[2] Some generally accepted criteria for a living polymerization system include:

1) complete monomer conversion and chain growth upon further monomer addition;
2) linear increase of number average molecular weight as a function of conversion;
3) constant number of active centers for duration of polymerization;
4) precise control of molecular weight through stoichiometry;
5) narrow polymer molecular weight distributions;
6) preparation of block copolymers by sequential monomer addition;
7) synthesis of end-functionalized polymers.

It is important to define "living polymerization" as it pertains to the work presented in this thesis. Scheme I.1 represents a typical polymerization process.

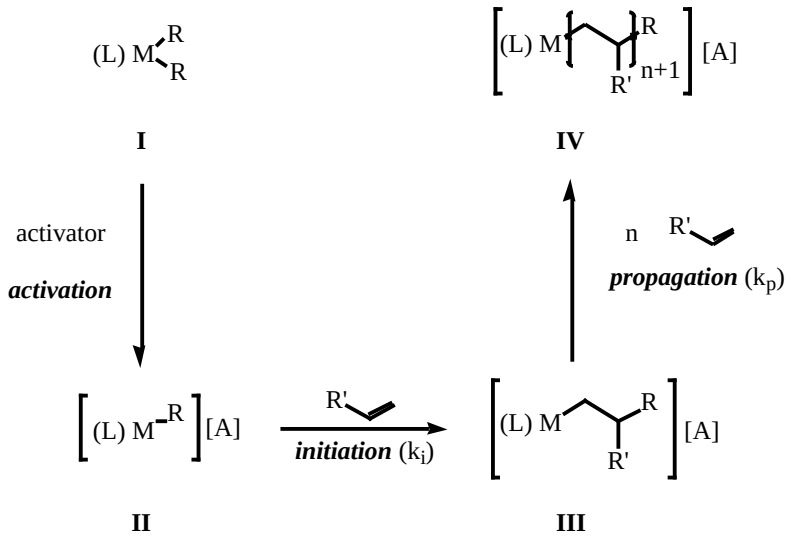

Scheme I.1. The Ziegler-Natta polymerization process.

In typical reactions, the precatalyst, **I**, is converted to the initiator, **II**, by an appropriate activator. In a well-behaved living polymerization system all the precatalyst is converted to the initiator in the activation process. If the activation process is not complete, and only a fraction of metal centers catalyzes polymerization, the number average molecular weight (M_n) for a given number of equivalents of olefin, versus initial metal concentration, could be higher than expected.

Addition of olefin to **II** constitutes an initiation process and proceeds with an initiation rate constant, k_i, to yield the product of the first insertion of olefin, **III**. Species **III** should theoretically be observable and stable in the absence of excess olefin. Addition of olefin to **III** results in propagation with the rate constant k_p and generates the propagating species, **IV**. If $k_i > k_p$, all the metal centers are initiated and carry out polymerization, and the number of active centers remains constant. Thus the polymerization rate has a first order dependence on metal concentration as well as on olefin concentration, and k_p can be determined from the observed rate constant, k_{obs}, by simply dividing k_{obs} by [catalyst]. Species **IV** should be stable in the absence of olefin and be able to carry out consecutive polymerization reactions with approximately the same k_p. If no decomposition of species **IV** is observed, then the system is living.

Polymerization progresses by successive olefin insertion into the metal-carbon bond of the catalyst[3] until, in the case of non-living systems, chain termination occurs. Some chain termination events include β-hydrogen or β-alkyl elimination as well as chain transfer, most commonly to alkylaluminum cocatalysts.[4] In some cases, C-H activation of the ligand terminates the polymerization process.[5] Scheme I.2 is a summary of possible chain termination events in metal-catalyzed olefin polymerization.

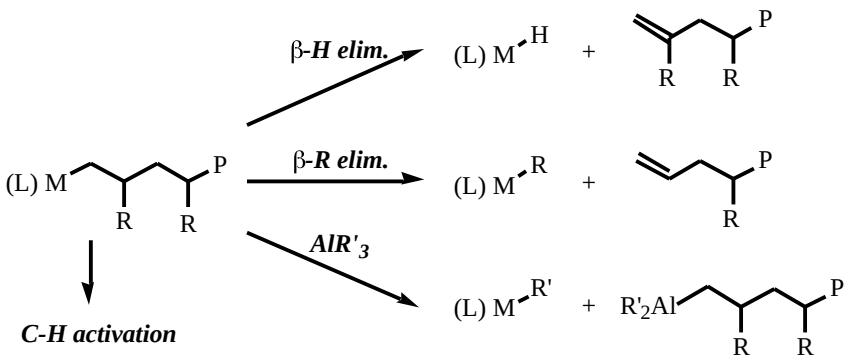

Scheme I.2. Termination events for metal-catalyzed polymerizations.

The insertion processes usually proceed with 1,2 regiochemistry to result in primary metal alkyls. Theoretical studies show a clear preference for 1,2-insertion of olefin due to both electronic as well as steric factors.[6,7] However, regio-errors due to 2,1-insertion of olefin (~1%) are commonly observed in metallocene systems (Scheme I.3).[4] In these cases, catalyst activity and polymer molecular weights are lowered as chain termination competes with propagation.[8]

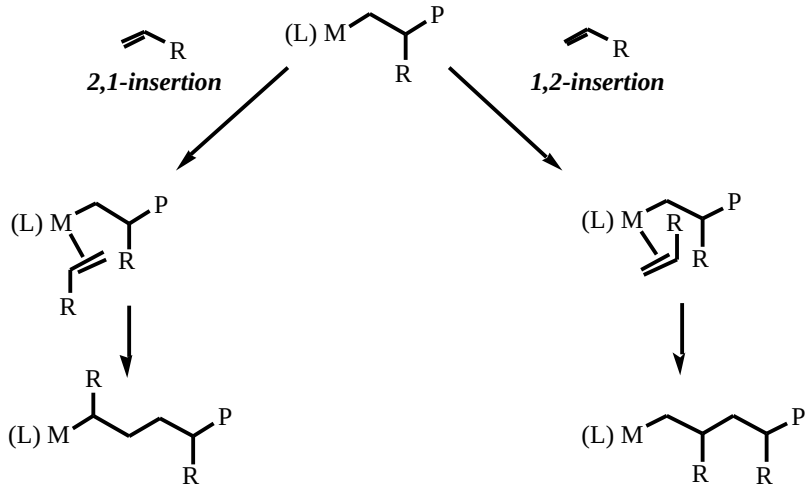

Scheme I.3. 1,2- versus 2,1-insertion in metal-catalyzed polymerizations.

A living polymerization system yields polymer samples with narrow molecular weight distributions and low polydispersity indices (PDI's). A plot of added equivalents of olefin vs. M_n for a living system should be linear, enabling prediction of M_n on the basis of added olefin. It is

important to carry out this type of experiment for large equivalents of olefin (~500), as in systems with high k_p, a small amount of olefin can be consumed before the catalyst decomposes, *i.e.* the rate of catalyst decomposition, k_d, is significantly less than k_p.

It is important to have a basis for comparison and evaluation of different catalyst systems. In 1996, McConville *et al.* reported a diamido titanium system which carried out living α-olefin polymerization at room temperature,[9,10] but which decomposed in the absence of olefin.[11] Since that report many groups have reported group IV catalysts, supported by non-metallocene ligands,[12-14] that carry out living α-olefin polymerization.[15-24] However, the term "living polymerization" is used with a slightly different connotation in each report.[25] The following chapters describe a system for the living polymerization of 1-hexene that adheres very closely to the above criteria, and shows great promise for potential application and study of block polymerization processes.[26,27]

Chapter 1

Synthesis and activation of dimethyl zirconium and hafnium complexes of arylated diamidopyridine ligands: The importance of methyl bridges in a system with an open coordination environment

1.1 Introduction

In the past few years, a variety of group IV complexes bearing diamido-donor ligands has been developed.[5,15,16,28-39] The diamido-donor ligands are highly modular and allow for the investigation of a variety of systems (Figure 1.1).

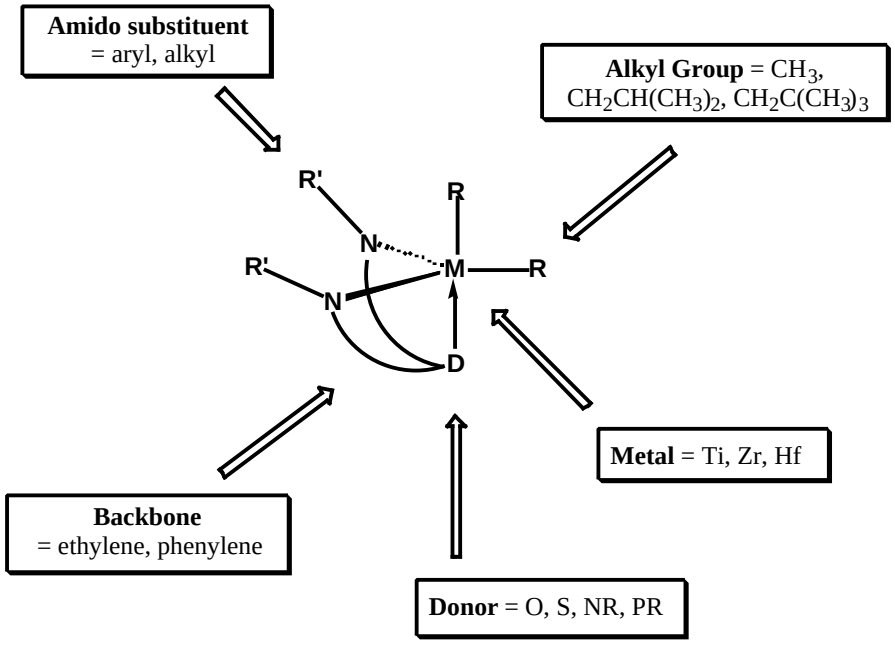

Figure 1.1. Different catalyst systems developed in the Schrock group.

Complexes bearing diamido-donor ligands can adopt a *pseudo*-meridional (*mer*) or *pseudo*-facial (*fac*) conformation in the solid state. In some dialkyl complexes, the two conformations equilibrate in solution such that the geometry of the resulting cation is ambiguous.

The goal of the present project was to investigate ligands that force the *fac* conformation in complexes, and to study the influence of this geometry on catalyst activity. The ligands that were investigated are based on a system developed by Gade *et al.* (Figure 1.2).[14,40,41]

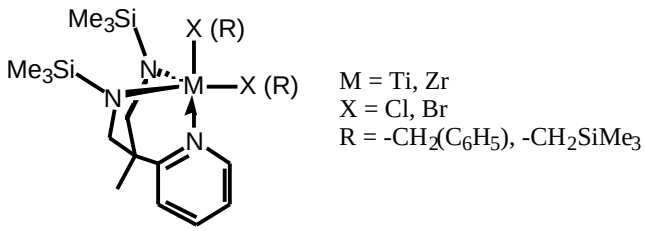

Figure 1.2. Group IV complexes developed by Gade *et al.* bearing a diamidopyridine ligand.

In the ligand used in this project, the trimethylsilyl groups have been replaced by 2,6-disubstituted aryl groups. This substitution may serve to avoid the decomposition of the catalyst due to the lability of the Si-N bond or C-H activation of the TMS groups.[42] The new ligand would be similar to the diamidoamine systems developed in the Schrock group, but the central pyridine ring and the "tied back" backbone would ensure a *fac* conformation.

Dimethyl complexes of group IV complexes have been widely studied because of their ease of synthesis and stability, and therefore they provide a starting point for catalyst synthesis. An important aspect of the chemistry of these compounds is the ability of methyl groups to form intermolecular bonds to other neutral or cationic metal centers.[43-51] Interaction of neutral dimethyl complexes with cationic centers to form dinuclear monocations has also been reported.[52] One example of such a complex was reported by Schrock *et al.* where 1 equiv of $[MesN_2NMe]ZrMe_2$ ($[MesN_2NMe]^{2-}$ = $[(MesNCH_2CH_2)_2NMe]^{2-}$) was activated with 0.5 equiv of $[Ph_3C][B(C_6F_5)_4]$ to yield the dinuclear complex, $\{[(MesN_2NMe)ZrMe]_2Me\}\{B(C_6F_5)_4\}$.[38] The bridging methyl group in this complex is thought to be sp^2 hybridized and has a J_{CH} of 133 Hz.

Usually these dinuclear monocations are formed by activation of dimethyl complexes with only 0.5 equiv of activator; however, in some cases a dinuclear complex is the only product, regardless of the amount of activator employed. Marks *et al.* activated $Cp"_2ZrMe_2$ with an excess of the $B[C_6F_4(2\text{-}C_6F_5)]_3$ (PPB) to yield only the dinuclear complex $[(Cp"_2ZrMe)_2Me][MePPB]$. This complex has one bridging methyl group with a J_{CH} value of ~130 Hz, again characteristic of sp^2 hybridization (Figure 1.3 a).[53]

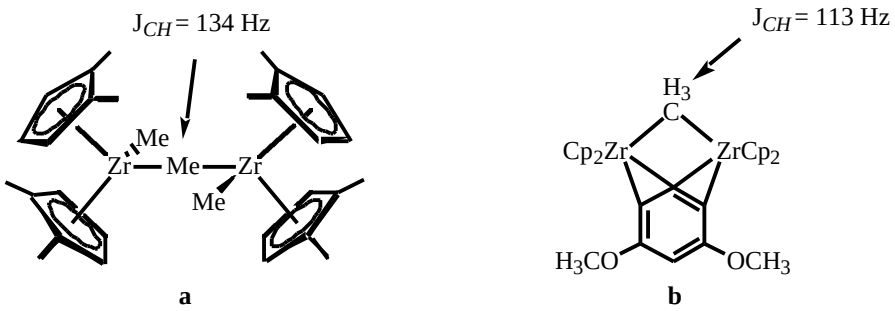

Figure 1.3. Two dinuclear monocations with a bridging methyl group.

In contrast, complex **b** in Figure 1.3 has a non-linear, sp^3 hybridized bridging methyl group, and in this case the J_{CH} is significantly lower at 113 Hz.[48]

1.2 Ligand Synthesis

The synthesis of the arylated diamidopyridine ligands $[H_3CC(2\text{-}C_5H_4N)(CH_2NAr)_2]^{2-}$ ($[ArNpy]^{2-}$; Ar = 2,4,6-$Me_3C_6H_2$ (Mes), 2,4,6-$(i\text{-}Pr)_3C_6H_2$ (Trip)) is a modification of the H_2[TMSNpy] ligand synthesis reported by Gade *et al.* (Scheme 1.1).[40]

The first step of the synthesis involves reaction of 2-ethylpyridine with an excess of formaldehyde at 140 ˚C to yield mono- and di-substituted alcohols, **I** and **II**, which can be separated by fractional vacuum distillation. Alcohol **I** can be converted to **II** by further treatment with formaldehyde, thus increasing the overall yield of the reaction to *ca.* 50%. The tosylate (**III**), azide (**IV**) and amine (**V**) derivatives were obtained in 70-90% yield. They were judged sufficiently pure by ^{1}H NMR spectroscopy.[40] It should be noted that **IV** is a potentially explosive compound and thus should not be isolated or stored over long periods of time.

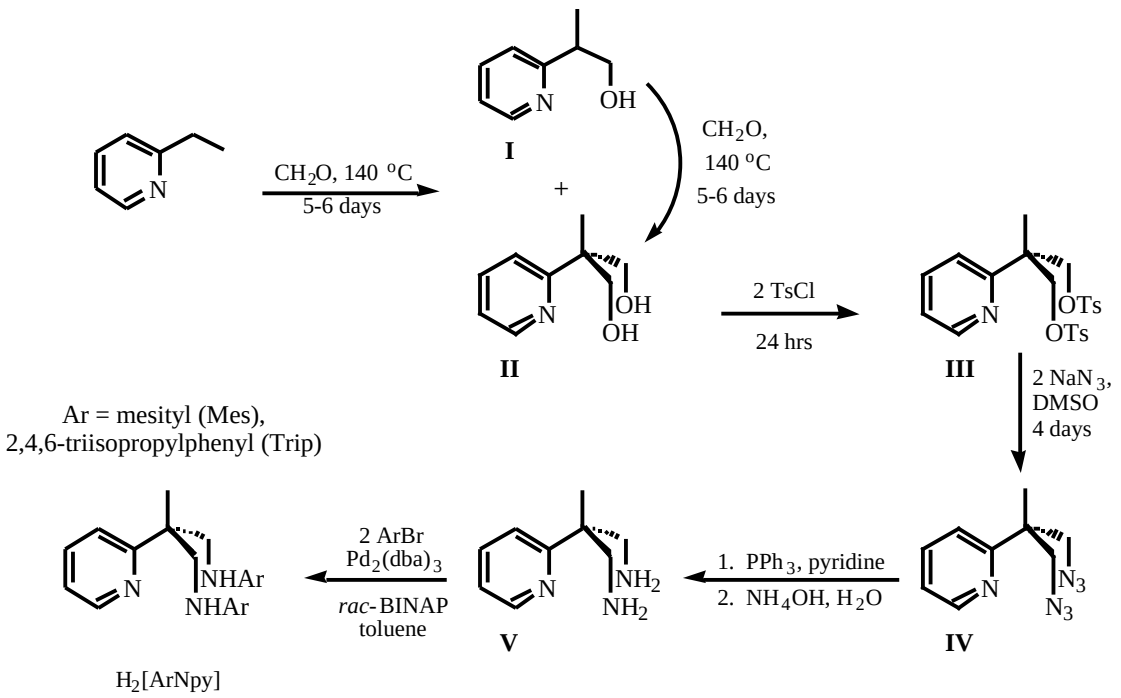

Scheme 1.1. Synthesis of H_2[ArNpy].

An unsuccessful synthetic route was amination of the tosylate derivative (**III**) with 2,6-disubstituted lithium anilide (Scheme 1.2). Direct substitution of the tosyl groups with anilide would have afforded the ligand in a substantially shorter synthesis. This reaction was attempted

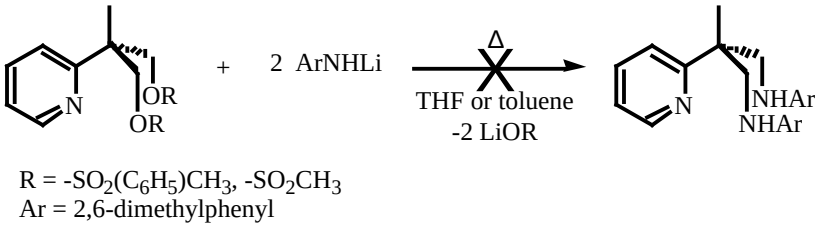

Scheme 1.2. Failed attempt at ligand synthesis.

at room temperature as well as in refluxing THF or toluene. It was monitored by ^{1}H NMR spectroscopy, but none of the desired product was observed even after several days. The difficulty with this reaction was attributed to the steric hindrance imposed by the adjacent

quaternary carbon. Using the less bulky mesylate derivative, similarly synthesized, also failed to yield the desired ligand. In light of the success of the Gade route, the route in Scheme 1.2 was abandoned.

The final step of ligand preparation involved an C-N bond formation using a Buchwald coupling reaction.[54,55] A 3% catalyst loading (Pd_2dba_3, BINAP) was used for the preparation of both H_2[MesNpy] and H_2[TripNpy]. Reaction times were dependent on the steric bulk of the aryl group. Synthesis of H_2[MesNpy] was complete after only 1-2 d at 100 ˚C, whereas synthesis of H_2[TripNpy] required 7-14 d to complete. H_2[MesNpy] can be recrystallized readily from pentane to yield pure product, while H_2[TripNpy] was obtained only as a waxy solid.

1.3 Complications during synthesis of [MesNpy]$ZrMe_2$

The first attempts at the synthesis of zirconium dialkyl complexes of the [MesNpy] ligand were carried out according to the "direct method" developed by Liang.[34] This route involves the formation of an adduct between $ZrCl_4$ and protonated ligand, followed by deprotonation and alkylation with an appropriate Grignard reagent. Magnesium salts generated in this process are precipitated with dioxane and removed from the system.

The direct method was unsatisfactory for the formation of [MesNpy]$ZrMe_2$ (**1**) due to low yield (~10%) and formation of intractable products. The formation of a solvent adduct, [MesNpy]Zr(THF)Me_2 (**2**), when THF was introduced during addition of a MeMgBr solution to the reaction mixture (eq 1.1) introduces further complications.

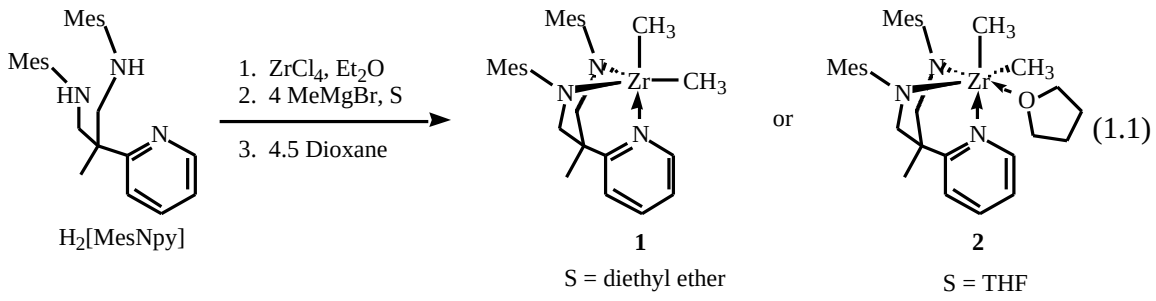

H_2[MesNpy]

1

S = diethyl ether

2

S = THF

The X-ray crystal structure of **2** revealed a *pseudo*-octahedral complex with one molecule of THF coordinated *trans* to an amido nitrogen (Figure 1.4). The bond lengths from the zirconium center to the amido nitrogen atoms, N(2) and N(3), are 2.063(4) and 2.115(4) Å respectively, while that to the pyridyl nitrogen, N(1), is 2.471(4) Å. The axial methyl group, C(28), has a slightly shorter bond length to zirconium (2.288(6) Å) than its equatorial counterpart (2.361(5) Å). The Zr-O bond length is 2.387(4) Å. The N(2)-Zr-N(3) bond angle is 90.73(16)˚. The N(2)-Zr-N(1) angle is 79.93(15)˚, and that for N(3)-Zr-N(1) is 76.6(15)˚, indicating that the ligand is "tied down" by the ligand backbone. The angle between the two methyl groups is 89.7(2)˚. The two mesityl groups are pushed back from one face of the molecule, leaving a large unhindered region where THF can bind.

The dimethyl complex [MesNpy]$ZrMe_2$ (**1**) has a great affinity toward donating solvents, in the following order: THF >> dioxane > diethyl ether. Tetrahydrofuran must be strictly avoided to prevent the formation of **2**. Addition of excess dioxane results in the formation of a solid consisting of the desired product and approximately 0.25 equiv of dioxane which cannot be removed. The affinity of **1** for coordinating solvents may be caused by the easy access of these molecules to the metal center (*vide infra*). In systems bearing more crowded environments, such as [$MesN_2NMe$]$ZrMe_2$ ([$MesN_2NMe$]$^{2-}$ = [$(MesNCH_2CH_2)_2NMe$]$^{2-}$)[38] and [(t-Bu)NON]$ZrMe_2$ ([(t-Bu)NON]$^{2-}$ = [$((t\text{-Bu})NCH_2CH_2)_2O$]$^{2-}$),[30] association of ethers with the complex is not significant.

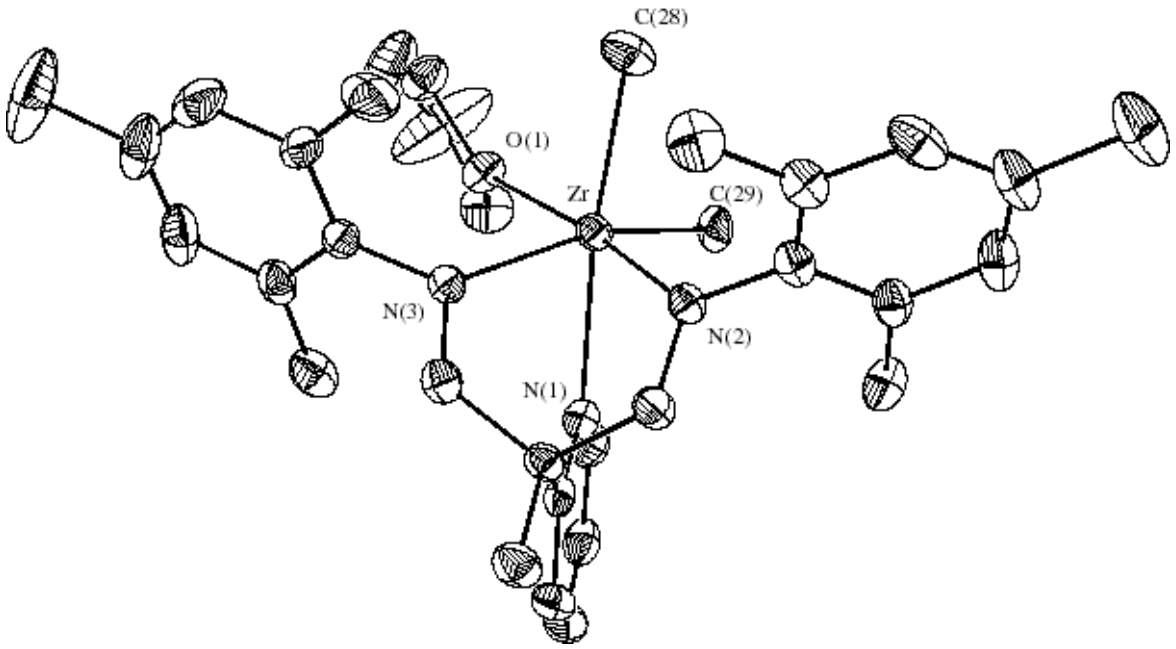

Figure 1.4. Thermal ellipsoid diagram (35% probability level) of [MesNpy]Zr(THF)Me_2 (**2**).

Table 1.1. Selected bond lengths (Å) and angles (˚) for [MesNpy]Zr(THF)Me_2 (**2**).

Bond Lengths

Zr-N(1)	2.471(4)	Zr-C(28)	2.288(6)
Zr-N(2)	2.063(4)	Zr-C(29)	2.361(5)
Zr-N(3)	2.115(4)	Zr-O(1)	2.387(4)

Bond Angles

N(2)-Zr-N(3)	90.73(16)	O(1)-Zr-C(28)	85.84(18)
N(2)-Zr-N(1)	79.93(15)	O(1)-Zr-C(29)	82.56(16)
N(3)-Zr-N(1)	76.66(15)	C(28)-Zr-C(29)	89.7(2)
N(2)-Zr-C(29)	118.49(14)	C(28)-Zr-N(1)	172.1(2)
N(3)-Zr-O(1)	84.23(14)	C(29)-Zr-N(1)	82.69(18)

The ^{1}H NMR spectrum (20 ˚C, C_6D_6) for [MesNpy]Zr(THF)Me_2 (**2**) shows a singlet at 0.54 ppm corresponding to 6 Zr-CH_3 protons, along with 1 equiv of THF. The ^{13}C{^{1}H} spectrum shows a broad signal at 35.8 ppm. Observation of only one signal for the two methyl groups, which are in inequivalent positions, may indicate an exchange of methyl groups in this system at room temperature. This phenomenon is also observed in the solvent-free species (*vide infra*).

Use of excess MeMgBr or MeLi, or long reaction times, resulted in the formation of intractable anionic "zirconate" species. One such complex was independently synthesized by addition of 1.0 equiv of MeLi to [MesNpy]ZrMe_2 (**1**), prepared *via* an alternate route (*vide infra*),

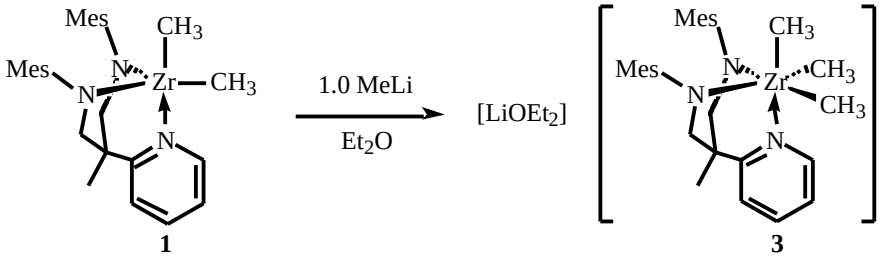

(1.2)

to yield [Li·OEt_2][(MesNpy)ZrMe_3] (**3**) (eq 1.2). The ^{1}H NMR spectrum (C_6D_6, 20 ˚C) of **3** shows a singlet at –0.06 ppm corresponding to 9 Zr-CH_3 protons. One equiv of free diethyl ether is observed in solution. Two signals for the *ortho* methyl groups on the mesityl rings are observed, which indicates restricted rotation of the aryl groups.

The X-ray crystal structure of [Li·OEt_2][(MesNpy)ZrMe_3] (**3**) shows an etherated Li cation interacting approximately equally with the methyl groups of a complex with *pseudo*-octahedral geometry (Figure 1.5). The angle between the two amido nitrogens, N(1) and N(2), is 91.48(18)˚, comparable to that obtained in the *pseudo*-octahedral [MesNpy]Zr(THF)Me_2 (**2**) complex. The equatorial Zr-C bonds are ~ 0.1 Å longer than the axial Zr-C bonds, potentially due to steric crowding. The C(1)-Zr-N_{amido} angle is 105˚, while the C(2) and C(3) are both at < 90˚ to the other carbon and nitrogen atoms. One example of a similar zirconate species involves the interaction of the methyl groups of $[ZrMe_6]^{2-}$ with 2 equiv of $[Li(tmed)]^{+}$.[56]

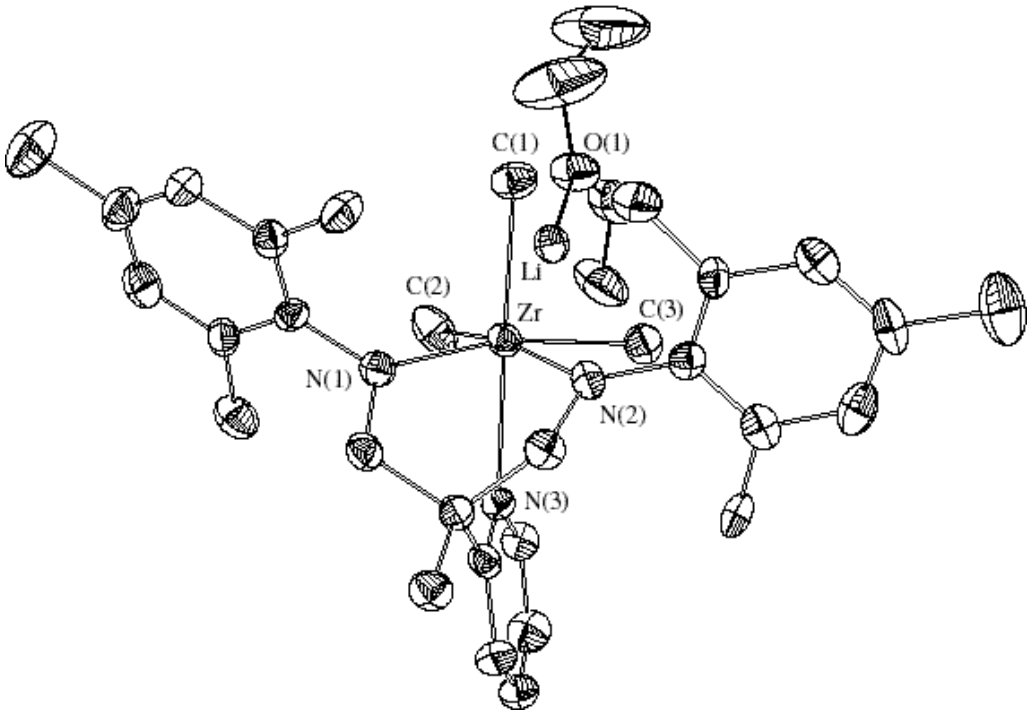

Figure 1.5. Thermal ellipsoid diagram (35% probability level) of $[Li{\cdot}OEt_2][(MesNpy)ZrMe_3]$ (**3**).

Table 1.2. Selected bond lengths (Å) and angles (˚) for $[Li{\cdot}OEt_2][(MesNpy)ZrMe_3]$ (**3**).

Bond Lengths

Zr-N(1)	2.101(5)	Zr-C(1)	2.319(6)
Zr-N(2)	2.113(5)	Zr-C(2)	2.421(7)
Zr-N(3)	2.399(5)	Zr-C(3)	2.461(6)
Li-C(1)	2.267(14)	Li-O(1)	1.970(12)
Li-C(2)	2.204(14)	Li-Zr	2.691(11)
Li-C(3)	2.194(17)		

Bond Angles

N(1)-Zr-N(2)	91.48(18)	C(1)-Zr-C(2)	85.4(2)
N(1)-Zr-C(1)	105.6(2)	C(1)-Zr-C(3)	87.0(2)
N(2)-Zr-C(1)	105.5(2)	C(2)-Zr-N(3)	84.1(2)
N(3)-Zr-C(1)	171.62(18)	C(3)-Zr-N(3)	87.40(18)

1.4 Synthesis of [ArNpy]ZrMe$_2$

A more effective way to form metal complexes with the [ArNpy] ligands is an amine elimination reaction between M(NMe$_2$)$_4$ and H$_2$[ArNpy] to form [ArNpy]M(NMe$_2$)$_2$. This compound is then treated with Me$_3$SiCl to form [ArNpy]MCl$_2$ which can serve as a starting material for the synthesis of a variety of dialkyl complexes using the appropriate Grignard or alkyl lithium reagent (Scheme 1.3).

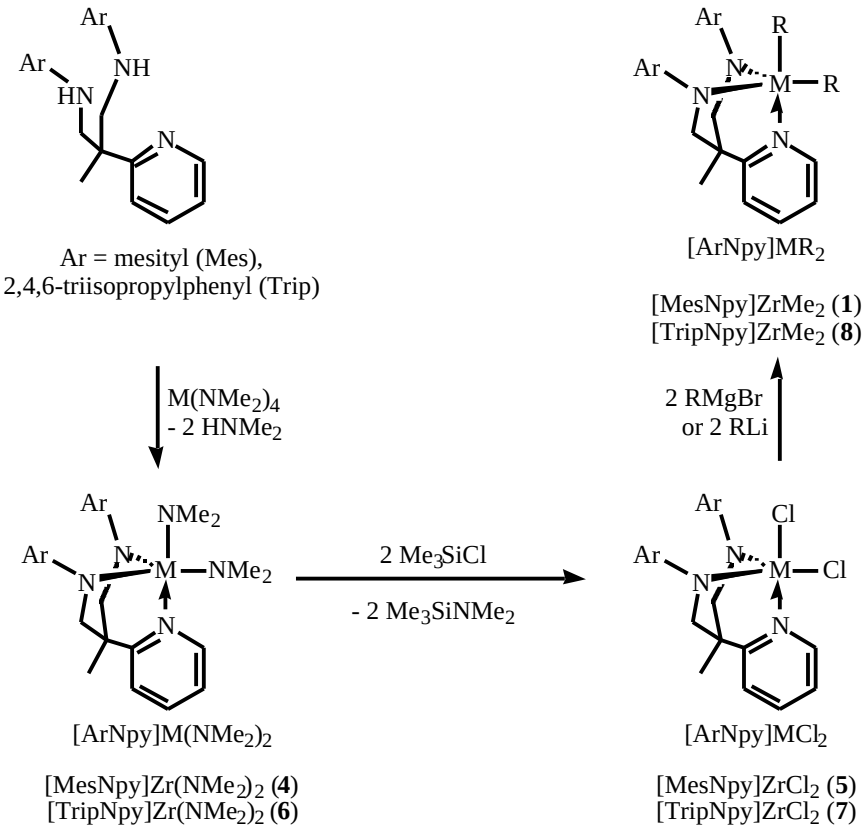

Scheme 1.3. Synthesis of [ArNpy] containing dialkyl complexes.

Complexes [MesNpy]Zr(NMe$_2$)$_2$ (**4**) and [MesNpy]ZrCl$_2$ (**5**) were prepared in ~ 90% yield according to the method outlined in Scheme 1.3. Complex **1** is rather difficult to prepare due to reasons discussed in Section 1.3, however it can be synthesized in moderate yields with strict control of reaction conditions, which includes careful titration of the Grignard reagent.

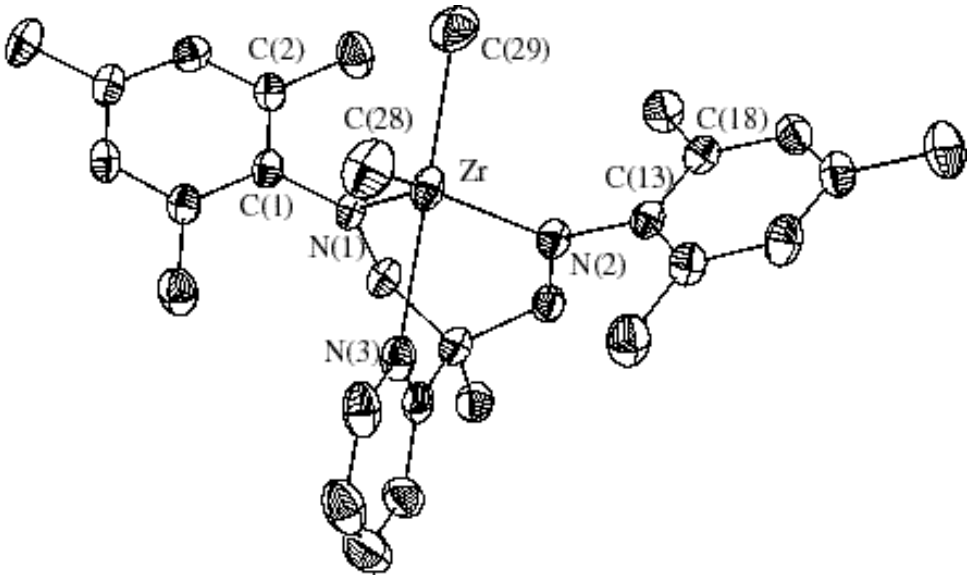

Figure 1.6. Thermal ellipsoid diagram (35% probability level) of [MesNpy]$ZrMe_2$ (**1**).

Table 1.3. Selected bond lengths (Å) and angles (˚) for [MesNpy]$ZrMe_2$ (**1**).

Bond Lengths

Zr-N(1)	2.027(3)	Zr-C(29)	2.284(6)
Zr-N(2)	2.034(3)	Zr-C(28)	2.294(5)
Zr-N(3)	2.444(4)		

Bond Angles

N(1)-Zr-N(2)	102.24(12)	C(29)-Zr-C(28)	89.1(2)
N(1)-Zr-C(29)	102.2(2)	N(1)-Zr-N(3)	80.81(14)
N(2)-Zr-C(29)	101.2(2)	N(2)-Zr-N(3)	80.58(14)
N(1)-Zr-C(28)	122.55(19)	C(29)-Zr-N(3)	175.96(19)
N(2)-Zr-C(28)	127.74(19)	C(28)-Zr-N(3)	86.9(2)

A single crystal X-ray study of **1** reveals a trigonal bipyramidal structure with *pseudo* C_s symmetry. The ligand is coordinated with *pseudo*-facial geometry, as expected (Figure 1.6 and Table 1.3). The angle between the two methyl groups, C(28) and C(29), is 89.1(2)˚, and the respective Zr-C bond lengths are 2.294(5) Å and 2.284(6) Å. The Zr-N_{amine} bonds are significantly longer than those reported for similar compounds [$MesN_2NMe$]$ZrMe_2$ or [BDPP]$ZrMe_2$ (Figure 1.7, Table 1.4).[34,57]

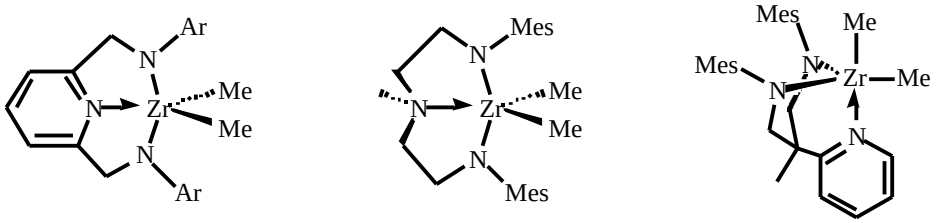

[BDPP]$ZrMe_2$ [$MesN_2NMe$]$ZrMe_2$ [MesNpy]$ZrMe_2$

Figure 1.7. Comparison of three diamidoamine zirconium complexes.

Table 1.4. A comparison of selected bond lengths (Å) and angles (˚) in five-coordinate diamido-donor complexes.

	Zr-N_{amine}	**Zr-N_{amido}**	**Zr-C**	**N_{amido}-Zr-N_{amido}**	**C-Zr-C**
[MesNpy]$ZrMe_2$	2.44	2.03	2.29	102.2	89.1
[$MesN_2NMe$]$ZrMe_2$ [a]	2.37	2.10	2.24	140.5	103.2
[BDPP]$ZrMe_2$ [b]	2.33	2.10	2.25	139.6	102.4

[a] 34; [b] 57.

The N(1)-Zr(1)-N(2) angle in [MesNpy]$ZrMe_2$ (**1**) is 102.24(12)˚, which is significantly smaller than the angle in analogous complexes where the ligand is coordinated with *pseudo*-meridional geometry, 140.5(2)˚ and 139.6(2)˚ for [$MesN_2NMe$]$ZrMe_2$ and [BDPP]$ZrMe_2$, respectively. The planes of the mesityl rings are at 65.4˚ and 56.3˚ angles to the equatorial plane defined by the N(1)-N(2)-Zr-C(28) atoms (Figure 1.8).

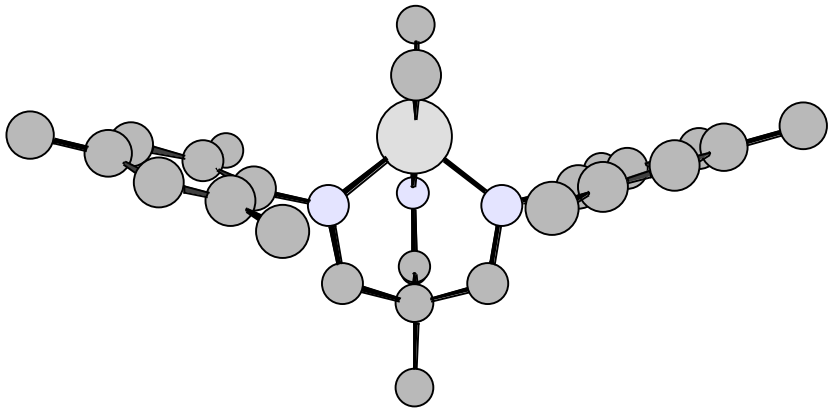

Figure 1.8. A Chem 3D drawing of **1** with the view along the C(29)-Zr-N(3) axis.

The rigid nature of the ligand backbone enforces a *pseudo*-facial geometry, which creates an open face on the molecule containing only the Zr-bound methyl groups. This open environment explains the affinity of **1** for coordinating solvents as well as its reactivity with excess Grignard or lithium reagents. It is also an important factor in the reactivity of activated [ArNpy]MR_2 complexes which will be discussed in this and the following chapters. Solution studies of **1** are discussed at length in the following sections.

In order to avoid some of the problems discussed in Section 1.3, dimethyl complexes of the bulkier [TripNpy] ligand were prepared. Complexes [TripNpy]Zr$(NMe_2)_2$ (**6**) and [TripNpy]$ZrCl_2$ (**7**) were prepared in 60-90% yield according to the method outlined in Scheme 1.3. A benefit of the bulkier ligand system was greater ease of synthesis of [TripNpy]$ZrMe_2$ (**8**), as there were no complications due to solvent coordination or zirconate formation. The ^{1}H NMR spectrum (20 ˚C, C_6D_6) of **8** clearly shows two signals for the Zr-CH_3 groups at 0.53 and 0.61 ppm. The ^{13}C-labeled complex [TripNpy]Zr$(^{13}Me)_2$ (**8***) can be prepared in good yield on a large scale and was used in the majority of the labeling studies discussed. The $^{13}C\{^1H\}$ NMR spectrum of **8*** shows two signals for Zr-CH_3 carbons at 34.2 and 38.3 ppm.

1.5 Methyl exchange in the [MesNpy]ZrMe$_2$ system

The ^{1}H and ^{13}C{^{1}H} NMR spectra of [MesNpy]ZrMe$_2$ (**1**) show significant solvent and temperature dependence. In C_6D_6 at 20 ˚C, the ^{1}H NMR spectrum shows a singlet at 0.56 ppm corresponding to 6 Zr-CH_3 protons and the ^{13}C{^{1}H} NMR spectrum shows one broad resonance at 36.5 ppm for the Zr-CH$_3$ carbon.

In C_6D_5Br at 20 ˚C, the ^{1}H NMR spectrum shows two singlets at 0.22 and 0.32 ppm and the ^{13}C{^{1}H} NMR spectrum shows two peaks at 35.46 and 36.65 ppm. Variable temperature NMR studies of **1** (80 mM) in C_6D_5Br show that at –25 ˚C two distinct signals, corresponding to the axial and equatorial methyl groups, can be observed. As the temperature is raised, the peaks broaden and finally coalesce to a broad singlet at 90 ˚C, indicating an exchange of methyl groups (Figure 1.9). At temperatures above 70 ˚C, **1** starts to decompose to yield methane (0.15 ppm in the ^{1}H NMR spectrum) as well as other by-products.

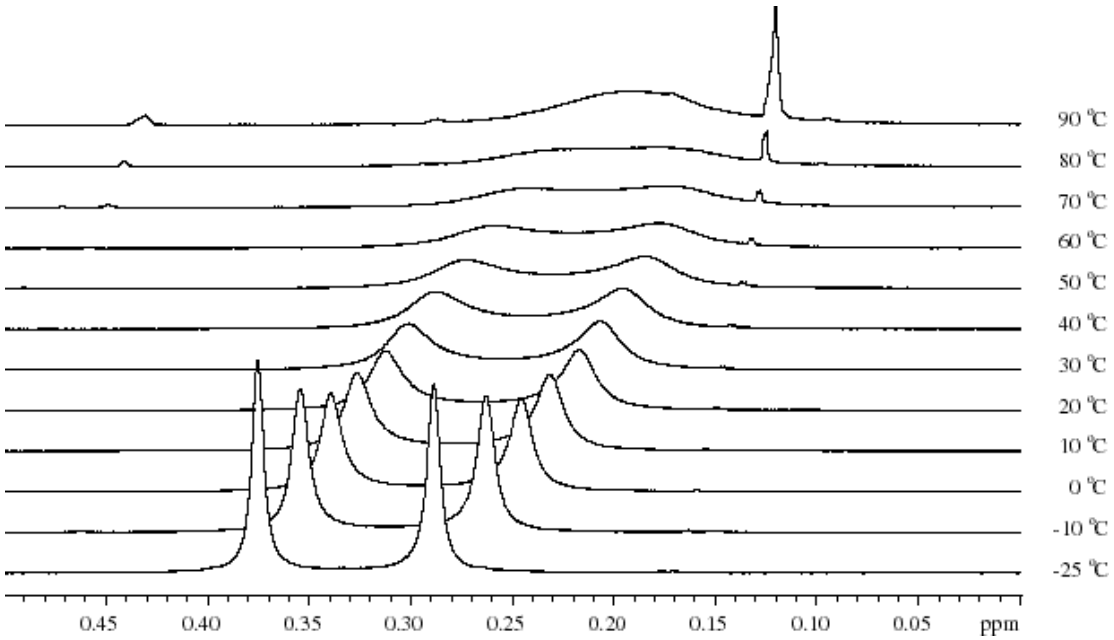

Figure 1.9. Variable temperature ^{1}H NMR spectra (500 MHz, C_6D_5Br, ZrCH_3) of **1**.

These results indicate a solvent dependent exchange of the methyl groups. In C_6D_5Br, the exchange is slow on the NMR time scale, potentially due to solvent coordination, and at room temperature two signals can be observed, while in poorly donating C_6D_6 this exchange is rapid at room temperature and only one signal can be observed (Scheme 1.4). A slower exchange between the methyl groups has been observed in the $[MesN_2NX]ZrMe_2$ (X = H, Me) system.[38]

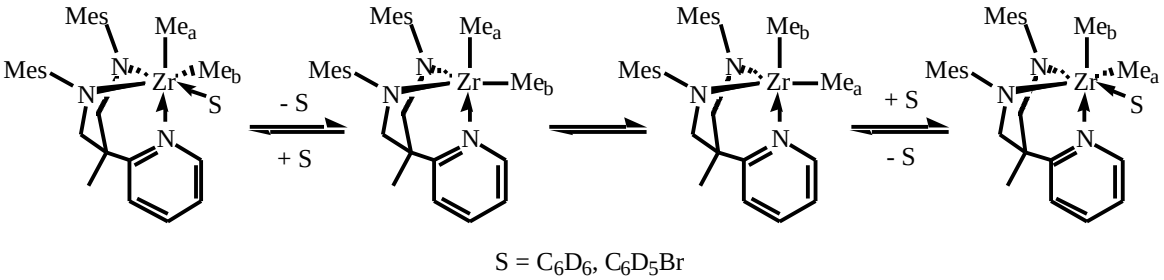

Scheme 1.4. Exchange of axial and equatorial methyl groups in $[MesNpy]ZrMe_2$ (**1**).

A double labeling study was carried out in the [ArNpy] system where equimolar amounts of **1** and the related ^{13}C-labeled complex, $[TripNpy]Zr(^{13}Me)_2$ (**8***), were taken up in C_6D_6 and mixed as solutions of varying concentration between 1.8 and 17.7 mM. The $^{13}C\{^1H\}$ NMR spectra (20 ˚C, C_6D_6) of these solutions show two signals at 39.8 and 34.9 ppm corresponding to the two methyl groups in **8*** which do not readily exchange in C_6D_6 at this temperature. A broad singlet at 36.9 ppm is also observed and corresponds to a ^{13}C-labeled methyl group that is transferred from **8*** to **1** to yield the labeled species **1*** (Figure 1.10). This broad signal is due to the rapid exchange of axial and equatorial methyl groups in **1*** (*vide supra*). Scheme 1.5 is a summary of the possible inter and intramolecular methyl exchange equilibria in the $[ArNpy]ZrMe_2$ systems.

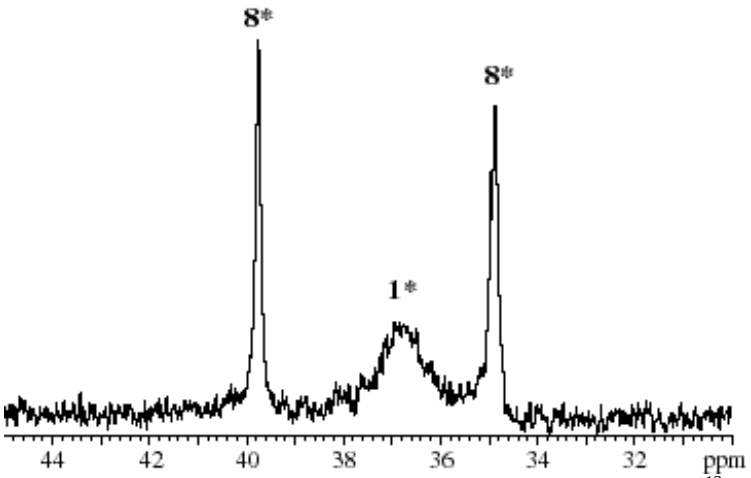

Figure 1.10. Exchange of methyl groups between [TripNpy]Zr(^{13}Me)$_2$ (**8***) and [MesNpy]ZrMe$_2$ (**1**) (20 ˚C, C_6D_6, 0.018M)

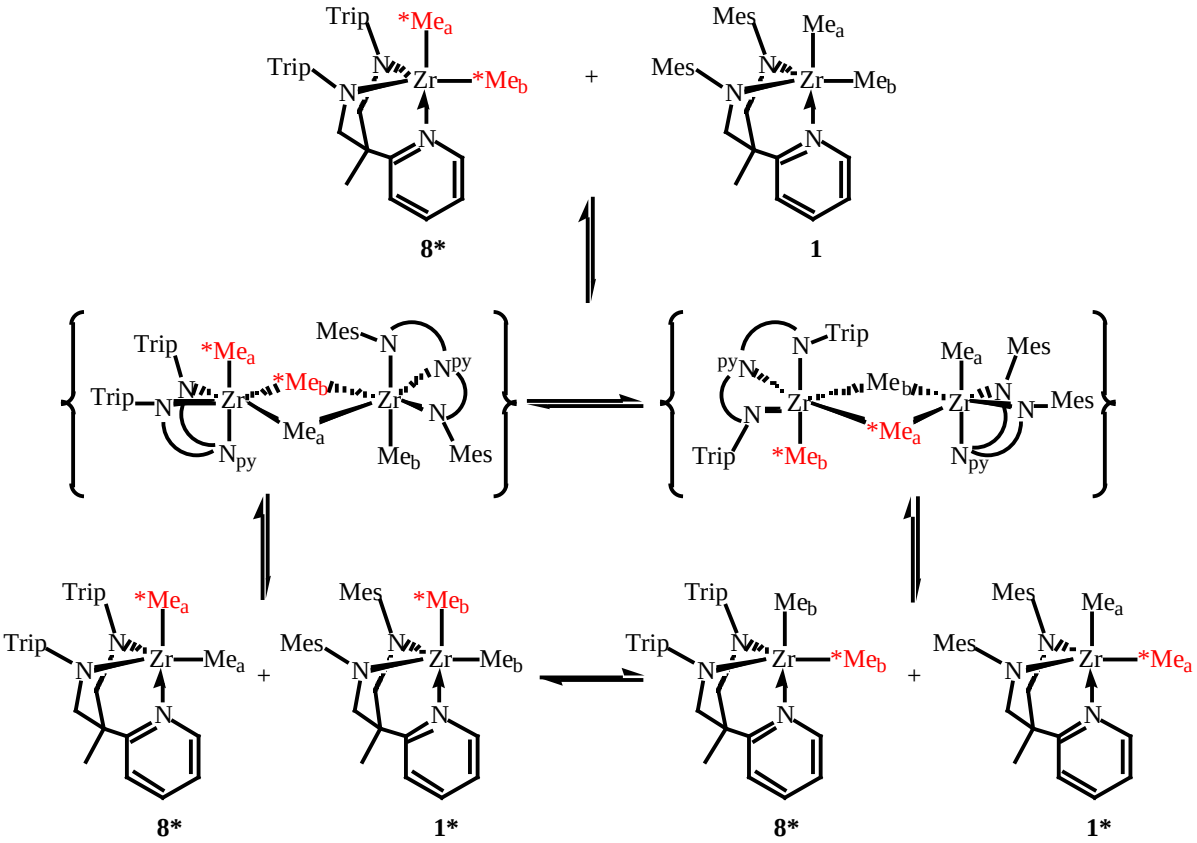

Scheme 1.5. A possible explanation for the methyl exchange between **1** and **8***.

Transfer of the ^{13}C label from **8*** to **1** is support for intermolecular methyl exchange on the chemical time scale. In order to show that the line broadening is due to intermolecular methyl exchange on the NMR time scale, a concentration dependent experiment was carried out. The ^{1}H NMR spectrum of a 96.0 mM solution of **1** (20 ˚C, C_6D_5Br) shows one broad signal at 0.26 ppm for the Zr-CH_3 protons. When this solution is diluted by a factor of 10, *i.e.* it is 9.6 mM, the Zr-CH_3 signal splits into two signals at 0.22 and 0.31 ppm. Possible intermediates for the intermolecular exchange are the dimeric species depicted in Scheme 1.5 consisting of two octahedral zirconium centers.

It is possible to draw parallels between the processes presented in Scheme 1.4 and Scheme 1.5. It appears that [ArNpy]$ZrMe_2$ complexes have a great affinity for filling their open coordination sphere and achieving octahedral geometry. This is accomplished by interaction with solvent molecules as well as with other dimethyl complexes. Interaction of dimethyl complexes with other metal centers will be discussed in the following sections.

1.6 Activation of [ArNpy]$ZrMe_2$ and labeling studies

Activation of [MesNpy]$ZrMe_2$ (**1**) with 1.0 equiv of $[Ph_3C][B(C_6F_5)_4]$ (20 ˚C, C_6D_5Br) results in direct methyl abstraction to yield Ph_3CMe and a zirconium cation. The resulting cationic species were studied by various NMR techniques and labeling studies. The ^{1}H NMR spectrum of this solution shows a sharp resonance at 2.03 ppm, which corresponds to the 3 protons of Ph_3CCH_3, and a broader resonance at 0.66 ppm corresponding to roughly 9 protons. In the ^{1}H NMR spectrum of activated [MesNpy]$Zr(^{13}Me)_2$ (**1***) this resonance splits into two signals with a J_{CH} of 108 Hz. This value is lower than that for $[(MesN_2NMe)Zr(^{13}Me)][B(C_6F_5)_4]$, which is 117 Hz.[38] The $^{13}C\{^{1}H\}$ NMR spectrum of activated **1*** shows a broad singlet at 38 ppm at room temperature.

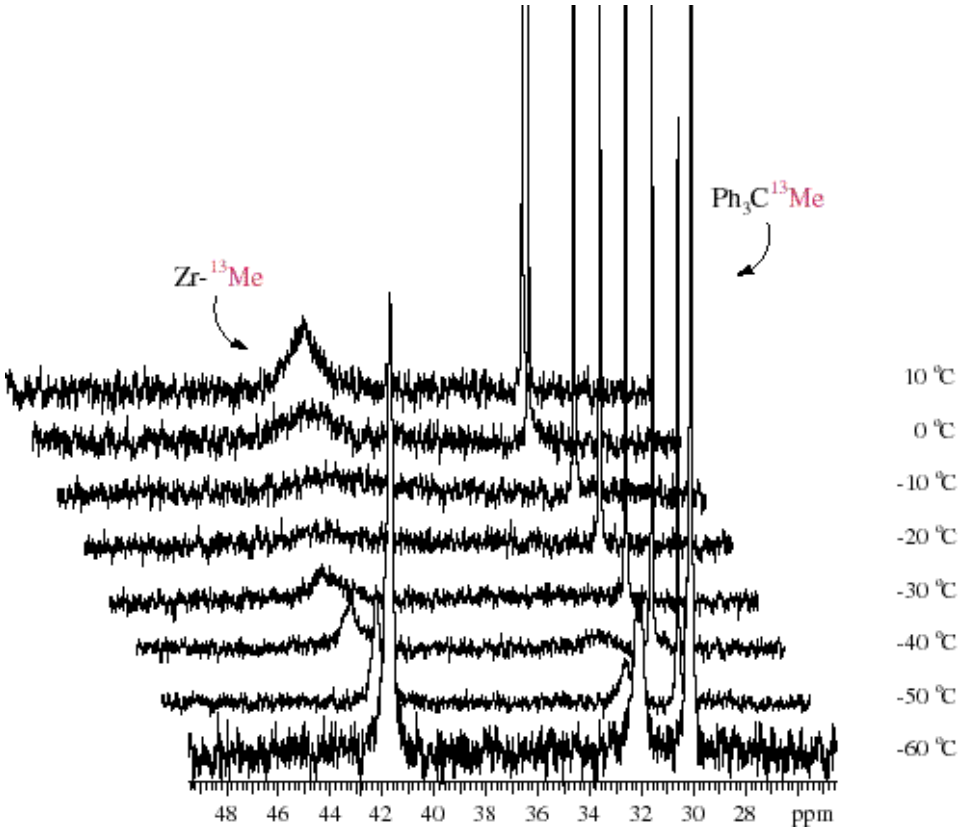

Figure 1.11. Variable temperature $^{13}C\{^{1}H\}$ NMR spectra (1:1 C_6D_5Br : $C_6D_5CD_3$) of **1*** activated with 1.0 equiv $[Ph_3C][B(C_6F_5)_4]$.

The cation generated from activation of **1** with $[Ph_3C][B(C_6F_5)_4]$ is stable at -30 ˚C for at least one month and at 40 ˚C for a few hours. Variable temperature $^{13}C\{^{1}H\}$ NMR studies of the labeled species were carried out in a 1:1 mixture of C_6D_5Br and $C_6D_5CD_3$ (Figure 1.11). These studies show that as the solution is cooled to -60 ˚C, the signal at 38 ppm splits into two peaks (41.9 and 32.1 ppm) in a 2:1 ratio. A proton coupled ^{13}C NMR experiment at -60 ˚C showed the J_{CH} for both signals to be 108 Hz. This indicates that both signals belong to methyl groups with the same hybridization.

A ^{1}H ROESY experiment (-25 ˚C, C_6D_5Br) shows NOE cross-peaks between the Zr-CH_3 and the *ortho* pyridyl proton signals, and between Zr-CH_3 and one set of the mesityl *ortho*

methyls. These results indicate that either the Zr-CH_3 group is in a position intermediate between axial and equatorial, or that it can exchange between these two positions.

Activation of [TripNpy]$ZrMe_2$ (**8**) with 1 equiv of $[Ph_3C][B(C_6F_5)_4]$ results in a cationic species as well as Ph_3CMe. The ^1H NMR spectrum (20 ˚C, C_6D_5Br) shows a single broad peak at 0.9 ppm corresponding to the Zr-CH_3 group, with a J_{CH} value of 109 Hz (obtained from activation of **8***). Variable temperature studies of the ^{13}C-labeled cation, in a 1:1 mixture of C_6D_5Br and $C_6D_5CD_3$, reveal two signals at –70 ˚C (36.3 and 47.2 ppm) in a 2:1 ratio (Figure 1.12). Notably, in Figure 1.12 the resonance for the most upfield Zr-^{13}Me is the most intense, while in Figure 1.11 the downfield signal is the most intense. These results indicate that activation of [ArNpy]$ZrMe_2$ complexes with 1.0 equiv $[Ph_3C][B(C_6F_5)_4]$ does not result in the formation of [(MesNpy)ZrMe]$[B(C_6F_5)_4]$ (**9**) and [(TripNpy)ZrMe]$[B(C_6F_5)_4]$ (**10**) as expected.

Based on studies carried out in the [$MesN_2$NMe] system by Casado, formation of dinuclear species {[(MesNpy)Zr]$_2$$Me_3$}$\{B(C_6F_5)_4\}$ (**11**) and {[(TripNpy)Zr]$_2$$Me_3$}$\{B(C_6F_5)_4\}$ (**12**)

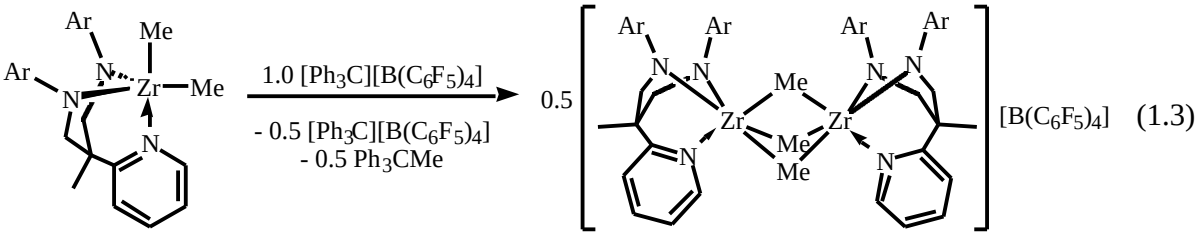

(1.3)

is a possibility (eq 1.3).[38] Equation 1.3 indicates that only 0.5 equiv of $[Ph_3C][B(C_6F_5)_4]$ is used in the activation process. Thus the solutions of cation generated with greater than 0.5 equiv of activator are always dark orange, the color of unreacted $[Ph_3C][B(C_6F_5)_4]$.

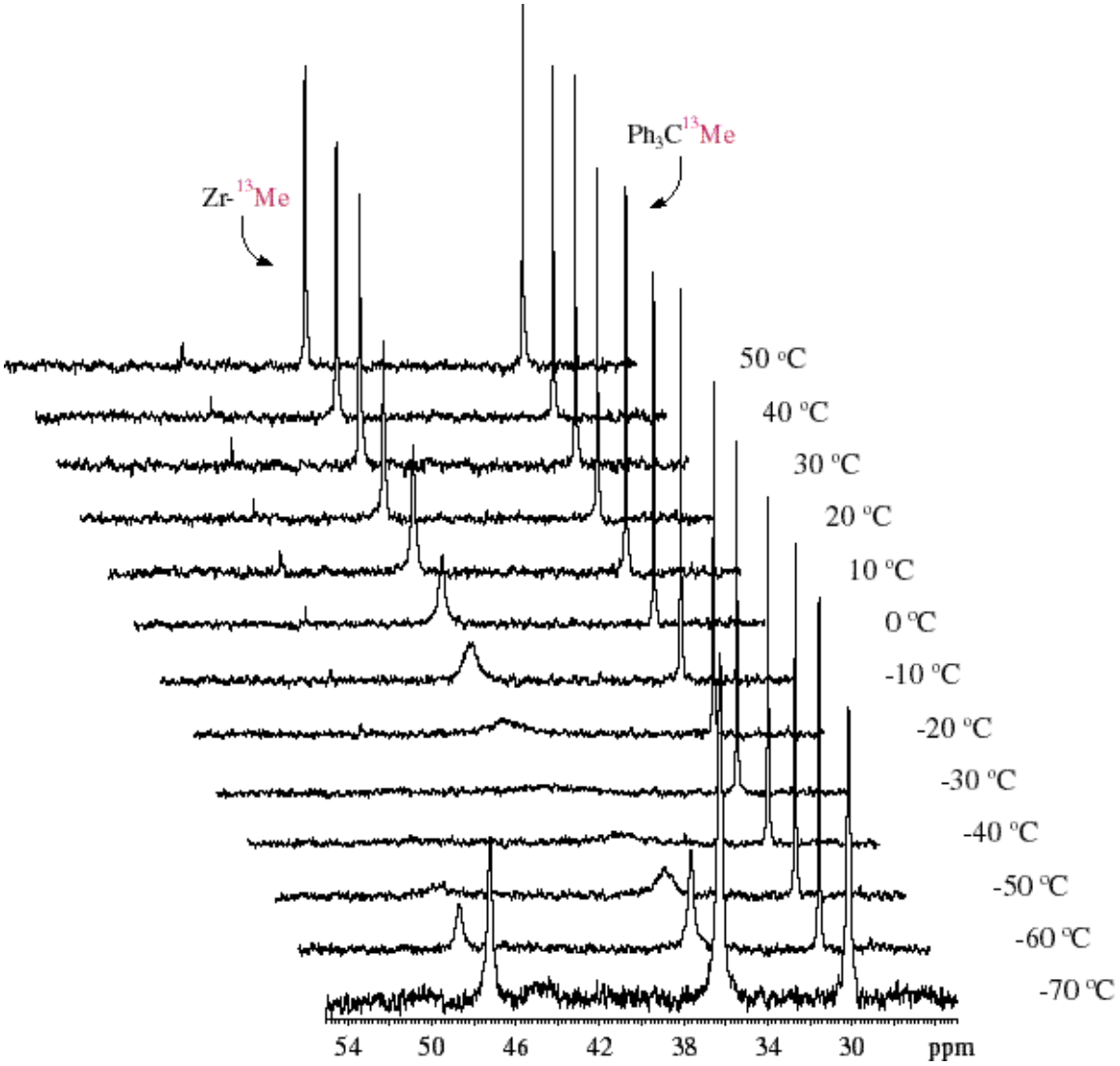

Figure 1.12. Variable temperature $^{13}C\{^{1}H\}$ studies of **8*** activated with 1.0 equiv $[Ph_3C][B(C_6F_5)_4]$ in 1:1 C_6D_5Br : $C_6D_5CD_3$.

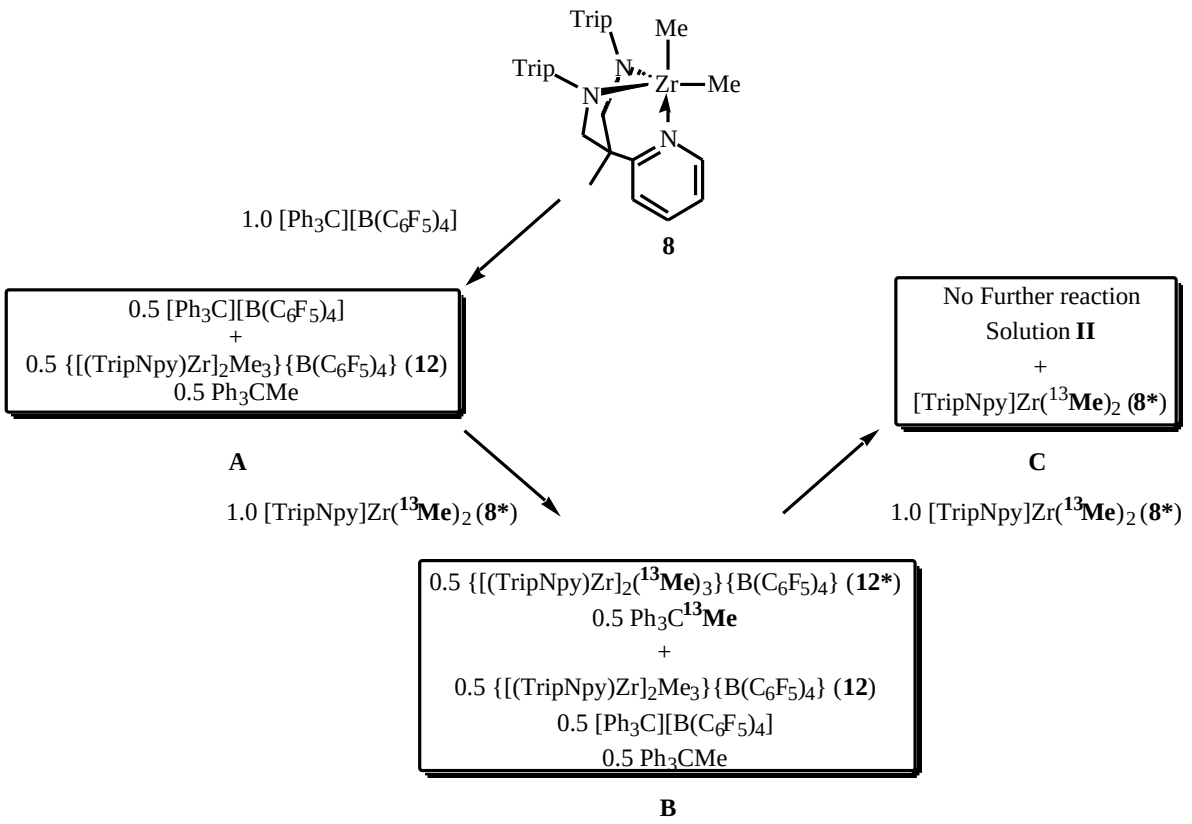

Scheme 1.6. Summary of NMR studies in the activated [TripNpy]$ZrMe_2$ (**8**) system.

Further experiments which were carried out on this system are summarized in Scheme 1.6. One equiv of **8** was activated with 1.0 equiv of $[Ph_3C][B(C_6F_5)_4]$ to yield an orange solution, **A**. The ^1H NMR spectrum (20 ˚C, C_6D_5Br) of this solution showed signals for $\{[(TripNpy)Zr]_2Me_3\}\{B(C_6F_5)_4\}$ (**12**) and Ph_3CMe. One equiv of ^{13}C-labeled dimethyl complex, **8***, was then added to solution **A** to give a yellow solution, **B**. The ^1H NMR spectrum of this solution showed signals for both Ph_3CMe and $Ph_3C^{13}Me$ in approximately a 1:1 ratio. The $^{13}C\{^1H\}$ NMR spectrum showed signals for $Ph_3C^{13}Me$ as well as for **12***. These results indicated that 0.5 equiv of activator remained in solution **A** to further activate **8***. Addition of another 1.0 equiv of **8*** to solution **B** led to no further reaction and free **8*** was observed in solution **C**.

To further study the nature of the activated species, [TripNpy]Zr(^{13}Me)$_2$ (**8***) was activated with 0.5 equiv of [Ph_3C][$B(C_6F_5)_4$] to generate {[(TripNpy)Zr]$_2$(^{13}Me)$_3$}{$B(C_6F_5)_4$}

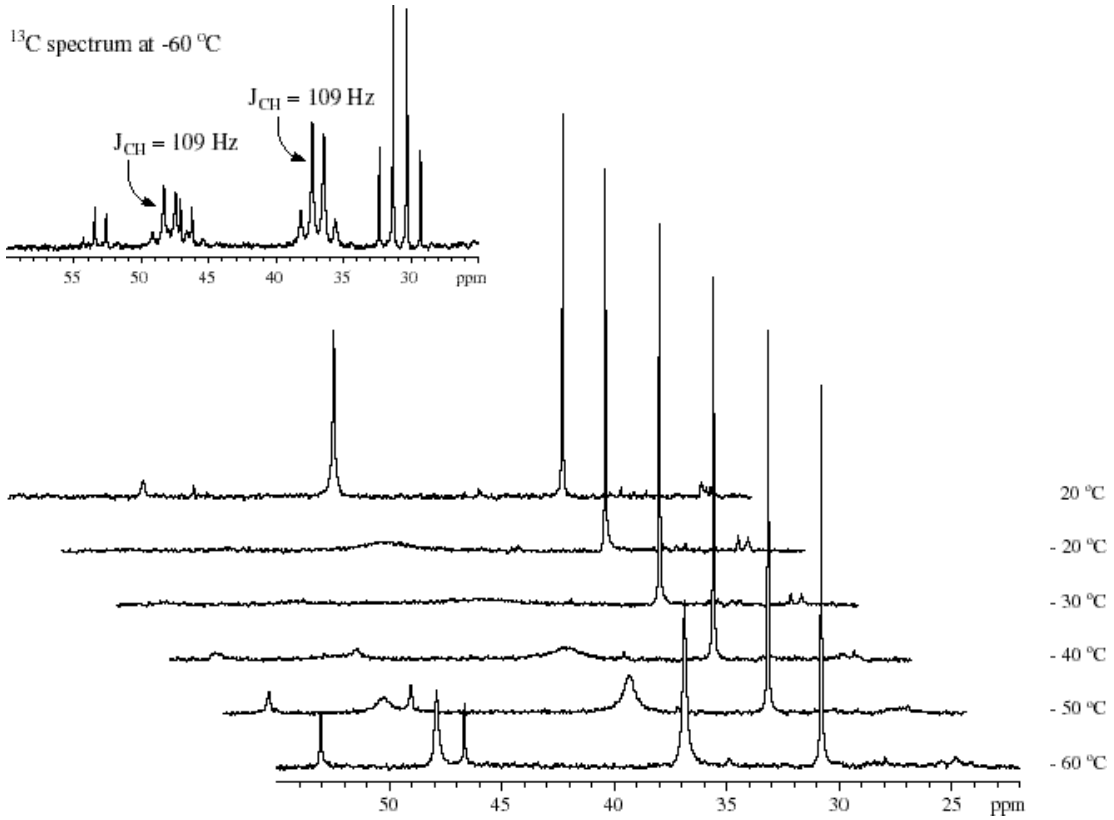

Figure 1.13. Variable temperature $^{13}C\{^1H\}$ studies of [TripNpy]ZrMe_2 (**8***) + 0.5 [Ph_3C][$B(C_6F_5)_4$] in 1:1 C_6D_5Br : $C_6D_5CD_3$.

(**12***) (Figure 1.13). Variable temperature $^{13}C\{^1H\}$ studies of this yellow solution in a 1:1 mixture of C_6D_5Br and $C_6D_5CD_3$ are similar to those of **8** activated with 1.0 equiv [Ph_3C][$B(C_6F_5)_4$] (Figure 1.12) (the minor set of signals at 46.5 and 53.1 ppm are due to an impurity.) The ^{13}C NMR spectrum (inset, Figure 1.13) shows that all of the signals belong to CH_3 groups, and that J_{CH} is 109 Hz for both Zr-^{13}CH$_3$ peaks. This supports a dinuclear structure with three bridging methyl groups. In the dinuclear compound bearing the diamidoamine ligand, [($Mes N_2$NMe)ZrMe)$_2$Me][$B(C_6F_5)_4$], coupling constants are distinct for bridging and terminal

methyl groups, 133 and 115 Hz, respectively (Figure 1.14).[38] As observed by Casado[38] and

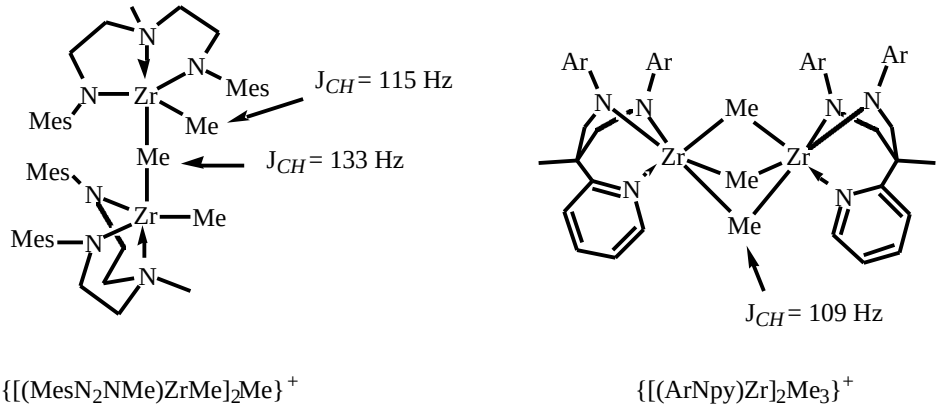

Figure 1.14. Structures of $\{[(MesN_2NMe)ZrMe]_2Me\}^+$ and $\{[(ArNpy)Zr]_2Me_3\}^+$. Anion = $[B(C_6F_5)_4]^-$.

others,[43-51,58,59] the bridging methyl group in such a species has greater sp^2 character and thus J_{CH} values are closer to 130 Hz. Based on these results, and the results obtained by Buchwald[48] (Figure 1.3) and others,[58] we propose a structure with three bridging methyl groups for activated $[ArNpy]ZrMe_2$ complexes.

Attempts were made to break up the dinuclear species $\{[(MesNpy)Zr]_2Me_3\}\{B(C_6F_5)_4\}$ (**11**) and $\{[(TripNpy)Zr]_2Me_3\}\{B(C_6F_5)_4\}$ (**12**) and generate solvent adducts of the mononuclear cations $[(MesNpy]ZrMe][B(C_6F_5)_4]$ (**9**) and $[(TripNpy]ZrMe][B(C_6F_5)_4]$ (**10**). Complexes **11** and **12** are stable toward coordinating solvents; addition of excess diethyl ether, THF or DME to these complexes at room temperature does not lead to a solvent adduct. However, heating **12*** at 50 ˚C in the presence of 2.5 equiv of DME led to the appearance of signals for **8*** (34.2 and 38.3 ppm) as well as a new set of resonances at 39.4 and 46.5 ppm (Figure 1.15). The new peaks may belong to DME adducts of **10***, $[(TripNpy]Zr(DME)(^{13}Me)][B(C_6F_5)_4]$, in which the methyl group can be *trans* (**13**) or *cis* (**13'**) to the pyridyl nitrogen (Scheme 1.7). The Zr-CH_3 resonance for a similar compound, $\{[(t\text{-}Bu)NON]Zr(DME)Me\}\{BPh_4\}$, is observed at 52.5 ppm.[30]

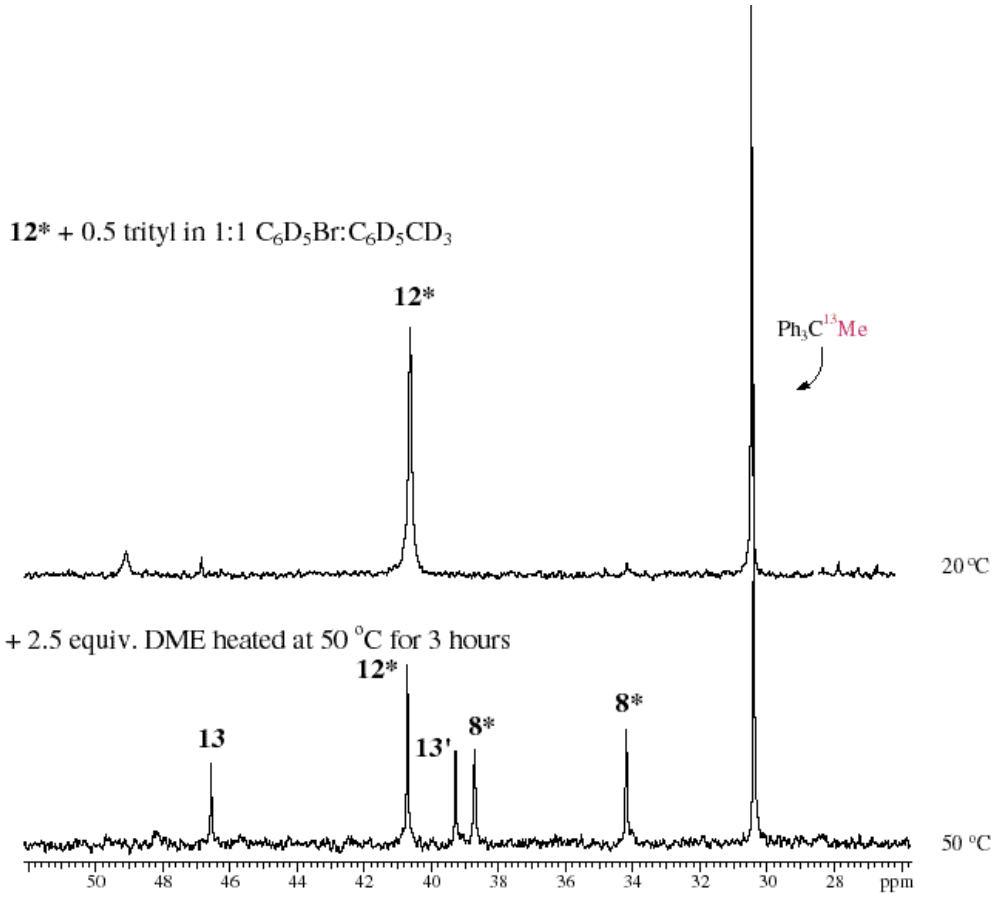

Figure 1.15. Attempt at isolating a DME adduct of **10***. $^{13}C\{^{1}H\}$ spectrum (1:1 C_6D_5Br : $C_6D_5CD_3$) of **12*** at 20 ˚C (top) and with added DME 50 ˚C (bottom).

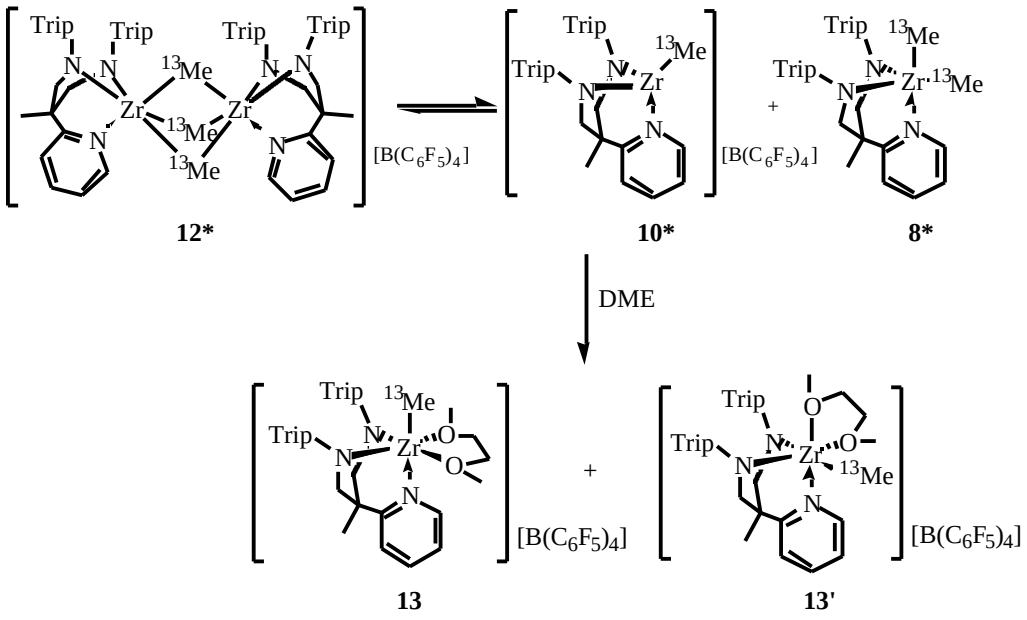

Scheme 1.7. Potential pathway for formation of DME adducts of **10***.

No exchange between solutions of {[(TripNpy)Zr]$_2$(^{13}Me)$_3$}{B(C$_6$F$_5$)$_4$} (**12***) and {[MesNpy)Zr]$_2$Me$_3$}{B(C$_6$F$_5$)$_4$} (**11**) was observed. Both dimethyl complexes **1** and **8*** were treated with 1 equiv of [Ph$_3$C][B(C$_6$F$_5$)$_4$] and the activated solutions mixed at room temperature. Variable temperature ^{13}C{^{1}H} studies (1:1 C$_6$D$_5$Br : C$_6$D$_5$CD$_3$) show only signals for **12***, indicating that the dinuclear complexes do not readily exchange methyl groups with one another.

In order to further study the dinuclear complexes, both **11** and **12**, and their ^{13}C-labeled analogues, **11*** and **12***, were independently prepared and isolated as yellow powders. These compounds were characterized by elemental analysis, as well as by ^{1}H and ^{13}C{^{1}H} NMR spectroscopy, and had spectra identical to their counterparts generated *in situ*. A series of experiments was carried out to further test the stability of these complexes (Scheme 1.8).

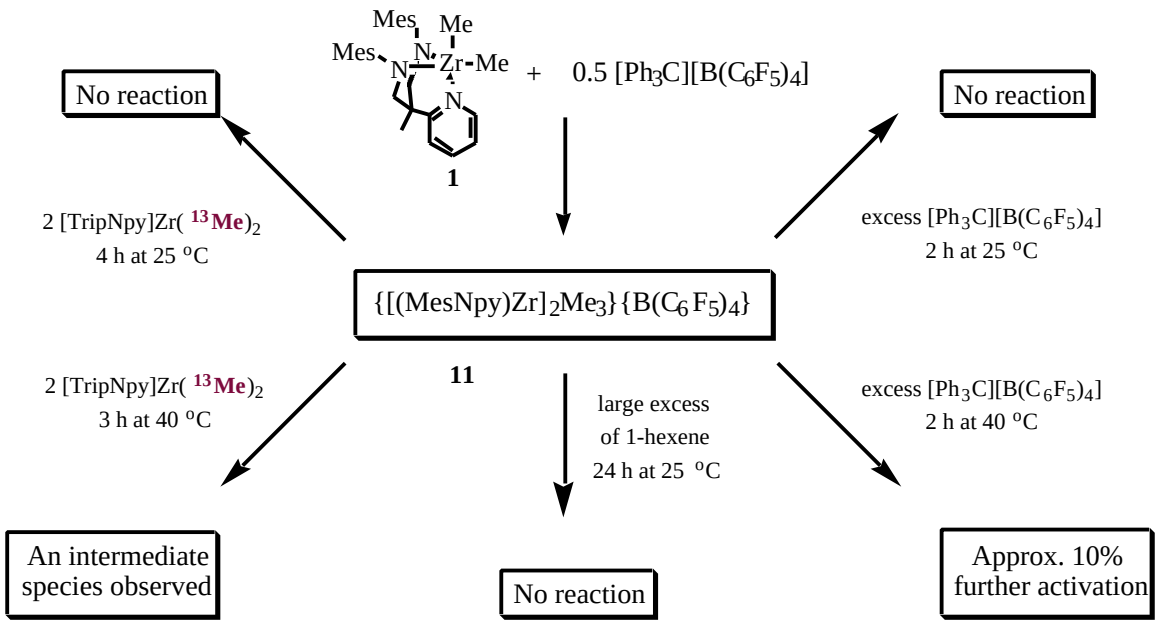

Scheme 1.8. Experiment carried out with $\{[(MesNpy)Zr]_2Me_3\}\{B(C_6F_5)_4\}$ (**11**).

Treatment of **11** with 2 equiv of **8*** led to very little change over 4 h at 25 ˚C. Heating this solution to 40 ˚C, however, caused an exchange of methyl groups between these two species

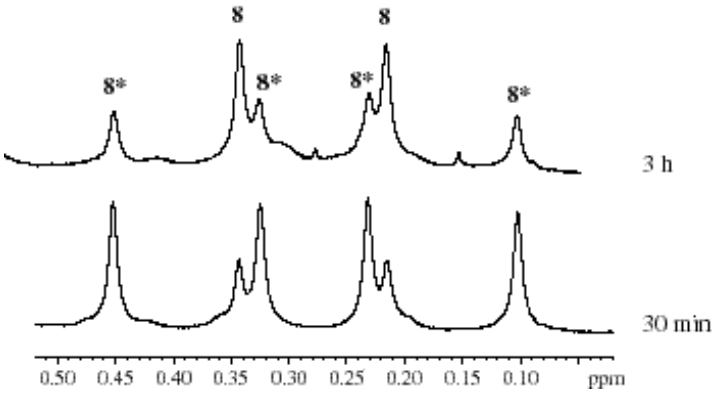

Figure 1.16. ^{1}H NMR spectra (40 ˚C, C_6D_5Br) of methyl exchange between **11** and **8***.

(Figure 1.16). The ^{1}H NMR spectrum (C_6D_5Br) of this solution after 30 min at 40 ˚C shows the presence of both **8*** and **8** which results from exchange of methyl groups between **11** and **8***. The signals for **8** increase significantly after 3 h at 40 ˚C. The $^{13}C\{^1H\}$ NMR spectrum (40 ˚C,

C_6D_5Br) shows signals for **8*** as well as a broad resonance at 40.5 ppm corresponding to a ^{13}C-labeled dinuclear species (Figure 1.17).

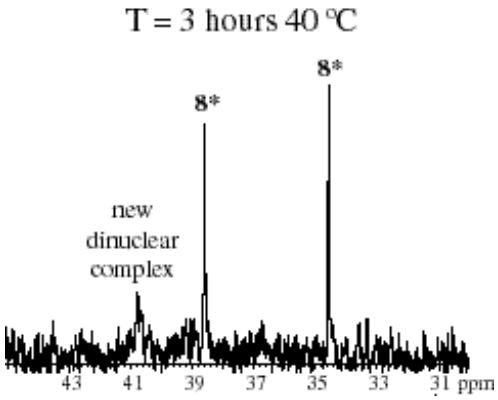

Figure 1.17. $^{13}C\{^1H\}$ NMR spectrum (40 ˚C, C_6D_5Br) of **11** + **8*** after 3 h.

Observation of unlabelled **8** and a ^{13}C-labeled dinuclear species indicates that there is an exchange of methyl groups between **11** and **8***. For this methyl exchange to occur, there must be an equilibrium between **11** and a mononuclear cation $[(MesNpy)ZrMe][B(C_6F_5)_4]$ (**9**), as well as the neutral dialkyl complex $[MesNpy]ZrMe_2$ (**1**) (Scheme 1.9). At room temperature this equilibrium lies far towards **11**, however at 40 ˚C, some **9** is produced which is captured by **8*** to yield the new ^{13}C-labeled dinuclear species shown in Figure 1.17. Complex **8** can then be generated by further methyl group exchange between the new cation and **1**, or by methyl group exchange between **8*** and **1**. An exchange between the dialkyl components in this system has not been included in Scheme 1.9, but is assumed to be present throughout the process.

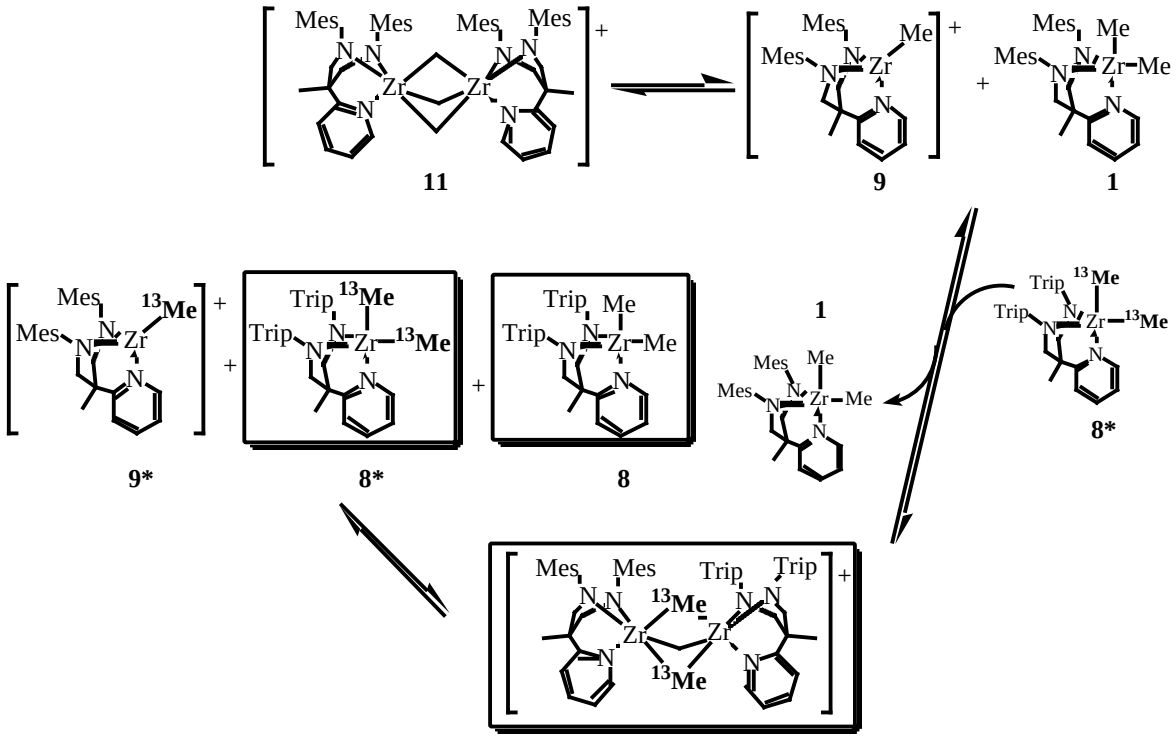

Scheme 1.9. An explanation for methyl exchange in the activated [ArNpy]$ZrMe_2$ system. Observed species are in shaded boxes.

Treatment of **11** with excess $[Ph_3C][B(C_6F_5)_4]$ at 25 ˚C for 2 h led to no further activation of the cationic dinuclear species. However, heating the sample to 40 ˚C for a further 2 h led to approximately 10% further activation, as evident by the presence of $Ph_3C^{13}Me$ signals in the ^1H and $^{13}C\{^1H\}$ NMR spectra (40 ˚C, C_6D_5Br) (Scheme 1.8). Addition of a large excess of 1-hexene to a solution of **11** (isolated as a powder and dissolved in chlorobenzene) leads to no polymerization over 24 h at 25 ˚C.

Activation of **1** with 1 equiv of $[Ph_3C][B(C_6F_5)_4]$ in minimal chlorobenzene and immediate addition of 400 equiv of 1-hexene leads to a polymer sample with molecular weight of 62000 (expected 34000) and PDI of 1.16. This is in contrast to other polymerization experiments where M_n values up to ten times higher than expected were obtained (Chapter 2). This result can be explained if one assumes that the formation of the dimeric species was

hindered by the "capture" of a monomeric monocation with the large excess of 1-hexene. Further polymerization results with activated **1** will be presented in Chapter 2.

1.7 Synthesis and activation of [MesNpy]HfMe$_2$ and labeling studies

Hafnium complexes of the [MesNpy] ligand, [MesNpy]Hf(NMe$_2$)$_2$ (**14**) and [MesNpy]HfCl$_2$ (**15**) can be prepared readily according to the procedure outlined in Scheme 1.3. [MesNpy]HfMe$_2$ (**16**) and its ^{13}C-labeled analogue (**16***) have been prepared and show signals at 0.06 and 0.14 ppm for Hf-C*H*$_3$ protons and at 45.2 and 49.4 ppm for Hf-*C*H$_3$ carbons (20 ˚C, C$_6$D$_5$Br). The ^{1}H NMR spectrum in C$_6$D$_6$ shows only one signal corresponding to 6 protons for the two methyl groups. Thus, the exchange process observed in the [ArNpy]ZrMe$_2$ system also occurs in the hafnium system.

Activation of **16** with 1 equiv [Ph$_3$C][B(C$_6$F$_5$)$_4$] results in the formation of the dinuclear complex {[(MesNpy)Hf]$_2$Me$_3$}{B(C$_6$F$_5$)$_4$} (**17**). The ^{1}H NMR spectrum shows a broadened signal at 1.14 ppm corresponding to 9 protons, which accounts for three Hf-C*H*$_3$ groups for each molecule of **17**. The chemical shifts for **17** correspond closely to those for the analogous zirconium complex {[(MesNpy)Zr]$_2$Me$_3$}{B(C$_6$F$_5$)$_4$} (**11**).

Activation of [MesNpy]HfMe$_2$ with B(C$_6$F$_5$)$_3$ results in methyl abstraction and the formation of the dinuclear monocation {[(MesNpy)Hf]$_2$Me$_3$}{MeB(C$_6$F$_5$)$_3$} (**18**) (eq 1.4).

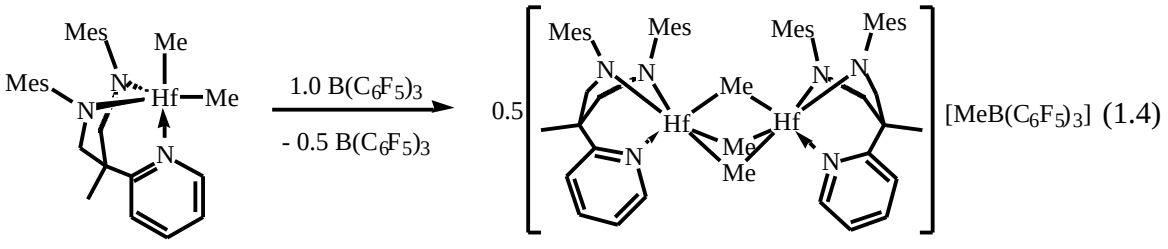

(1.4)

16 **18**

Complexes **18** and the ^{13}C-labeled analogue **18*** have also been synthesized by addition of 0.5 equiv of $B(C_6F_5)_3$ to **16** or **16*** and characterized by NMR spectroscopy as well as by elemental analysis.

The ^{1}H NMR spectrum ($C_6D_5CD_3$, 20 ˚C) of **18** shows one broad signal for the *ortho* pyridyl proton at 7.9 ppm. The backbone signals and the aliphatic region of the spectrum are similar to those for **17**, with a broad resonance at 1.1 ppm for the bridging methyl groups and a sharp signal at 0.95 ppm for the B-C*H*$_3$ protons. The ^{19}F NMR spectrum shows two major sets of signals, corresponding to $[MeB(C_6F_5)_3]^-$ and unreacted $B(C_6F_5)_3$. Addition of 96 equiv of 1-hexene to a solution of **18** resulted in no polymerization.

The $^{13}C\{^1H\}$ NMR spectrum of **18*** at 20 ˚C shows a very broad signal at ~40 ppm. As the solution (1:1 $C_6D_5CD_3$: C_6D_5Br) is cooled to -40 ˚C, this signal splits into two resonances at 41.4 and 32.5 ppm (Figure 1.18). In the proton coupled ^{13}C NMR spectrum, these signals split into quartets with J_{CH} = 108 Hz. The signal for the B-^{13}*C*H$_3$ of $[MeB(C_6F_5)_3]^-$ is observed at ~11 ppm and has a J_{CH} of 116 Hz. This value is similar to that for B-*C*H$_3$ in $[(n\text{-}Bu)_4N][MeB(C_6F_5)_3]$.

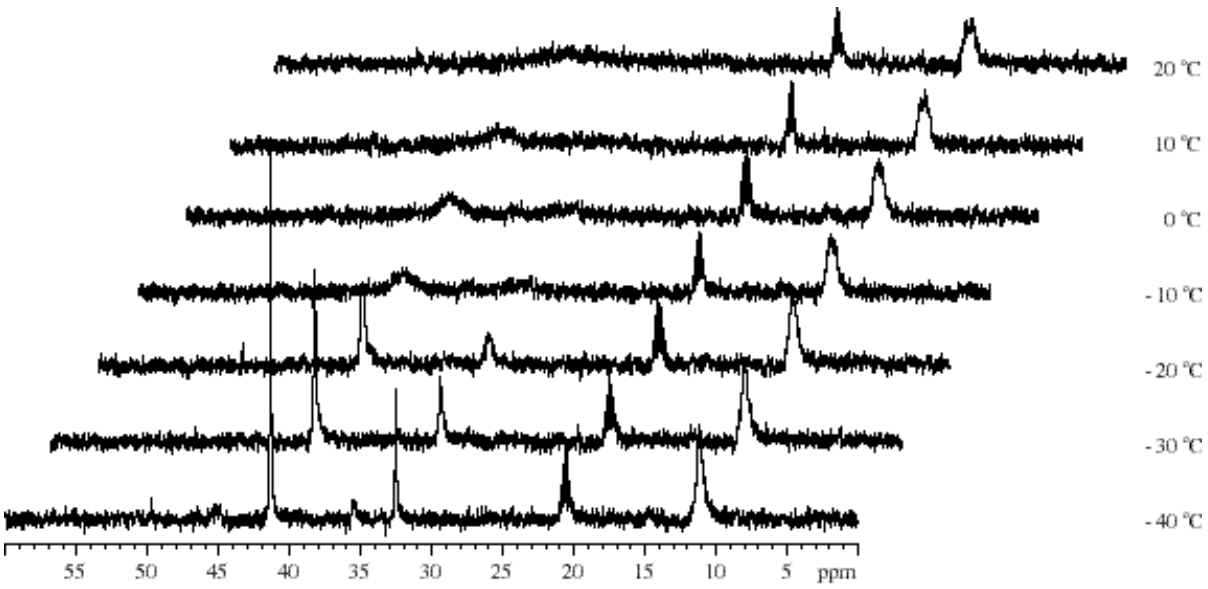

Figure 1.18. Variable temperature $^{13}C\{^1H\}$ studies of $\{[(MesNpy)Hf]_2(^{13}Me)_3\}\{MeB(C_6F_5)_3\}$ (**18***) (1:1 C_6D_5Br : $C_6D_5CD_3$).

In activation of [(t-Bu)NON]$ZrMe_2$ with $B(C_6F_5)_3$ by Baumann,[30] the product of the reaction is {[(t-Bu)NON]ZrMe}{$MeB(C_6F_5)_3$} in which the anion is coordinated to the metal center through a bridging methyl group (eq 1.5). The ^{13}C signal for the coordinated B-*C*H_3 group is reported at 29.5 ppm.

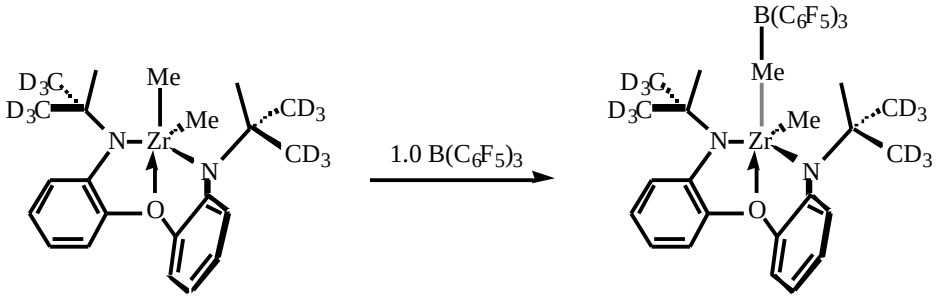

[(t-Bu)NON]$ZrMe_2$ {[(t-Bu)NON]ZrMe}{$MeB(C_6F_5)_3$}

(1.5)

It is apparent that $[(MesNpy)HfMe]^+$ has a greater affinity for an equivalent of [MesNpy]$HfMe_2$ than for the $[MeB(C_6F_5)_3]$ anion. This highlights the importance of the interaction of neutral dimethyl complexes with open cationic centers in the [ArNpy] systems.

1.8 Conclusions

Chapter 1 describes the preparation of arylated diamidopyridine ligands H_2[MesNpy] and H_2[TripNpy]. These ligands coordinate to zirconium with strictly *pseudo*-facial geometry. Dimethyl complexes [MesNpy]$ZrMe_2$ (**1**) and [TripNpy]$ZrMe_2$ (**8**) were prepared. The synthesis of **1** was complicated by formation of ether adducts as well as zirconate species. Methyl exchange was observed in both [ArNpy]$ZrMe_2$ systems. These complications are due to the open coordination geometry of these complexes which is enforced by the ligand.

Activation of these dimethyl complexes with 1.0 or 0.5 equiv of $[Ph_3C][B(C_6F_5)_4]$ resulted in the dinuclear monocations $\{[(ArNpy)Zr]_2Me_3\}\{B(C_6F_5)_4\}$. These complexes were

also synthesized independently and were shown to be unreactive towards various reagents at room temperature. Solution studies of these dinuclear complexes suggest a structure with three bridging methyl groups.

Activation of the analogous hafnium dimethyl complex [MesNpy]$HfMe_2$ (**16**) with either 1.0 equiv $[Ph_3C][B(C_6F_5)_4]$ or with $B(C_6F_5)_3$ also led to the formation of a dinuclear species, $\{[(MesNpy)Hf]_2Me_3\}\{MeB(C_6F_5)_3\}$ (**19**). Interaction of the anion generated in the latter case, $[MeB(C_6F_5)_3]$, with the cation was not observed.

The [ArNpy] ligand system provides an open coordination environment that fosters a variety of interactions not observed in more sterically encumbered systems. This property of [ArNpy]MR_2 complexes will be discussed in depth in the following chapters.

1.9 Experimental section

General Procedures. All manipulations, with the exception of the synthesis of ligand precursors, were performed under N_2 in a glove-box or using standard Schlenk procedures. Solvents were dried using conventional procedures.[60] Chlorobenzene (HPLC grade) and deuterated solvents were degassed, stored over and distilled from CaH_2. Commercial reagents were used without further purification. NMR spectra were recorded on a Varian INOVA 500 spectrometer. ^1H NMR chemical shifts are given in ppm versus residual protons in the deuterated solvents as follows: δ 7.27 $CDCl_3$, δ 7.16 C_6D_6, δ 2.09 toluene-d_8 (methyl), δ 7.29 C_6D_5Br (most downfield resonance). $^{13}C\{^1H\}$ NMR chemical shifts are given in ppm versus residual ^{13}C in the solvents as follows: δ 77.23 $CDCl_3$, δ 128.39 C_6D_6, δ 20.4 toluene-d_8 (methyl), δ 122.25 C_6D_5Br (most upfield resonance). Some aryl resonances in ^1H and $^{13}C\{^1H\}$ spectra are not given.

Elemental analyses were performed by H. Kolbe, Mikroanalytisches Laboratorium (Mülheim an der Ruhr, Germany). X-ray data were collected on a Siemens SMART/CCD

diffractometer with λ(MoKα) = 0.71073 Å and solved using a full-matrix least squares refinement on F^2. HRMS (EI, 70 eV) were obtained with a MAT 731 spectrometer.

All Grignard reagents were carefully titrated with 2-butanol in the presence of 1,10-phenanthroline prior to use. $Zr(NMe_2)_4$ and $Hf(NMe_2)_4$ have been prepared according to previously reported methods.[61]

H_2[MesNpy]. A Schlenk flask was charged with $H_3CC(2\text{-}C_5H_4N)(CH_2NH_2)_2$ (5.00 g, 30 mmol), mesityl bromide (11.74 g, 59 mmol), tris(dibenzylideneacetone)dipalladium(0) (0.419 g, 0.45 mmol), racemic-2,2'-diphenylphosphino-1,1'-binaphthyl (0.717 g, 1.15 mmol), sodium *t*-butoxide (8.75 g, 91 mmol) and toluene (200 mL). The reaction mixture was stirred and heated to 110 ˚C under a stream of N_2. The reaction was judged complete after one day, with H_2[MesNpy] being the only significant product in the reaction mixture. The hot solution was filtered through Celite to remove NaBr and washed with pentane. The solvent was removed *in vacuo* and the red residue was dissolved in refluxing pentane (200 mL) and filtered while hot. Clear, colorless crystals of H_2[MesNpy] were obtained from pentane. Yield: 7.5 g, 63%. ^{1}H NMR (500 MHz, $CDCl_3/C_6D_6$, 295 K) δ 1.71/1.59 (s, 3H, C*H*$_3$), 2.16/2.21 (s, 12H, *o*-C*H*$_3$), 2.21/2.19 (s, 6H , *p*-C*H*$_3$), 3.17/3.25 (d, 2H, C*H*$_2$), 3.45/3.49 (d, 2H, C*H*$_2$), 3.45/3.70 (s, 2H, N*H*), 6.79/6.79 (s, 4H, C*H*), 7.22/6.63 (m, 1H, py-C*H*), 7.49/7.06 (m, 1H, py-C*H*), 7.71/7.07 (m, 1H, py-C*H*), 8.69/8.41 (m, 1H, py-o-C*H*). $^{13}C\{^1H\}$ NMR (125 MHz, C_6D_6, 295 K) δ 18.86 (s, *o*-*C*H$_3$), 21.17 (s, *p*-*C*H$_3$), 23.31 (s, *C*H$_3$), 46.97 (s, *C*R$_4$), 57.97 (s, *C*H$_2$), 121.76 (s, Ar-*C*), 122.00 (s, Ar-*C*), 130.25 (s, Ar-*C*), 130.83 (s, Ar-*C*), 131.59 (s, Ar-*C*), 136.65 (s, Ar-*C*), 144.99 (s, Ar-*C*), 149.25 (s, Ar-*C*), 165.77 (s, Ar-*C*). HRMS (EI, 70 eV) *m/z* Calcd for $C_{27}H_{35}N_3$: 401.283098; found: 401.2840 (12).

[MesNpy]Zr(THF)Me_2 (2). $ZrCl_4$ (0.89 g, 3.80 mmol) was added to a cold (–30 ˚C) solution of H_2[MesNpy] (2.00g, 3.84 mmol) in diethyl ether (30 mL). The mixture was stirred

at room temperature for 1 h to yield a pink-orange solid. The mixture was cooled to –30 ˚C, and MeMgCl (3.0 M in THF, 5.2 mL, 15.58 mmol) was added. The reaction mixture was stirred for 20 min at room temperature. Dioxane (1.51 g, 17.11 mmol) was added to the mixture, the ensuing white solid filtered through Celite, and the orange filtrate taken to dryness *in vacuo*. After trituration with pentane (3 × 15 mL), [MesNpy]Zr(THF)Me_2 was obtained as a yellow powder, which was washed with cold pentane (3 × 10 mL) and vacuum-dried. Yield: 1.6 g, 70%. Yellow crystals suitable for a single crystal X-ray diffraction study were grown by slow crystallization from diethyl ether at -30 ˚C. ^{1}H NMR (C_6D_6, 295 K) δ 0.45 (s, 6H, CH_3), 0.98 (s, 3H, CH_3), 1.21 (m, 4H, O(CH_2CH_2)$_2$), 2.15 (s, 6H, *p*-CH_3), 2.23 (s, 12H, *o*-CH_3), 2.76 (d, 2H, CH_2), 3.48 (m, 4, O(CH_2CH_2)$_2$), 3.90 (d, 2H, CH_2), 6.62 (m, 1H, py-C*H*), 6.84 (s, 4H, C*H*), 6.86 (m, 1H, py-C*H*), 7.05 (m, 1H, py-C*H*), 8.85 (m, 1H, py-C*H*). ^{13}C{^{1}H} NMR (125 MHz, C_6D_6, 295 K) δ 18.61 (s, *o*-CH_3), 20.83 (s, *p*-CH_3), 24.85 (s, CH_3), 35.04 (s, O(CH_2CH_2)$_2$) 35.8 (broad s, Zr-CH_3), 46.29 (s, CR_4), 65.82 (s, CH_2), 35.04 (s, O(CH_2CH_2)$_2$), 120.67 (s, Ar-*C*), 121.83 (s, Ar-*C*), 129.63 (s, Ar-*C*), 133.09 (s, Ar-*C*), 134.86 (s, Ar-*C*), 138.51 (s, Ar-*C*), 147.05 (s, Ar-*C*), 147.98 (s, Ar-*C*), 162.87 (s, Ar-*C*). Anal. Calcd for $C_{29}H_{39}N_3Zr$: C, 66.84; H, 7.99; N, 7.09. Found: C, 66.69; H, 7.91; N, 6.99.

[MesNpy]Zr(NMe_2)$_2$ (4). Zr(NMe_2)$_4$ (2.00 g, 7.48 mmol) and H_2[MesNpy] (3.16 g, 7.86 mmol) were dissolved in pentane (60 mL). The reaction mixture was stirred at room temperature for 16 h, filtered, and the solvent evaporated to yield an orange solid. Yield: 3.90 g, 86%. [MesNpy]Zr(NMe_2)$_2$ can be recrystallized from pentane at -30 ˚C to yield yellow-orange crystals. ^{1}H NMR (500 MHz, C_6D_6, 295 K) δ 1.07 (s, 3H, CH_3), 2.20 (s, 6H, *p*-CH_3), 2.30 (s, 12H, *o*-CH_3), 2.83 (d, 2H, CH_2), 2.99 (s, 6H, N(CH_3)$_2$), 3.00 (s, 6H, N(CH_3)$_2$), 4.12 (d, 2H, CH_2), 6.68 (m, 1H, py-C*H*), 6.87 (m, 1H, py-C*H*), 6.89 (s, 4H, C*H*), 7.09 (m, 1H, py-C*H*), 8.69 (m, 1H, py-*o*-C*H*). ^{13}C{^{1}H} NMR (125 MHz, C_6D_6, 295 K) δ 19.68 (s, *o*-CH_3), 21.28 (s, *p*-CH_3), 25.29 (s, CH_3), 42.53 (s, N(CH_3)$_2$), 45.14 (s, N(CH_3)$_2$), 47.01 (s, CR_4), 67.03 (s, CH_2), 120.65 (s, Ar-*C*),

122.18 (s, Ar-*C*), 130.07 (s, Ar-*C*), 132.12 (s, Ar-*C*), 134.14 (s, Ar-*C*), 138.92 (s, Ar-*C*), 148.63 (s, Ar-*C*), 149.96 (s, Ar-*C*), 163.94 (s, Ar-*C*). Anal. Calcd for $C_{31}H_{45}N_5Zr$: C, 64.31; H, 7.83; N, 12.10. Found: C, 64.39; H, 7.76; N, 11.94.

[MesNpy]ZrCl$_2$ (5). To a solution of [MesNpy]Zr(NMe$_2$)$_2$ (7.74 g, 13.4 mmol) in diethyl ether (200 mL) was added TMSCl (5.09 mL, 40.0 mmol) and the reaction mixture was stirred at room temperature for 1 h. The resulting white solid was filtered, washed with pentane (3 × 10 mL) and dried *in vacuo* for 4 h. Yield: 6.50 g, 86%. [MesNpy]ZrCl$_2$ can be recrystallized from toluene at room temperature to yield clear, colorless crystals. ^{1}H NMR (500 MHz, C_6D_6, 295 K) δ 0.86 (s, 3H, C*H*$_3$), 1.51 (s, 6H, *o*-C*H*$_3$), 2.16 (s, 6H, *p*-C*H*$_3$), 2.76 (d, 2H, C*H*$_2$), 2.90 (s, 6H, *o*-C*H*$_3$), 3.83 (d, 2H, C*H*$_2$), 6.65 (m, 1H, py-C*H*), 6.70 (s, 2H, C*H*), 6.89 (m, 1H, py-C*H*), 6.90 (s, 2H, C*H*), 6.98 (m, 1H, py-C*H*), 10.41 (m, 1H, py-*o*-C*H*). ^{13}C{^{1}H} NMR (125 MHz, C_6D_6, 295 K) δ 18.63 (s, *o*-*C*H$_3$), 19.08 (s, *o*-*C*H$_3$), 19.85 (s, *p*-*C*H$_3$), 21.30 (s, *C*H$_3$), 46.89 (s, *C*R$_4$), 65.82 (s, *C*H$_2$), some aryl peaks omitted here. Anal. Calcd for $C_{27}H_{33}N_3Cl_2Zr$: C, 57.73; H, 5.92; N, 7.48; Cl, 12.62. Found: C, 57.61; H, 6.11; N, 7.42; Cl, 12.47.

[MesNpy]ZrMe$_2$ (1). A suspension of [MesNpy]ZrCl$_2$ (0.606 g, 1.079 mmol) in diethyl ether (30 mL) was cooled to -30 ˚C. To the cold solution was added MeMgBr (3.4 M in diethyl ether, 0.666 mL, 2.266 mmol) and the resulting mixture was stirred at room temperature for 15 min until the cloudy suspension became clear. (*Note: Correct stoichiometry is very important to the success of the reaction*.) Dioxane (0.216 mL, 2.535 mmol) was added to the solution and the resulting white solid was filtered through Celite. The filtrate was reduced to *ca* 5 mL and stored at -30 ˚C for 1 d to yield [MesNpy]ZrMe$_2$ as clear, colorless crystals. Yield: 0.33 g, 59%. The ^{13}C-labeled complex, [MesNpy]Zr(^{13}Me)$_2$, was prepared in a similar manner with ^{13}MeMgI. White crystals suitable for a single crystal X-ray diffraction study were grown by slow crystallization from diethyl ether at -30 ˚C. ^{1}H NMR (500 MHz, C_6D_6, 295 K) δ 0.56 (s, 6H, Zr-

CH_3), 0.95 (s, 3H, CH_3), 2.18 (s, 6H, *p*-CH_3), 2.27 (s, 12H, *o*-CH_3), 2.73 (d, 2H, CH_2), 4.04 (d, 2H, CH_2), 6.56 (m, 1H, py-C*H*), 6.77 (m, 1H, py-C*H*), 6.87 (s, 4H, C*H*), 7.02 (m, 1H, py-C*H*), 8.77 (m, 1H, py-*o*-C*H*). ^{1}H NMR (500 MHz, C_6D_5Br, 295 K) δ 0.22 (s, 3H, Zr-CH_3), 0.32 (s, 3H, Zr-CH_3), 1.24 (s, 3H, CH_3), 2.16 (s, 12H, *o*-CH_3), 2.18 (s, 6H, *p*-CH_3), 2.74 (d, 2H, CH_2), 4.05 (d, 2H, CH_2), 6.80 (s, 4H, C*H*), 6.97 (m, 1H, py-C*H*), 7.18 (m, 1H, py-C*H*), 7.47 (m, 1H, py-C*H*), 8.83 (m, 1H, py-*o*-C*H*). ^{13}C{^{1}H} NMR (125 MHz, C_6D_6, 295 K) δ 19.28 (s, *o*-*C*H$_3$), 21.31 (s, *p*-*C*H$_3$), 25.47 (s, *C*H$_3$), 36.5 (broad s, Zr-*C*H$_3$), 46.31 (s, *C*R$_4$), 66.13 (s, *C*H$_2$), 120.89 (s, Ar-*C*), 122.61 (s, Ar-*C*), 130.28 (s, Ar-*C*), 134.18 (s, Ar-*C*), 135.08 (s, Ar-*C*), 139.33 (s, Ar-*C*), 145.97 (s, Ar-*C*), 147.41 (s, Ar-*C*), 162.75 (s, Ar-*C*). ^{13}C{^{1}H} NMR (125 MHz, C_6D_5Br, 295 K) δ 19.92 (s, *o*-*C*H$_3$), 21.08 (s, *p*-*C*H$_3$), 25.33 (s, *C*H$_3$), 35.46 (s, Zr-*C*H$_3$), 36.65 (s, Zr-*C*H$_3$), 45.85 (s, *C*R$_4$), 65.42 (s, *C*H$_2$), 120.65 (s, Ar-*C*), 122.14 (s, Ar-*C*), 131.44 (s, Ar-*C*), 133.43 (s, Ar-*C*), 134.46 (s, Ar-*C*), 139.26 (s, Ar-*C*), 145.36 (s, Ar-*C*), 146.78 (s, Ar-*C*), 162.13 (s, Ar-*C*). Anal. Calcd for $C_{29}H_{39}N_3Zr$: C, 66.87; H, 7.55; N, 8.07. Found: C, 67.02; H, 7.46; N, 7.94.

[Li·OEt$_2$] [(MesNpy)ZrMe$_3$] (3). A suspension of [MesNpy]ZrMe$_2$ (0.092 g, 1.079 mmol) in diethyl ether (5 mL) was cooled to -30 ˚C. To the cold solution was added MeLi (4.4 M in diethyl ether, 0.126 mL, 1.76 mmol) and the mixture stirred at room temperature for 10 min. The resulting solution was filtered through Celite and the filtrate was dried *in vacuo* to yield [Li·OEt$_2$][(MesNpy)ZrMe$_3$] as a white powder. Yield: 0.109 g, 100%. White crystals suitable for a single crystal X-ray diffraction study were grown by slow crystallization from diethyl ether at -30 ˚C. ^{1}H NMR (500 MHz, C_6D_6, 295 K) δ -0.06 (s, 9H, Zr-CH_3), 1.00 (t, 6H, O-CH$_2$CH_3), 1.12 (s, 3H, CH_3), 1.78 (s, 6H, *o*-CH_3), 2.21 (s, 6H, *p*-CH_3), 2.94 (s, 6H, *o*-CH_3), 3.02 (d, 2H, CH_2), 3.16 (q, 4H, O-CH$_2$CH_3), 3.85 (d, 2H, CH_2), 6.64 (m, 1H, py-C*H*), 6.92 (s, 2H, C*H*), 7.02 (m, 1H, py-C*H*), 7.07 (s, 2H, C*H*), 7.10 (m, 1H, py-C*H*), 9.10 (m, 1H, py-*o*-C*H*). Anal. Calcd for $C_{37}H_{52}N_3LiOZr$: C, 66.19; H, 8.50; N, 6.81. Found: C, 66.26; H, 8.43; N, 6.89.

Activation of [MesNpy]ZrMe$_2$ with [Ph$_3$C][B(C$_6$F$_5$)$_4$]. Solutions of [MesNpy]ZrMe$_2$ (0.021 g, 0.040 mmol) and [Ph$_3$C][B(C$_6$F$_5$)$_4$] (0.037 g, 0.040 mmol), each in C$_6$D$_5$Br (0.6 mL) were prepared and cooled to -30 ˚C. The solutions were mixed while still cold and the resulting orange solution was transferred to an NMR tube. The following NMR data correspond to activated [MesNpy]Zr(^{13}Me)$_2$ which was obtained in an analogous process. ^{1}H NMR (500 MHz, C$_6$D$_5$Br, 295 K) δ 0.66 (d, J$_{CH}$ = 108 Hz, 3H, Zr-^{13}C*H*$_3$), 1.21 (s, 3H, C*H*$_3$), 1.22 (s, 6H, *o*-C*H*$_3$), 2.03 (d, J$_{CH}$ = 128 Hz, 3H, ^{13}C*H*$_3$Ph$_3$), 2.15 (s, 6H, *p*-C*H*$_3$), 2.29 (s, 6H, *o*-C*H*$_3$), 2.78 (d, 2H, C*H*$_2$), 3.67 (d, 2H, C*H*$_2$), 6.70 (s, 2H, C*H*), 6.80 (s, 2H, C*H*), some aryl peaks omitted here, 6.87 (m, 1H, py-C*H*), 7.51 (m, 1H, py-C*H*), 7.92 (m, 1H, py-*o*-C*H*). ^{13}C{^{1}H} NMR (125 MHz, C$_6$D$_5$Br, 295 K) δ 17.14 (s, *o*-*C*H$_3$), 18.10 (s, *o*-*C*H$_3$), 20.80 (s, *p*-*C*H$_3$), 23.81 (s, *C*H$_3$), 30.42 (s, ^{13}*C*H$_3$Ph$_3$), 38.81 (broad s, Zr-^{13}*C*H$_3$), 48.95 (s, *C*R$_4$), 67.40 (s, *C*H$_2$), some aryl peaks omitted here.

{[(MesNpy)ZrMe]$_2$Me}{B(C$_6$F$_5$)$_4$} (11). Solutions of [MesNpy]ZrMe$_2$ (0.205 g, 0.394 mmol) and [Ph$_3$C][B(C$_6$F$_5$)$_4$] (0.182 g, 0.197 mmol), each in C$_6$H$_5$Cl (1.5 mL) were prepared and cooled to -30 ˚C. The solutions were mixed while still cold and the resulting yellow solution was stirred at room temperature for 5 min. The solvent was removed *in vacuo* and the remaining residue triturated with pentane for 2 h. The resulting yellow powder was washed with pentane to remove Ph$_3$CMe and dried *in vacuo*. Yield: 0.233 g, 64%. Complex {[(MesNpy)Zr]$_2$(^{13}Me)$_3$}{B(C$_6$F$_5$)$_4$} was prepared in a similar fashion from [MesNpy]Zr(^{13}Me)$_2$. ^{1}H NMR (500 MHz, C$_6$D$_6$, 295 K) δ 0.74 (s, 4.5 H, Zr-C*H*$_3$), 0.86 (s, 3H, C*H*$_3$), 1.22 (s, 6H, *o*-C*H*$_3$), 2.14 (s, 6H, *p*-C*H*$_3$), 2.27 (s, 6H, *o*-C*H*$_3$), 2.65 (d, 2H, C*H*$_2$), 3.67 (d, 2H, C*H*$_2$), 6.67 (m, 1H, py-C*H*), 6.73 (s, 2H, C*H*), 6.78 (s, 2H, C*H*), 6.88 (m, 1H, py-C*H*), 7.18 (m, 1H, py-C*H*), 7.99 (m, 1H, py-*o*-C*H*). ^{1}H NMR (500 MHz, C$_6$D$_5$Br, 295 K) δ 0.66 (d, J$_{CH}$ = 108 Hz, H, Zr-^{13}C*H*$_3$), 1.21 (s, 3H, C*H*$_3$), 1.22 (s, 6H, *o*-C*H*$_3$), 2.15 (s, 6H, *p*-C*H*$_3$), 2.29 (s, 6H, *o*-C*H*$_3$), 2.78 (d, 2H, C*H*$_2$), 3.67 (d, 2H, C*H*$_2$), 6.70 (s, 2H, C*H*), 6.80 (s, 2H, C*H*), 6.87 (m, 1H, py-C*H*), 7.25 (m,

1H, py-C*H*), 7.51 (m, 1H, py-C*H*), 7.92 (m, 1H, py-*o*-C*H*). Anal. Calcd for $C_{93}H_{75}N_6Zr_2BF_{20}$: C, 60.38; H, 4.09; N, 4.54. Found: C, 60.46; H, 4.19; N, 4.59.

H_2[TripNpy]. A Schlenk flask was charged with $H_3CC(2\text{-}C_5H_4N)(CH_2NH_2)_2$ (5.16 g, 31.2 mmol), 1-bromo-2,4,6-triisopropylphenyl (17.25 g, 60.9 mmol), tris(dibenzylideneacetone) dipalladium(0) (0.429 g, 0.468 mmol), racemic-2,2'-diphenylphosphino-1,1'-binaphthyl (0.603 g, 0.968 mmol), sodium t-butoxide (9.06 g, 94.3 mmol) and toluene (400 mL). The reaction mixture was refluxed under a stream of N_2, and the reaction was judged complete after 8 d, with H_2[TripNpy] the only significant product in the reaction mixture. The solvent was removed *in vacuo* and the purple residue taken up in diethyl ether (100 mL). The solution was washed with H_2O (4 × 100 mL) and saturated NaCl (3 × 100 mL). The organic phase was dried over $MgSO_4$. Evaporation of the solvent yielded a red solid which was used without further purification. Yield: 14.4 g, 81%. ^{1}H NMR (500 MHz, $CDCl_3/C_6D_6$, 295 K) δ 1.13/1.23 (d, 12H, CH_3), 1.90/1.25 (d, 12H, CH_3), 1.23/1.30 (d, 12H, CH_3), 1.77/1.76 (s, 3H, CH_3), 2.83/2.84 (m, 2H, C*H*), 3.03/3.27 (d/m, 2H, CH_2), 3.14/3.42 (m, 4H, C*H*), 3.43/3.63 (d/m, 2H, CH_2), 3.26/3.67 (s/m, 2H, N*H*), 6.91/7.10 (s, 4H, C*H*), 7.22/6.68 (m, 1H, py-C*H*), 7.51/7.10 (m, 1H, py-C*H*), 7.70/7.10 (m, 1H, py-C*H*), 8.68/8.50 (m, 1H, py-o-C*H*). ^{13}C{^{1}H} NMR (125 MHz, C_6D_6, 295 K) δ 23.08 (s, *C*H_3), 24.80 (s, *C*H_3), 24.94 (s, *C*H_3), 28.18 (s, *C*H_3), 34.96 (s, *C*H), 35.15 (s, *C*H), 47.15 (s, *C*R_4), 61.55 (s, *C*H_2), 121.77 (s, Ar-*C*), 122.00 (s, Ar-*C*), 122.91 (s, Ar-*C*), 122.77 (s, Ar-*C*), 128.68 (s, Ar-*C*), 136.63 (s, Ar-*C*), 142.47 (s, Ar-*C*), 143.56 (s, Ar-*C*), 144.55 (s, Ar-*C*), 149.27 (s, Ar-*C*), 165.89 (s, Ar-*C*). HRMS (EI, 70 eV) *m/z* Calcd for $C_{39}H_{59}N_3$: 569.4704; found: 569.4708.

[TripNpy]Zr(NMe_2)$_2$ (6). Zr(NMe_2)$_4$ (2.53 g, 9.43 mmol) and H_2[TripNpy] (6.45 g, 11.3 mmol) were dissolved in pentane (80 mL). The reaction mixture was stirred at room temperature for 16 h, residual insoluble precipitate filtered, and the solution stirred at room temperature for a

further 16 h. The solvent was reduced to yield a white precipitate which was filtered and washed with small amounts of cold pentane. Yield: 1.5g, 60%. ^{1}H NMR (500 MHz, C_6D_6, 295 K) δ 0.67 (d, 6H, C*H*$_3$), 1.08 (s, 3H, C*H*$_3$), 1.28 (d, 12H, C*H*$_3$), 1.33 (d, 6H, C*H*$_3$), 1.57 (d, 6H, C*H*$_3$), 1.58 (d, 6H, C*H*$_3$), 2.86 (m, 4H, C*H*), 2.89 (s, 6H, N(C*H*$_3$)$_2$), 3.01 (d, 2H, C*H*$_2$), 3.04 (s, 6H, N(C*H*$_3$)$_2$), 4.08 (m, 2H, C*H*), 4.19 (d, 2H, C*H*$_2$), 6.69 (m, 1H, py-C*H*), 6.79 (m, 1H, py-C*H*), 7.05 (m, 1H, py-C*H*), 7.10 (d, 2H, C*H*), 7.25 (d, 2H, C*H*), 8.71 (m, 1H, py-*o*-C*H*). ^{13}C{^{1}H} NMR (125 MHz, C_6D_6, 295 K) δ 24.81 (s, *C*H$_3$), 24.89 (s, *C*H$_3$), 24.93 (s, *C*H$_3$), 25.50 (s, *C*H$_3$), 26.50 (s, *C*H$_3$), 27.80 (s, *C*H), 29.01 (s, *C*H), 29.71 (s, *C*H), 34.87 (s, *C*H$_3$), 43.29 (s, N(*C*H$_3$)$_2$), 45.04 (s, N(*C*H$_3$)$_2$), 47.75 (s, *C*R$_4$), 70.09 (s, *C*H$_2$), 120.65 (s, Ar-*C*), 121.55 (s, Ar-*C*), 122.08 (s, Ar-*C*), 122.75 (s, Ar-*C*), 128.04 (s, Ar-*C*), 139.00 (s, Ar-*C*), 144.28 (s, Ar-*C*), 144.33 (s, Ar-*C*), 146.00 (s, Ar-*C*), 149.09 (s, Ar-*C*). Anal. Calcd for $C_{43}H_{69}N_5Zr$: C, 69.02; H, 9.31; N, 9.43. Found: C, 69.02; H, 9.30; N, 9.43.

[TripNpy]ZrCl$_2$ (7). To a solution of [TripNpy]Zr(NMe$_2$)$_2$ (3.07 g, 4.11 mmol) in diethyl ether (80 mL) was added TMSCl (1.56 mL, 12.3 mmol) and the reaction mixture was stirred at room tempera*ture* for 4 h. The resulting white solid was filtered, washed with pentane (3 (10 mL) and dried in vacuo for 4 h. Yield: 2.8 g, 93%. δ 0.63 (d, 6H, C*H*$_3$), 0.93 (s, 3H, C*H*$_3$), 1.02 (br d, 6H, C*H*$_3$), 1.29 (d, 6H, C*H*$_3$), 1.32 (d, 6H, C*H*$_3$), 1.55 (d, 6H, C*H*$_3$), 1.87 (d, 6H, C*H*$_3$), 2.31 (br m, 2H, C*H*), 2.87 (m, 2H, C*H*), 3.06 (d, 2H, C*H*$_2$), 4.03 (d, 2H, C*H*$_2$), 4.33 (br m, 2H, C*H*), 6.68 (m, 1H, py-C*H*), 6.73 (m, 1H, py-C*H*), 6.93 (m, 1H, py-C*H*), 6.95 (s, 2H, C*H*), 7.25 (d, 2H, C*H*), 10.24 (m, 1H, py-*o*-C*H*).

[TripNpy]ZrMe$_2$ (8). A suspension of [TripNpy]ZrCl$_2$ (1.32 g, 1.81 mmol) in diethyl ether (20 mL) was cooled to -30 ˚C. To the cold solution was added MeMgBr (3.6 M in diethyl ether, 1.00 mL, 3.62 mmol) and the resulting mixture was stirred at room temperature for 30 min until the cloudy suspension became clear. Dioxane (0.39 mL, 4.5 mmol) was added to the

solution and the resulting white solid was filtered through Celite. The filtrate was reduced to *ca* 5 mL and stored at -30 ˚C for 1 d to yield [TripNpy]ZrMe$_2$ as clear, colorless crystals. Yield: 0.61 g, 49%. The ^{13}C-labeled complex, [TripNpy]Zr(^{13}Me)$_2$, was prepared in a similar manner with ^{13}MeMgI. ^{1}H NMR (500 MHz, C_6D_6, 295 K) δ 0.53 (s, 3H, Zr-CH_3), 0.61 (s, 3H, Zr-CH_3), 0.73 (d, 6H, CH_3), 0.95 (s, 3H, CH_3), 1.25 (d, 12H, CH_3), 1.40 (d, 6H, CH_3), 1.55 (d, 6H, CH_3), 1.65 (d, 6H, CH_3), 2.88 (m, 4H, C*H*), 2.89 (d, 2H, CH_2), 4.11 (d, 2H, CH_2), 4.18 (m, 2H, C*H*), 6.61 (m, 1H, py-C*H*), 6.75 (m, 1H, py-C*H*), 7.05 (m, 1H, py-C*H*), 7.12 (s, 2H, C*H*), 7.23 (s, 2H, C*H*), 8.90 (m, 1H, py-*o*-C*H*). ^{1}H NMR (500 MHz, C_6D_5Br, 295 K) δ 0.21 (s, 3H, Zr-CH_3), 0.33 (s, 3H, Zr-CH_3), 0.66 (d, 6H, CH_3), 1.21 (s, 3H, CH_3), 1.20 (d, 12H, CH_3), 1.26 (d, 6H, CH_3), 1.45 (d, 6H, CH_3), 1.50 (d, 6H, CH_3), 2.77 (m, 2H, C*H*), 2.83 (m, 2H, C*H*), 2.86 (d, 2H, CH_2), 4.00 (m, 2H, C*H*), 4.06 (d, 2H, CH_2), 7.00 (s, 2H, C*H*), 7.04 (m, 1H, py-C*H*), 7.13 (m, 1H, py-C*H*), 7.14 (s, 2H, C*H*), 7.45 (m, 1H, py-C*H*), 8.92 (m, 1H, py-*o*-C*H*). ^{13}C{^{1}H} NMR (125 MHz, C_6D_6, 295 K) δ 24.82 (s, *C*H$_3$), 25.16 (s, *C*H$_3$), 25.76 (s, *C*H$_3$), 25.93 (s, *C*H$_3$), 27.58 (s, *C*H$_3$), 28.96 (s, *C*H), 29.05 (s, *C*H), 34.86 (s, Zr-*C*H$_3$), 34.96 (s, *C*H$_3$), 39.71 (s, Zr-*C*H$_3$), 46.44 (s, *C*R$_4$), 69.67 (s, *C*H$_2$), 120.82 (s, Ar-*C*), 121.97 (s, Ar-*C*), 122.57 (s, Ar-*C*), 123.08 (s, Ar-*C*), 139.62 (s, Ar-*C*), 144.84 (s, Ar-*C*), 145.28 (s, Ar-*C*), 146.03 (s, Ar-*C*), 146.46 (s, Ar-*C*), 147.62 (s, Ar-*C*), 163.04 (s, Ar-*C*). Anal. Calcd for $C_{41}H_{63}N_3Zr$: C, 71.45; H, 9.21; N, 6.10. Found: C, 71.33; H, 9.22; N, 6.18.

Activation of [TripNpy]ZrMe$_2$ with [Ph$_3$C][B(C$_6$F$_5$)$_4$]. Solutions of [TripNpy]ZrMe$_2$ (0.0102 g, 0.0148 mmol) and [Ph$_3$C][B(C$_6$F$_5$)$_4$] (0.0139 g, 0.0151 mmol), each in C_6D_5Br (0.5 mL) were prepared and cooled to -30 ˚C. The solutions were mixed while still cold and the resulting orange solution was transferred to an NMR tube.

{[(TripNpy)ZrMe]$_2$Me}{B(C$_6$F$_5$)$_4$} (12). Solutions of [TripNpy]ZrMe$_2$ (0.290 g, 0.421 mmol) and [Ph$_3$C][B(C$_6$F$_5$)$_4$] (0.194 g, 0.210 mmol), each in C_6H_5Cl (1.5 mL) were prepared and

cooled to –30 ˚C. The solutions were mixed while still cold and the resulting yellow solution was stirred at room temperature for 5 min. The solvent was removed *in vacuo* and remaining residue triturated with pentane for 2 h. The resulting yellow powder was washed with pentane to remove Ph_3CMe and dried *in vacuo*. Yield: 0.320 g, 75%. Complex $\{[(TripNpy)Zr]_2(^{13}Me)_3\}\{B(C_6F_5)_4\}$ was prepared in a similar fashion from $[TripNpy]Zr(^{13}Me)_2$. ^{1}H NMR (500 MHz, C_6D_6, 295 K) δ 0.64 (d, 6H, C*H*$_3$), 0.81 (d, 6H, C*H*$_3$), 0.89 (s, 3H, C*H*$_3$), 1.02 (s, 4.5H, Zr-C*H*$_3$), 1.05 (d, 6H, C*H*$_3$), 1.26 (d, 6H, C*H*$_3$), 1.33 (d, 12H, C*H*$_3$), 1.67 (m, 2H, C*H*), 2.83 (m, 2H, C*H*), 3.00 (d, 2H, C*H*$_2$), 3.56 (m, 2H, C*H*), 3.73 (d, 2H, C*H*$_2$), 6.84 (m, 1H, py-C*H*), 6.85 (s, 2H, C*H*), 6.91 (m, 1H, py-C*H*), 6.93 (s, 2H, C*H*), 7.39 (m, 1H, py-C*H*), 8.59 (m, 1H, py-*o*-C*H*). Anal. Calcd for $C_{105}H_{123}N_6Zr_2BF_{20}$: C, 61.75; H, 6.07; N, 4.11. Found: C, 61.64; H, 6.18; N, 3.98.

[MesNpy]Hf(NMe$_2$)$_2$ (14). $Hf(NMe_2)_4$ (4.00 g, 11.0 mmol) and H_2[MesNpy] (4.75 g, 12.0 mmol) were dissolved in pentane (80 mL). The reaction mixture was stirred at room temperature for 16 h, filtered, and the solvent evaporated to yield yellow solid. Yield: 7.75 g, 95%. ^{1}H NMR (500 MHz, C_6D_6, 295 K) δ 1.02 (s, 3H, C*H*$_3$), 2.21 (s, 6H, *p*-C*H*$_3$), 2.33 (s, 12H, *o*-C*H*$_3$), 2.95 (d, 2H, C*H*$_2$), 3.02 (s, 6H, N(C*H*$_3$)$_2$), 3.06 (s, 6H, N(C*H*$_3$)$_2$), 4.18 (d, 2H, C*H*$_2$), 6.67 (m, 1H, py-C*H*), 6.83 (m, 1H, py-C*H*), 6.91 (s, 4H, C*H*), 7.04 (m, 1H, py-C*H*), 8.77 (m, 1H, py-*o*-C*H*). Anal. Calcd for $C_{31}H_{45}N_5Hf$: C, 55.89; H, 6.81; N, 10.51. Found: C, 55.96; H, 6.88; N, 10.40.

[MesNpy]HfCl$_2$ (15). To a solution of $[MesNpy]Hf(NMe_2)_2$ (7.75 g, 11.0 mmol) in diethyl ether (80 mL) was added TMSCl (4.35 mL, 34.0 mmol) and the reaction mixture was stirred at room temperature for 1 h. The resulting white solid was filtered, washed with pentane (3 × 10 mL) and dried *in vacuo* for 4 h. Yield: 6.82 g, 95%. ^{1}H NMR (500 MHz, C_6D_6, 295 K) δ 0.81 (s, 3H, C*H*$_3$), 1.59 (s, 6H, *o*-C*H*$_3$), 2.20 (s, 6H, *p*-C*H*$_3$), 2.97 (d, 2H, C*H*$_2$), 2.97 (s, 6H, *o*-

C*H*$_3$), 4.10 (d, 2H, C*H*$_2$), 6.65 (m, 1H, py-C*H*), 6.71 (s, 2H, C*H*), 6.89 (m, 1H, py-C*H*), 6.89 (m, 1H, py-C*H*), 6.94 (s, 2H, C*H*), 10.41 (m, 1H, py-*o*-C*H*). Anal. Calcd for $C_{27}H_{33}N_3Cl_2Hf$: C, 49.97; H, 5.13; N, 6.47; Cl, 10.93. Found: C, 49.90; H, 5.08; N, 6.42; Cl, 11.06.

[MesNpy]HfMe$_2$ (16). A suspension of [MesNpy]HfCl$_2$ (1.17 g, 1.80 mmol) in diethyl ether (50 mL) was cooled to –30 ˚C. To the cold solution was added MeMgBr (3.5 M in diethyl ether, 1.30 mL, 4.55 mmol) and the resulting mixture was stirred at room temperature for 1 h until the cloudy suspension became clear. Dioxane (0.50 mL, 5.87 mmol) was added to the solution and the resulting white solid was filtered through Celite. The filtrate was reduced to *ca* 5 mL and stored at –30 ˚C for 1 d to yield [MesNpy]HfMe$_2$ as clear, colorless crystals. Yield: 1.09 g, 64%. The ^{13}C-labeled complex, [MesNpy]Hf(^{13}Me)$_2$, was prepared in a similar manner with ^{13}MeMgI. ^{1}H NMR (500 MHz, C_6D_5Br, 295 K) δ 0.06 (s, 3H, Hf-C*H*$_3$), 0.14 (s, 3H, Hf-C*H*$_3$), 1.22 (s, 3H, C*H*$_3$), 2.16 (s, 6H, *p*-C*H*$_3$), 2.20 (s, 12H, *o*-C*H*$_3$), 2.86 (d, 2H, C*H*$_2$), 4.15 (d, 2H, C*H*$_2$), 6.81 (s, 4H, C*H*), 6.99 (m, 1H, py-C*H*), 7.18 (m, 1H, py-C*H*), 7.48 (m, 1H, py-C*H*), 8.91 (m, 1H, py-*o*-C*H*). ^{13}C{^{1}H} NMR (125 MHz, C_6D_5Br, 295 K) δ 18.72 (s, *o*-*C*H$_3$), 20.88 (s, *p*-*C*H$_3$), 24.91 (s, *C*H$_3$), 45.21 (s, Hf-*C*H$_3$), 45.85 (s, *C*R$_4$), 49.36 (s, Hf-*C*H$_3$), 64.98 (s, *C*H$_2$), 120.39 (s, Ar-*C*), some aryl signal omitted here, 134.81 (s, Ar-*C*), 139.15 (s, Ar-*C*). Anal. Calcd for $C_{29}H_{39}N_3Hf$: C, 57.28; H, 6.46; N, 6.91. Found: C, 57.21; H, 6.55; N, 6.84.

Activation of [MesNpy]HfMe$_2$ with [Ph$_3$C][B(C$_6$F$_5$)$_4$]. Solutions of [MesNpy]HfMe$_2$ (0.0102 g, 0.0168 mmol) and [Ph$_3$C][B(C$_6$F$_5$)$_4$] (0.0162 g, 0.0176 mmol), each in C_6D_5Br (0.5 mL) were prepared and cooled to –30 ˚C. The solutions were mixed while still cold and the resulting orange solution was transferred to an NMR tube.

{[(MesNpy)HfMe]$_2$Me}{MeB(C$_6$F$_5$)$_3$} (19). Solutions of [MesNpy]HfMe$_2$ (0.318 g, 0.523 mmol) in C_6H_5Cl (1.5 mL) and B(C$_6$F$_5$)$_3$ (0.139 g, 0.271 mmol) in toluene (1.5 mL) were

prepared and cooled to –30 ˚C. The solutions were mixed while still cold and the resulting clear, colorless solution was stirred at room temperature for 15 min. The solvent was removed *in vacuo* and the remaining white residue triturated with pentane for 2 h and dried *in vacuo*. Yield: 0.628 g, 69%. Complex {[(MesNpy)Hf]$_2$(^{13}Me)$_3$}{MeB(C_6F_5)$_3$} (**19***) was prepared in a similar fashion from [MesNpy]Hf(^{13}Me)$_2$ (**16***). ^{1}H NMR (500 MHz, C_6D_5Br, 295 K) δ 1.00 (s, 4.5 H, Zr-C*H*$_3$), 1.17 (s, 3H, B-C*H*$_3$), 1.18 (s, 3H, C*H*$_3$), 1.23 (s, 6H, *o*-C*H*$_3$), 2.17 (s, 6H, *o*-C*H*$_3$), 2.31 (s, 6H, *p*-C*H*$_3$), 2.90 (d, 2H, C*H*$_2$), 3.86 (d, 2H, C*H*$_2$), 6.72 (s, 2H, C*H*), 6.81 (s, 2H, C*H*), 6.92 (m, 1H, py-C*H*), 7.31 (m, 1H, py-C*H*), 7.52 (m, 1H, py-C*H*), 7.89 (m, 1H, py-*o*-C*H*). ^{13}C{^{1}H} NMR (125 MHz, C_6D_5Br, 233 K) δ 11.12 (broad s, B-^{13}*C*H$_3$), 32.52 (s, Hf-^{13}*C*H$_3$), 41.35 (s, Hf-^{13}*C*H$_3$). Anal. Calcd for $C_{76}H_{78}N_6Hf_2BF_{15}$: C, 52.82; H, 4.55; N, 4.86. Found: C, 52.67; H, 4.62; N, 4.73.

Chapter 2

Polymerization of 1-hexene with activated zirconium alkyl complexes: Elucidation of a dramatic alkyl initiator effect

2.1 Introduction

Activation of dialkyl complexes of group IV metals with an appropriate activator yields a cationic species which can undergo alkene coordination followed by insertion in the metal alkyl.[62] In the majority of reported systems, this alkyl group is methyl (Me), although examples of catalysts bearing a variety of other alkyl groups have been studied.[52]

There have been reports of the initiator alkyl groups having a significant effect on the polymerization process. Fink *et al.* have shown that the rate of monomer insertion into a metal-alkyl bond (alkyl ≠ Me) can be up to 100 times faster than insertion into a metal-Me bond.[63-66] Bochmann *et al.* have reported that the use of $Al(i\text{-}Bu)_3$ as a co-catalyst with L_2ZrMe_2 systems (L_2 = Cp_2, *rac*-$Me_2Si(Ind)_2$) has beneficial effects due to alkyl exchange with the co-catalyst to yield Zr-(i-Bu) species.[67] In this case, the bulkier alkyl group is thought to prevent the formation of catalytically dormant aluminum adducts, and thereby increase catalyst efficiency. Marks *et al.* have also reported significant Zr-alkyl effects on ion pair formation thermodynamics.[68]

Schrock *et al.* have reported a number of group IV complexes bearing different alkyl groups;[5,28-30,35,36,39,69] however, extensive comparative studies on the effects of alkyl groups on olefin polymerization have not been reported.

In Chapter 2 polymerization of 1-hexene with activated dialkyl complexes $[MesNpy]ZrR_2$ (R = Me, Bn, Np, i-Bu) is discussed and a significant alkyl initiator effect presented.[26] The polymerization processes discussed in this chapter have been treated based on simple first order kinetics.[70] The polymerization is presumed to occur *via* elementary steps, eq 2.1 and 2.2, where C(S) is the solvated cation, C is the active cationic species, S is the coordinating solvent or anion in solution, M is 1-hexene, and C(M) is the first propagating species.

$$\mathbf{C(S)} \underset{k_{-1}}{\overset{k_1}{\rightleftharpoons}} \mathbf{C + S} \qquad (2.1)$$

$$C + M \xrightarrow{k} C(M) \qquad (2.2)$$

The rates of consumption of M and production of C can be expressed by eq 2.3 and 2.4.

$$\frac{-d[M]}{dt} = k_2[C][M] \tag{2.3}$$

$$\frac{d[C]}{dt} = k_1[C(S)] - k_{-1}[C][S] - k_2[C][M]. \tag{2.4}$$

A steady state approximation, *i.e.* $\frac{d[C]}{dt} = 0$, yields eq 2.5.

$$[C] = \frac{k_1[C(S)]}{k_{-1}[S] + k_2[M]} \tag{2.5}$$

If the dimethyl complex has an open coordination sphere and binds coordinating solvents readily one can argue that the cation has a similar or greater affinity for such solvent molecules. If the majority of the total concentration of zirconium in the system, C_{total}, is in the form of C(S), *i.e.* $C_{total} \approx C(S)$, and $k_{-1}[S] >> k_2[M]$, then eq 2.5 reduces to eq 2.6.

$$[C] = \frac{k_1[C_{total}]}{k_{-1}[S]} = \frac{K_{eq}[C_{total}]}{[S]} \tag{2.6}$$

Inserting eq 2.6 into eq 2.3 gives

$$\frac{-d[M]}{dt} = \frac{k_2 K_{eq}[C_{total}]}{[S]}[M] = k_{obs}[M] \tag{2.7}$$

where $$k_{obs} = \frac{k_2 K_{eq}[C_{total}]}{[S]}. \tag{2.8}$$

Integrating eq 2.7 gives

$$\ln[M] = \ln[M_\circ] - k_{obs}t \tag{2.9}$$

and k_{obs} (in units of s^{-1}) can be extracted from a plot of ln[M] vs. t. Using these rates, the Eyring equation (eq 2.10) can be used to determine the free energy of activation, $\Delta G^{\ddagger}$, for a kinetic process.

$$k_{obs} = \frac{k_\beta T}{h} e^{\frac{-\Delta G^{\ddagger}}{RT}} \tag{2.10}$$

Rearrangement of eq 2.10 yields eq 2.11 from which the entropy and enthalpy of activation, $\Delta S^{\ddagger}$ and $\Delta H^{\ddagger}$, can be derived by plotting $\ln(k_{obs}/T)$ vs. 1/T.

$$\ln\left(\frac{k_{obs}}{T}\right) = \ln\left(\frac{k_{\beta}}{h}\right) + \frac{\Delta S^{\ddagger}}{R} - \frac{\Delta H^{\ddagger}}{RT} \qquad (2.11)$$

2.2 1-Hexene polymerization by activated [ArNpy]ZrMe$_2$

As illustrated in Chapter 1, when a dimethyl species of the type [ArNpy]ZrMe$_2$ (Ar = Mes, Trip) reacts with an activator, a stable dinuclear monocation, {[(ArNpy)Zr]$_2$Me$_3$}, forms (eq 2.11).

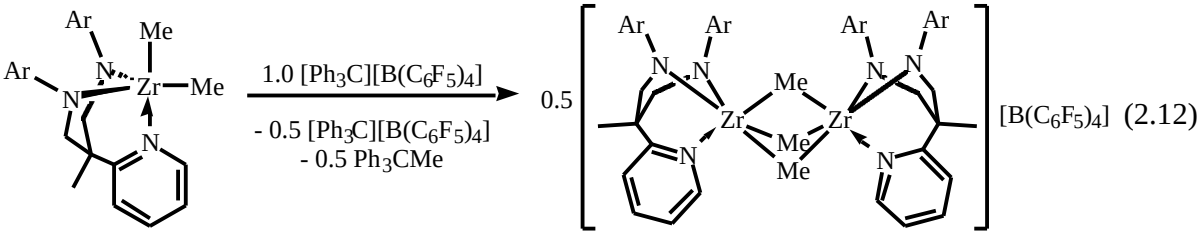

(2.12)

Double labeling experiments in Chapter 1 showed that this dinuclear species is capable of methyl group exchange with a neutral dimethyl complex (Scheme 1.10), however this exchange is very slow, even at 40 ˚C. It was possible to isolate the dinuclear complex and demonstrate that it has very limited reactivity with dimethyl complexes, [Ph$_3$C][B(C$_6$F$_5$)$_4$], and 1-hexene at room temperature. Chapter 2 discusses 1-hexene polymerization by activated [ArNpy]ZrMe$_2$ complexes.

Activation of [MesNpy]ZrMe$_2$ with 1 equiv [Ph$_3$C][B(C$_6$F$_5$)$_4$]. [MesNpy]ZrMe$_2$ (**1**) was activated with 1 equiv of [Ph$_3$C][B(C$_6$F$_5$)$_4$] to yield the dinuclear monocation {[(MesNpy)Zr]$_2$Me$_3$}{B(C$_6$F$_5$)$_4$} (**11**) which, when isolated by using only 0.5 equiv of

$[Ph_3C][B(C_6F_5)_4]$, was shown to be unreactive towards 1-hexene. Complex **11** is presumably generated by methyl abstraction from **1** to yield a mononuclear cation, $[(MesNpy)ZrMe][B(C_6F_5)_4]$ (**9**), which is then captured by a molecule of the dimethyl complex. As the following kinetics studies will show, some of **9** is not trapped by **1** and is therefore available to act as an initiator in polymerization reactions.

Rates of olefin consumption in reactions with up to 200 equiv 1-hexene were determined by monitoring the decrease in 1-hexene concentration with respect to an internal standard using ^{1}H NMR spectroscopy (eq 2.12).

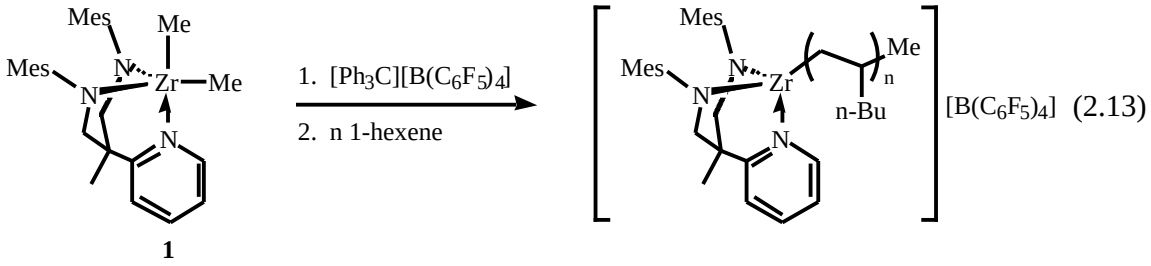

(2.13)

In one experiment, 160 equiv 1-hexene was added to a solution of $[MesNpy]ZrMe_2$ (**1**) activated with 1 equiv $[Ph_3C][B(C_6F_5)_4]$. The plot of ln(1-hexene) vs. time for the consumption of 1-hexene at 25 ˚C is presented in Figure 2.1. This plot is curved for the first 100 min, but becomes essentially linear as polymerization continues. Assuming that polymerization progresses according to first order kinetics with respect to monomer, the observed rate constant for olefin consumption, k_{obs}, can be obtained if only the linear part of this plot is considered. ^{1}H and ^{13}C NMR spectra (25 ˚C, C_6D_5Br) indicate that after all the olefin is consumed, approximately 50% of the unreacted cation remains in solution. The non-linearity in the early part of the plot may be attributed to a slow initiation process that is able to compete with chain growth in the early stages of polymerization.

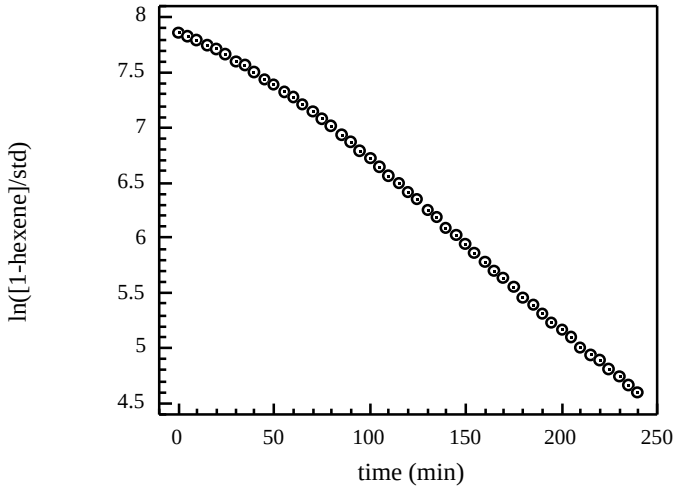

Figure 2.1. Plot of ln[1-hexene/Ph_2CH_2] vs. time (min) for addition of 160 equiv of 1-hexene to **1** (0.007 M) activated with 1 equiv $[Ph_3C][B(C_6F_5)_4]$ (25 ˚C, C_6D_5Br).

Variable temperature ^1H NMR studies in C_6D_5Br showed that the catalyst generated by activation of **1** with 1 equiv $[Ph_3C][B(C_6F_5)_4]$ was stable up to 40 ˚C for at least 1 h. Observed rate constants were obtained at 21, 25, 30 and 40 ˚C in different experiments with approximately 80 equiv of 1-hexene (Figure 2.2).

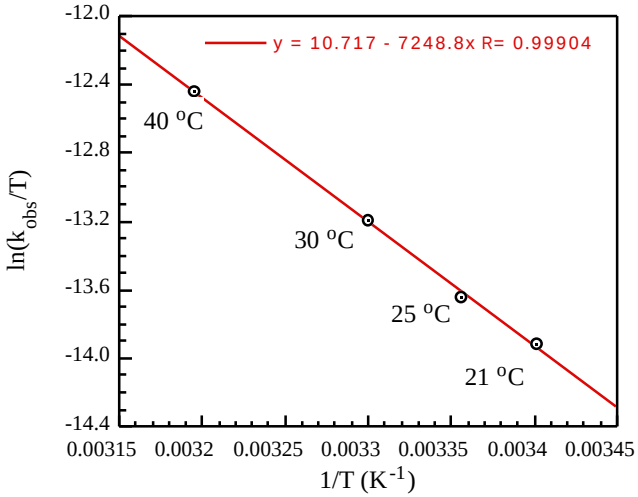

T (K)	k_{obs} (min^{-1})	$[Zr]_o$ (M)
294	0.0159(2)	0.0110
298	0.0211(4)	0.0099
303	0.0340(6)	0.0099
313	0.0742(17)	0.0099

Figure 2.2. Eyring plot for consumption of 1-hexene with an activated solution of **1**.

The Eyring plot for these limited data was linear and led to $\Delta H^{\ddagger}$ and $\Delta S^{\ddagger}$ values of 14.40(49) kcal/mol and –23.1(19) cal/(mol K) (60.3(19) kJ mol^{-1} and –108(4) J mol^{-1} K^{-1}), respectively.

To determine the stability of the active species, 80 equiv of 1-hexene were added to a sample of catalyst and the consumption of olefin was monitored at 25 ˚C. After all the olefin was consumed, a further 80 equiv 1-hexene was added to the solution and the polymerization process was again monitored. The observed rate constant (k_{obs}) values were 0.016(1) min^{-1} (2.7(2) × 10^{-4} s^{-1}) and 0.018(1) min^{-1} (3.0(2) × 10^{-4} s^{-1}) for the first and second additions respectively (Figure 2.3). This showed the propagating species to be stable and active in the absence of monomer; the activity of the catalyst system did not diminish over a 7 h period.

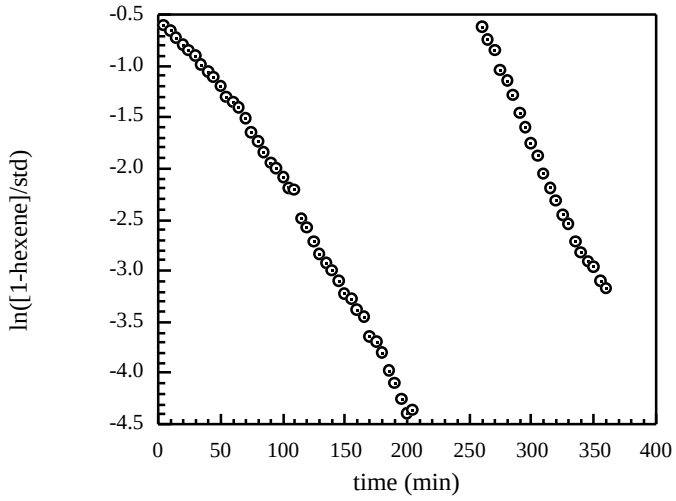

Figure 2.3. Plot of ln[1-hexene] vs. time (min) for two consecutive additions of 80 equiv of 1-hexene to **1** (0.01 M) activated with 1 equiv $[Ph_3C][B(C_6F_5)_4]$ (25 ˚C, C_6D_5Br).

No significant initiation period was observed for the second addition, which may have contributed to the slightly greater observed rate of olefin consumption. A significant amount of **11** was observed by ^1H NMR spectroscopy after both additions.

^{13}C-labeling studies. It was possible to observe the insertion of 1-hexene into the Zr-CH_3 bond of the catalyst by treating a solution of [MesNpy]Zr(^{13}Me)$_2$ (**1***) (0.01 M) activated with 1 equiv [Ph_3C][$B(C_6F_5)_4$] with only 2 equiv of 1-hexene and tracking the olefin by ^{1}H and ^{13}C{^{1}H} NMR spectroscopy (20 ˚C, C_6D_5Br). No appreciable amount of polymer was evident after 90 min; however, after 24 h signals for poly(1-hexene) were observed in the ^{1}H NMR spectrum. The ^{13}C{^{1}H} NMR spectrum showed a peak at 21 ppm as a result of multiple insertion products, as well as peaks corresponding to the unreacted cation and the by-product, Ph_3CMe (Figure 2.4).

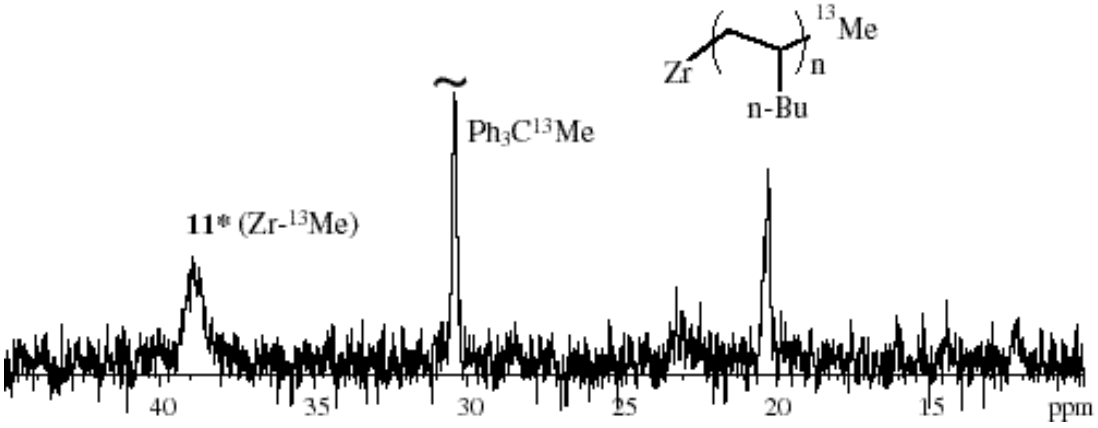

Figure 2.4. ^{13}C{^{1}H} NMR spectrum (20 ˚C, C_6D_5Br, *C*H_3 signals) of **1** activated with 1 equiv [Ph_3C][$B(C_6F_5)_4$] after addition of 2 equiv of 1-hexene.

Activation of [MesNpy]ZrMe$_2$ with 0.5 equiv of [Ph_3C][$B(C_6F_5)_4$]. Activation of [MesNpy]$ZrMe_2$ (**1**) with 0.5 equiv of [Ph_3C][$B(C_6F_5)_4$] yields the dinuclear monocation, {[(MesNpy)Zr]$_2Me_3$}{$B(C_6F_5)_4$} (**11**). The ^{1}H NMR (25 ˚C, C_6D_5Br) resonances are completely analogous to those of a solution of **1** activated with 1 equiv of [Ph_3C][$B(C_6F_5)_4$]. Addition of 43 equiv of 1-hexene to a solution of **11** at room temperature leads to polymer formation; however, there is a substantial initiation period followed by slow first order consumption of monomer (Figure 2.5). The polymerization was followed over less than one half-life, with a k_{obs} = 0.0035(1) min^{-1} (5.8(2) × 10^{-5} s^{-1}) for these limited data. Not all of the olefin was consumed even

after 24 h at room temperature. Activation of **1** with only 0.4 equiv of $[Ph_3C][B(C_6F_5)_4]$ led to the formation of a species that is inactive as a catalyst for the polymerization of 1-hexene under the same conditions.

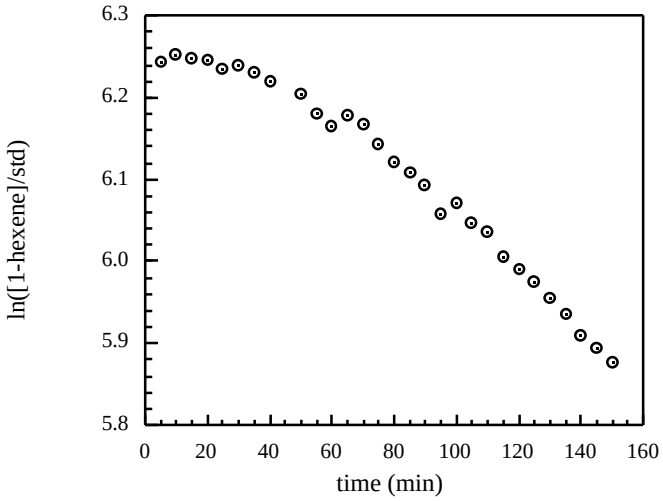

Figure 2.5. Plot of ln[1-hexene/std] vs. time after addition of 43 equiv of 1-hexene to **11**.

As discussed in Chapter 1, and as the above experiments show, $\{[(MesNpy)Zr]_2Me_3\}\{[B(C_6F_5)_4\}$ (**11**) is unreactive towards 1-hexene. The active catalyst must be the mononuclear cation $[(MesNpy)ZrMe][B(C_6F_5)_4]$ (**9**) (Scheme 2.1).

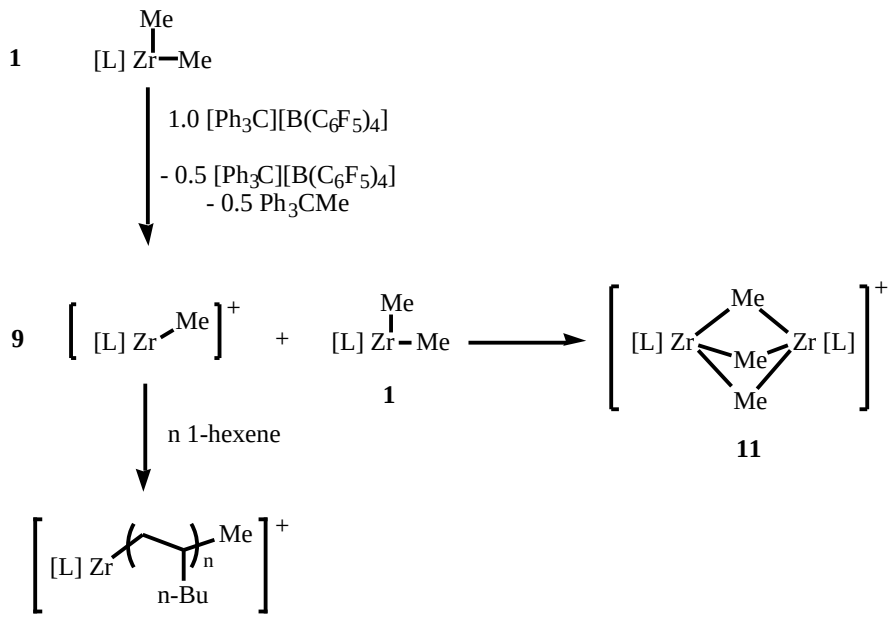

Scheme 2.1. Polymerization of 1-hexene in the activated [MesNpy]$ZrMe_2$ system. L = $[MesNpy]^{2-}$, anion = $[B(C_6F_5)_4]^-$.

It should be noted that in all the kinetics studies carried out with activated solutions of **1**, signals for **11** are always detected after the complete consumption of olefin, which indicates that only a small fraction of metal centers catalyzes polymerization. Bulk polymerization results obtained for this system support this assertion. Polymer samples obtained from a solution of **1** activated with 1 equiv $[Ph_3C][B(C_6F_5)_4]$ at 25 ˚C have M_n values that are approximately ten times greater than expected (Table 2.1), thus only ~10% of the catalyst is active for polymerization.

Table 2.1. Polymer characteristics for [MesNpy]$ZrMe_2$ (**1**) at 25 ˚C.

[MesNpy]$ZrMe_2$ (M)	Equiv of 1–hexene	Expected M_n	Observed M_n	PDI
0.012	63	5300	60000	1.02
0.010	77	6480	65000	1.07

Equiv 1-hexene are calculated in excess of [Zr].

In order to determine the effect of increased ligand steric bulk on the polymerization rate, [TripNpy]$ZrMe_2$ (**8**) was investigated. Activation of **8** (0.01 M) with 1 equiv of $[Ph_3C][B(C_6F_5)_4]$ at 25 ˚C also led to a dinuclear cation, $\{[(TripNpy)Zr]_2Me_3\}\{B(C_6F_5)_4\}$ (**12**), along with Ph_3CMe. Addition of 61 equiv of 1-hexene to this solution led to first order consumption of 1-hexene to yield k_{obs} = 0.025(1) min^{-1}, a rate higher than that obtained with activated **1** (k_{obs} = 0.016(1) min^{-1}). Excess cation was observed after consumption of all the 1-hexene. A polymer sample generated by addition of 187 equiv 1-hexene to a solution of **8** activated with 1 equiv of $[Ph_3C][B(C_6F_5)_4]$ (25 ˚C, C_6H_5Cl) had a PDI value of 1.2 and an M_n value of 94000, six times greater than the expected molecular weight.

These preliminary results showed that, as in the case of **1**, only a fraction of the catalyst was utilized in the polymerization process. The dinuclear species **12** is unreactive towards 1-hexene and the increased steric bulk of the [TripNpy] ligand did not have a significant effect on the polymerization rate. Further studies with this system are required.

2.3 2,1-Insertion of 1-hexene into activated [MesNpy]$ZrMe_2$

In the early stages of polymerization with the [MesNpy]$ZrMe_2$ (**1**) system, two sets of weak resonances appear in the olefinic region of the ^1H NMR spectra (between 5.3 and 5.5 ppm) and integrate to about 4% of the expected catalyst concentration in solution. These signals have been attributed to β-hydride elimination products. The rate of appearance of these olefins was monitored with respect to an internal standard, C_6Me_6 (Figure 2.6).

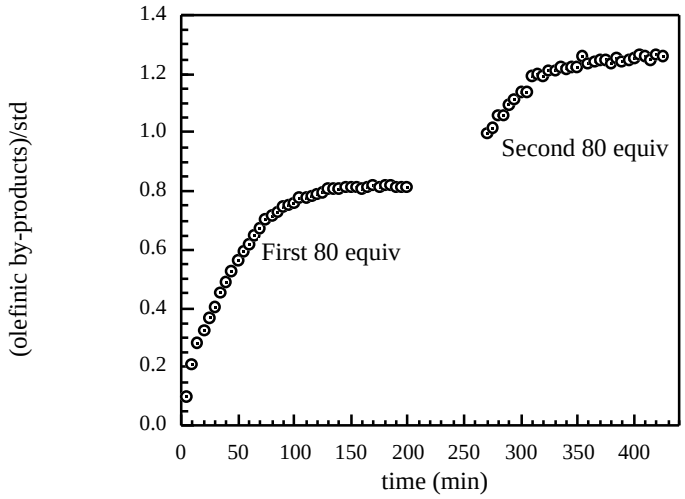

Figure 2.6. Plot of [olefinic by-products]/C_6Me_6 vs. time (min) for two consecutive additions of 80 equiv of 1-hexene to **1** (0.01 M) activated with 1 equiv $[Ph_3C][B(C_6F_5)_4]$ (25 ˚C, C_6D_5Br).

The rate of formation of by-products is greatest at the early stages of polymerization and decreases after the initiation period. No increase in the elimination products was observed after the 1-hexene was fully consumed. A similar pattern was observed after a second addition of 80 equiv of 1-hexene.

One possible explanation for the formation of these olefins is 2,1-insertion of 1-hexene into the Zr-CH_3 bond of $[(MesNpy)ZrMe][B(C_6F_5)_4]$ (**9**) in the early stages of polymerization. This results in the formation of an unstable secondary alkyl cation which can β-hydride eliminate to yield internal heptenes. The ^1H NMR spectra of reaction mixtures containing these by-products show a splitting pattern similar to that of a mixture of *cis* and *trans* 2-heptene (Figure 2.7). Scheme 2.2 is a summary of the possible pathways for olefin insertion into **9**. 3-Heptenes were not observed, possibly due to more favorable rotation around the less hindered bond as shown in Scheme 2.2.

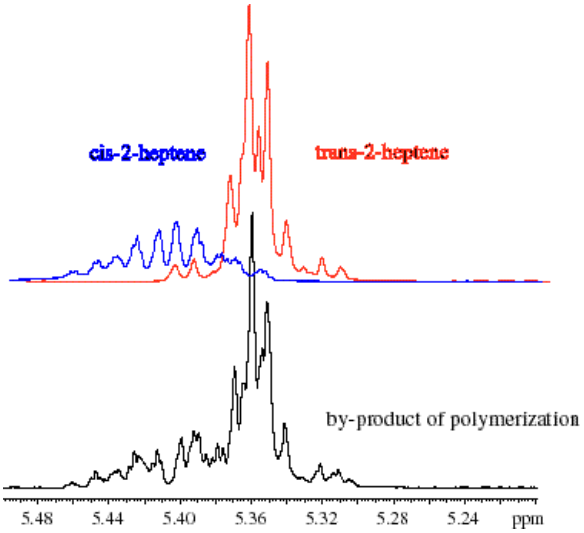

Figure 2.7. ^{1}H NMR spectra of the olefinic by-products of 1-hexene polymerization by activated **1**.

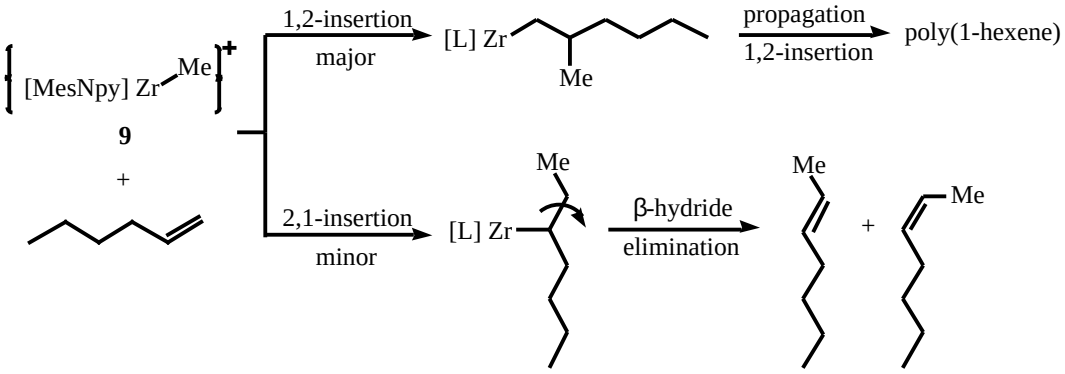

Scheme 2.2. Possible origin of 2-heptenes. L = $[MesNpy]^{2-}$, anion = $[B(C_6F_5)_4]^-$.

Activated dimethyl systems are inefficient catalysts for living 1-hexene polymerization. Formation of unreactive dinuclear complexes drastically decreases the concentration of active catalyst centers in solution and results in polymer samples with molecular weights significantly higher than expected. The open nature of the active catalyst, [(MesNpy)ZrMe][$B(C_6F_5)_4$] (**9**), allows 2,1-insertion of 1-hexene, leading to a secondary alkyl cation which is significantly less

stable than a primary alkyl cation. The 2,1-insertion product then β-hydride eliminates and leads to catalyst decomposition. The rest of this chapter is devoted to exploration of other dialkyl complexes in an effort to solve the previous problems encountered in the methyl systems.

2.4 Synthesis and activation of [MesNpy]ZrBn$_2$

The dibenzyl compound, [MesNpy]ZrBn$_2$ (**20**), was quite robust and easy to isolate in 83% yield. The ^{1}H NMR (21 ˚C, C_6D_6) spectrum of **20** showed one broad resonance at 2.5 ppm corresponding to the four Zr-C*H*$_2$ protons of the two benzyl groups. Similar fluxionality has been observed with the benzyl groups of other dibenzyl complexes.[71] At –40 ˚C in $C_6D_5CD_3$, the peak at 2.5 ppm splits into two separate resonances for two distinct sets of Zr-C*H*$_2$ protons at 2.92 and 3.44 ppm, respectively.

Activation of **20** with [Ph_3C][$B(C_6F_5)_4$] proceeds smoothly to yield the benzyl cation [(MesNpy)ZrBn][$B(C_6F_5)_4$] (**21**) (eq 2.13).

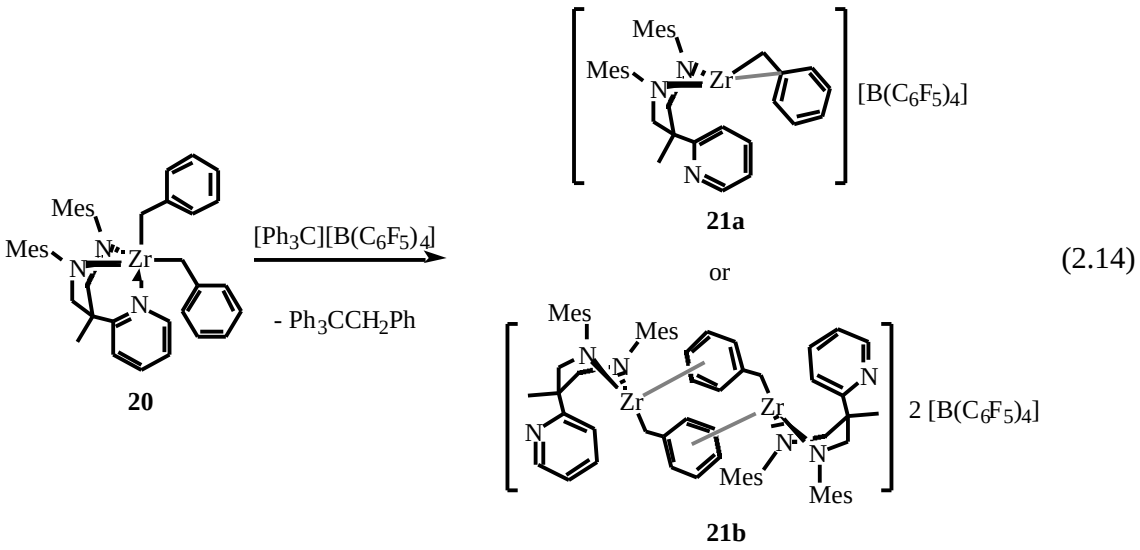

(2.14)

The ^{1}H NMR spectrum (25 ˚C, C_6D_5Br) of **21** shows two sharp resonances at 2.53 and 2.84 ppm

corresponding to the Zr-CH_2 and Ph_3CCH_2Ph groups, respectively.

An unusual feature of the ^{1}H NMR spectrum of **21** is the *ortho* pyridyl proton. In all other isolated dialkyl complexes as well as cations bearing [ArNpy] ligands, the *ortho* pyridyl peak is the most downfield signal in the spectrum. In **21** this resonance is shifted to 7.55 ppm, upfield of the resonance for the *meta* pyridyl proton. This upfield shift indicates that the pyridine ring is not coordinated to the metal, since similar observations have been made by Gade *et al.*[40]

A ^{1}H ROESY experiment carried out at –25 ˚C shows NOE cross peaks between the ligand CH_3 signal and the *ortho* and one *meta* proton of the pyridyl ring. This suggests that the pyridyl ring is not coordinated and freely rotates (Figure 2.8). No correlation is observed between Zr-CH_2 and the *ortho* pyridyl proton signals. In similar studies carried out in the activated [MesNpy]ZrMe_2 system where the pyridine ring is coordinated, no interaction between the ligand CH_3 protons and the *ortho* or *meta* pyridyl protons is observed.

Two possible structures for **21** are proposed in eq 2.13. One structure, **21a**, involves the interaction of the benzyl group aromatic ring with the metal center. The signal for the *ortho* benzyl protons is shifted upfield to 6.09 ppm, pointing towards a strong interaction of the aryl ring with the metal center. However, the intermolecular interaction of two cations to yield **21b**, cannot be ruled out.

Compound **21** catalyzes the polymerization of 1-hexene at 25 ˚C, however the rate of polymerization was very slow compared to other systems, and only a small amount of polymer was observed after 90 min at 25 ˚C. A reliable rate constant was not obtained and this compound was not further investigated.

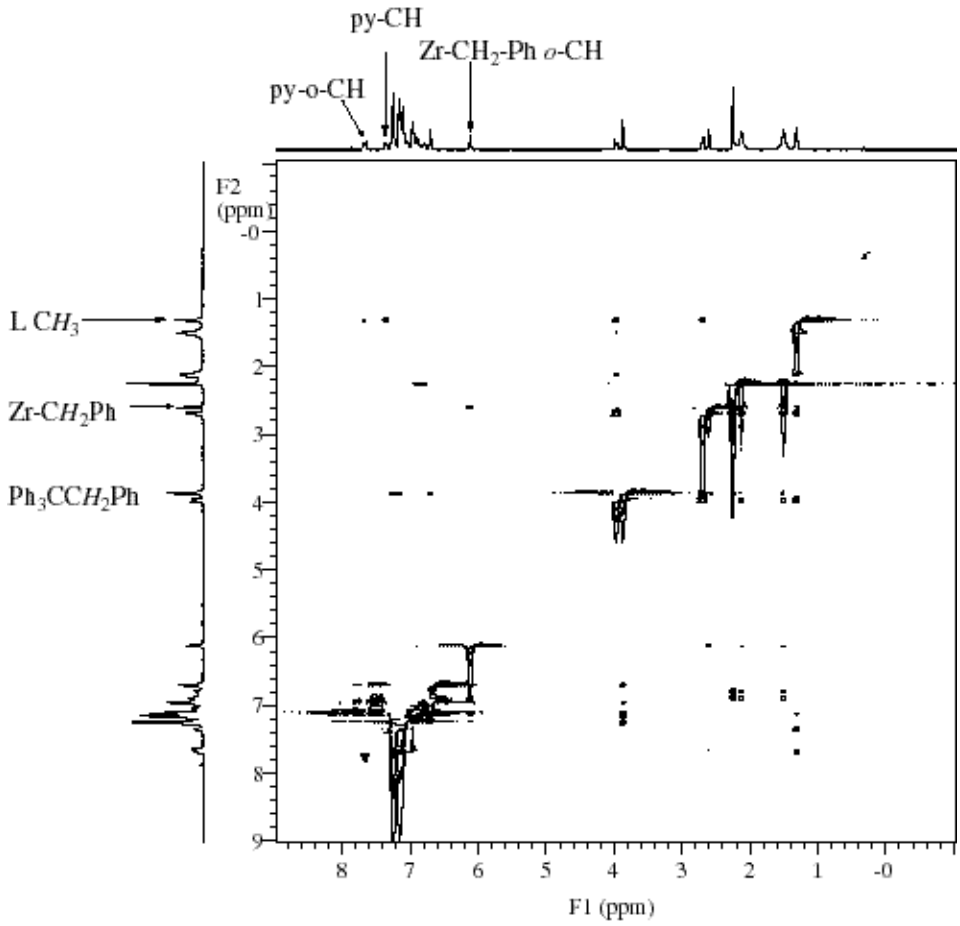

Figure 2.8. ^{1}H ROESY (500 MHz, 300 ms mixing time, C_6D_5Br, –25 ˚C) of the reaction of **20** and 1.1 equiv of $[Ph_3C][B(C_6F_5)_4]$ leading to **21**. Only NOE cross peaks are included.

2.5 Synthesis and activation of [MesNpy]ZrNp$_2$

In order to isolate a more stable and reactive catalyst, one without β-hydrogens, [MesNpy]ZrNp$_2$ (**22**) was synthesized and activated. Complex **22** was readily isolated from the reaction of [MesNpy]ZrCl$_2$ with 2 equiv of neopentyllithium. Similar reactions with neopentyl magnesium chloride were unsuccessful. The ^{1}H NMR spectrum (20 ˚C, C_6D_6) of **22** showed two resonances for the t-butyl protons at 1.10 and 1.36 ppm, and another set of signals for the Zr-CH_2 groups at 1.27 and 1.46 ppm.

Treatment of **22** with 1 equiv of $[Ph_3C][B(C_6F_5)_4]$ led to the generation of a yellow solution containing $[(MesNpy)ZrNp][B(C_6F_5)_4]$ (**23**) (eq 2.14).

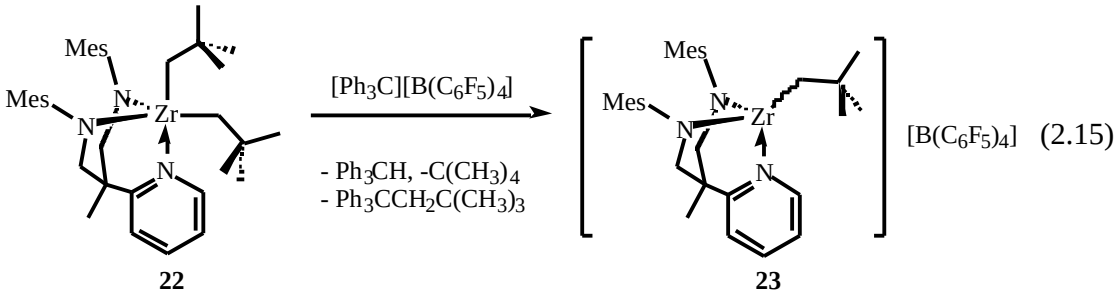

22 **23** (2.15)

The major by-products in this reaction are $Ph_3CCH_2C(CH_3)_3$ (77%), Ph_3CH (23%) and neopentane. The ^1H NMR spectrum (–25 ˚C, C_6D_5Br) of **23** showed only one zirconium-neopentyl group with signals at 0.64 and 0.96 ppm for the t-butyl and methylene protons, respectively. ^1H NMR studies showed **23** to decompose at 0 ˚C to yield a second major species as well as neopentane. The nature of the second species has not been determined.

One possibility encountered in other diamidoamine systems is C-H activation of the mesityl rings leading to an aryl bridged dinuclear dication, analogous to one determined by Schrodi.[5] This is not likely because the resulting species shows signals for a structure with C_s symmetry as evidenced by equivalent signals for the backbone methylene groups. If the temperature is increased to 25 ˚C, the sample decomposes completely and the only distinguishable signals are those for the above-mentioned organic by-products.

Addition of 89 equiv of 1-hexene to a 9 mM solution of **23** (0 ˚C, C_6D_5Br) led to first order consumption of olefin to yield poly(1-hexene) with a k_p value of 8.0(2) M^{-1} min^{-1} (0.133(4) M^{-1} s^{-1}). This value is higher than the rate obtained for the $[(MesNpy)Zr(i\text{-}Bu)][B(C_6F_5)_4]$ (**25**) system, 4.8(1) M^{-1} min^{-1} (0.079(2) M^{-1} s^{-1}) (*vide infra*). The $[(MesNpy)ZrNp][B(C_6F_5)_4]$ (**23**) system has solved the problem of catalyst activity encountered in the dibenzyl system, however the activation and decomposition processes are not well understood.

2.6 Polymerization of 1-hexene with activated [MesNpy]Zr(i-Bu)$_2$

Polymerization studies carried out in the Schrock group have thus far involved mainly dimethyl zirconium compounds of diamido-donor ligands. However, diisobutyl derivatives of some ligand systems have also been prepared and activated.[29,30,36,37,39,69] Reaction of [MesNpy]ZrCl$_2$ with 2 equiv (i-Bu)MgBr results in the formation of [MesNpy]Zr(i-Bu)$_2$ (**24**) in 92% yield. Complex **24** is thermally unstable and starts to decompose in solution or in the solid state at room temperature after several hours. The ^{1}H and ^{13}C{^{1}H} NMR spectra (–20 ˚C, C_6D_5Br) show signals for the Zr-CH_2 protons at 1.04 ppm, and the carbons at 72.6 and 74.2 ppm, respectively.

Activation of **24** with 1 equiv of [Ph_3C][$B(C_6F_5)_4$] (–20 ˚C, C_6D_5Br) resulted in the quantitative generation of [(MesNpy)Zr(i-Bu)][$B(C_6F_5)_4$] (**25**) (eq 2.15).

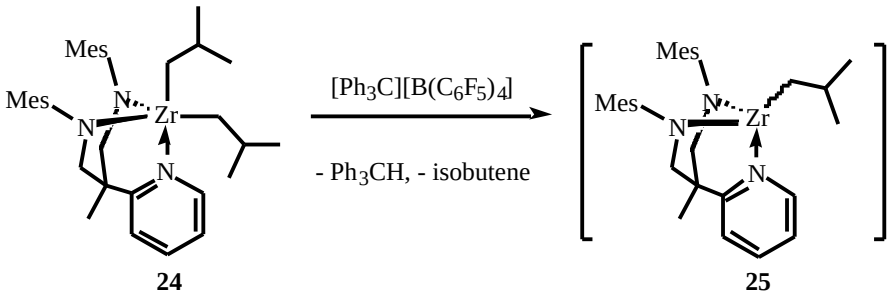

24 **25** (2.16)

The ^{1}H and ^{13}C{^{1}H} NMR spectra (–30 ˚C, C_6D_5Br) of **25** show only one set of peaks corresponding to the Zr-CH_2 group protons and carbon at 0.62 and 83.3 ppm, respectively. The sample begins to decompose irreversibly at 0 ˚C, possibly as a result of β-hydride elimination. At 30 ˚C the sample exhibits signals indicative of at least three distinct species.

Decomposition of **25** was followed by ^{1}H NMR spectroscopy (0 ˚C, C_6D_5Br) with respect to an internal standard, Ph_2CH_2.

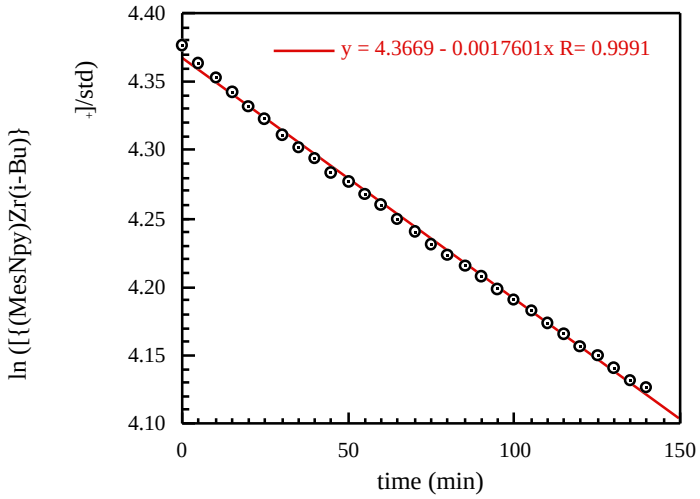

Figure 2.9. Plot of ln([**25**]/Ph_2CH_2) vs. time (0 ˚C, C_6D_5Br).

Complex **25** decomposed in a first order manner with a k_{obs} value of 0.00176(2) min^{-1} (2.93(8) × 10^{-5} s^{-1}) and $t_{1/2}$ of 390 min. As the decomposition progressed, the concentration of isobutene in solution increased, but then decreased as it was polymerized by a slight excess of $[Ph_3C][B(C_6F_5)_4]$. The decomposition process likely proceeded *via* β-hydride elimination to yield isobutene and a zirconium hydride species which did not participate in the polymerization process. The rate of polymerization of 1-hexene by **25** at 0 ˚C is 4.8(1) M^{-1} min^{-1} (0.079(2) M^{-1} s^{-1}).

Addition of 100 equiv of 1-hexene to **25** in C_6D_5Br at room temperature resulted in an exothermic reaction and complete conversion of monomer within less than 5 min. Repeating the procedure at lower temperatures allowed kinetics studies of polymerization. Unlike polymerizations catalyzed by activated $[MesNpy]ZrMe_2$, no significant initiation period was observed for those catalyzed by **25** and plots of ln[1-hexene] vs. time for this catalyst were linear (Figure 2.10).

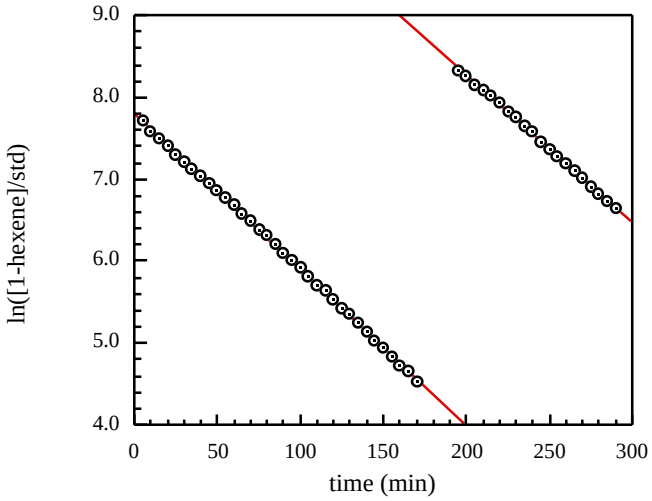

Figure 2.10. Plot of ln(1-hexene/Ph_3CH) vs. time (min) for two consecutive additions of 88 equiv of 1-hexene to **25** (0.007M) (–10 ˚C, C_6D_5Br).

As in the methyl system, the propagating species in the isobutyl system appeared to be stable in the absence of monomer at –10 ˚C. The observed rates of olefin consumption for two consecutive additions of 1-hexene to solution of **25** at –10 ˚C are identical at 0.019(1) min^{-1} (The k_p value is 2.6(2) $M^{-1}\,min^{-1}$ (0.044(3) $M^{-1}\,s^{-1}$)). This rate is similar to those obtained for activated [MesNpy]$ZrMe_2$ *at room temperature*. The ^1H NMR spectrum (–10 ˚C, C_6D_5Br) of this solution after addition of 1-hexene shows that all of **25** is consumed when monitoring the polymerization begins (no signals for the isobutyl methyl or methylene groups are observed). These observations suggest that the slow rates of initiation and polymerization with the methyl catalyst are due to the participation of only a fraction of the metal centers in catalysis.

The Eyring plot for polymerization of approximately 100 equiv 1-hexene obtained with **25**, with k_{obs} values of 0.01086(6) min^{-1} at 253K, 0.01903(7) min^{-1} at 263K, 0.0333(2) min^{-1} at 273 K and 0.0523(4) min^{-1} at 283K, was linear and led to $\Delta H^{\ddagger}$ and $\Delta S^{\ddagger}$ values of 34(3) kJ mol^{-1} (8.1(7) kcal mol^{-1}) and –140(10) J $mol^{-1}\,K^{-1}$ (–33 (3) cal $mol^{-1}\,K^{-1}$), respectively. Signals for internal heptenes were not observed for samples catalyzed by **25**, which indicates that 2,1-insertion by-products are not generated with the bulkier alkyl initiator.

Bulk polymerization reactions with solutions of **25** (0 ˚C, 6 mM in C_6H_5Cl) yield polymer samples with low polydispersity values (1.01-1.06), but higher than expected molecular weights (Figure 2.11, Table 2.2).

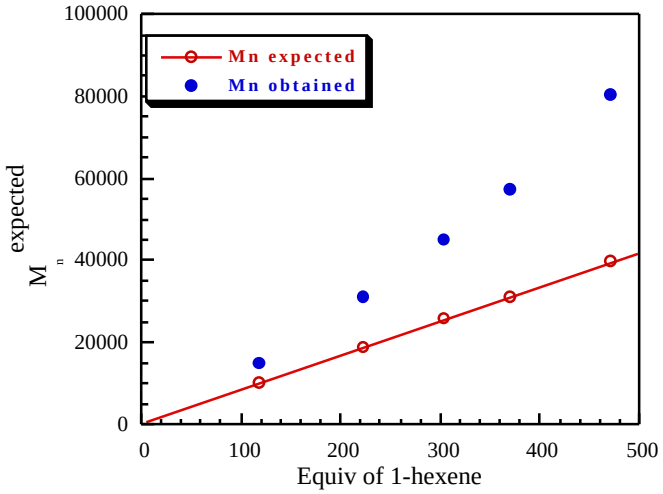

Figure 2.11. Polymerization of 1-hexene catalyzed by **25** (0 ˚C, 10 mM in C_6H_5Cl).

Table 2.2. Polymers generated with **25** at 0 ˚C.

[MesNpy]Zr(i–bu)$_2$ (M)	Equiv of 1–hexene	Expected M_n	Observed M_n	PDI
0.0062	118	9930	14700	1.06
0.0068	223	18767	31030	1.03
0.0066	304	25584	44900	1.01
0.0054	370	31139	57160	1.02
0.0048	472	39723	80250	1.02

A reason for the discrepancy in the molecular weights may be catalyst decomposition prior to and during polymer formation. Further studies of the decomposition process are required.

2.7 Polymerization of 1-hexene with activated [TripNpy]Zr(i-Bu)$_2$

To investigate the effect of increased ligand steric bulk on catalyst activity, the [TripNpy]Zr(i-Bu)$_2$ (**26**) system was studied. The ^{1}H NMR spectrum (20 ˚C, C_6D_5Br) of **26** showed signals for two Zr-C*H*$_2$ groups at 0.75 and 0.97 ppm. The $^{13}C\{^1H\}$ resonances are observed at 70.5 and 76.2 ppm.

An X-ray structural study of **26** showed the ligand bound in *pseudo*-facial manner with the alkyl groups in axial and equatorial positions (Figure 2.12, Table 2.3). The structural features are similar to those of the dimethyl compound, with an approximately trigonal bipyramidal geometry around the zirconium center. Although the isopropyl groups have increased the steric bulk of the ligand, the orientation of the aryl rings still creates an open face around the alkyl groups (Figure 2.12, Table 2.3).

Compound **26** was activated with 1 equiv of $[Ph_3C][B(C_6F_5)_4]$ to generate [(TripNpy)Zr(i-Bu)][$B(C_6F_5)_4$] (**27**) in a yellow solution. ^{1}H NMR studies (–10 ˚C, C_6D_5Br) showed only one set of signals for the zirconium-bound isobutyl group. Signals for Ph_3CH and isobutene were also detected.

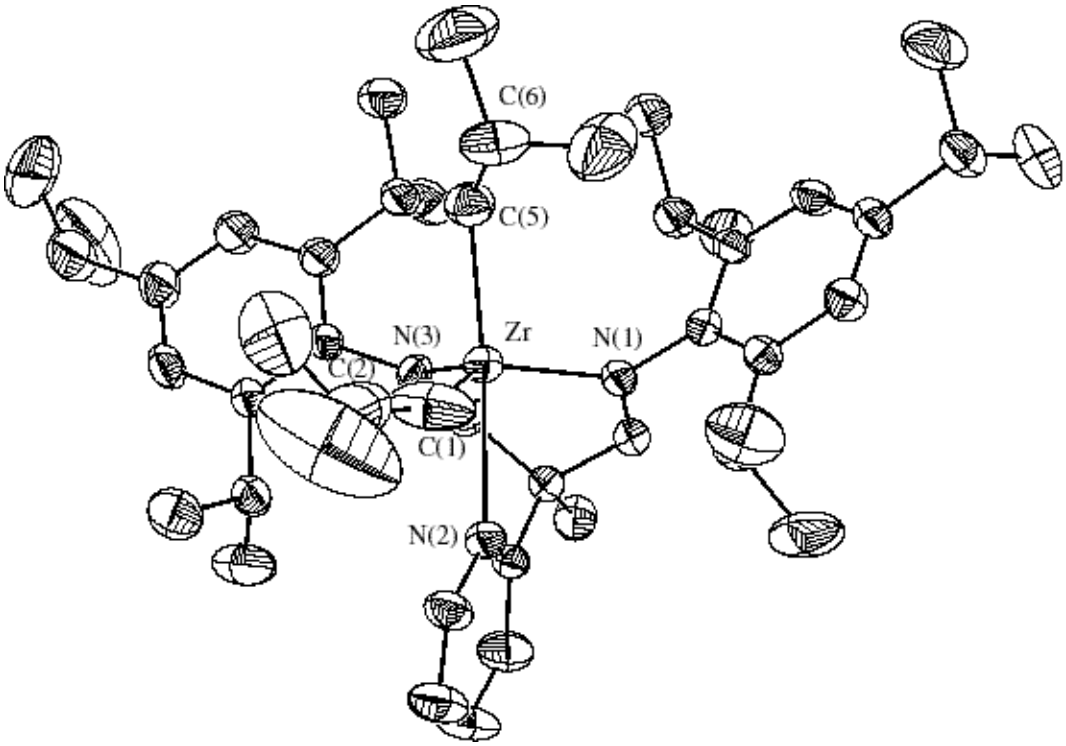

Figure 2.12. Thermal ellipsoid diagram (35% probability level) of [TripNpy]Zr(i-Bu)$_2$ (**26**).

Table 2.3. Selected bond lengths (Å) and angles (˚) for [TripNpy]Zr(i-Bu)$_2$ (**26**).

Bond Lengths

Zr-N(1)	2.047(4)	Zr-C(1)	2.258(7)
Zr-N(2)	2.483(4)	Zr-C(5)	2.253(5)
Zr-N(3)	2.047(4)		

Bond Angles

N(1)-Zr-N(3)	98.46(16)	C(1)-Zr-C(5)	90.4(2)
N(1)-Zr-C(5)	104.35(18)	N(1)-Zr-N(2)	81.18(14)
N(3)-Zr-C(5)	102.31(17)	N(3)-Zr-N(2)	80.03(13)
N(1)-Zr-C(1)	125.0(3)	C(5)-Zr-N(2)	173.46(18)
N(3)-Zr-C(1)	130.2(3)	C(1)-Zr-N(2)	83.5(2)

Unlike **25**, **27** is stable to β-hydride elimination at 0 ˚C for several hours, but decomposes slowly at room temperature. This increased stability is evident in the kinetics results obtained for this system; a plot of ln[1-hexene/std] vs. time is linear for this system and leads to a k_p value of 2.7(1) M^{-1} min^{-1} (0.044(2) M^{-1} s^{-1}) (Figure 2.13). This rate is smaller than that obtained with **25** (k_p = 4.8(1) M^{-1} min^{-1} (0.079(2) M^{-1} s^{-1})), perhaps due to greater catalyst bulk which can hinder olefin approach.

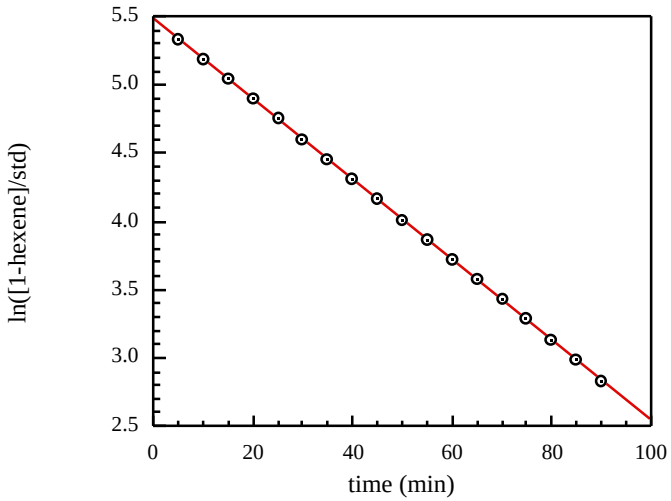

Figure 2.13. Plot of ln[1-hexene/std] vs. time after addition of 60 equiv of 1-hexene (0.8 M) to **27**.

The polydispersity values of polymer samples obtained with this system show significant temperature dependence. At room temperature, polymer samples with a PDI value of 1.35 and molecular weights four times the expected values were obtained. If the polymerization was carried out at 0 ˚C, the PDI was lowered to 1.02 and the molecular weights were three times greater than expected. In this case, the persistently higher molecular weights observed are likely due to catalyst decomposition during the propagation period. Studies with analogous hafnium complexes (Chapter 4) show that β-hydride elimination from the polymer chain is more severe in the bulkier [TripNpy] systems compared to the [MesNpy] system. Further investigation of this system is required.

2.8 Conclusions

Chapter 2 discussed polymerization of 1-hexene with activated dialkyl zirconium complexes of the type [ArNpy]ZrR_2 (Ar = Mes, Trip; R = Me, Bn, Np, i-Bu).

Activation of [MesNpy]$ZrMe_2$ (**1**) with [Ph_3C][$B(C_6F_5)_4$] leads to methyl abstraction and formation of [(MesNpy)ZrMe][$B(C_6F_5)_4$] (**9**), which is captured by **1** to form a stable dinuclear complex, {[(MesNpy)$Zr]_2Me_3$}{$B(C_6F_5)_4$} (**11**). Complex **11** does not react with 1-hexene; the active species in the system is [(MesNpy)ZrMe][$B(C_6F_5)_4$] (**9**) which is present in solution in low concentrations (~10%). A large fraction of unreacted **11** is observed in reactions carried out in solution, and poly(1-hexene) samples obtained with this system have M_n values an order of magnitude higher than expected, confirming low catalyst efficiency.

Although the mononuclear species [(MesNpy)ZrMe][$B(C_6F_5)_4$] (**9**) catalyzes 1-hexene polymerization, the open coordination environment provided by the [MesNpy] ligand allows 2,1-insertion of 1-hexene in the initiation step, which results in a secondary alkyl cation. This species is prone to β-hydride elimination and yields 2-heptenes, which can be isolated and characterized. For these reasons, methyl systems were judged to be unsuitable for further polymerization studies.

In an effort to form stable mononuclear cations, dibenzyl and dineopentyl complexes, [MesNpy]$ZrBn_2$ (**20**) and [MesNpy]$ZrNp_2$ (**22**) were synthesized and activated. The activated complex [(MesNpy)ZrBn][$B(C_6F_5)_4$] (**21**) was stable at room temperature; however, NMR studies showed that the pyridyl group was not coordinated to the metal, resulting in either a dinuclear species or interaction of zirconium with the coordinated benzyl group. Polymerization of 1-hexene with **21** was very slow. Activation of **22** proceeded *via* an unknown mechanism to yield [(MesNpy)ZrNp][$B(C_6F_5)_4$] (**23**) as well as Ph_3CH and $Ph_3CCH_2CMe_3$. Although **23** was an active catalyst for 1-hexene polymerization, it was unstable at 0 ˚C and decomposed in an unknown manner.

Diisobutyl complexes [MesNpy]Zr(i-Bu)$_2$ (**24**) and [TripNpy]Zr(i-Bu)$_2$ (**26**) were more suitable precatalysts for 1-hexene polymerization. Activation with [Ph_3C][$B(C_6F_5)_4$] proceeded *via* β-hydride abstraction to yield [(MesNpy)Zr(i-Bu)][$B(C_6F_5)_4$] (**25**) and [(TripNpy)Zr(i-Bu)][$B(C_6F_5)_4$] (**27**) as well as Ph_3CH and isobutene. Polymerization of 1-hexene with either **25** or **27** progressed with first order kinetics, however GPC data for polymer samples obtained with both catalysts were indicative of low catalyst efficiency.

For polymer samples obtained with **25** at 0 ˚C, M_n values were higher than expected due to β-hydride elimination at this temperature. The decomposition process for **27** was significantly slower at this temperature, however the M_n values obtained were still higher than expected and pointed towards catalyst decomposition during the propagation period.

To develop a suitable catalyst for living α-olefin polymerization, more stable, well-behaved systems had to be developed. Chapters 3 and 4 are devoted to solving this problem by investigating a variety of hafnium dialkyl complexes bearing the [ArNpy] ligands.

2.9 Experimental section

General Procedures. All manipulations, with the exception of the synthesis of ligand precursors, were performed under N_2 in a glove-box or using standard Schlenk procedures. Solvents were dried using conventional procedures.[60] Chlorobenzene (HPLC grade) and deuterated solvents were degassed, stored over and distilled from CaH_2. Commercial reagents were used without further purification. NMR spectra were recorded on a Varian INOVA 500 spectrometer. ^{1}H NMR chemical shifts are given in ppm versus residual protons in the deuterated solvents as follows: δ 7.16 C_6D_6, δ 2.09 toluene-d_8 (methyl), δ 7.29 C_6D_5Br (most downfield resonance). $^{13}C\{^1H\}$ NMR chemical shifts are given in ppm versus residual ^{13}C in the solvents as follows: δ 128.39 C_6D_6, δ 20.4 toluene-d_8 (methyl), δ 122.25 C_6D_5Br (most upfield resonance). Some aryl resonances in ^{1}H and $^{13}C\{^1H\}$ spectra are not given.

Elemental analyses were performed by H. Kolbe, Mikroanalytisches Laboratorium (Mülheim an der Ruhr, Germany). GPC analyses were carried out on a system equipped with two Jordi-Gel DVB mixed bed columns (250 mm length × 10 mm inner diameter) in series. HPLC grade THF was supplied at a flow rate of 1.0 mL/min with a Knauer 64 HPLC pump. A Wyatt Technology mini Dawn light scattering detector coupled with a Knauer differential refractometer was employed. Data analysis was carried out using Astrette 1.2 software (Whatt Technology). M_n and M_w values for poly(1-hexene) were obtained using dn/dc = 0.076 mL/gr (Wyatt Technology) and the auxiliary constant of the apparatus (5.9×10^{-4}) calibrated using a polystyrene standard ($M_n = 2.2 \times 10^5$). X-ray data were collected on a Siemens SMART/CCD diffractometer with λ(MoKα) = 0.71073 Å and solved using a full-matrix least squares refinement on F^2.

All Grignard reagents were carefully titrated with 2-butanol in the presence of 1,10-phenanthroline prior to use. [MesNpy]H_2[26] and Zr(NMe_2)$_4$[61] have been prepared according to previously reported methods.

Reactions of activated [MesNpy]ZrMe_2 (1) with 1-hexene, kinetics studies. Solutions of [MesNpy]$ZrMe_2$ (0.0298 g, 0.0572 mmol) and [Ph_3C][B(C_6F_5)$_4$] (0.0535 g, 0.0580 mmol), each in C_6D_5Br (2 mL) were prepared and cooled to –30 °C. The solutions were mixed while still cold and hexamethylbenzene (HMB) (0.0582, 0.0359 mmol) was added to the resulting orange solution. The total volume was increased to 5 mL in a volumetric flask and the solution was stored at –30 °C for further use for up to 5 d. ^{13}C labeling studies were carried out in a similar fashion using [MesNpy]Zr(^{13}Me)$_2$.

The NMR samples were prepared by adding 1-hexene (0.100 mL, 0.800 mmol) to the above stock solution (0.900 mL, 0.0099 mmol) in a calibrated NMR tube. ^{1}H NMR (500 MHz, C_6D_5Br) spectra were obtained by comparison of the most downfield methylene peak of 1-hexene δ 1.96 (m, 2H, CH_2=CHCH_2(CH_2)$_2$$CH_3$) to the HMB peak 2.10 (s, 18H, CH_3).

Reactions of activated [TripNpy]ZrMe$_2$ (8) with 1-hexene, kinetics studies. Solutions of [TripNpy]ZrMe$_2$ (0.0091 g, 0.0132 mmol), [Ph$_3$C][B(C$_6$F$_5$)$_4$] (0.0130 g, 0.0141 mmol) and the internal standard diphenylmethane (0.0056 g, 0.0333 mmol), each in C$_6$D$_5$Br were prepared and cooled to –30 ˚C. 1-hexene (0.100 mL, 0.800 mmol) was added to the mixture and the total volume increased to 1.00 mL. Further studies were carried out in an analogous manner to activated **1**.

[MesNpy]ZrBn$_2$ (20). A suspension of [MesNpy]ZrCl$_2$ (0.206 g, 0.367 mmol) in diethyl ether (30 mL) was cooled to –30 ˚C. To the cold solution was added BnMgCl (1.0 M in diethyl ether, 0.73 mL, 0.73 mmol) and the resulting mixture was stirred at room temperature for 15 min until the cloudy suspension became clear. Dioxane (0.06 mL, 0.73 mmol) was added to the solution and the resulting white solid was filtered through Celite. The filtrate was reduced to *ca* 5 mL and stored at –30 ˚C for 1 d to yield [MesNpy]ZrBn$_2$ as yellow crystals. Yield: 0.21 g, 83%. ^{1}H NMR (500 MHz, C$_6$D$_6$, 295 K) δ 0.87 (s, 3H, C*H*$_3$), ~2 (v. broad s, 12H, *o*-C*H*$_3$), 2.26 (s, 6H, *p*-C*H*$_3$), ~2.5 (broad s, 2H, C*H*$_2$Ph), 2.65 (d, 2H, C*H*$_2$), 4.01 (d, 2H, C*H*$_2$), 6.53 (m, 1H, py-C*H*), 6.68 (m, 1H, py-C*H*), 6.78 (m, 1H, py-C*H*), ~6.8 (broad s, 4H, C*H*), 6.91 (broad s, 4H, Bn-C*H*), 6.93 (m, 2H, Bn-C*H*), 7.04 (m, 4H, Bn-C*H*), 8.65 (m, 1H, py-*o*-C*H*). Anal. Calcd for C$_{41}$H$_{47}$N$_3$Zr: C, 73.17; H, 7.04; N, 6.24. Found: C, 73.25; H, 7.07; N, 6.19.

Solutions of [(MesNpy)ZrBn][B(C$_6$F$_5$)$_4$] (21). Solutions of [MesNpy]ZrBn$_2$ (0.021 g, 0.031 mmol) and [Ph$_3$C][B(C$_6$F$_5$)$_4$] (0.029 g, 0.031 mmol), each in C$_6$D$_5$Br (0.5 mL) were prepared and cooled to –30 ˚C. The solutions were mixed while still cold and the resulting yellow solution was transferred to an NMR tube. ^{1}H NMR (500 MHz, C$_6$D$_5$Br, 295 K) δ 1.30 (s, 3H, C*H*$_3$), ~1.7 (broad s, 12H, *o*-C*H*$_3$), 2.18 (s, 6H, *p*-C*H*$_3$), 2.29 (s, 6H, *o*-C*H*$_3$), 2.53 (s, 2H, Zr-C*H*$_2$Ph), 2.75 (d, 2H, C*H*$_2$), 2.84 (s, 2H, Ph$_3$CC*H*$_2$Ph), 3.95 (d, 2H, C*H*$_2$), 6.08 (d, J_{HH} = 7 Hz, 2H,

Zr-CH_2-ph-*o*-C*H*), 6.64 (d, J_{HH} = 8 Hz, 2H, C*H*), some aryl peaks omitted here, 7.37 (m, 1H, py-C*H*), 7.55 (m, 1H, py-*o*-C*H*), 7.69 (m, 1H, py-C*H*). $^{13}C\{^1H\}$ NMR (125 MHz, C_6D_5Br, 295 K) δ 18.25 (s, *o*-*C*H_3), 20.74 (s, *p*-*C*H_3), 24.88 (s, *C*H_3), 44.62 (s, Ph_3CCH_2Ph), 38.81 (broad s, Zr-^{13}*C*H_3), 46.20 (s, *C*R_4), 58.55 (s, *C*H_2), 64.59 (s, Zr-*C*H_2Ph), 74.40 (s, Ph_3CCH_2Ph), some aryl peaks omitted here.

Reaction of [(MesNpy)ZrBn][B(C_6F_5)$_4$] with 1-hexene. The NMR sample were prepared by adding 1-hexene (0.400 mL, 3.2 mmol) to the above sample.

[MesNpy]ZrNp$_2$ (22). A suspension of [MesNpy]$ZrCl_2$ (1.01 g, 1.80 mmol) in diethyl ether (30 mL) was cooled to –30 ˚C. To the cold solution was added a solution of NpLi (0.280 g, 3.60 mmol) in diethyl ether at –30 ˚C and the resulting mixture was stirred at room temperature for 45 min until the cloudy suspension became a clear orange color. The resulting white solid was filtered through Celite and the filtrate was reduced to *ca* 15 mL and stored at –30 ˚C for 1 d to yield [MesNpy]$ZrNp_2$ as a white powder. Yield: 0.59 g, 52%. ^{1}H NMR (500 MHz, C_6D_6, 295 K) δ 0.95 (s, 3H, C*H*$_3$), 1.10 (s, 9H, Zr-$CH_2C(CH_3)_3$), 1.27 (s, 2H, Zr-C*H*$_2$C(CH_3)$_3$), 1.36 (s, 9H, Zr-$CH_2C(CH_3)_3$), 1.46 (s, 2H, Zr-C*H*$_2$C(CH_3)$_3$), 2.14 (s, 6H, *p*-C*H*$_3$), ~2.3 (v. broad s, 12H, *o*-C*H*$_3$), 2.75 (d, 2H, C*H*$_2$), 4.03 (d, 2H, C*H*$_2$), 6.67 (m, 1H, py-C*H*), 6.78 (m, 1H, py-C*H*), 6.88 (s, 4H, C*H*), 7.05 (m, 1H, py-C*H*), 9.17 (m, 1H, py-*o*-C*H*). $^{13}C\{^1H\}$ NMR (125 MHz, C_6D_6, 295 K) δ 19.76 (s, *o*-*C*H_3), 21.25 (s, *o*-*C*H_3), 23.07 (s, *p*-*C*H_3), 25.46 (s, *C*H_3), 34.40 (s, Zr-$CH_2C(CH_3)_3$), 35.47 (s, Zr-$CH_2C(CH_3)_3$), 36.26 (s, Zr-$CH_2C(CH_3)_3$), 36.32 (s, Zr-$CH_2C(CH_3)_3$), 46.28 (s, *C*R_4), 67.07 (s, *C*H_2), 79.61 (s, Zr-*C*$H_2C(CH_3)_3$), 82.07 (s, Zr-*C*$H_2C(CH_3)_3$), 120.54 (s, Ar-*C*), 122.02 (s, Ar-*C*), 128.68 (s, Ar-*C*), 134.02 (s, Ar-*C*), 139.07 (s, Ar-*C*), 147.48 (s, Ar-*C*), 148.38 (s, Ar-*C*), 163.47 (s, Ar-*C*). Anal. Calcd for $C_{37}H_{55}N_3Zr$: C, 70.20; H, 8.76; N, 6.64. Found: C, 70.08; H, 8.65; N, 6.86.

Solutions of [(MesNpy)ZrNp][B(C_6F_5)$_4$] (23). Solutions of [MesNpy]ZrNp_2 (0.0105 g, 0.0166 mmol) and [Ph_3C][B(C_6F_5)$_4$] (0.0165 g, 0.0179 mmol), each in C_6D_5Br (0.5 mL) were prepared and cooled to –30 ˚C. The solutions were mixed while still cold and the resulting yellow/orange solution was transferred to an NMR tube and frozen in $N_{2(l)}$ within 2 min of the preparation of the sample. ^{1}H NMR (500 MHz, C_6D_5Br, 243 K) δ 0.61 (s, $Ph_3CCH_2C(CH_3)_3$), 0.64 (s, 9H, Zr-$CH_2C(CH_3)_3$), 0.89 (s, $C(CH_3)_4$), 0.96 (s, 2H, $Ph_3CCH_2C(CH_3)_3$), 1.3 (s, 3H, CH_3), ~1.55 (broad s, 6H, *o*-CH_3), 2.16 (s, 6H, *p*-CH_3), ~2.32 (broad s, 6H, *o*-CH_3), 2.72 (s, $Ph_3CCH_2C(CH_3)_3$), 2.78 (d, 2H, CH_2), 3.98 (d, 2H, CH_2), 5.45 (s, Ph_3CH), some aryl peaks omitted here, 7.66 (m, 1H, py-*o*-C*H*), 8.49 (m, 1H, py-C*H*).

Reactions of [(MesNpy)ZrNp][B(C_6F_5)$_4$] with 1-hexene, kinetics studies. Solutions of [MesNpy]ZrNp_2 (0.0057 g, 0.0090 mmol), [Ph_3C][B(C_6F_5)$_4$] (0.0087 g, 0.0094 mmol) and diphenylmethane (0.0100g, 0.0594 mmol), each in C_6D_5Br were prepared and cooled to –30 ˚C. 1-hexene (0.100 mL, 0.800 mmol) was added to the mixture and the total volume was increased to 1 mL in a graduated NMR tube. Kinetics data were obtained from the ^{1}H NMR (500 MHz, C_6D_5Br) spectra by comparison of the most downfield olefin peak of 1-hexene δ 5.67 (m, 2H, CH_2=C*H*$CH_2(CH_2)_2CH_3$) to the Ph_2CH_2 peak 3.81 (s, 2H, Ph_2CH_2).

[MesNpy]Zr(i-Bu)$_2$ (24). *Note: all of the following manipulations were carried out in the absence of light.* A suspension of [MesNpy]ZrCl_2 (0.212 g, 0.377 mmol) in diethyl ether (10 mL) was cooled to –30 °C. To the cold solution was added (i-Bu)MgBr (2.0 M in diethyl ether, 0.377 mL, 0.755 mmol) and the resulting mixture was stirred at room temperature for 10 min until the cloudy suspension became clear. Dioxane (0.080 mL, 0.944 mmol) was added to the solution and the resulting white solid was filtered through Celite. The solvent was removed *in vacuo* to yield a white powder. Yield: 0.21 g, 92%. [MesNpy]Zr(i-Bu)$_2$ can be recrystallized from diethyl ether at –30 °C to yield clear, colorless crystals. ^{1}H NMR (500 MHz, C_6D_6, 295 K)

δ 0.94 (s, 3H, CH_3), 0.97 (d, 6H, Zr-CH_2CH(CH_3)$_2$), 1.04 (m, 4H, Zr-CH_2CH(CH_3)$_2$), 1.27 (d, 6H, Zr-CH_2CH(CH_3)$_2$), 2.16 (s, 6H, *p*-CH_3), 2.29 (broad s, 12H, *o*-CH_3), 2.35 (m, 1H, Zr-CH_2C*H*(CH_3)$_2$), 2.52 (m, 1H, Zr-CH_2C*H*(CH_3)$_2$), 2.72 (d, 2H, CH_2), 4.00 (d, 2H, CH_2), 6.62 (m, 1H, py-C*H*), 6.78 (m, 1H, py-C*H*), 6.89 (s, 4H, C*H*), 7.02 (m, 1H, py-C*H*), 8.87 (m, 1H, py-*o*-C*H*). ^{1}H NMR (500 MHz, C_6D_5Br, 295 K) δ 0.74 (d, 6H, Zr-CH_2CH(CH_3)$_2$), 0.81 (d, 2H, Zr-CH_2CH(CH_3)$_2$), 0.88 (d, 2H, Zr-CH_2CH(CH_3)$_2$), 1.11 (d, 6H, Zr-CH_2CH(CH_3)$_2$), 1.22 (s, 3H, CH_3), 2.14 (s, 6H, *p*-CH_3), 2.19 (broad s, 13H, *o*-CH_3, Zr-CH_2C*H*(CH_3)$_2$), 2.39 (m, 1H, Zr-CH_2C*H*(CH_3)$_2$), 2.73 (d, 2H, CH_2), 4.02 (d, 2H, CH_2), 6.82 (s, 4H, C*H*), 7.02 (m, 1H, py-C*H*), 7.17 (m, 1H, py-C*H*), 7.48 (m, 1H, py-C*H*), 8.89 (m, 1H, py-*o*-C*H*). ^{13}C{^{1}H} NMR (125 MHz, C_6D_6, 295 K) δ 19.25 (s, *o*-*C*H_3), 21.31 (s, *p*-*C*H_3), 25.67 (s, *C*H_3), 29.03 (s, Zr-CH_2CH(*C*H_3)$_2$), 29.63 (s, Zr-CH_2CH(*C*H_3)$_2$), 30.51 (s, Zr-CH_2*C*H(CH_3)$_2$), 32.72 (s, Zr-CH_2*C*H(CH_3)$_2$), 46.18 (s, *C*R_4), 66.52 (s, *C*H_2), 72.59 (s, Zr-*C*H_2CH(CH_3)$_2$), 74.21 (s, Zr-*C*H_2CH(CH_3)$_2$), 120.93 (s, Ar-*C*), 122.60 (s, Ar-*C*), 130.18 (s, Ar-*C*), 134.19 (s, Ar-*C*), 135.18 (s, Ar-*C*), 139.19 (s, Ar-*C*), 146.79 (s, Ar-*C*), 147.42 (s, Ar-*C*), 163.22 (s, Ar-*C*). Anal. Calcd for $C_{35}H_{51}N_3Zr$: C, 69.48; H, 8.50; N, 6.95. Found: C, 69.37; H, 8.48; N, 6.86.

Solutions of {[MesNpy]Zr(i-Bu)}[B(C_6F_5)$_4$] (25). *Note: all of the following manipulations were carried out in the absence of light.* Solutions of [MesNpy]Zr(i-Bu)$_2$ (0.022 g, 0.036 mmol) and [Ph_3C][B(C_6F_5)$_4$] (0.034 g, 0.036 mmol), each in C_6D_5Br (0.5 mL) were prepared and cooled to –30 ˚C. The solutions were mixed while still cold and the resulting yellow/orange solution was transferred to an NMR tube and frozen in $N_{2(l)}$ within 2 min of the preparation of the sample. ^{1}H NMR (500 MHz, C_6D_5Br, 243 K) δ 0.60 (d, 6H, Zr-CH_2CH(CH_3)$_2$), 0.62 (d, 2H, Zr-CH_2CH(CH_3)$_2$), 0.84 (m, 1H, CH_2C*H*(CH_3)$_2$), 1.31 (s, 3H, CH_3), ~1.5 (broad s, 6H, *o*-CH_3), 1.62 (s, 6H, CH_2C(CH_3)$_2$), 2.18 (s, 6H, *p*-CH_3), 2.32 (broad s, 6H, *o*-CH_3), 2.79 (d, 2H, CH_2), 3.98 (d, 2H, CH_2), 4.73 (s, 1H, Ph_3C*H*), 5.45 (s, 2H, CH_2C(CH_3)$_2$), some aryl peaks omitted here, 7.36 (m, 1H, py-C*H*), 7.65 (m, 1H, py-C*H*), 8.39 (m, 1H, py-*o*-

C*H*). $^{13}C\{^{1}H\}$ NMR (125 MHz, C_6D_5Br, 243 K) δ 18.65 (s, *o*-*C*H_3), 20.79 (s, *p*-*C*H_3), 24.30 (s, $CH_2C(CH_3)_2$), 24.96 (s, *C*H_3), 26.28 (s, Zr-$CH_2CH(CH_3)_2$), 27.533 (s, Zr-$CH_2CH(CH_3)_2$), 44.76 (s, *C*R_4), 56.64 (s, Ph_3CH), 64.77 (s, *C*H_2), 83.33 (s, Zr-*C*$H_2CH(CH_3)_2$), 111.23 (s, *C*$H_2C(CH_3)_2$), some aryl peaks omitted here.

Reactions of {[MesNpy]Zr(i-Bu)}[B(C_6F_5)$_4$] (25) with 1-hexene, kinetics studies. *Note: all of the following manipulations were carried out in the absence of light.* Solutions of [MesNpy]Zr(i-Bu)$_2$ (0.0082 g, 0.0136 mmol) and [Ph_3C][B(C_6F_5)$_4$] (0.0136 g, 0.0147 mmol), each in C_6D_5Br (0.8 mL) were prepared and cooled to –30 ˚C. The solutions were mixed while still cold and 1-hexene (0.170 mL, 1.36 mmol) was added to the mixture. The total volume was increased to 2 mL in a volumetric flask. The NMR samples were obtained directly from this solution, and frozen with liquid nitrogen prior to experimentation.

Bulk polymerization reactions: All bulk polymerization reactions were carried out in a similar manner as the following procedure.

Reactions of [(MesNpy)Zr(i-Bu)][B(C_6F_5)$_4$] (25) with 1-hexene: bulk polymerization. Solutions of [MesNpy]Zr(i-Bu)$_2$ (0.0131 g, 0.0217 mmol) and [Ph_3C][B(C_6F_5)$_4$] (0.0204 g, 0.0221 mmol), each in C_6H_5Cl (1.5 mL) were prepared and cooled to –30 ˚C. The solutions were mixed while still cold and 1-hexene (1.00 mL, 8.00 mmol) was added to the mixture. The samples stirred at 0 ˚C for 2 hrs, quenched with methanol, and the solvent removed *in vacuo*. The sample was then redissolved in pentane, passed through silica, and dried *in vacuo* for 16 h.

[TripNpy]Zr(i-Bu)$_2$ (26). A suspension of [TripNpy]$ZrCl_2$ (1.02 g, 1.40 mmol) in diethyl ether (50 mL) was cooled to –30 ˚C. To the cold solution was added (i-Bu)MgBr (2.3 M in diethyl ether, 1.40 mL, 3.21 mmol) and the resulting mixture was stirred at room temperature

for 10 min until the cloudy suspension became clear. Dioxane (0.30 mL, 3.49 mmol) was added to the solution and the resulting white solid was filtered through Celite. The solvent was removed in *vacuo* to yield a white powder. [TripNpy]Zr(i-Bu)$_2$ was recrystallized from diethyl ether at room temperature to yield clear, colorless crystals. ^{1}H NMR (500 MHz, C_6D_5Br, 295 K) δ 0.54 (d, 6H, Zr-$CH_2CH(CH_3)_2$), 0.62 (d, 6H, Zr-$CH_2CH(CH_3)_2$), 0.75 (d, 2H, Zr-$CH_2CH(CH_3)_2$), 0.97 (d, 2H, Zr-$CH_2CH(CH_3)_2$), 1.11 (d, 6H, CH_3), 1.21 (d, 6H, CH_3), 1.22 (s, 3H, CH_3), 1.33 (d, 6H, CH_3), 1.46 (d, 6H, CH_3), 1.60 (d, 6H, CH_3), 2.12 (m, 1H, Zr-$CH_2CH(CH_3)_2$), 2.35 (m, 1H, Zr-$CH_2CH(CH_3)_2$), 2.83 (m, 2H, CH), 2.95 (d, 2H, CH_2), 3.05 (m, 2H, CH), 3.87 (m, 2H, CH), 4.07 (d, 2H, CH_2), 7.02 (s, 2H, CH), 7.09 (m, 1H, py-CH), 7.12 (m, 1H, py-CH), 7.14 (s, 2H, CH), 7.45 (m, 1H, py-CH), 8.98 (m, 1H, py-*o*-CH). ^{13}C{^{1}H} NMR (125 MHz, C_6D_5Br, 295 K) δ 23.67 (s, CH_3), 24.32 (s, CH_3), 24.35 (s, CH_3), 24.96 (s, CH_3), 25.70 (s, CH_3), 27.47 (s, Zr-$CH_2CH(CH_3)_2$), 27.52(s, Zr-$CH_2CH(CH_3)_2$), 28.69 (s, Zr-$CH_2CH(CH_3)_2$), 29.28 (s, CH), 29.48 (s, CH), 32.13 (s, Zr-$CH_2CH(CH_3)_2$), 34.18 (s, CH_3), 45.85 (s, CR_4), 68.71 (s, CH_2), 70.52 (s, Zr-$CH_2CH(CH_3)_2$), 76.18 (s, Zr-$CH_2CH(CH_3)_2$), 120.41 (s, Ar-*C*), 121.06 (s, Ar-*C*), 121.97 (s, Ar-*C*), 122.48 (s, Ar-*C*), 139.14 (s, Ar-*C*), 144.32 (s, Ar-*C*), 144.88 (s, Ar-*C*), 145.11 (s, Ar-*C*), 145.28 (s, Ar-*C*), 146.83 (s, Ar-*C*), 162.65 (s, Ar-*C*). Anal. Calcd for $C_{47}H_{75}N_3Zr$: C, 73.00; H, 9.78; N, 5.43. Found: C, 73.11; H, 9.71; N, 5.36.

Solutions of [(TripNpy]Zr(i-Bu)][B(C$_6$F$_5$)$_4$] (27). Solutions of [TripNpy]Zr(i-Bu)$_2$ (0.0103 g, 0.0133 mmol), [Ph_3C][B(C_6F_5)$_4$] (0.0127 g, 0.0138 mmol) and Ph_2CH_2 (0.0058, 0.0345 mmol), each in C_6D_5Br (0.5 mL) were prepared and cooled to –30 ˚C. The solutions were mixed while still cold and the resulting yellow/orange solution was transferred to an NMR tube and frozen in $N_{2(l)}$ within 2 min of the preparation of the sample. ^{1}H NMR (500 MHz, C_6D_5Br, 263 K) δ 0.56 (d, 6H, Zr-$CH_2CH(CH_3)_2$), 0.71 (d, 6H, CH_3), 0.85 (d, 2H, Zr-$CH_2CH(CH_3)_2$), 1.02 (d, 6H, CH_3), 1.21 (d, 12H, CH_3), 1.32 (d, 12H, CH_3), 1.62 (d, 3H, $CH_2C(CH_3)_2$), 1.65 (m, 2H, CH), 2.83 (m, 2H, CH), 3.03 (d, 2H, CH_2), 3.23 (m, 2H, CH), 4.13 (d, 2H, CH_2), 4.72 (s, 2H,

C*H*$_2$C(CH$_3$)$_2$), 5.45 (s, 1H, Ph$_3$C*H*), some aryl peaks omitted here, 7.38 (s, 2H, C*H*), 7.71 (m, 1H, py-C*H*), 8.23 (m, 1H, py-*o*-C*H*).

Reactions of [(TripNpy]Zr(i-Bu)][B(C$_6$F$_5$)$_4$] (27) with 1-hexene, kinetics studies. Solutions of [TripNpy]Zr(i-Bu)$_2$ (0.0093 g, 0.0120 mmol), [Ph$_3$C][B(C$_6$F$_5$)$_4$] (0.0110 g, 0.0120 mmol) and diphenylmethane (0.0048 g, 0.0285 mmol), each in C$_6$D$_5$Br were prepared and cooled to –30 ˚C. 1-hexene (0.090 mL, 0.800 mmol) was added to the mixture and the total volume increased to 1.09 mL. Further studies were carried out in an analogous manner to **25**.

Chapter 3

Synthesis and activation of stable hafnium dialkyl complexes: Examining the initiator / activator relationship

3.1 Introduction

In Chapter 2, [ArNpy]Zr(i-Bu)$_2$ complexes were investigated and were found to be relatively stable toward decomposition. However, the respective zirconium isobutyl cations were not stable and decomposed *via* β-hydride elimination at 0 ˚C. Although a number of β-hydride containing dialkyl zirconium complexes are reported in the literature,[72-77] in many of these systems the β C-H bonds are thermally labile. In contrast, the corresponding dialkyl hafnium complexes are more stable towards manipulation at room temperature.[27,78] In an attempt to generate cationic species stable toward β-hydride elimination, hafnium dialkyl complexes were investigated.

Examples involving reactions of dialkyl complexes with various activators have been reported in the literature.[79] The [Ph$_3$C][B(C$_6$F$_5$)$_4$] activator reacts with β-hydrogen containing dialkyl complexes mainly *via* a β-hydride abstraction mechanism, while with dimethyl or dibenzyl complexes alkyl abstraction is the sole activation mechanism (*vide supra*). The [HNMe$_2$Ph][B(C$_6$F$_5$)$_4$] activator reacts by protonation of the alkyl group to yield a cation and the respective alkane by-product. The neutral B(C$_6$F$_5$)$_3$ activator, which can react by direct alkyl abstraction in the case of dimethyl and dibenzyl complexes,[52] has been shown to react predominantly by β-hydride abstraction in the case of β-hydride containing dialkyl complexes.

Scheme 3.1 is a summary of the different activation pathways for the above activators. Chapter 3 is concerned with the synthesis and activation of β-hydride-containing dialkyl hafnium systems of the type [MesNpy]HfR$_2$, where R = Et, n-Pr, n-Bu, i-Pr. The dialkyl complexes were synthesized similarly to their zirconium counterparts (Scheme 1.3). In particular, the activated [MesNpy]Hf(i-Bu)$_2$ system was found to be a catalyst for the living polymerization of α-olefins, and will be discussed in detail in Chapter 4. The reactivity of these complexes with various activators was studied.

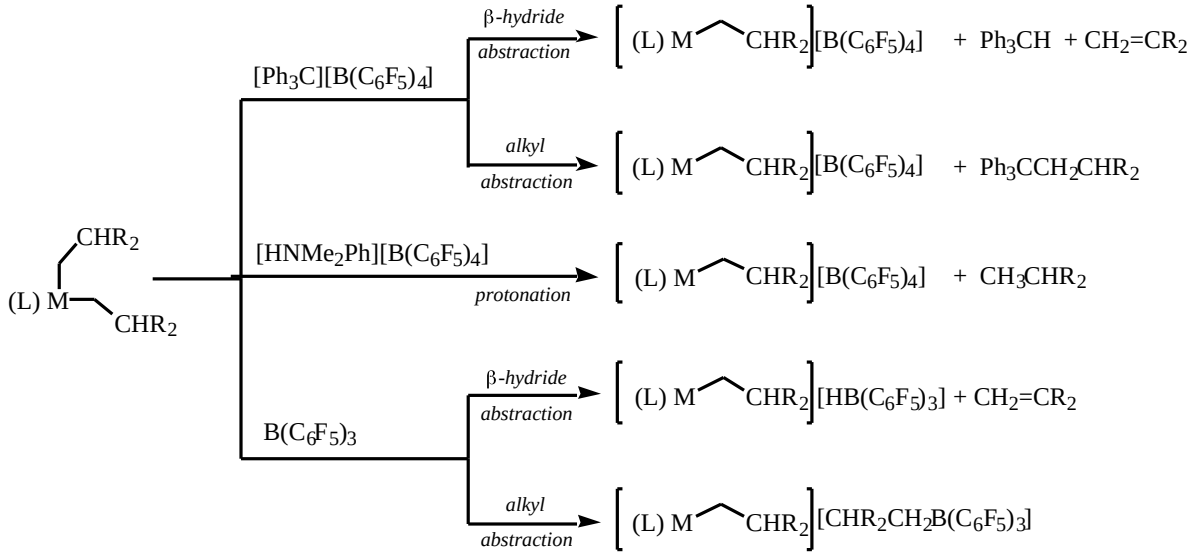

Scheme 3.1. Activation of β-hydride containing dialkyl complexes by different activators.

3.2 Activation of [MesNpy]HfEt$_2$

The [MesNpy]HfEt$_2$ complex (**28**) was stable at room temperature in the solid state and in solution for several hours (The zirconium analogue of **28**, [MesNpy]ZrEt$_2$, was also prepared and was found to decompose in solution at room temperature in under 20 min). The ^{1}H NMR (–20 ˚C, C_6D_5Br) resonances for the Hf-C*H*$_2$ protons overlap at 0.53 ppm, while the corresponding $^{13}C\{^1H\}$ NMR resonances are observed at 57.2 and 59.3 ppm.

When **28** is activated with [Ph$_3$C][B(C$_6$F$_5$)$_4$], the resulting reaction mixture is composed of two major cationic species as well as by-products of activation (Scheme 3.2). Path **A** in Scheme 3.2 involves the direct abstraction of an ethyl group from **28** to yield [(MesNpy)HfEt][B(C$_6$F$_5$)$_4$] (**29**) as well as the by-product Ph$_3$CCH$_2$CH$_3$. A gCOSY experiment (0 ˚C, C_6D_5Br) of the solution mixture shows a quartet and a triplet at 0.26 and 0.92 ppm, respectively. These resonances correlate to each other only and are assigned to the Hf-C*H*$_2$CH$_3$ and Hf-CH$_2$C*H*$_3$ protons of **29**, respectively. The aliphatic signals for Ph$_3$CCH$_2$CH$_3$ can be observed as a triplet and quartet at 0.69 and 2.47 ppm, respectively.

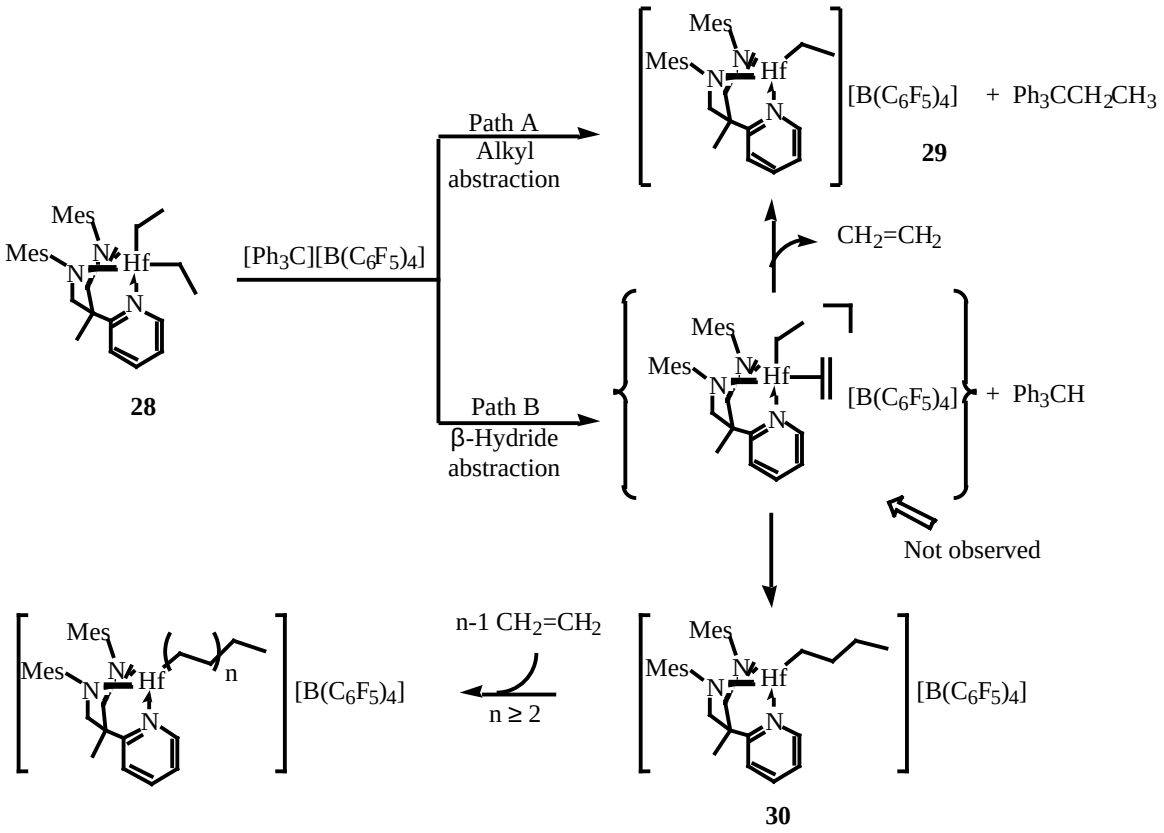

Scheme 3.2. Activation of **28** with $[Ph_3C][B(C_6F_5)_4]$ (–20 ˚C, C_6D_5Br).

Path **B** in Scheme 3.2 involves the abstraction of a β-hydride from **28** to yield Ph_3CH and a putative hafnium(ethyl)(ethylene) intermediate. This intermediate can lose ethylene to yield **29**, or can insert ethylene to yield a new cationic species, $[(MesNpy)Hf(n\text{-}Bu)][B(C_6F_5)_4]$ (**30**). Thus it is possible to generate sub-stoichiometric quantities of an olefin *in situ* and observe the first insertion product of a variety of olefins in this manner.

A ^{13}C DEPT experiment (0 ˚C, C_6D_5Br) on the solution resulting from the activation of **28** with $[Ph_3C][B(C_6F_5)_4]$ confirms the presence of two cationic hafnium alkyl species in solution. The Hf-CH_2 of **29** can be observed at 71.5 ppm, and that for **30** can be observed at 80.0 ppm. ^1H and $^{13}C\{^1H\}$ NMR assignments for **30** can be confirmed by comparison with signals for this cation generated *via* activation of $[MesNpy]Hf(n\text{-}Bu)_2$ with 1 equiv of $[Ph_3C][B(C_6F_5)_4]$ (*vide*

infra). Figure 3.1 is a summary of the relevant chemical shifts for all the species present in solution as well as their relative amounts with respect to an internal standard (Ph_2CH_2).

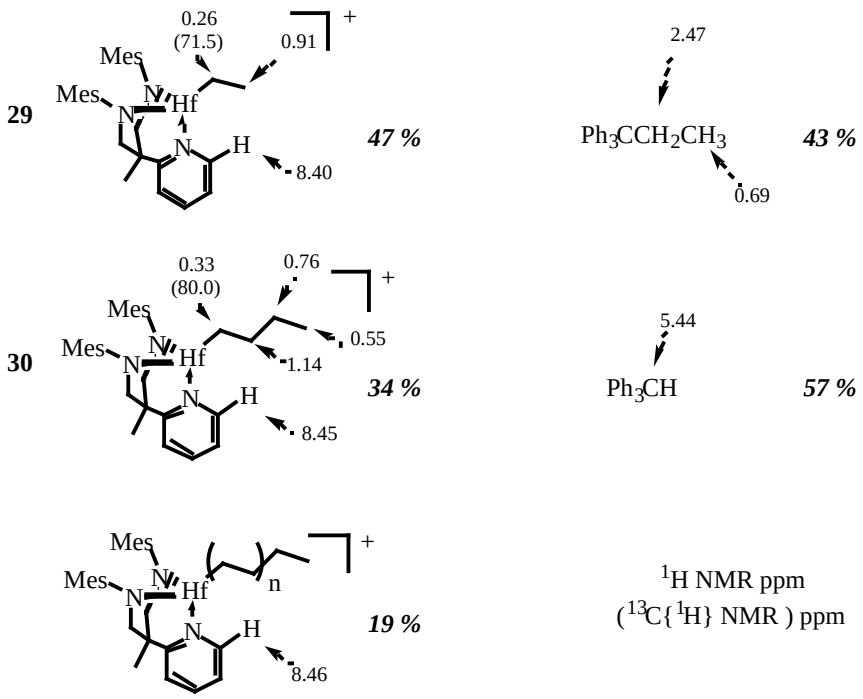

Figure 3.1. Species present in solution upon activation of **28** with $[Ph_3C][B(C_6F_5)_4]$ (–20 ˚C, C_6D_5Br) and their relative amounts with respect to Ph_2CH_2. Anion = $[B(C_6F_5)_4]^-$.

These NMR spectroscopic data show that the ratio of Ph_3CH to $Ph_3CCH_2CH_3$ is 1.3:1, thus β-abstraction appears to be the more prominent activation mode in this system. The amount of **30** is 23% less than Ph_3CH, potentially due to ethylene loss from the ethyl ethylene intermediate (Scheme 3.2). The lost ethylene can insert into **29** to yield **30**, or it can insert into **30** to yield multiple insertion products.

Addition of 1-2 equiv of 1-hexene to a solution containing the activated species **29** and **30** led to a mixture of two major species. Useful information was gained from a ^{13}C DEPT experiment (0 ˚C, C_6D_5Br) of this mixture, leading to the identification of signals for two 1,2-

insertion products (Scheme 3.3). Only a signal at 88.7 ppm corresponding to a methylene of the

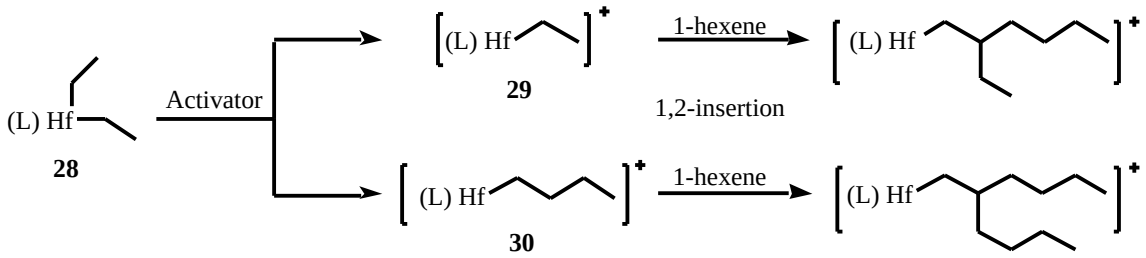

Scheme 3.3. Addition of 1-2 equiv of 1-hexene to a mixture of **29** and **30** (0 ˚C, C_6D_5Br). Activator = $[Ph_3C][B(C_6F_5)_4]$. L = $[MesNpy]^{2-}$, anion = $[B(C_6F_5)_4]^-$.

type Hf-*C*H_2CHR'R" (where R' and R" are alkyl groups) is present. A signal for a hafnium-bound methine carbon, Hf-*C*HR'R", was not observed. The absence of a methine carbon indicates that either no 2,1-insertion of 1-hexene has occurred, or that the amount of 2,1-insertion product is low and undetectable *via* these NMR spectroscopic techniques.

The diethyl system yields valuable information about the mode of activation with $[Ph_3C][B(C_6F_5)_4]$. As discussed in Chapters 1 and 2, activation of dimethyl precatalysts proceeds exclusively *via* alkyl abstraction, whereas activation of the diisobutyl analogues proceeds exclusively *via* β-hydride abstraction. In the case of the hafnium diethyl system, however, both pathways are observed, illustrating that activation of some β-hydride containing dialkyl complexes may be considered a competition between the two mechanisms.

3.3 Activation of [MesNpy]Hf(n-Pr)$_2$ and [MesNpy]Hf(n-Bu)$_2$

Complexes [MesNpy]Hf(n-Pr)$_2$ (**31**) and [MesNpy]Hf(n-Bu)$_2$ (**32**) were found to be stable at room temperature in both solution and solid state for several hours. Complexes **31** and **32** were activated with 1 equiv of $[Ph_3C][B(C_6F_5)_4]$ to yield alkyl cations resulting from β-hydride abstraction, $[(MesNpy)HfR][B(C_6F_5)_4]$ (R = n-Pr, **33**; n-Bu, **30**), their respective first

insertion products, and Ph_3CH as the sole by-product. These mixtures are more difficult to identify fully because of many overlapping signals in the ^1H and $^{13}C\{^1H\}$ NMR spectra (Scheme 3.4).

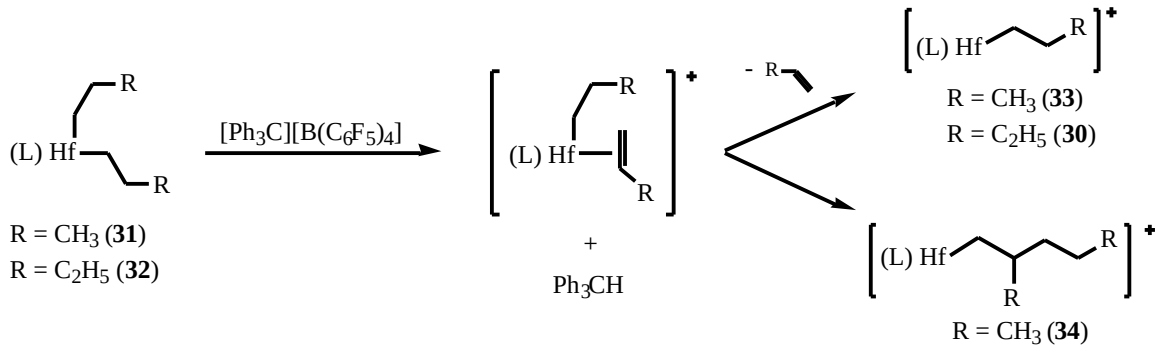

Scheme 3.4. Activation of **31** and **32** with $[Ph_3C][B(C_6F_5)_4]$ (0 ˚C, C_6D_5Br). L = $[MesNpy]^{2-}$, anion = $[B(C_6F_5)_4]^-$.

^1H and gCOSY NMR spectra (–20 ˚C, C_6D_5Br) of the reaction mixture resulting from activation of **31** show signals at 0.32, 1.22 and 0.53 ppm for the Hf-C*H*$_2$CH$_2$CH$_3$, Hf-CH$_2$C*H*$_2$CH$_3$, and Hf-CH$_2$CH$_2$C*H*$_3$ protons, respectively. Signals for the first 1,2-insertion product of propene, $[(MesNpy)Hf(CH_2CH(CH_3)(n\text{-}Pr))][B(C_6F_5)_4]$, **34**, are also observed in this region but cannot be clearly assigned. The *ortho* pyridyl region of the ^1H NMR spectrum shows resonances at 8.48, 8.52, and 8.61 ppm with a ratio of 6.2:4.3:1. These signals correspond to **33**, **34**, and the product of multiple propene insertions, respectively. Signals for $Ph_3CCH_2CH_2CH_3$, the product of direct alkyl abstraction, were not observed. This indicates that with the bulkier alkyl group, β-hydride abstraction is the preferred mechanism of activation by $[Ph_3C][B(C_6F_5)_4]$. A ^{13}C DEPT experiment (-20 ˚C, C_6D_5Br) of the reaction mixture shows resonances at 92.5 and 82.7 ppm corresponding to the Hf-*C*H$_2$ carbon atoms of **33** and **34**, respectively.

The ^1H NMR spectrum of the mixture generated by activation of **32** with $[Ph_3C][B(C_6F_5)_4]$ was difficult to interpret due to many overlapping signals. However a trace of free 1-butene was observed in solution, while ethylene and propene were not observed in

analogous activation reactions of [MesNpy]HfEt$_2$ (**28**), [MesNpy]Hf(n-Pr)$_2$ (**31**) and [MesNpy]Hf(i-Pr)$_2$ (**37**) (*vide infra*), indicating that ethylene and propene are more reactive than the bulkier 1-butene.

3.4 Synthesis and activation of mixed alkyl hafnium complexes

To prepare and study the isopropyl cation, [(MesNpy)Hf(i-Pr)][B(C_6F_5)$_4$], independently, the mixed alkyl complex, [MesNpy]Hf(i-Pr)(Me) (**35**), was synthesized (eq 3.1) and activated.

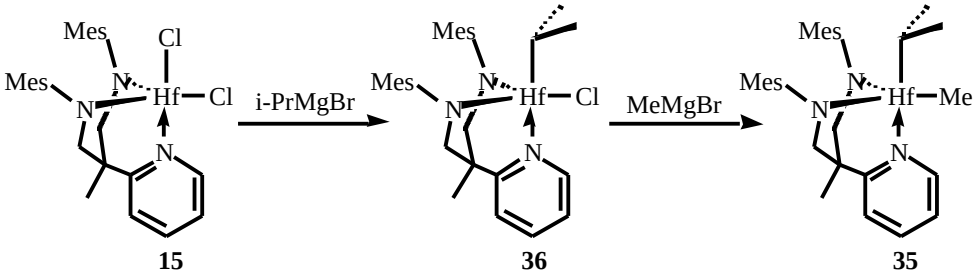

15 **36** **35** (3.1)

The mono-alkylated complex, [MesNpy]Hf(i-Pr)(Cl) (**36**), was prepared by addition of 1 equiv of (i-Pr)MgCl to [MesNpy]HfCl$_2$. Complex **36** is readily isolated and recrystallized from diethyl ether. The ^{1}H NMR spectrum (21 ˚C, C_6D_6) shows a doublet at 1.48 ppm (6H) and a septet at 0.98 ppm (1H) corresponding to the Hf-CH(CH$_3$)$_2$ methyl and methine protons, respectively. The pyridyl proton is observed at 9.67 ppm, about 1 ppm downfield of the signal for [MesNpy]Hf(i-Pr)$_2$ (**37**) (8.72 ppm). As discussed in Chapter 1, a downfield shift in the *ortho* pyridyl proton is often an indication of halide coordination. Sharp singlets at 2.66 and 1.92 ppm, corresponding to *ortho* methyl groups, indicate that the aryl rings of **36** are subject to restricted rotation. In contrast, for **37** a broad singlet at ~2.3 ppm is observed, which indicates slow rotation of the rings on the NMR time scale.

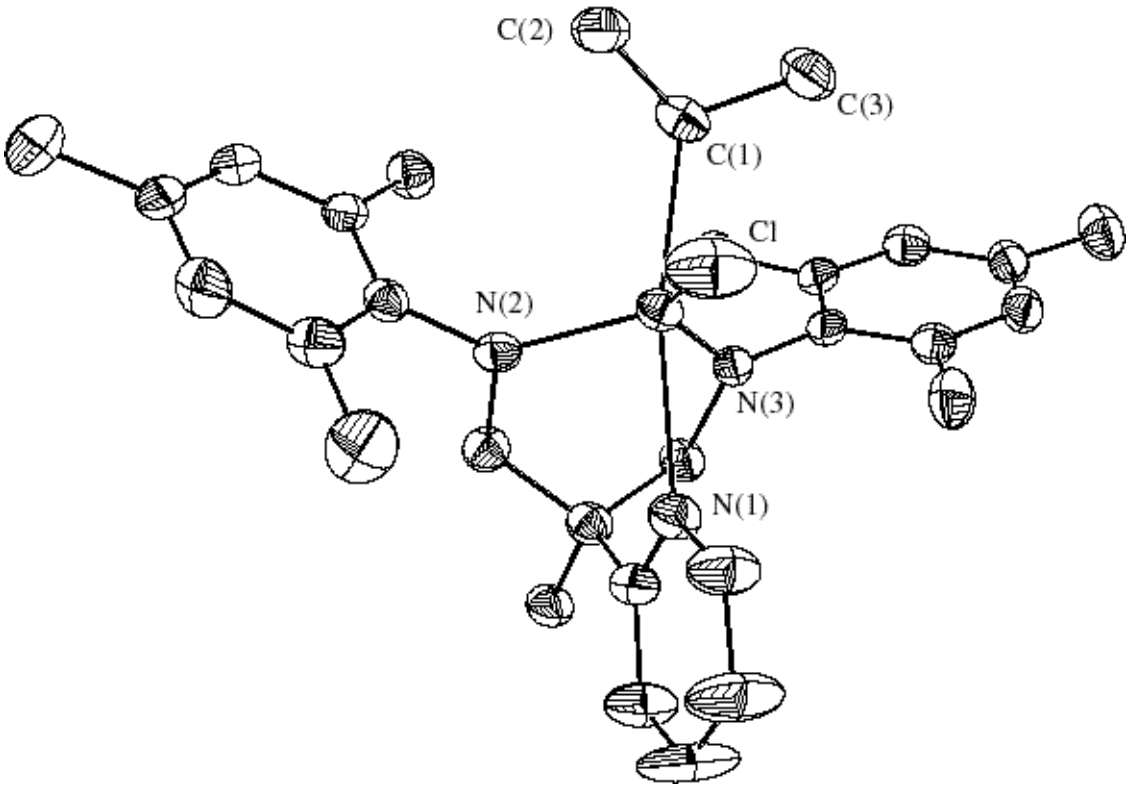

Figure 3.2. Thermal ellipsoid diagram (35% probability level) of [MesNpy]Hf(i-Pr)Cl (**36**).

Table 3.1. Selected bond lengths (Å) and angles (˚) for [MesNpy]Hf(i-Pr)Cl (**36**).

Bond Lengths

Hf-N(1)	2.399(5)	Hf-C(1)	2.252(7)
Hf-N(2)	1.997(5)	Hf-Cl	2.4452(19)
Hf-N(3)	2.031(5)		

Bond Angles

N(1)-Hf-N(2)	83.78(18)	C(1)-Hf-Cl	87.98(19)
N(1)-Hf-C(1)	168.1(2)	N(1)-Hf-N(3)	82.08(18)
N(2)-Hf-C(1)	108.0(2)	N(2)-Hf-N(3)	97.53(18)
N(1)-Hf-Cl	84.96(13)	C(1)-Hf-N(3)	97.4(2)
N(2)-Hf-Cl	118.49(14)	Cl-Hf-N(3)	139.98(15)

The X-ray crystal structure of **36** is similar to that of **37** (Figure 3.2, Table 3.1). The isopropyl group is coordinated in the axial position of a trigonal bipyramid. The Hf-C(1) bond length is 2.252(7) Å and the Hf-Cl bond length is 2.4452(19) Å. Despite the Cl-Hf-N_{amido} angles of 118.49(14)˚ and 139.98(15)˚, the molecule can be considered to have approximately C_s symmetry.

Treatment of **36** with 1.2 equiv of MeMgBr leads to two major products, [MesNpy]Hf(i-Pr)(Me) (**35**) and [MesNpy]Hf(Me)(i-Pr) (**35'**), in which the isopropyl group is coordinated in the axial and equatorial positions, respectively. Two minor species, [MesNpy]$HfMe_2$ (**16**) and [MesNpy]Hf(i-$Pr)_2$ (**37**), are also present in solution. These minor products may be the result of intermolecular alkyl exchange between **35**, **35'** and excess MeMgBr.

Activation of **35** with 1 equiv of $[Ph_3C][B(C_6F_5)_4]$ leads to a mixture of $\{[(MesNpy)Hf]_2Me_3\}\{B(C_6F_5)_4\}$ (**17**) and $[(MesNpy)Hf(CH_2CH(CH_3)(i\text{-}Pr))][B(C_6F_5)_4]$ (**39**). Signals for $[(MesNpy)Hf(i\text{-}Pr)][B(C_6F_5)_4]$ (**38**) and Ph_3CCH_3, resulting from direct methyl abstraction from **35** or **35'**, were not observed. Scheme 3.5 outlines a possible route to the observed complexes.

The activation proceeds exclusively *via* β-hydride abstraction to yield Ph_3CH and $[(MesNpy)Hf(Me)(CH_2{=}CH(CH_3)][B(C_6F_5)_4]$, which affords $[(MesNpy)HfMe][B(C_6F_5)_4]$ *via* loss of propene. Signals for $[(MesNpy)HfCH_2CH(CH_3)_2][B(C_6F_5)_4]$, the first 1,2 insertion product of propene into a hafnium methyl cation, were not observed. The hafnium methyl cation is likely immediately bridged by **35** to yield a methyl bridged complex. These methyl-bridged dinuclear species have been shown to be labile in solution, and it is possible to envision a pathway that leads to **17** (Scheme 3.5) *via* this species. The dinuclear species, **17**, has been independently prepared by activation of [MesNpy]$HfMe_2$ (**16**) with $[Ph_3C][B(C_6F_5)_4]$ (Chapter 1). Important ^{1}H NMR chemical shifts for **17** are a broad methyl signal at ~1.1 ppm and a broad pyridyl signal at ~8.1 ppm (20 ˚C, C_6D_5Br). The backbone signals are the usually observed doublets. The pyridyl signal for **39** is observed at 8.4 ppm, and the backbone signals are split

into AB doublets as asymmetry is introduced in the molecule. A trace of methane is also observed.

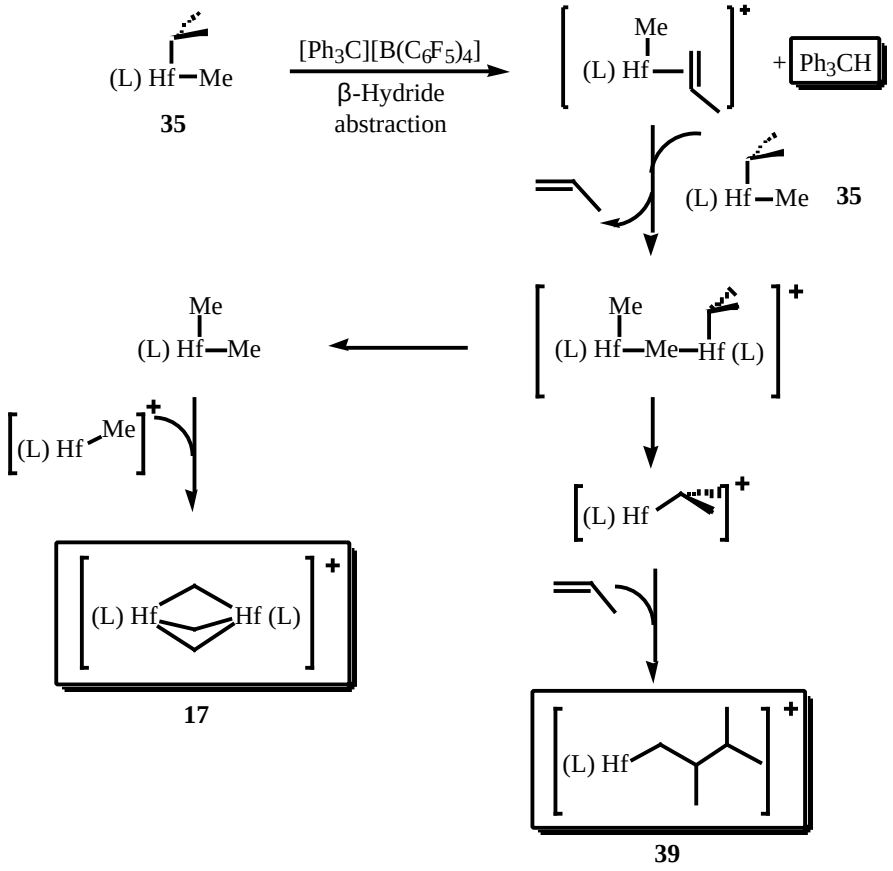

Scheme 3.5. Activation of **35** with 1 equiv of $[Ph_3C][B(C_6F_5)_4]$ (0 ˚C, C_6D_5Br). L = $[MesNpy]^{2-}$, anion = $[B(C_6F_5)_4]^-$. Observed species are framed.

A similar phenomenon is observed when **35** is activated with $[HNMe_2Ph][B(C_6F_5)_4]$, however in this case the major products are $\{[(MesNpy)Hf]_2Me_3\}\{B(C_6F_5)_4\}$ (**17**) and $[(MesNpy)Hf(i\text{-}Pr)][B(C_6F_5)_4]$ (**38**) (Scheme 3.6). The methyl and methine ^1H NMR signals (20 ˚C, C_6D_5Br) for the isopropyl group of **38** are clearly discernable at 0.91 and 0.66 ppm. Association of dimethylaniline to stabilize **38** is a possibility, although only sharp signals suggestive of free base were observed in solution.

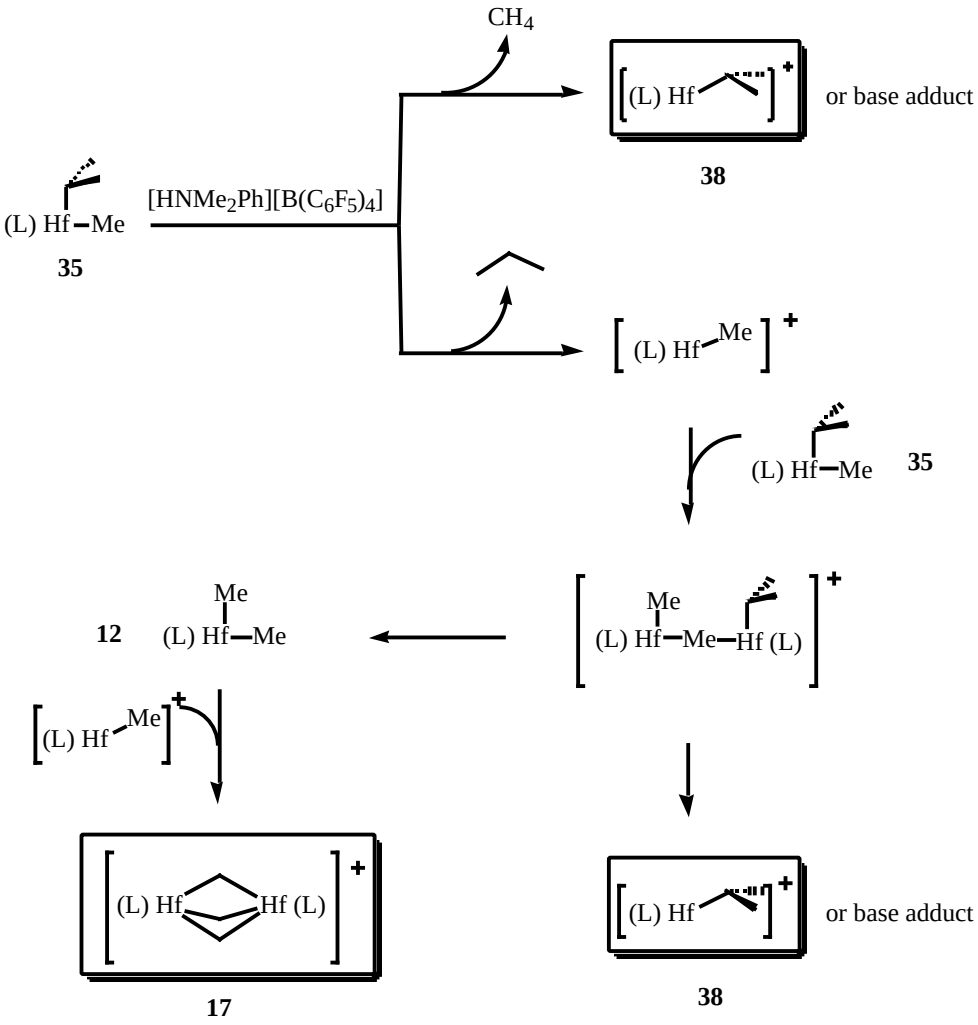

Scheme 3.6 Activation of **35** with 1 equiv of $[HNMe_2Ph][B(C_6F_5)_4]$ (0 ˚C, C_6D_5Br). L = $[MesNpy]^{2-}$, anion = $[B(C_6F_5)_4]^-$.

These experiments highlight the importance of methyl bridges discussed at length in Chapter 1. It appears that mixed alkyl complexes containing methyl groups are not suitable precatalysts in the diamidopyridine systems, due to methyl exchange equilibria in both the neutral and cationic complexes.

3.5 [MesNpy]Hf(i-Pr)$_2$

The complex [MesNpy]Hf(i-Pr)$_2$, **37**, was also found to be stable in solution at room temperature for several hours in solution or in the solid state. The ^{1}H NMR (22 ˚C, C_6D_5Br) resonances for the Hf-C*H* protons are observed at 0.09 and 0.51 ppm, while the respective $^{13}C\{^1H\}$ signals are observed at 65.9 and 68.2 ppm.

Due to lack of structural information about group IV diisopropyl complexes, complex **37** was characterized by X-ray crystallography (Figure 3.3, Table 3.2). Examples of isopropyl complexes of later transition metals have been reported.[80-85] The structure of **37** is similar to that of other dialkyl complexes which bear a diamidopyridine ligand, however there is some asymmetry in the molecule. Table 3.3 is a summary of bond lengths and angles for various diamidopyridine dialkyl complexes of zirconium and hafnium. The Hf-C bond lengths in **37** (2.3 Å) are quite similar to those found for [MesNpy]ZrMe$_2$ and [TripNpy]Zr(i-Bu)$_2$. In **37** the N(1)-Hf-C(ax) angle is 105.57(15)˚, while the N(2)-Hf-C(ax) angle is 98.94(14)˚, indicating that the axial isopropyl group is closer to N(2). Conversely, the equatorial isopropyl group is closer to N(1); N(1)-Hf-C(eq) = 122.75(17)˚ and N(2)-Hf-C(ax) = 134.62(17)˚. Again, these angles are nearly identical in the other two zirconium dialkyl complexes. Thus the geometry of **37** seems to be slightly skewed to accommodate the steric bulk of the isopropyl groups.

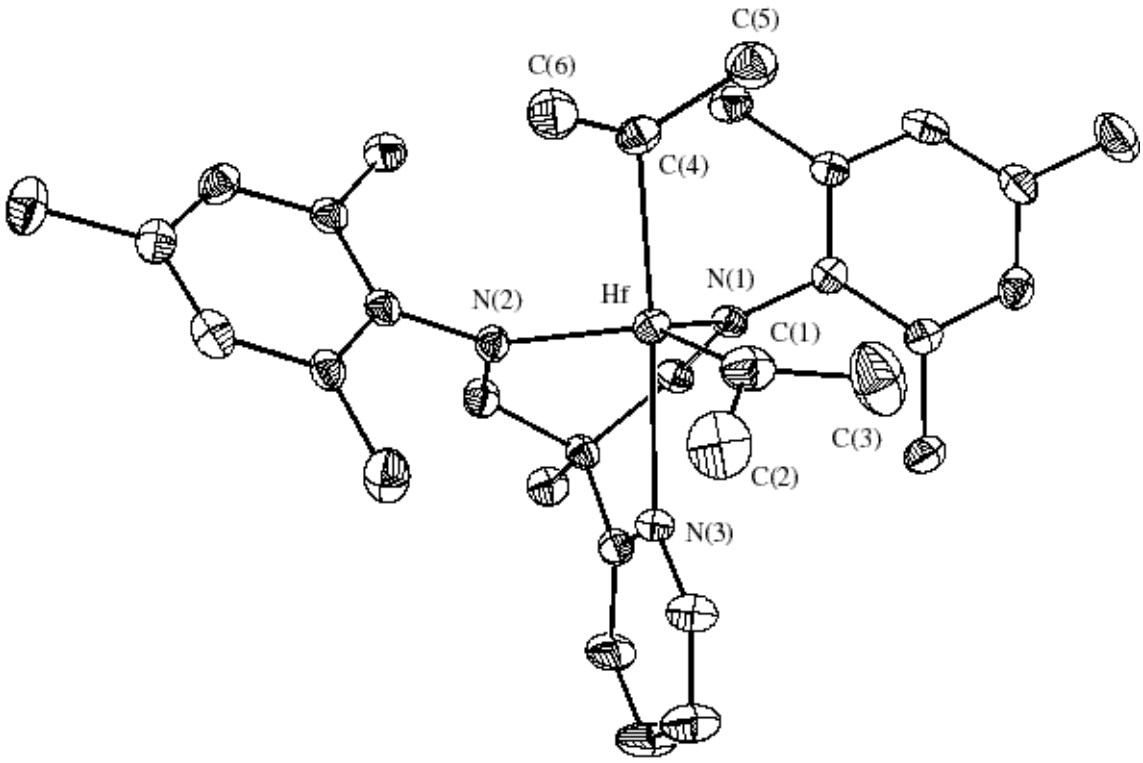

Figure 3.3. Thermal ellipsoid diagram (35% probability level) of [MesNpy]Hf(i-Pr)$_2$ (**37**).

Table 3.2. Selected bond lengths (Å) and angles (˚) for [MesNpy]Hf(i-Pr)$_2$ (**37**).

Bond Lengths

Hf-N(1)	2.032(3)	Hf-C(4)	2.297(4)
Hf-N(2)	2.035(3)	Hf-C(1)	2.268(5)
Hf-N(3)	2.412(3)		

Bond Angles

N(1)-Hf-N(2)	98.94(14)	C(4)-Hf-C(1)	88.24(18)
N(1)-Hf-C(4)	105.57(15)	N(1)-Hf-N(3)	81.14(12)
N(2)-Hf-C(4)	97.72(15)	N(2)-Hf-N(3)	81.34(13)
N(1)-Hf-C(1)	122.75(17)	C(4)-Hf-N(3)	173.28(14)
N(2)-Hf-C(1)	134.62(17)	C(1)-Hf-N(3)	87.73(16)

Table 3.3. A comparison of bond lengths (Å) and angles (˚) for three different dialkyl complexes bearing a diamidopyridine ligand.

	[MesNpy]ZrMe$_2$	[TripNpy]Zr(i-Bu)$_2$	[MesNpy]Hf(i-Pr)Cl	[MesNpy]Hf(i-Pr)$_2$
M-N(1)	2.027(3)	2.047(4)	1.997(5)	2.032(3)
M-N(2)	2.034(3)	2.047(4)	2.031(5)	2.035(3)
M-N(py)	2.444(4)	2.483(4)	2.339(5)	2.412(3)
M-C(ax)	2.284(6)	2.253(5)	2.252(7)	2.297(4)
M-X	2.294(5)	2.258(7)	2.445(2)	2.268(5)
N(2)-M-N(1)	102.24(12)	98.46(16)	97.35(18)	98.94(14)
N(1)-M-C(ax)	102.2(2)	102.31(17)	108.0(2)	105.57(15)
N(2)-M-C(ax)	101.2(2)	104.35(18)	97.4(2)	97.72(15)
N(1)-M-X	125.55(19)	130.2(3)	118.49(14)	122.75(17)
N(2)-M-X	127.74(19)	125.0(3)	139.98(15)	134.62(17)
C(ax)-M-X	89.1(2)	90.4(2)	87.98(19)	88.24(18)
N(1)-M-N(py)	80.81(14)	80.03(13)	83.78(18)	81.14(12)
N(2)-M-N(py)	80.58(14)	81.18(14)	82.08(18)	81.34(13)
C(ax)-M-N(py)	175.96(19)	173.46(18)	168.1(2)	173.28(14)
X-M-N(py)	86.9(2)	83.5(2)	84.96(13)	87.73(16)

N(1) and N(2) = Equatorial amido nitrogens; N(py) = Pyridyl nitrogen;
C(ax) and C(eq) = Metal-bound carbon of axial and equatorial alkyl groups, X = C(eq) or Cl for **36**

3.5.1 Activation of [MesNpy]Hf(i-Pr)$_2$ with [Ph$_3$C][B(C$_6$F$_5$)$_4$]

Activation of [MesNpy]Hf(i-Pr)$_2$ (**37**) with 1 equiv of [Ph$_3$C][B(C$_6$F$_5$)$_4$] leads to two major cationic species: the isopropyl cation [(MesNpy)Hf(i-Pr)][B(C$_6$F$_5$)$_4$] (**38**) and the product of 1,2-insertion of propene [(MesNpy)Hf(CH$_2$CH(CH$_3$)(i-Pr))][B(C$_6$F$_5$)$_4$] (**39**) (Scheme 3.7). The main by-product of this reaction is Ph$_3$CH. Signals for the alkyl abstraction product, Ph$_3$CCH(CH$_3$)$_2$ were not detected, indicating that β-hydride abstraction is the sole mechanism of activation in this system. Observation of **38** is attributed to the dissociation of propene from the putative Hf(propyl)(propene) intermediate. Liberated propene then reinserts into **38** to form **39**, or into **39** to form other hafnium alkyl cations, traces of which are observed in the ^{1}H NMR spectra of the solution mixture.

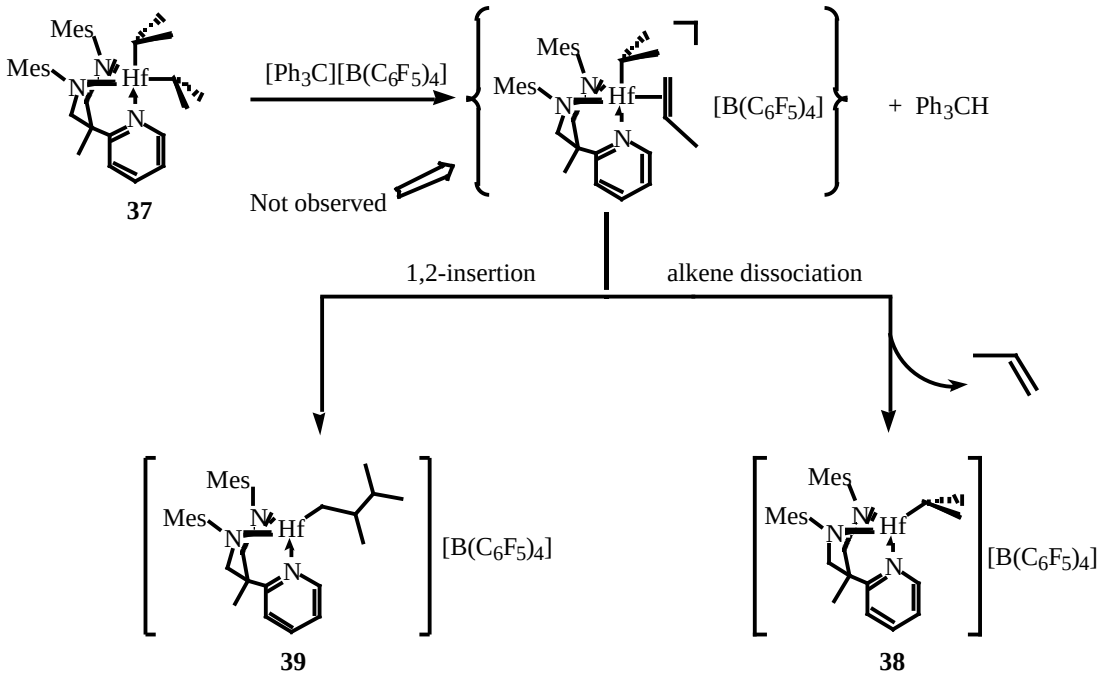

Scheme 3.7. Activation of **37** with $[Ph_3C][B(C_6F_5)_4]$ (–20 ˚C, C_6D_5Br). L = $[MesNpy]^{2-}$, anion = $[B(C_6F_5)_4]^-$.

A ^{13}C DEPT experiment (0 ˚C, C_6D_5Br) reveals a signal at 88.5 ppm corresponding to the Hf-*C*H_2R carbon in **39** and a signal at 79.0 ppm corresponding to the Hf-*C*HMe_2 carbon in **38**. Signals for two other methine carbon atoms belonging to **39** were observed at 41.5 and 37.5 ppm, as well as four methyl signals corresponding to the non-ligand methyls on **38** and **39** (Figure 3.4). Assignment of the ^1H NMR spectrum was complicated by overlapping peaks, however the signal for the *ortho* pyridyl proton is quite distinctive and it is possible to assign the signal at 8.47 ppm to **39** and the one at 8.35 ppm to **38**. The ratio of **39**:**38** is 4.2:1 at –20 ˚C, however if the temperature is raised to 0 ˚C, this ratio changes to 6.7:1, *i.e.* the amount of **38** is decreased at 0 ˚C due to irreversible decomposition.

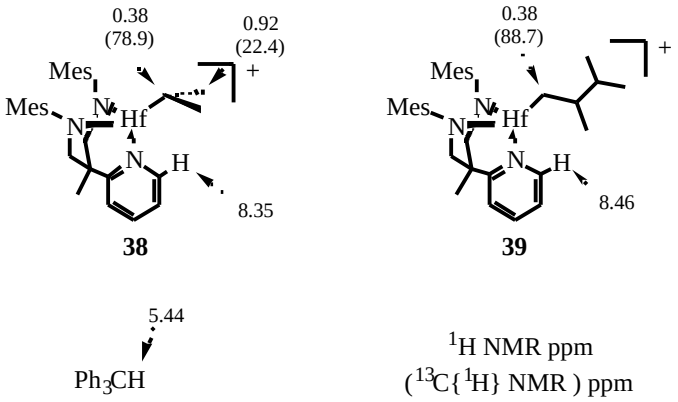

Figure 3.4. Species present in solution upon activation of **37** with $[Ph_3C][B(C_6F_5)_4]$ (–20 ˚C, C_6D_5Br).

Rearrangement of **38** to a hafnium n-propyl cation, **33**, is not observed. A solution containing a mixture of **38** and **39** showed no change over 1 h at 0 ˚C. Storage of the same solution at 10 ˚C for 24 h leads to the disappearance of the signals for **38** and the appearance of two new ^{1}H NMR signals at 4.68 and 4.73 ppm corresponding to vinylidene protons of a β-hydride elimination product (most likely CH_2=CMeCHMe_2, *vide infra*). The ^{13}C DEPT spectrum also shows a signal at 107 ppm corresponding to a *C*H_2=R'R" methylene carbon. This mode of decomposition is to be expected, as β-hydride elimination above 0 ˚C was responsible for chain termination in olefin polymerization reactions with $[(MesNpy)Zr(i\text{-}Bu)][B(C_6F_5)_4]$ (Chapter 2).

Decomposition may occur *via* β-hydride elimination of **38** to yield propene and an unstable hydride complex which is consumed in various side reactions. The propene can then insert into unreacted **38** to yield **39**, or further insert in **39** to yield multiple insertion products. If one assumes that **38** and **39** decompose *via* β-hydride elimination processes, it is possible to propose a pathway for the disappearance of the cation signals belonging to these species and the appearance of the olefinic peaks belonging to CH_2=CMeCHMe_2 (Scheme 3.8). Signals for free propene are not observed.

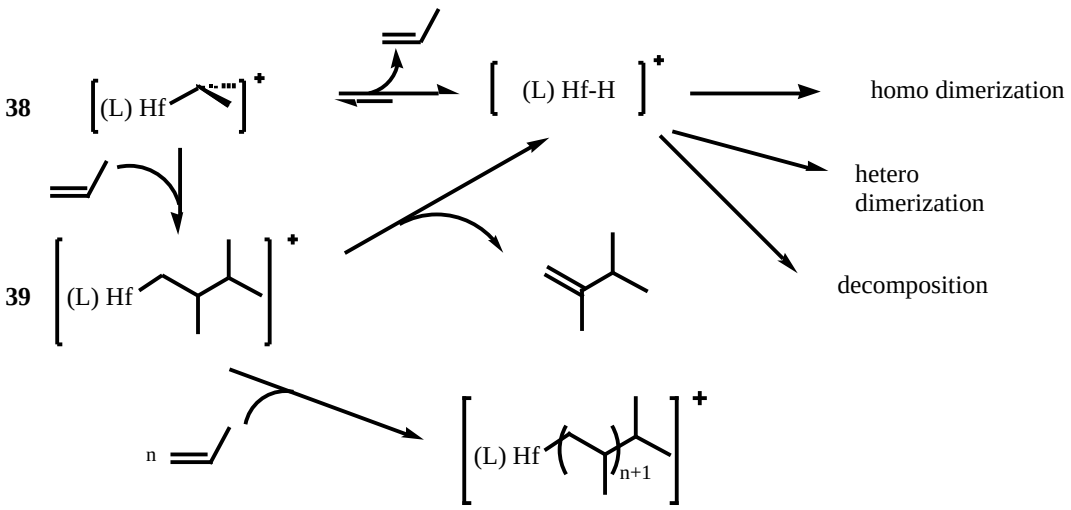

Scheme 3.8. Decomposition pathways for a $[Ph_3C][B(C_6F_5)_4]$ activated solution of **37**. L = $[MesNpy]^{2-}$, $[B(C_6F_5)_4]^-$.

Attempts were made to study the kinetics of decomposition for the various species in solution at 10 and 25 ˚C. No significant change was observed at 10 ˚C for these species over the course of 2 h. However, the decomposition processes could be studied at 25 ˚C. The isopropyl cation, **38**, is significantly less stable than the first insertion product, **39**. Thus **38** is completely decomposed after 80 min at 25 ˚C, while decomposition of **39** has not yet spanned one half life.

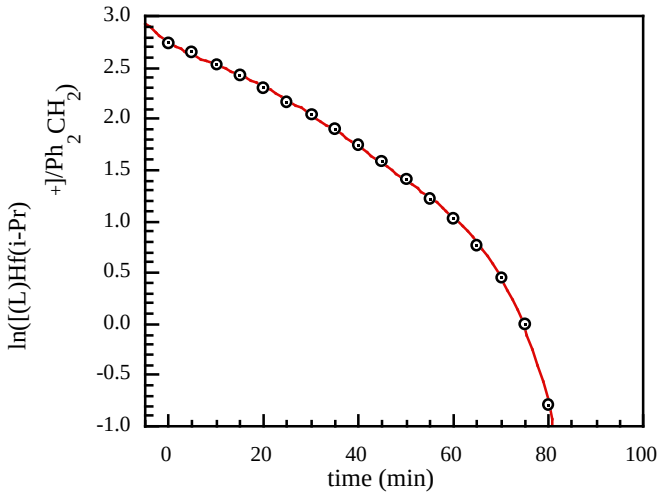

Figure 3.5. Plot of ln[**38**/Ph_2CH_2] vs. time (min) for decomposition of an activated solution of **37** (0.024 M) (25 ˚C, C_6D_5Br).

The plot of ln(**38**/Ph_2CH_2) vs. time is not linear, indicating that disappearance of the isopropyl cation is not a first order process (Figure 3.5). From the first 8 data points in the plot, a decomposition rate of 0.0242(7) min^{-1} (4.03(12) × 10^{-4} s^{-1}). This result may be partially explained by the mechanism outlined in Scheme 3.8, as **38** would be converted to **39** in a second order process, as well as a hafnium hydride species. In contrast, the decomposition of the first insertion product **39** proceeds *via* an apparent first order route with an observed rate of 0.0081(1) min^{-1} (1.3(2) × 10^{-4} s^{-1}) (Figure 3.6). These observations confirm that the complex containing a secondary alkyl group, **38**, is significantly less stable than the complex with a primary alkyl group, **39**.

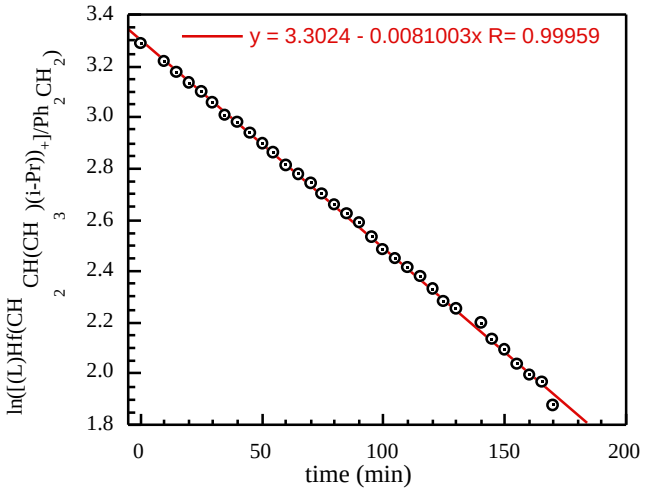

Figure 3.6. Plot of ln[**39**/Ph_2CH_2] vs. time (min) for decomposition of an activated solution of **37** (0.024 M) (25 ˚C, C_6D_5Br).

3.5.2 Activation of [MesNpy]Hf(i-Pr)$_2$ with [HNMe$_2$Ph][B(C$_6$F$_5$)$_4$]

When **37** is activated with [$HNMe_2Ph$][$B(C_6F_5)_4$] the only possible mode of activation is protonation of one isopropyl group to yield **38** along with the by-products NMe_2Ph and propane (eq 3.2).

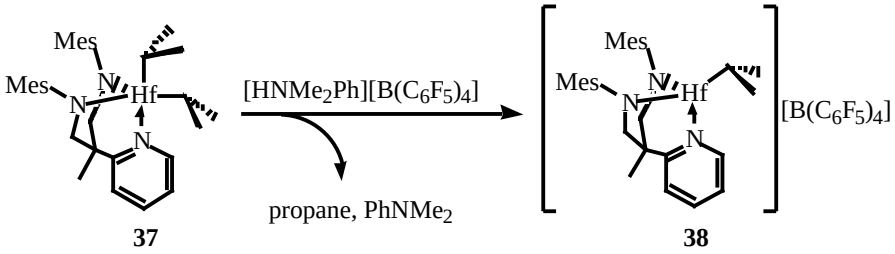

(3.2)

The ^{1}H NMR (20 ˚C, C_6D_5Br) spectrum for **38** is presented in Figure 3.7. The resonances correspond closely to those previously assigned in a mixture (Figure 3.4). In the ^{1}H NMR

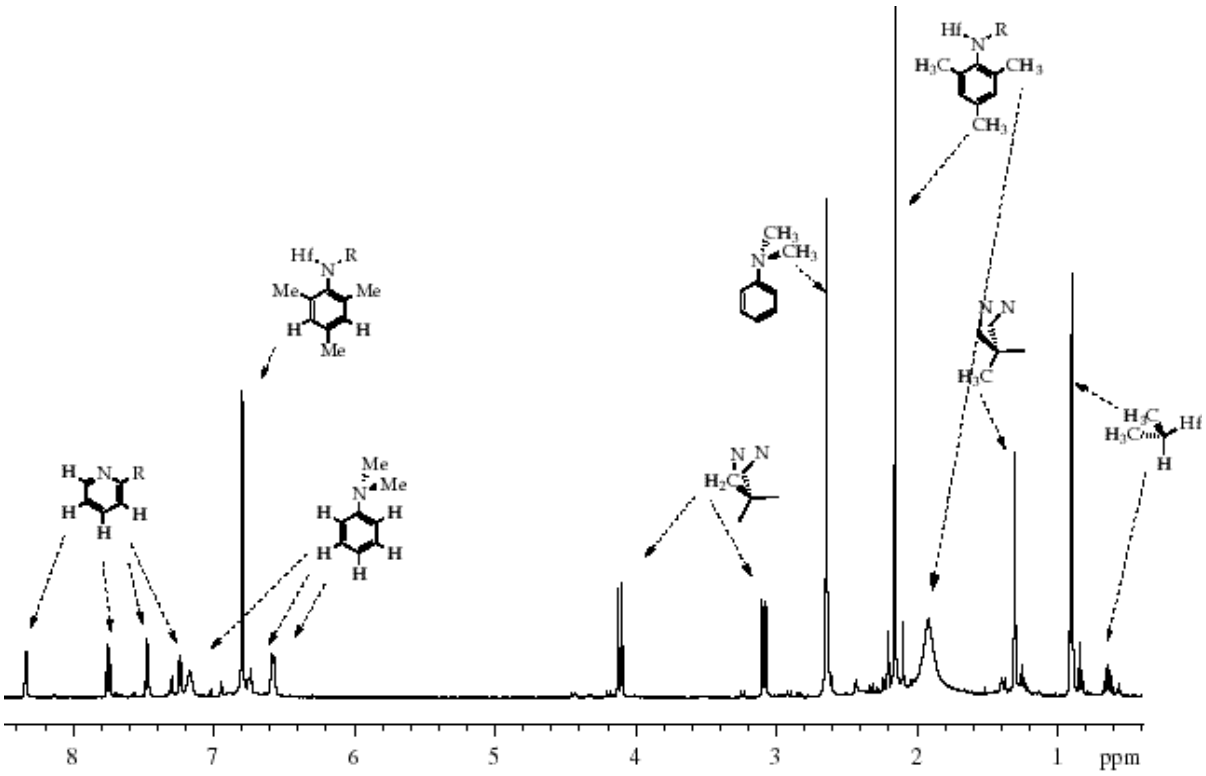

Figure 3.7. ^{1}H NMR spectrum (20 ˚C, C_6D_5Br) of **37** activated with $[HNMe_2Ph][B(C_6F_5)_4]$.

spectrum, the *ortho* pyridyl proton is observed at 8.33 ppm, and a doublet (6H) and a multiplet (1H) corresponding to the methyl and methine protons of the hafnium-bound isopropyl group are

observed at 0.90 and 0.64 ppm, respectively. Signals for free dimethyl aniline are observed at 2.64, 6.58, 6.74 and 7.17 ppm.

Addition of 80 equiv of 1-hexene to a solution of **37** activated with $[HNMe_2Ph][B(C_6F_5)_4]$ at 0 ˚C results in the consumption of all the olefin within the first 50 min in two independent experiments (Figure 3.8). The plots of ln([1-hexene]/Ph_2CH_2) vs. time are linear in this time period, leading to k_p values of 4.5(2) and 4.4(2) M^{-1} min^{-1} (0.075(3) and 0.074(3) M^{-1} s^{-1}).

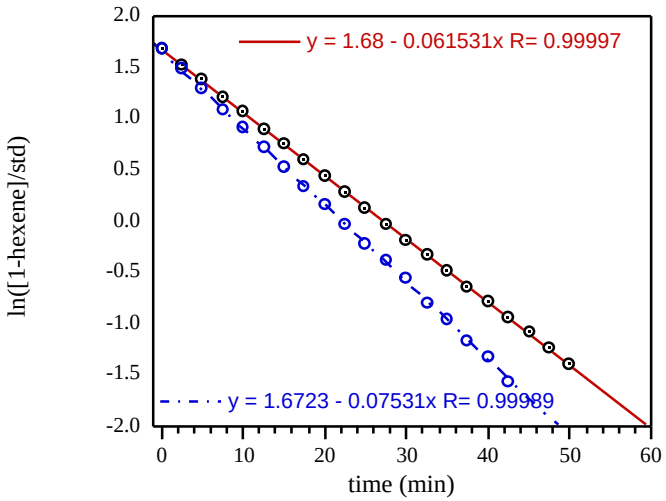

Figure 3.8. Plots of ln([1-hexene]/Ph_2CH_2) vs. time (min) for additions of 1-hexene to **38** (0.015 M) in the presence of 1 equiv NMe_2Ph (0 ˚C, C_6D_5Br).

During the polymerization process, a new doublet at 9.01 ppm is observed in the ^1H NMR spectrum (Figure 3.9). The signal for this *ortho* pyridyl proton as well as signals for the ligand backbone correspond to the product of dimethylaniline C-H activation $[(MesNpy)Hf(C_6H_4NMe_2)][B(C_6F_5)_4]$ (**40**). This compound is also observed in inhibition studies with NMe_2Ph and has been independently isolated and characterized (Chapter 4). Equation 3.3 summarizes the process observed during polymerization of 1-hexene with **37** activated with $[HNMe_2Ph][B(C_6F_5)_4]$.

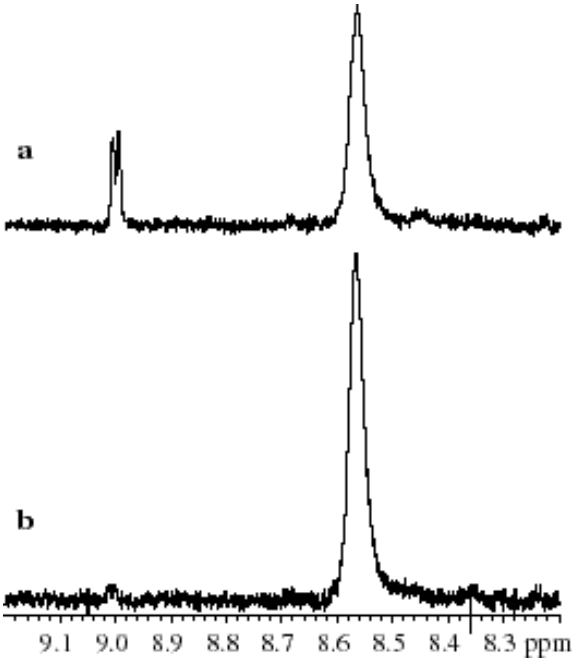

Figure 3.9. ^{1}H NMR spectra (0 ˚C, C_6D_5Br) for the *ortho* pyridyl region after addition of 1-hexene to a solution of **37** activated with $[HNMe_2Ph][B(C_6F_5)_4]$ a) after 1 h; b) initially.

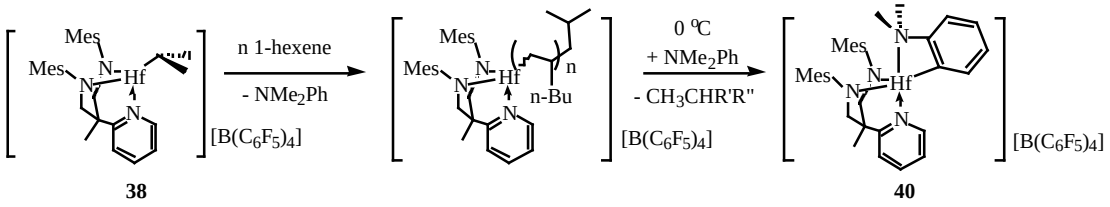

38 **40** (3.3)

The generation of NMe_2Ph which is prone to C-H activation makes $[HNMe_2Ph][B(C_6F_5)_4]$ an unsuitable activator for the diamidopyridine dialkyl complexes. Reaction of NMe_2Ph with hafnium isobutyl cations will be discussed further in Chapter 4.

3.5.3 Activation of [MesNpy]Hf(i-Pr)$_2$ with B(C_6F_5)$_3$

Activation of [MesNpy]Hf(i-Pr)$_2$ (**37**) with $B(C_6F_5)_3$ results in β-hydride abstraction to yield the first insertion product $[(MesNpy)Hf(CH_2CHMe(i\text{-}Pr))][HB(C_6F_5)_3]$ (**41**) exclusively (eq

3.4). The chemical shifts for **41** are similar to those for the first insertion product **39** generated

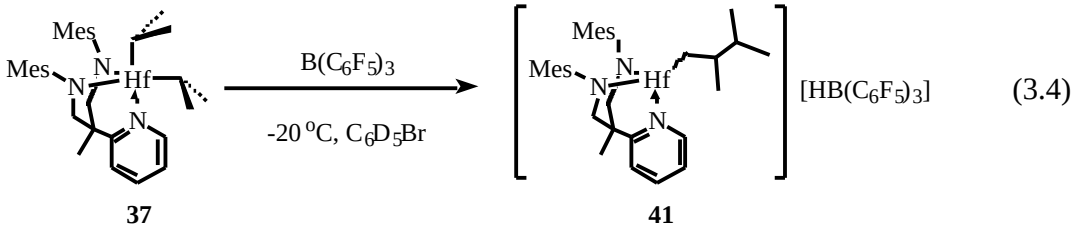

37 **41** (3.4)

by activation of **37** with $[Ph_3C][B(C_6F_5)_4]$ (Figure 3.4). In the ^{1}H NMR spectrum (0 ˚C, C_6D_5Br), the *ortho* pyridyl proton is observed at 8.65 ppm, the backbone signals are asymmetric as the plane of symmetry present in **38** is not present in **41** (Figure 3.10). The aliphatic methyl, methylene and methine protons can be observed and assigned by a gCOSY experiment.

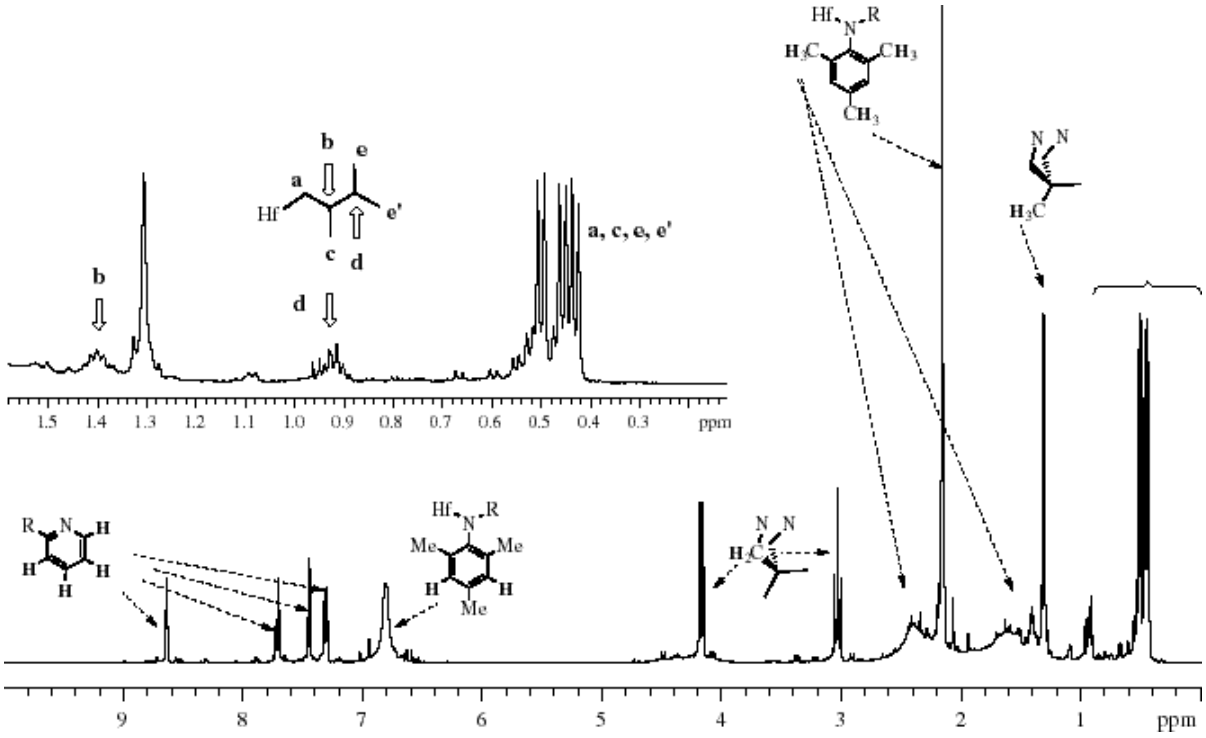

Figure 3.10. ^{1}H NMR spectrum (0 ˚C, C_6D_5Br) of **41**.

The $^{13}C\{^{1}H\}$ spectrum (0 ˚C, C_6D_5Br) shows a signal for Hf-*C*H_2R'R" at 87.42 ppm, and the ^{19}F NMR spectrum shows only one set of signals for the anion, $[HB(C_6F_5)_3]^-$. Signals for unreacted $B(C_6F_5)_3$ are not observed.

Addition of 90 equiv of 1-hexene to a solution of **41** in two independent experiments results in the first order consumption of olefin in both runs (Figure 3.11). The k_p values obtained are 2.75(6) M^{-1} min^{-1} (0.046(1) M^{-1} s^{-1}) and 3.1(1) M^{-1} min^{-1} (0.051(2) M^{-1} s^{-1}). These values correspond closely to polymerization rates obtained for $[(MesNpy)Hf(i\text{-}Bu)][HB(C_6F_5)_3]$ (2.87(7) M^{-1} min^{-1}, 0.048(1) M^{-1} s^{-1}) and illustrate an anion effect more fully explored in Chapter 4.

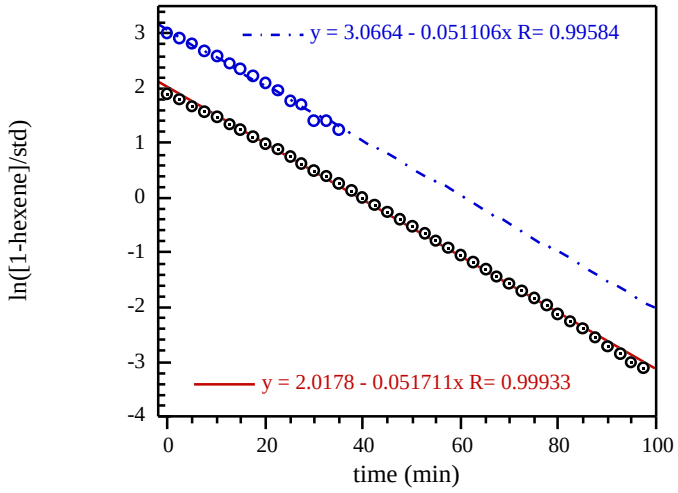

Figure 3.11. Plots of ln([1-hexene]/Ph_2CH_2) vs. time (min) for additions of 1-hexene to **41** (0.015 M) (0 ˚C, C_6D_5Br).

The diisopropyl system highlights the importance of the activator to the activation process. Activation of **37** with $[Ph_3C][B(C_6F_5)_4]$ leads to β-hydride abstraction which yields the isopropyl cation, **38**, and the first insertion product, **39**, both associated with the $[B(C_6F_5)_4]$ anion in solution. The $[HNMe_2Ph][B(C_6F_5)_4]$ activator leads to only one product, **38**, as protonation is the only activation mechanism in this case.

The neutral $B(C_6F_5)_3$ activator reacts by β-hydride abstraction, but for reasons as yet unclear, results only in the first insertion product bearing the $[HB(C_6F_5)_3]$ anion, **41**. One can speculate that the anion has a role in preventing olefin dissociation from the hafnium (isopropyl) (propene) intermediate that would have resulted in the formation of the [(MesNpy)Hf(i-Pr)][$HB(C_6F_5)_3$] cation, in a manner represented in Scheme 3.7.

Scheme 3.9 is a summary of the activation pathways for **37**.

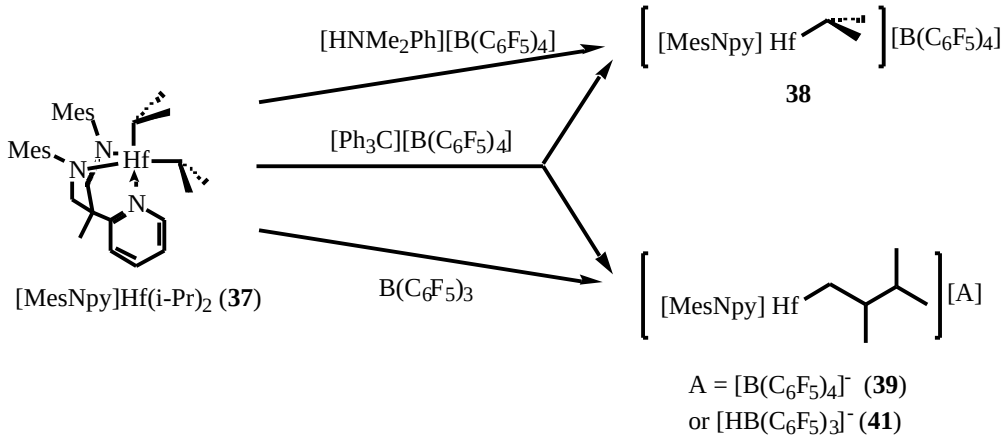

Scheme 3.9. Activation of [MesNpy]Hf(i-Pr)$_2$ with three different activators**.**

3.6 Conclusions

Chapter 3 described the synthesis and activation of series of β C-H containing dialkyl hafnium complexes of the type [MesNpy]HfR_2 where R = Et, n-Pr, n-Bu and i-Pr. Activation of these complexes with the $[Ph_3C][B(C_6F_5)_4]$, $[HNMe_2Ph][B(C_6F_5)_4]$, and $B(C_6F_5)_3$ activators afforded important insights into the activator initiator relationship in these systems.

Activation of [MesNpy]$HfEt_2$ (**28**) with $[Ph_3C][B(C_6F_5)_4]$ led to both β-hydride abstraction as well as direct alkyl abstraction. This case illustrates the two competing pathways when $[Ph_3C][B(C_6F_5)_4]$ is used as an activator for a β-hydride containing system. In systems with bulkier alkyl groups β-hydride abstraction is the only mode of activation.

Activation of [MesNpy]Hf(i-Pr)$_2$ (**37**) with each of the three activators gave a different result. When [Ph_3C][$B(C_6F_5)_4$] was used, β-hydride abstraction was the only activation mechanism, leading to generation of [(MesNpy)Hf(i-Pr)][$B(C_6F_5)_4$] (**38**) and [(MesNpy)Hf($CH_2CH(CH_3)$(i-Pr))][$B(C_6F_5)_4$] (**39**), the product of propene 1,2-insertion. It was possible to study the decomposition rates of **38** and **39** and determine that **38**, the secondary alkyl cation, is considerably less stable than **39**, a primary alkyl cation. When [$HNMe_2Ph$][$B(C_6F_5)_4$] is used to activate **37**, the sole product is **38**. However if $B(C_6F_5)_3$ is used, β-hydride abstraction occurs to yield the first 1,2-insertion product, [(MesNpy)Hf($CH_2CH(CH_3)$(i-Pr))][$HB(C_6F_5)_3$] (**41**), exclusively. In this case $[HB(C_6F_5)_3]^-$ is the anion, and it may play a role in the selectivity of this reaction.

The hafnium [MesNpy] system leads to relatively stable alkyl cations. The living polymerization of α-olefins with this system will be discussed in the next chapter.

3.7 Experimental section

General Procedures. All manipulations, with the exception of the synthesis of ligand precursors, were performed under N_2 in a glove-box or using standard Schlenk procedures. Solvents were dried using conventional procedures.[60] Chlorobenzene (HPLC grade) and deuterated solvents were degassed, stored over and distilled from CaH_2. Commercial reagents were used without further purification. NMR spectra were recorded on a Varian INOVA 500 spectrometer. ^{1}H NMR chemical shifts are given in ppm versus residual protons in the deuterated solvents as follows: δ 7.16 C_6D_6, δ 2.09 toluene-d_8 (methyl), δ 7.29 C_6D_5Br (most downfield resonance). $^{13}C\{^1H\}$ NMR chemical shifts are given in ppm versus residual ^{13}C in the solvents as follows: δ 128.39 C_6D_6, δ 20.4 toluene-d_8 (methyl), δ 122.25 C_6D_5Br (most upfield resonance). Some aryl resonances in ^{1}H and $^{13}C\{^1H\}$ spectra are not given.

Elemental analyses were performed by H. Kolbe, Mikroanalytisches Laboratorium (Mülheim an der Ruhr, Germany). X-ray data were collected on a Siemens SMART/CCD diffractometer with λ(MoKα) = 0.71073 Å and solved using a full-matrix least squares refinement on F^2.

All Grignard reagents were carefully titrated with 2-butanol in the presence of 1,10-phenanthroline prior to use. [MesNpy]H_2[26] and Hf(NMe_2)$_4$[61] have been prepared according to previously reported methods. Syntheses of [MesNpy]Hf(NMe_2)$_2$ and [MesNpy]$HfCl_2$ are described in Chapter 1.

[MesNpy]$HfEt_2$ (28). A suspension of [MesNpy]$HfCl_2$ (0.210 g, 0.324 mmol) in diethyl ether (50 mL) was cooled to -30 ˚C. To the cold solution was added EtMgBr (2.0 M in diethyl ether, 0.34 mL, 0.68 mmol) and the resulting mixture was stirred at room temperature for 10 min until the cloudy suspension became clear. Dioxane (0.07 mL, 0.81 mmol) was added to the solution and the resulting white solid was filtered through Celite. The solvent was removed *in vacuo* to yield a white powder, which was redissolved in 5 mL diethyl ether and crystallized at -30 ˚C for 16 h as white crystals. Yield: 0.098g, 48%. ^{1}H NMR (500 MHz, C_6D_5Br, 255 K) δ 0.53 (m, 4H, Hf-CH_2CH$_3$), 1.19 (s, 3H, CH_3), 1.34 (t, 3H, Hf-CH$_2$CH_3), 1.57 (d, 3H, Hf-CH$_2$CH_3), 2.17 (s, 6H, *p*-CH_3), ~2.2 (broad s, 12H, *o*-CH_3), 2.83 (d, 2H, CH_2), 4.13 (d, 2H, CH_2), 6.83 (s, 4H, C*H*), 6.99 (m, 1H, py-C*H*), 7.12 (m, 1H, py-C*H*), 7.45 (m, 1H, py-C*H*), 8.81 (m, 1H, py-*o*-C*H*). ^{13}C{^{1}H} NMR (125 MHz, C_6D_5Br, 255 K) δ 11.74 (s, Hf-CH$_2$*C*H$_3$), 13.63 (s, Hf-CH$_2$*C*H$_3$), 18.78 (s, *o*-*C*H$_3$), 20.99 (s, *p*-*C*H$_3$), 25.13 (s, *C*H$_3$), 44.91 (s, *C*R$_4$), 57.24 (s, Hf-*C*H$_2$CH$_3$), 59.39 (s, Hf-*C*H$_2$CH$_3$), 64.97 (s, *C*H$_2$), 120.65 (s, Ar-*C*), 121.97 (s, Ar-*C*), 122.61 (s, Ar-*C*), 131.16 (s, Ar-*C*), 132.89 (s, Ar-*C*), 139.15 (s, Ar-*C*), 146.07 (s, Ar-*C*), 146.19 (s, Ar-*C*), 162.05 (s, Ar-*C*). Anal. Calcd for $C_3H_{43}N_3Hf$: C, 58.53; H, 6.81; N, 6.60. Found: C, 58.40; H, 6.88; N, 6.53.

[MesNpy]Hf(n-Bu)$_2$ (32). A suspension of [MesNpy]HfCl$_2$ (0.265 g, 0.408 mmol) in diethyl ether (10 mL) was cooled to -30 ˚C. To the cold solution was added (n-Bu)MgBr (2.0 M in diethyl ether, 0.43 mL, 0.81 mmol) and the resulting mixture was stirred at room temperature for 10 min until the cloudy suspension became clear. Dioxane (0.1 mL, 1 mmol) was added to the solution and the resulting white solid was filtered through Celite. The solvent was removed *in vacuo* to yield a white powder, which was redissolved in 2 mL diethyl ether and crystallized at -30 ˚C for 16 h and the product isolated as white crystals. Yield: 0.14 g, 50%. ^{1}H NMR (500 MHz, C_6D_5Br, 295 K) δ 0.52 (m, 4H, Hf-C*H*$_2$CH$_2$CH$_2$CH$_3$), 0.73 (t, 3H, Hf-CH$_2$CH$_2$CH$_2$C*H*$_3$), 0.89 (t, 3H, Hf-CH$_2$CH$_2$CH$_2$C*H*$_3$), 1.11 (m, 2H, Hf-CH$_2$CH$_2$C*H*$_2$CH$_3$), 1.21 (s, 3H, C*H*$_3$), 1.40 (m, 2H, Hf-CH$_2$CH$_2$C*H*$_2$CH$_3$), 1.45 (m, 2H, Hf-CH$_2$C*H*$_2$CH$_2$CH$_3$), 1.83 (m, 2H, Hf-CH$_2$C*H*$_2$CH$_2$CH$_3$), 2.16 (s, 6H, *p*-C*H*$_3$), 2.2 (broad s, 12H, *o*-C*H*$_3$), 2.87 (d, 2H, C*H*$_2$), 4.13 (d, 2H, C*H*$_2$), 6.82 (s, 4H, C*H*), 7.02 (m, 1H, py-C*H*), 7.18 (m, 1H, py-C*H*), 7.49 (m, 1H, py-C*H*), 8.90 (m, 1H, py-*o*-C*H*). ^{13}C{^{1}H} NMR (125 MHz, C_6D_5Br, 295 K) δ 14.13 (s, Hf-CH$_2$CH$_2$CH$_2$*C*H$_3$), 14.17 (s, Hf-CH$_2$CH$_2$CH$_2$*C*H$_3$), 18.70 (s, *o*-*C*H$_3$), 20.85 (s, *p*-*C*H$_3$), 25.06 (s, *C*H$_3$), 30.33 (s, Hf-CH$_2$(*C*H$_2$)$_2$CH$_3$), 30.39 (s, Hf-CH$_2$(*C*H$_2$)$_2$CH$_3$), 30.58 (s, Hf-CH$_2$(*C*H$_2$)$_2$CH$_3$), 31.88 (s, Hf-CH$_2$(*C*H$_2$)$_2$CH$_3$), 45.26 (s, *C*R$_4$), 65.22 (s, *C*H$_2$), 66.85 (s, Hf-*C*H$_2$(CH$_2$)$_2$CH$_3$), 69.17 (s, Hf-*C*H$_2$(CH$_2$)$_2$CH$_3$), 120.44 (s, Ar-*C*), 122.46 (s, Ar-*C*), 129.31 (s, Ar-*C*), 129.69 (s, Ar-*C*), 131.27 (s, Ar-*C*), 134.86 (s, Ar-*C*), 139.00 (s, Ar-*C*), 146.06 (s, Ar-*C*), 146.48 (s, Ar-*C*). Anal. Calcd for $C_{35}H_{51}N_3Hf$: C, 60.72; H, 7.43; N, 6.07. Found: C, 60.65; H, 7.37; N, 5.94.

[MesNpy]Hf(n-Pr)$_2$ (31). A suspension of [MesNpy]HfCl$_2$ (0.312 g, 0.481 mmol) in diethyl ether (50 mL) was cooled to -30 ˚C. To the cold solution was added (n-Pr)MgCl (2.0 M in diethyl ether, 0.53 mL, 1.06 mmol) and the resulting mixture was stirred at room temperature for 10 min until the cloudy suspension became clear. Dioxane (0.12 mL, 0.14 mmol) was added to the solution and the resulting white solid was filtered through Celite. The solvent was removed

in vacuo to yield a white powder, which was redissolved in 5 mL diethyl ether, crystallized at -30 ˚C for 16 h, and the product isolated as white crystals. Yield: 0.175g, 55%. ^{1}H NMR (500 MHz, C_6D_5Br, 295 K) δ 0.82 (m, 2H, Hf-C*H*$_2$CH(CH$_3$)$_2$), 0.85 (m, 4H, Hf-C*H*$_2$CH(CH$_3$)$_2$), 0.92 (s, 3H, C*H*$_3$), 0.95 (d, 6H, Hf-CH$_2$CH(C*H*$_3$)$_2$), 1.27 (d, 6H, Hf-CH$_2$CH(C*H*$_3$)$_2$), 2.17 (s, 6H, *p*-C*H*$_3$), 2.3 (broad s, 12H, *o*-C*H*$_3$), 2.41 (m, 1H, Hf-CH$_2$C*H*(CH$_3$)$_2$), 2.54 (m, 1H, Zr-CH$_2$C*H*(CH$_3$)$_2$), 2.84 (d, 2H, C*H*$_2$), 4.12 (d, 2H, C*H*$_2$), 6.62 (m, 1H, py-C*H*), 6.78 (m, 1H, py-C*H*), 6.90 (s, 4H, C*H*), 7.04 (m, 1H, py-C*H*), 8.96 (m, 1H, py-*o*-C*H*). ^{13}C{^{1}H} NMR (125 MHz, C_6D_5Br, 295 K) δ 18.58 (s, *o*-*C*H$_3$), 29.85 (s, Hf-CH(*C*H$_3$)$_2$), 30.41 (s, Hf-CH(*C*H$_3$)$_2$), 21.29 (s, *p*-*C*H$_3$), 25.12 (s, *C*H$_3$), 45.05 (s, *C*R$_4$), 65.70 (s, *C*H$_2$), 68.21 (s, Hf-*C*H(CH$_3$)$_2$), 65.85 (s, Hf-*C*H(CH$_3$)$_2$), 120.80 (s, Ar-*C*), 122.83 (s, Ar-*C*), 130.15 (s, Ar-*C*), 134.13 (s, Ar-*C*), 135.70 (s, Ar-*C*), 139.27 (s, Ar-*C*), 146.92 (s, Ar-*C*), 147.40 (s, Ar-*C*), 163.40 (s, Ar-*C*). Anal. Calcd for $C_{33}H_{47}N_3Hf$: C, 59.67; H, 7.13; N, 6.33. Found: C, 59.67; H, 7.13; N, 6.41.

[MesNpy)Hf(i-Pr)Cl (36). A suspension of [MesNpy]HfCl$_2$ (0.744 g, 1.15 mmol) in diethyl ether (50 mL) was cooled to –20 ˚C. To the cold solution was added (i-Pr)MgCl (2.0 M in diethyl ether, 0.60 mL, 1.2 mmol) and the resulting mixture was stirred at room temperature for 1 h until the cloudy suspension became clear. Dioxane (0.15 mL, 1.7 mmol) was added to the solution and the resulting white solid was filtered through Celite. The solvent was removed *in vacuo* to yield a white powder, which was redissolved in 5 mL diethyl ether and crystallized at –20 ˚C to yield the product as white crystals. Yield: 0.35 g, 47%. ^{1}H NMR (500 MHz, C_6D_6, 295 K) δ 0.91 (s, 3H, C*H*$_3$), 0.98 (m, 1H, Hf-C*H*(CH$_3$)$_2$), 1.48 (d, 6H, Hf-CH(C*H*$_3$)$_2$), 1.92 (s, 6H, *o*-C*H*$_3$), 2.15 (s, 6H, *p*-C*H*$_3$), 2.66 (s, 6H, *o*-C*H*$_3$), 2.82 (d, 2H, C*H*$_2$), 4.19 (d, 2H, C*H*$_2$), 6.61 (m, 1H, py-C*H*), 6.73 (m, 1H, py-C*H*), 6.77 (s, 2H, C*H*), 6.95 (s, 2H, C*H*), 7.00 (m, 1H, py-C*H*), 9.67 (m, 1H, py-*o*-C*H*). ^{13}C{^{1}H} NMR (125 MHz, C_6D_6, 295 K) δ 18.74 (s, *o*-*C*H$_3$), 19.63 (s, *o*-*C*H$_3$), 21.28 (s, *p*-*C*H$_3$), 22.51 (s, Hf-CH(*C*H$_3$)$_2$), 25.22 (s, *C*H$_3$), 46.28 (s, *C*R$_4$), 65.47 (s, *C*H$_2$), 68.27 (s, Hf-*C*H(CH$_3$)$_2$), 120.57 (s, Ar-*C*), 123.04 (s, Ar-*C*), 130.14 (s, Ar-*C*), 130.50 (s, Ar-*C*),

134.89 (s, Ar-*C*), 135.92 (s, Ar-*C*), 139.70 (s, Ar-*C*), 145.02 (s, Ar-*C*), 149.20 (s, Ar-*C*). Anal. Calcd for $C_{30}H_{40}N_3ClHf$: C, 54.88; H, 6.14; N, 6.40; Cl, 5.40. Found: C, 55.07; H, 6.22; N, 6.34; Cl, 5.32.

[MesNpy]Hf(i-Pr)$_2$ (37). A suspension of [MesNpy]$HfCl_2$ (1.70 g, 2.62 mmol) in diethyl ether (50 mL) was cooled to -30 ˚C. To the cold solution was added (i-Bu)MgBr (2.0 M in diethyl ether, 2.88 mL, 5.76 mmol) and the resulting mixture was stirred at room temperature for 10 min until the cloudy suspension became clear. Dioxane (0.670 mL, 0.786 mmol) was added to the solution and the resulting white solid was filtered through Celite. The solvent was removed *in vacuo* to yield a white powder, which was redissolved in 5 mL diethyl ether and crystallized at -30 ˚C for 16 h as white crystals. Yield: 0.098g, 53%. ^{1}H NMR (500 MHz, C_6D_5Br, 295 K) δ 0.088 (m, 1H, Hf-C*H*$_2$(CH$_3$)$_2$), 0.51 (m, 1H, Hf-C*H*$_2$(CH$_3$)$_2$), 1.19 (s, 3H, C*H*$_3$), 1.22 (d, 6H, Hf-CH$_2$(C*H*$_3$)$_2$), 1.59 (d, 6H, Hf-CH$_2$(C*H*$_3$)$_2$), 2.14 (s, 6H, *p*-C*H*$_3$), 2.2 (broad s, 12H, *o*-C*H*$_3$), 2.85 (d, 2H, C*H*$_2$), 4.14 (d, 2H, C*H*$_2$), 6.84 (s, 4H, C*H*), 7.03 (m, 1H, py-C*H*), 7.17 (m, 1H, py-C*H*), 7.47 (m, 1H, py-C*H*), 8.77 (m, 1H, py-*o*-C*H*). ^{13}C{^{1}H} NMR (125 MHz, C_6D_5Br, 295 K) δ 18.58 (s, *o*-*C*H$_3$), 20.84 (s, Hf-CH(*C*H$_3$)$_2$), 21.32 (s, *p*-*C*H$_3$), 21.99 (s, Hf-CH(*C*H$_3$)$_2$), 25.12 (s, *C*H$_3$), 45.05 (s, *C*R$_4$), 65.70 (s, *C*H$_2$), 65.85 (s, Hf-*C*H(CH$_3$)$_2$), 68.21 (s, Hf-*C*H(CH$_3$)$_2$), 120.53 (s, Ar-*C*), 121.97 (s, Ar-*C*), 132.96 (s, Ar-*C*), 138.88 (s, Ar-*C*), 146.46 (s, Ar-*C*), 147.00 (s, Ar-*C*), 162.77 (s, Ar-*C*). Anal. Calcd for $C_{33}H_{47}N_3Hf$: C, 59.67; H, 7.13; N, 6.33. Found: C, 59.76; H, 7.20; N, 6.35.

Activation of dialkyl complexes. The above complexes were activated in a similar fashion. Some NMR signals are not included as overlapping signals make assignment difficult.

Activation of [MesNpy]HfEt$_2$ (28). Solutions of [MesNpy]$HfEt_2$ (0.0161 g, 0.0253 mmol), the internal standard Ph_2CH_2 (0.0063g, 0.037 mmol) and $[Ph_3C][B(C_6F_5)_4]$ (0.0238 g,

0.0258 mmol), each in C_6D_5Br (1.00 mL total) were prepared and cooled to -30 ˚C. The solutions were mixed while still cold and the resulting yellow solution was transferred to an NMR tube and frozen in $N_{2(l)}$ within 2 min of the preparation of the sample. The resulting solution contained five major compounds, [(MesNpy)HfEt][$B(C_6F_5)_4$] (**29**), [(MesNpy)Hf(n-Bu)][$B(C_6F_5)_4$] (**30**), $Ph_3CCH_2CH_3$, Ph_3CH and the internal standard Ph_2CH_2.

^{1}H NMR (500 MHz, C_6D_5Br, 253 K)

(**29**) δ 0.26 (q, 2H, Hf-C*H*$_2$CH$_3$), 0.91 (t, 3H, Hf-CH$_2$C*H*$_3$), 1.29 (s, 3H, C*H*$_3$), 1.57 (broad s, 6H, *o*-C*H*$_3$), 2.19 (s, 6H, *p*-C*H*$_3$), 2.37 (broad s, 6H, *o*-C*H*$_3$), 2.98 (d, 2H, C*H*$_2$), 4.18 (d, 2H, C*H*$_2$), 6.77 (broad s, 2H, C*H*), 6.85 (broad s, 2H, C*H*), some aryl peaks omitted here, 7.69 (m, 1H, py-C*H*), 8.40 (m, 1H, py-*o*-C*H*).

(**30**) δ 0.33 (q, 2H, Hf-C*H*$_2$CH$_2$CH$_2$CH$_3$), 0.56 (t, 3H, Hf-CH$_2$CH$_2$CH$_2$C*H*$_3$), 0.77 (m, 2H, Hf-CH$_2$CH$_2$C*H*$_2$CH$_3$), 1.14 (m, 2H, Hf-CH$_2$C*H*$_2$CH$_2$CH$_3$), 1.29 (s, 3H, C*H*$_3$), 1.57 (broad s, 6H, *o*-C*H*$_3$), 2.19 (s, 6H, *p*-C*H*$_3$), 2.37 (broad s, 6H, *o*-C*H*$_3$), 2.98 (d, 2H, C*H*$_2$), 4.18 (d, 2H, C*H*$_2$), 6.77 (broad s, 2H, C*H*), 6.85 (broad s, 2H, C*H*), some aryl peaks omitted here, 7.40 (m, 1H, py-C*H*), 8.51 (m, 1H, py-*o*-C*H*).

$Ph_3CCH_2CH_3$ δ 0.68 (t, 3H, Ph_3CCH_2C*H*$_3$), 2.46 (q, 2H, Ph_3CC*H*$_2$CH$_3$), some aryl peaks omitted here.

Ph_3CH δ 5.45 (s, 1H, Ph_3C*H*), some aryl peaks omitted here.

Ph_2CH_2 δ 3.80 (s, 1H, Ph_2C*H*$_2$), some aryl peaks omitted here.

^{13}C{^{1}H} NMR (125 MHz, C_6D_5Br, 253 K)

(**29**) δ 11.22 (s, Hf-CH$_2$*C*H$_3$), 19.6 (broad s, *o*-C*H*$_3$), 21.55 (s, *p*-C*H*$_3$), 25.76 (s, *C*H$_3$), 64.65 (s, *C*H$_2$), 71 (s, Hf-*C*H$_2$CH$_3$), some aryl peaks omitted here.

(**30**) δ 14.80 (s, Hf-CH$_2$(CH$_2$)$_2$*C*H$_3$), 19.6 (broad s, *o*-C*H*$_3$), 21.55 (s, *p*-C*H*$_3$), 25.76 (s, *C*H$_3$), 28.78 (s, Hf-CH$_2$(*C*H$_2$)$_2$CH$_3$), 29.36 (s, Hf-CH$_2$(*C*H$_2$)$_2$CH$_3$), 64.58 (s, *C*H$_2$), 80.02 (s, Hf-

$CH_2(CH_2)_2CH_3$), some aryl peaks omitted here.

$Ph_3CCH_2CH_3$ δ 9.77 (s, $Ph_3CCH_2CH_3$), 33.17 (s, $Ph_3CCH_2CH_3$), some aryl peaks omitted here.

Ph_3CH δ 57.49 (s, Ph_3CH), some aryl peaks omitted here.

Ph_2CH_2 δ 40.0 (s, 1H, Ph_2CH_2), some aryl peaks omitted here.

Reaction of an activated solution of [MesNpy]HfEt$_2$ (28) with 1-hexene. To a Solution of [MesNpy]HfEt$_2$ (0.0221 g, 0. 0347 mmol) in C_6D_5Br was added 1-hexene (0.0047, 0.056 mmol). This, along with a solution of $[Ph_3C][B(C_6F_5)_4]$ (0.0324 g, 0.0351 mmol) in C_6D_5Br (0.80 mL total) were cooled to -30 ˚C. The activator was added to the dialkyl while the solutions were still cold. The NMR samples were obtained directly from this solution, and frozen with $N_{2(l)}$ prior to experimentation.

Activation of [MesNpy]Hf(i-Pr)$_2$ (37). Solutions of [MesNpy]Hf(i-Pr)$_2$ (0.0103 g, 0.0155 mmol), the internal standard Ph_2CH_2 (0.0036g, 0.021 mmol) and $[Ph_3C][B(C_6F_5)_4]$ (0.0145 g, 0.0157 mmol), each in C_6D_5Br (1.00 mL total) were prepared and cooled to -30 ˚C. The solutions were mixed while still cold and the resulting yellow solution was transferred to an NMR tube and frozen in $N_{2(l)}$ within 2 min of the preparation of the sample. The resulting solution contained four major compounds, $[(MesNpy)Hf(CH(CH_3)_2)][B(C_6F_5)_4]$ (**38**), $[(MesNpy)HfCH_2CH(CH_3)(CH(CH_3)_2)][B(C_6F_5)_4]$ (**39**), Ph_3CH and the internal standard, Ph_2CH_2.

^{1}H NMR (500 MHz, C_6D_5Br, 253 K)

(**38**) δ ~0.38 (m, 1H, Hf-C*H*$(CH_3)_2$), 0.92 (t, 3H, Hf-CH(C*H*$_3)_2$), 1.25 (s, 3H, C*H*$_3$), 1.49 (broad s, 6H, *o*-C*H*$_3$), 2.14 (s, 6H, *p*-C*H*$_3$), 2.35 (broad s, 6H, *o*-C*H*$_3$), 3.01 (d, 2H, C*H*$_2$), 4.00 (d,

2H, CH_2), 6.77 (broad s, 2H, C*H*), 6.92 (broad s, 2H, C*H*), some aryl peaks omitted here, 7.65 (m, 1H, py-C*H*), 8.35 (m, 1H, py-*o*-C*H*).

(**39**) δ ~0.38 (m, 2H, Hf-CH_2CH(CH$_3$)(CH(CH$_3$)$_2$)), 0.43 (d, 3H, Hf-CH$_2$CH(CH$_3$)(CH(CH_3)$_2$)), 0.45 (d, 3H, Hf-CH$_2$CH(CH$_3$)(CH(CH_3)$_2$)), 0.49 (d, 3H, Hf-CH$_2$CH(CH_3)(CH(CH$_3$)$_2$)), 0.96 (m, 1H, Hf-CH$_2$CH(CH$_3$)(C*H*(CH$_3$)$_2$)), 1.29 (s, 3H, CH_3), 1.38 (m, 1H, Hf-CH$_2$C*H*(CH$_3$)(CH(CH$_3$)$_2$)), 1.57 (broad s, 6H, *o*-CH_3), 2.19 (s, 6H, *p*-CH_3), 2.37 (broad s, 6H, *o*-CH_3), 2.96 (dd, 2H, CH_2), 4.13 (dd, 2H, CH_2), 6.77 (broad s, 2H, C*H*), 6.85 (broad s, 2H, C*H*), some aryl peaks omitted here, 7.39 (m, 1H, py-C*H*), 7.68 (m, 1H, py-C*H*), 8.46 (m, 1H, py-*o*-C*H*).

^{13}C{^{1}H} NMR (125 MHz, C$_6$D$_5$Br, 253 K)

(**38**) δ 19.6 (broad s, *o*-CH_3), 21.94 (s, *p*-CH_3), 22.35 (s, Hf-CH(*C*H$_3$)$_2$), 26.13 (s, *C*H$_3$), 64.93 (s, *C*H$_2$), 78.90 (s, Hf-*C*H(CH$_3$)$_2$), some aryl peaks omitted here.

(**39**) δ 17.81 (s, Hf-CH$_2$CH(*C*H$_3$)(CH(CH$_3$)$_2$)), 19.6 (broad s, *o*-CH_3), 20.35 (s, Hf-CH$_2$CH(CH$_3$)(CH(*C*H$_3$)$_2$)), 20.84 (s, Hf-CH$_2$CH(CH$_3$)(CH(*C*H$_3$)$_2$)), 21.94 (s, *p*-CH_3), 25 (s, *C*H$_3$), 37.48 (s, Hf-CH$_2$CH(CH$_3$)(*C*H(CH$_3$)$_2$)), 41.35 (s, Hf-CH$_2$*C*H(CH$_3$)(CH(CH$_3$)$_2$)), 65.11 (s, *C*H$_2$), 88.65 (s, Hf-*C*H$_2$CH(CH$_3$)(CH(CH$_3$)$_2$)), some aryl peaks omitted here.

Chapter 4

Living polymerization of α-olefins with activated hafnium isobutyl complexes

4.1 Introduction

As outlined in the general introduction, a truly living polymerization system must follow a certain set of criteria. The rate of initiation, k_i, must be at least on the same order as the rate of propagation, k_p, to yield a constant number of active centers in solution.[2] These active species should be stable towards chain termination events [4] (Scheme I.2) and show sustained activity upon addition of further equivalents of monomer.

These properties of living systems make them especially amenable to kinetics investigations. In analogous non-living systems, it has been difficult to correlate empirical rate laws with molecular mechanism as the concentration and nature of catalytically active species was unknown. However, recently Landis *et al.* have reported a method of determining the number of active sites in solution.[86,87]

An issue that must be considered in cationic polymerization is the role of the anion. In general, bulky, fluorinated borates are considered to be non-coordinating and the polymerization process is discussed from the point of view of the cation only.[88] Recently, there has been a growing body of theoretical[89,90] as well as experimental[47,91,92] evidence that points toward the importance of the anion in the polymerization process. These studies indicate that in discussing a catalyst system, one must always discuss the ion pair.

Another aspect of the catalyst system that must be considered is the interaction of two cationic centers with each other. Although study of such interactions is sparse,[93-95] recently Sita *et al.* have reported the structure of a methyl-bridged dimeric dication[96] and demonstrated polymer chain transfer to a zirconium methyl cation.[97]

The previous chapters in this thesis have explored the chemistry of zirconium and hafnium complexes of ArNpy ligands. Chapter 4 describes the living polymerization of α-olefins with hafnium isobutyl complexes and investigates some of the factors affecting polymerization behavior described above.

4.2 1-Hexene polymerization with [(MesNpy)Hf(i-Bu)][B(C_6F_5)$_4$]

The limited success of the [(MesNpy)Zr(i-Bu)][B(C_6F_5)$_4$] system (Chapter 2) and the stability of β-hydride-bearing hafnium alkyl cations (Chapter 3) prompted us to investigate hafnium isobutyl complexes as catalysts for living α-olefin polymerization. It was hoped that the simple activation process associated with diisobutyl complexes as well as the stability imparted to the catalyst by the hafnium center would give these systems the desirable properties of a living catalyst.

The dialkyl complex [MesNpy]Hf(i-Bu)$_2$ (**42**) was synthesized by reaction of [MesNpy]$HfCl_2$ with 2 equiv of isobutylmagnesium bromide, in 83% recrystallized yield.[27] The ^{13}C-labeled analogue [MesNpy]Hf($^{13}CH_2CH(CH_3)_2$)$_2$ (**42***) was prepared similarly using $(CH_3)_2CH^{13}CH_2MgBr$. The ^{1}H NMR spectrum (22 ˚C, C_6D_5Br) of **42** shows two overlapping doublets at 0.6 ppm corresponding to two distinct Hf-C*H*$_2$ protons. The $^{13}C\{^1H\}$ NMR spectrum (22 ˚C, C_6D_5Br) shows two resonances at 80.9 and 83.0 ppm for the Hf-*C*H_2 carbons. These NMR data are indicative of a trigonal bipyramidal complex with two isobutyl groups coordinated in inequivalent axial and equatorial positions.

Compounds **42** and **42*** were activated with 1 equiv of [Ph_3C][B(C_6F_5)$_4$] to give a quantitative (with respect to Ph_3CH) yield of the respective cation, [(MesNpy)Hf(i-Bu)][B(C_6F_5)$_4$] (**43**, **43***), as well as isobutene and Ph_3CH as by-products (eq 4.1).

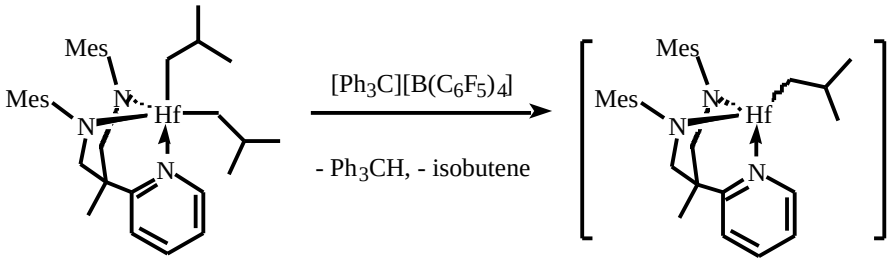

42 **43** (4.1)

The $^{13}C\{^1H\}$ NMR spectrum (0 ˚C, C_6D_5Br) of **43*** shows a singlet at 93.3 ppm corresponding to the Hf-$^{13}CH_2$ carbon. A signal for $^{13}CH_2=C(CH_3)_2$ is also observed at 111.1 ppm. Unlike its zirconium analogue, the hafnium cationic species is stable for over 2 h at 0 ˚C.[26] The ^1H NMR spectrum (–20 ˚C, C_6D_5Br) for **43** clearly shows signals for the methyl, methylene and methine protons at 0.55, 0.44, and 1.73 ppm, respectively. Variable temperature $^{13}C\{^1H\}$ NMR studies with **43*** show that the isobutyl signal at 93.3 ppm remains sharp as the temperature of the sample is lowered to –50 ˚C. This is in marked contrast to the methyl system, (Chapter 1) indicating that in the isobutyl system the dialkyl complex is completely activated and there is no evidence of a dinuclear monocation.

Addition of 1-2 equiv of 1-hexene to a solution of **43*** leads to a new $^{13}C\{^1H\}$ NMR signal at 49.0 ppm (Figure 4.1a). This sharp signal may be attributed to the first insertion product, [(MesNpy)Hf(CH_2CH(n-Bu)(*i-Bu)][B(C_6F_5)$_4$]. The weak signal at 44.2 ppm in Figure 4.1a may be due to a small amount of second insertion product. A signal for free **43*** was also observed at 93.3 ppm. Observation of the first insertion product indicates that k_i is on the same order as k_p. If k_p was significantly faster than k_i, one would expect signals for only **43*** and the multiple insertion product. It is difficult to quantify k_i and k_p in this experiment, as the 1-hexene mixing rate will have a great affect on the ratio of **43*** and first insertion product.

Addition of a further 44 equiv of 1-hexene leads to the disappearance of this signal and appearance of a more upfield signal at 44.3 ppm (Figure 4.1b). A $^{13}C\{^1H\}$ NMR signal at 93.3 ppm was not observed in this spectrum. In this case, all of **43*** as well as the first insertion product has been converted to the multiple insertion product observed in Figure 4.1a in very small amounts. Signals for atactic poly(1-hexene) were also observed.[98,99]

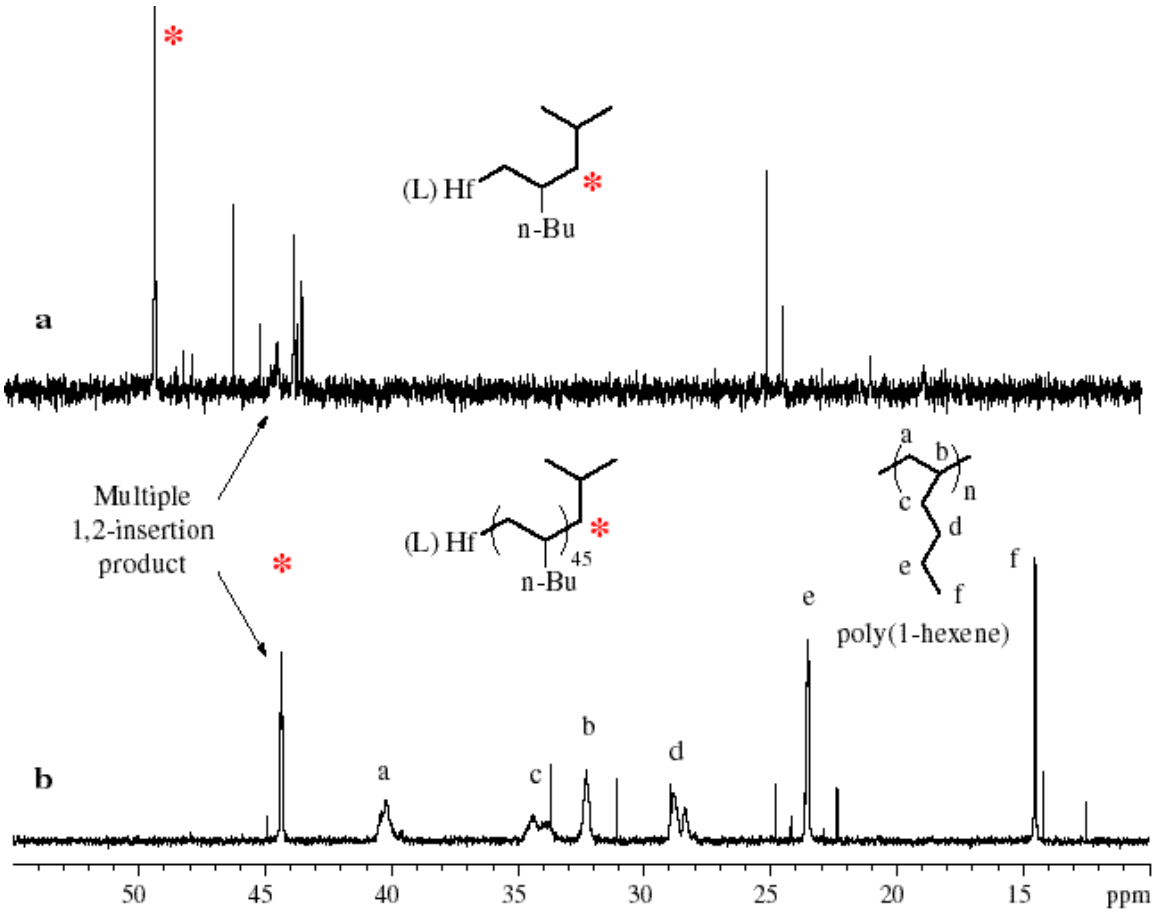

Figure 4.1. $^{13}C\{^{1}H\}$ NMR spectra (0 ˚C, C_6D_5Br) for addition of 1-hexene to **43***; a) 1-2 equiv 1-hexene, b) 45 equiv 1-hexene. (L = $[MesNpy]^{2-}$)

^{1}H NMR signals due to β-hydride elimination from a 1,2 or 2,1-insertion product were not observed. As work by Resconi *et al.* shows, the signals for vinylidene protons due to β-hydride elimination from a 1,2-insertion product are generally observed at 4.7 ppm, while those for 2-butenyl protons of 2,1-insertion elimination products are observed further downfield at 5.5 ppm.[100,101]

Polymerization reactions catalyzed by **43** follow strictly first order kinetics for the consumption of 1-hexene, as expected in a living system (Figure 4.2).

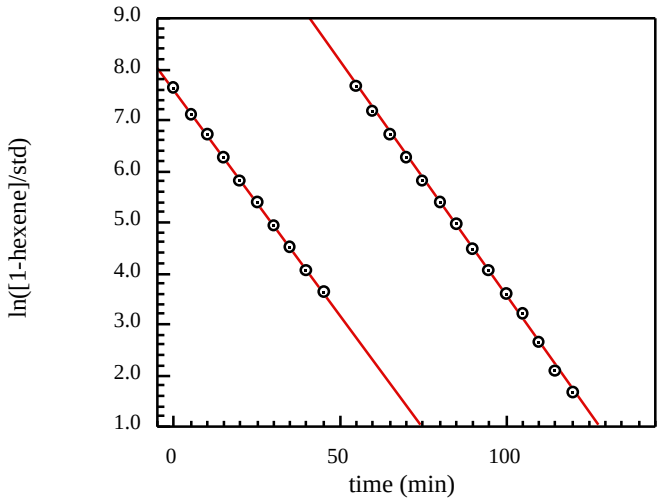

Figure 4.2. Plot of ln[1-hexene/Ph_2CH_2] vs. time (min) for two consecutive additions of 60 equiv of 1-hexene (0.80 M) to **43** (0.015 M) (0 ˚C, C_6D_5Br).

Two consecutive additions of 60 equiv of 1-hexene to a solution of **43** in C_6D_5Br at 0 ˚C resulted in plots of ln[1-hexene] vs. time which were linear, with k_p = 6.0(2) M^{-1} min^{-1} (0.10(2) M^{-1} s^{-1}). Addition of 1-hexene to this same solution stored at room temperature for more than 24 h leads to further first order olefin consumption, at a rate 1/3 that observed originally. Signals for vinylidene protons were observed at 4.83 and 4.85 ppm, indicating slow β-hydride elimination from the 1,2-insertion product at room temperature.

The rate of 1-hexene polymerization with **43** was monitored over an 8 - 23 mM concentration range. The plot of k_{obs} vs. $[Hf]_o$ is linear and indicates a first order dependence of polymerization rate on catalyst concentration (Figure 4.3). Propagation rate constants obtained over this concentration range result in an average k_p value of 6.0(6) M^{-1} min^{-1} (0.10(1) M^{-1} s^{-1}) at 0 ˚C.

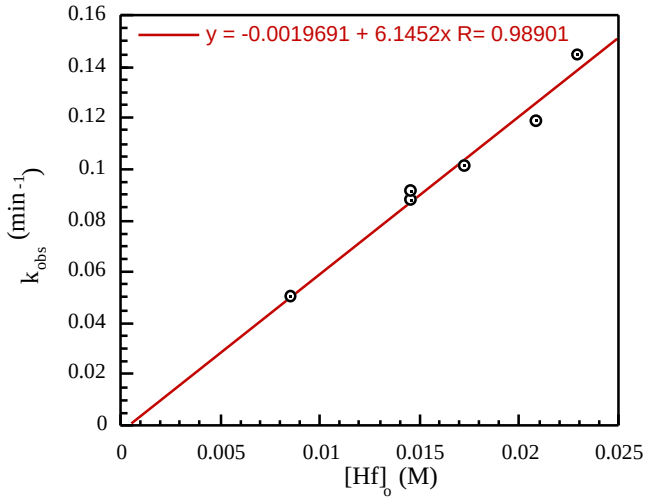

$[Hf]_o$ (M)	k_{obs} (min^{-1})
0.0229	0.144(4)
0.0209	0.119(3)
0.0172	0.101(3)
0.0146	0.0881(4)
0.0146	0.0913(7)
0.00858	0.0502(9)

Figure 4.3. Plot of k_{obs} (min^{-1}) vs. $[Hf]_o$ (M) for polymerization of 1-hexene catalyzed by **43** (0 ˚C, C_6D_5Br).

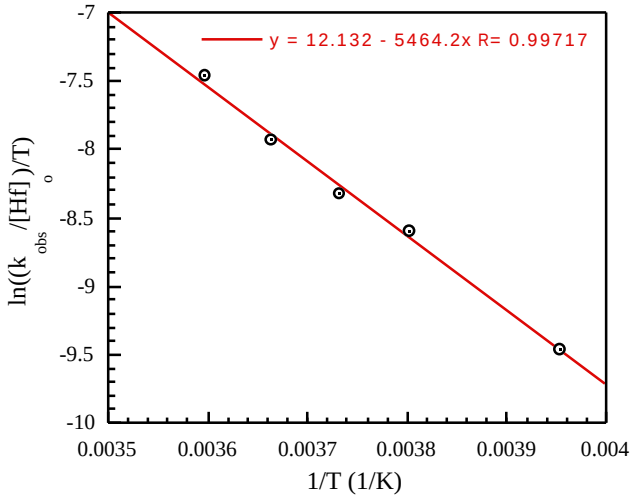

T (K)	k_{obs} (min^{-1})	$[Hf]_o$ (M)
253	0.01655(6)	0.0140
263	0.0450(5)	0.0154
268	0.0520(2)	0.0133
273	0.0881(4)	0.0150
278	0.138(2)	0.0144

Figure 4.4. Eyring plot for consumption of 1-hexene, catalyzed by **43**.

The Eyring plot for the polymerization process yields a $\Delta H^{\ddagger}$ value of 10.86(46) kcal mol^{-1} and a $\Delta S^{\ddagger}$ value of –28.6(28) cal mol^{-1} K^{-1}, with a $[Hf]_o$ value of 0.015 M (Figure 4.4). These values are in the range observed for the zirconium system ($\Delta H^{\ddagger}$ = 8.1(7) kcal mol^{-1} and $\Delta S^{\ddagger}$ = –33(2) cal mol^{-1} K^{-1}). Based on these results it is possible to predict the polymerization rate under conditions with varying temperatures and hafnium concentrations.

Addition of 100 equiv of 1-hexene to an initially cold (–20 ˚C) solution of **43** followed by polymerization at room temperature led to polymer samples with PDI = 1.04 and M_n = 7500 (expected M_n = 7900). Addition of 100 equiv of 1-hexene to this sample at room temperature led to polymer samples that clearly show bimodal GPC traces (by both refractive index and light scattering methods), which indicates that a substantial fraction of the polymer chains have β-eliminated after completion of the first polymerization process. However, β-hydride elimination is very slow at 0 ˚C, similar experiments carried out at this temperature gave significantly different results. In one experiment, 91 equiv of 1-hexene were added to a solution of **43** (8.8 mM, C_6D_5Br) and the polymerization completed after 2 h at 0 ˚C. A further 91 equiv of 1-hexene were added and polymerization resumed at 0 ˚C. The resulting polymer sample had PDI = 1.04 and M_n = 13650 (expected M_n = 14380) which is within the error limit of the desired molecular weight.

A plot of expected molecular weight vs. equiv of 1-hexene added for a series of batch-wise experiments was linear and indicated that this system is capable of the living polymerization of 1-hexene at 0 ˚C (Figure 4.5, Table 4.1). This plot shows that it is possible to predict M_n for a given polymer sample under these experimental conditions, and that there is little or no β-hydride elimination for conversion of up to 600 equiv of 1-hexene at 0 ˚C.[102]

The above results show that [(MesNpy)Hf(i-Bu)][$B(C_6F_5)_4$] fulfills all of the requirements for a living polymerization system as outlined in the introduction. The k_p values based on initial metal concentrations ($[M]_o$) are comparable to those obtained in the zirconium system (4.8(1) M^{-1} min^{-1}, 0.079(2) M^{-1} s^{-1}).

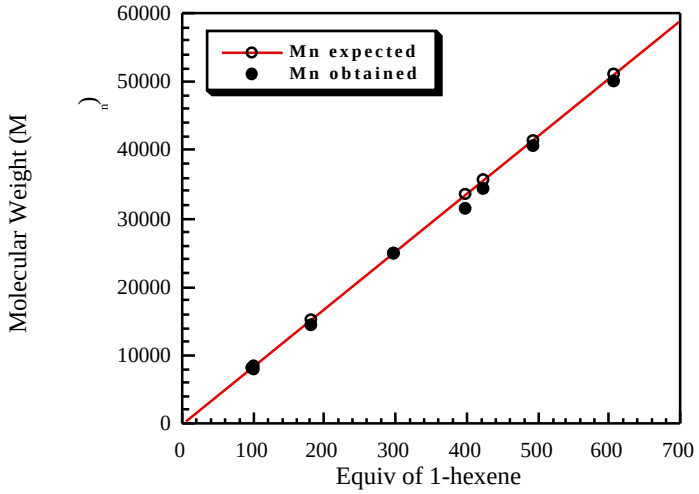

Figure 4.5. Polymerization of 1-hexene catalyzed by **43** (~10 mM, 0 ˚C, C_6H_5Cl). Polydispersity values are between 1.02 and 1.05. d*n*/dc = 0.076.

Table 4.1. Polymers generated with **43** at 0 ˚C.

[MesNpy]Hf(i–bu)$_2$ (M)	Equiv of 1–hexene	Expected M_n	Observed M_n	PDI
0.0106	98	8248	8012	1.04
0.0097	101	8500	7888	1.04
0.0053	182	15317	14380	1.04
0.0051	296	24911	24800	1.03
0.0057	398	33496	31370	1.03
0.0027	423	35600	34220	1.02
0.0052	493	41491	40610	1.03
0.0049	607	51085	49970	1.03

4.3 1-Hexene polymerization with [(TripNpy)Hf(i-Bu)][B(C_6F_5)$_4$]

In order to investigate the effects of increased ligand steric bulk on polymerization behavior, hafnium complexes of $[TripNpy]^{2-}$ were prepared. The precursors [TripNpy]Hf(NMe_2)$_2$ (**44**) and [TripNpy]$HfCl_2$ (**45**) were prepared in an analogous manner to their $[MesNpy]^{2-}$ counterparts.

Reaction of **45** with 2 equiv of (i-Bu)MgBr resulted in the isolation of [TripNpy]Hf(i-Bu)$_2$ (**46**) in 70% recrystallized yield. The slightly lower yield compared to that for **42** is due to the greater lipophilicity, and thus greater solubility, observed in all complexes bearing the [TripNpy]$^{2-}$ ligand. The ^{1}H NMR spectrum (22 ˚C, C_6D_5Br) of **46** shows resonances for the Hf-C*H*$_2$ protons at 0.55 and 0.72 ppm, and the $^{13}C\{^1H\}$ NMR spectrum (22 ˚C, C_6D_5Br) shows two resonances at 81.7 and 83.0 ppm for the Hf-*C*H$_2$ carbons.

Activation of **46** with 1 equiv of $[Ph_3C][B(C_6F_5)_4]$ results in β-hydride abstraction and formation of [(TripNpy)Hf(i-Bu)][B(C$_6$F$_5$)$_4$] (**47**) as well as Ph_3CH and isobutene (eq 4.2).

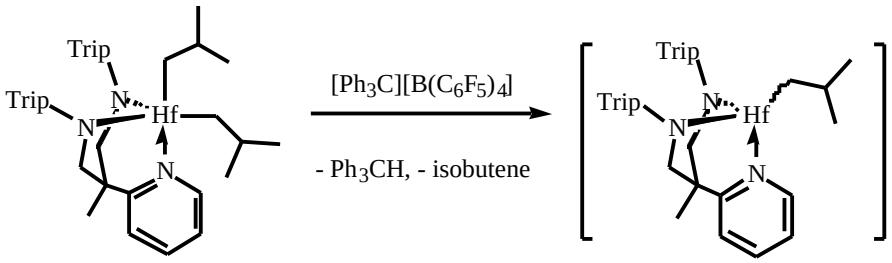

46 **47** (4.2)

The ^{1}H NMR spectrum (0 ˚C, C_6D_5Br) of **47** shows resonances for the methyl, methylene, and methine protons of the Hf-bound isobutyl group at 0.57, 0.58 and 1.65 ppm, respectively. The $^{13}C\{^1H\}$ NMR spectrum (0 ˚C, C_6D_5Br) shows a signal at 89.2 ppm for the Hf-*C*H$_2$ carbon. The cation is stable after 15 h at 0 ˚C. The same solution was monitored for up to 15 d, and after this time approximately 60% of the catalyst remained in solution in comparison to Ph_3CH.

Addition of 107 equiv of 1-hexene to a solution of **47** (0 ˚C, C_6D_5Br) resulted in first order polymerization with a k_p value of 1.71(8) M^{-1} min^{-1} (0.029(1) M^{-1} s^{-1}). The k_p value for **43** was 6.0(6) M^{-1} min^{-1} (0.10(6) M^{-1} s^{-1}). This decrease in rate is likely caused by increased steric bulk around the metal center, which may hinder olefin approach. Batch-wise polymerization reactions of 1-hexene (0 ˚C, C_6H_5Cl) with **47** were carried out and a plot of M_n vs. 1-hexene added for up to 700 equiv of olefin was obtained (Figure 4.6, Table 4.2). In contrast to Figure

4.5, the obtained molecular weights of polymers generated with **47** exceed the expected values with progressively higher equivalents of olefin. It should be noted that since the polymerization reaction is slower with **47**, the runs take approximately 3 times longer to complete than in the [MesNpy] system, leading to possible catalyst decomposition in the [TripNpy] system.

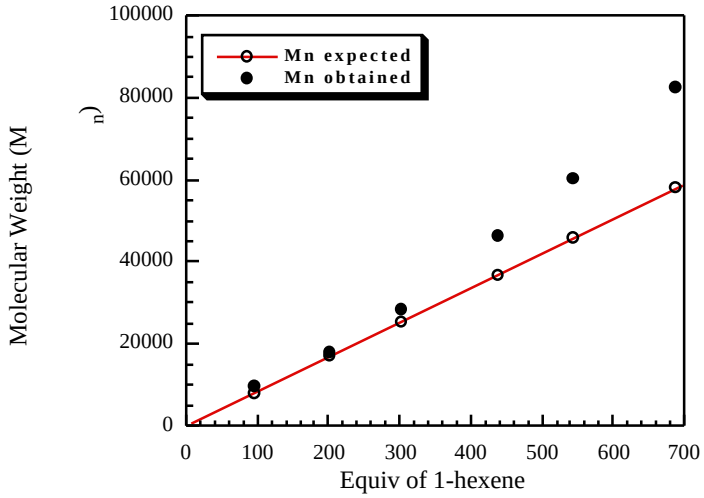

Figure 4.6. Polymerization of 1-hexene catalyzed by **47** (~10 mM, 0 ˚C, C_6H_5Cl). Polydispersities are between 1.02 and 1.05. d*n*/dc = 0.076.

Table 4.2. Polymers generated with **47** at 0 ˚C.

[TripNpy]Hf(i–bu)$_2$ (M)	Equiv of 1–hexene	Expected M_n	Observed M_n	PDI
0.0064	96	8079	9475	1.03
0.0061	202	17000	18050	1.01
0.0050	301	25332	28610	1.02
0.0052	437	36777	46250	1.01
0.0047	544	45783	60240	1.03
0.0033	688	57902	82380	1.02

In an experiment to determine the stability of oligomeric species in this system, 7 equiv of 1-hexene were added to a 21 mM solution (0 ˚C, C_6D_5Br) of **47**. The oligomer was stable after 28 min, however after 15 h vinylidene protons at around 4.8 ppm (~ 15%) were observed in

the ^{1}H NMR spectrum, indicating β-hydride elimination from a 1,2-insertion product. In contrast, **47** is stable over a 15 h period. This shows that in the bulkier $[TripNpy]^{2-}$ system, the propagating species with a coordinated polymer chain is more susceptible to β-hydride elimination than the initiator, **47**.

This instability may be due to increased steric congestion. Other possibilities include decreased interaction of anion with the cationic metal center leading to catalyst destabilization, and ligand C-H activation leading to decomposition. More work is required to better understand the decomposition process in this system, but it appears that **47** is unsuitable as a catalyst for polymerization reactions.

4.4 Investigation of the [(ArNpy)Hf(i-Bu)] cation

An important aspect of understanding a polymerization system involves investigating the true nature of the catalyst in solution. Studies in our group by Casado[38] as well as other recent reports[96,97] point towards the importance of cation-cation interactions in solution. Interaction of group IV methyl cations with neutral dimethyl compounds has been well documented.[52] Examples of other alkyl cations interacting with their respective dialkyl species are less common.

In an attempt to study this phenomenon in the [ArNpy] system a double labeling experiment was devised. A solution of **43*** was added to a solution of **46** (Scheme 4.1). The $^{13}C\{^{1}H\}$ NMR spectrum (0 ˚C, C_6D_5Br) of the resulting mixture showed signals for **43*** (93.3 ppm) as well as **42***, **46***, and **47***. A signal for **43***·OEt_2 (85.5 ppm) was also present, cause by the presence of a trace of diethyl ether in **42*** (Figure 4.7). One explanation for the observed scrambling is the formation of a dinuclear monocation in solution. This species is analogous to that seen in the methyl system, but with bridging isobutyl groups. Similar bridging species have been reported in rare earth systems.[103]

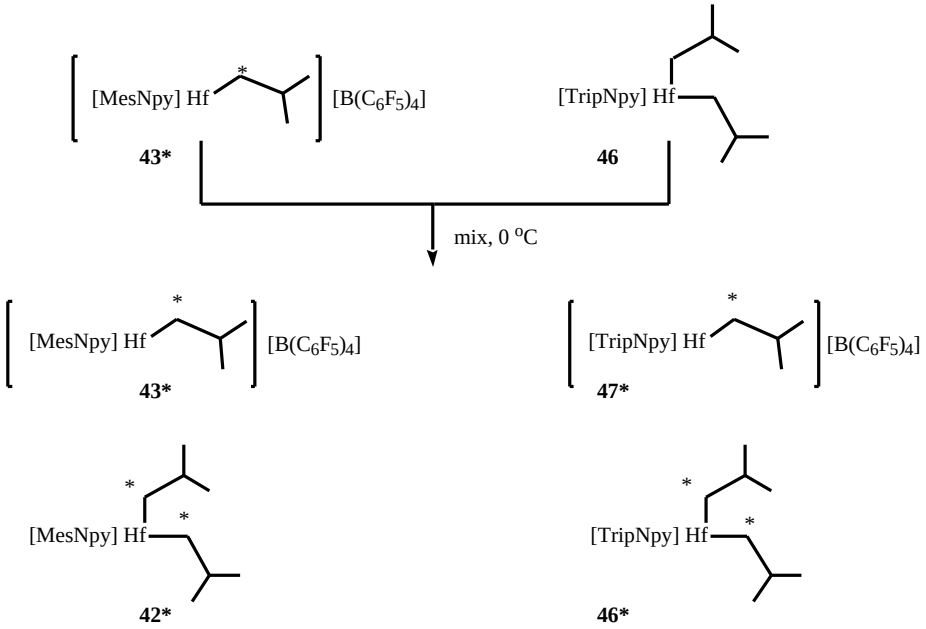

Scheme 4.1. Alkyl transfer between **43*** and **46**.

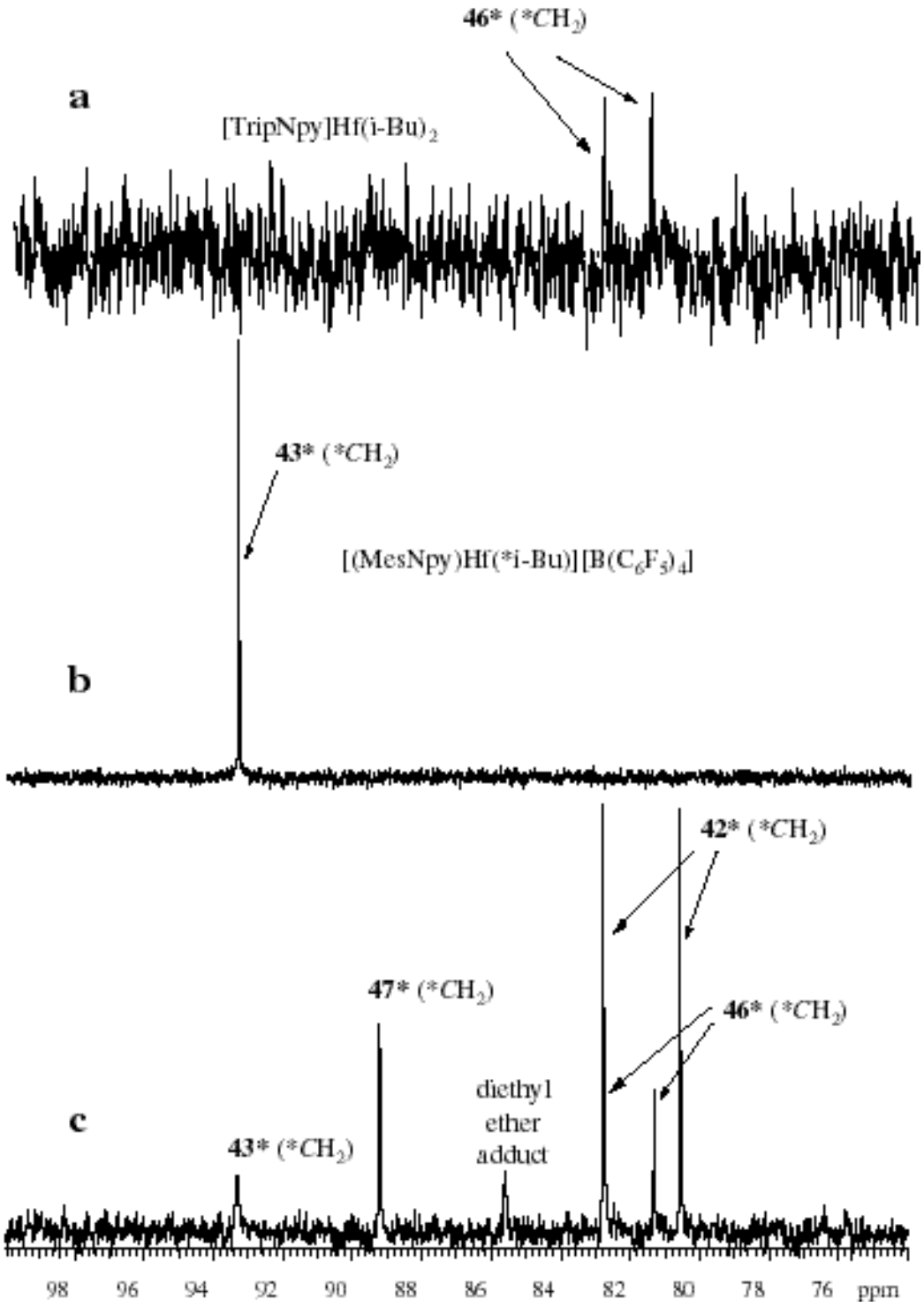

Figure 4.7. $^{13}C\{^{1}H\}$ NMR spectra (0 ˚C, C_6D_5Br) for Hf-CH_2 of: a) **46**; b) **43***; c) mixture of **43*** and **46**.

The next point of interest involves alkyl transfer between two cationic centers. In one experiment, **42*** and **46** were each activated with exactly 1.0 equiv of $[Ph_3C][B(C_6F_5)_4]$ and the resulting cations, **43*** and **47**, were mixed (Scheme 4.2, Figure 4.8). The $^{13}C\{^1H\}$ NMR spectrum (0 ˚C, C_6D_5Br) of the resulting mixture shows resonances for **47*** as well as **43*** (a trace of **43***·OEt_2 is observed again).

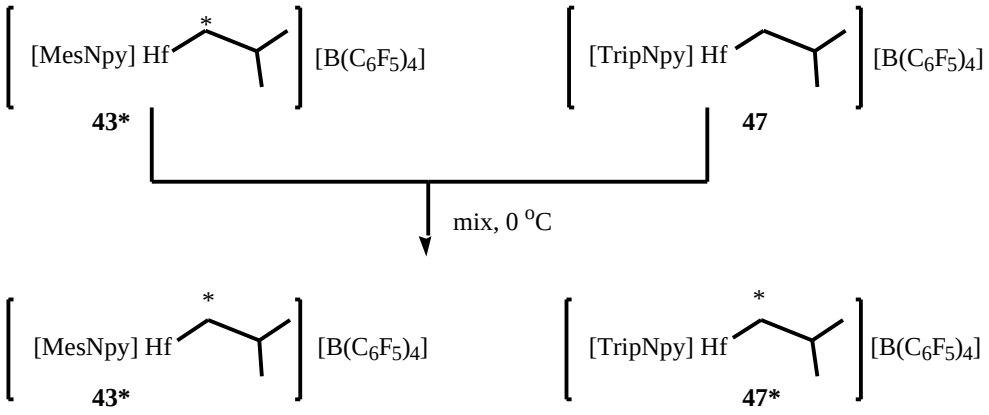

Scheme 4.2. Alkyl transfer between **43*** and **47**.

These results indicate that the labeled alkyl group has been transferred from **43*** to **47**. However, in light of the possibility of alkyl transfer mediated by a neutral species, it was important to ensure that no trace of dialkyl complex remains. To this end, **42*** and **46** were each activated with 2.0 equiv of $[Ph_3C][B(C_6F_5)_4]$ and the solutions examined by ^1H and $^{13}C\{^1H\}$ NMR spectroscopy prior to mixing. After 10 min of mixing at 0 ˚C only a trace of **47*** is present. This indicates that the neutral dialkyl species is promoting the alkyl transfer. Another difficulty in this experiment is caused by the decomposition of **43*** in the presence of excess $[Ph_3C][B(C_6F_5)_4]$ (**47** is stable in the same time period). Several other experiments in this vein were also inconclusive. In all cases, evidence for alkyl transfer was observed, but the mechanism of this transfer remains unclear.

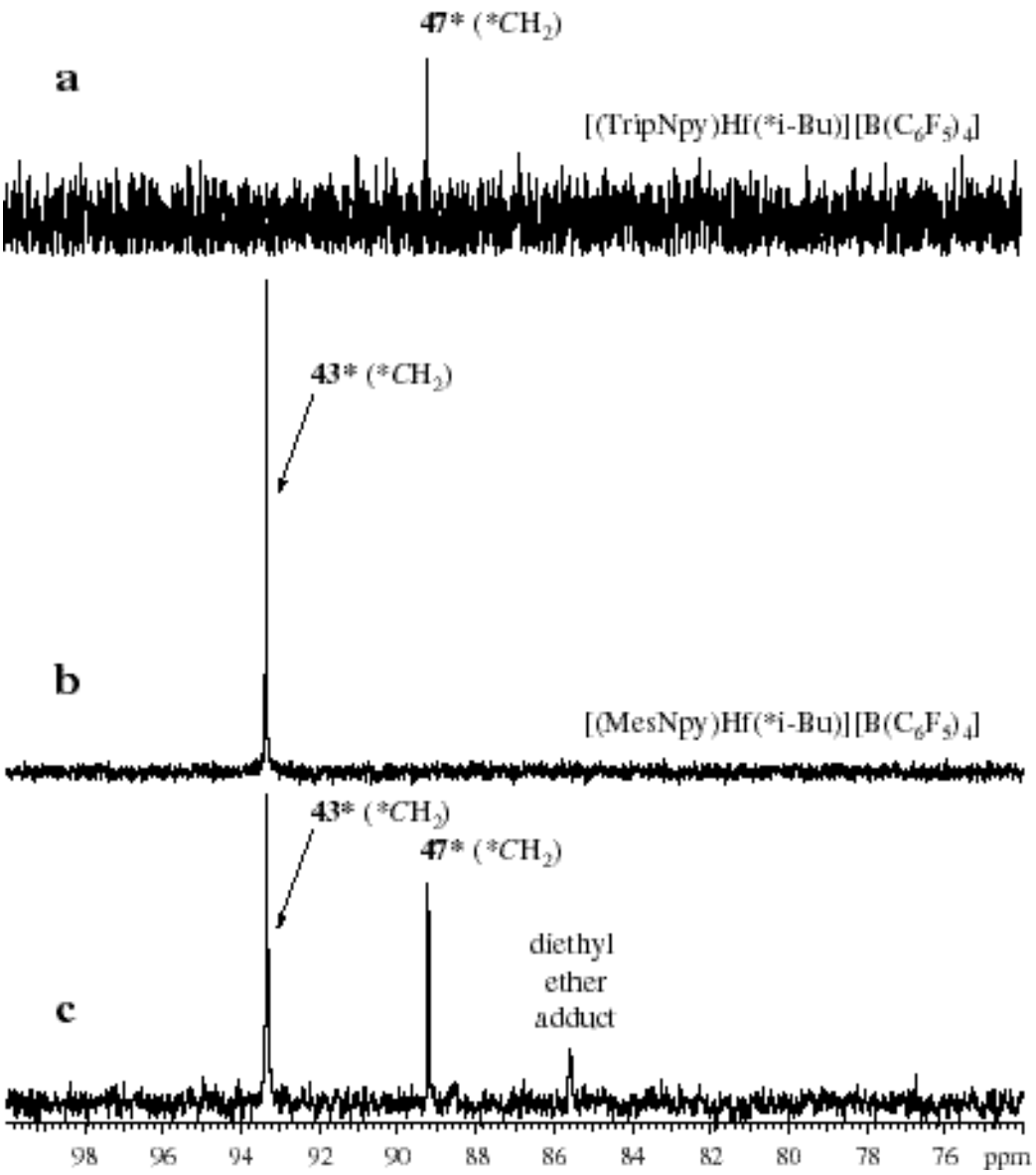

Figure 4.8. $^{13}C\{^{1}H\}$ NMR spectra (0 ˚C, C_6D_5Br) for Hf-CH_2 of: a) **47**; b) **43***; c) mixture of **43*** and **47**.

4.5 Investigating the role of activator and anion

The $[Ph_3C][B(C_6F_5)_4]$ activator has been used most frequently in this project. In order to study the role of activators on polymerization rates, $[HNMe_2Ph][B(C_6F_5)_4]$ and $B(C_6F_5)_3$ were also investigated.

Activation of [MesNpy]Hf(*i-Bu)$_2$ (**42***) with $[HNMe_2Ph][B(C_6F_5)_4]$ results in a complicated reaction mixture which includes $^{13}CH_2=C(CH_3)_2$ and $^{13}CH_3CH(CH_3)_2$, as well as the desired cation, **43***, and unreacted dialkyl compound. The activator had low solubility in C_6D_5Br and thus the reaction mixture was maintained at room temperature long enough to result in β-hydride elimination of **43*** to yield $^{13}CH_2=C(CH_3)_2$. The $^{13}CH_3CH(CH_3)_2$ results from C-H activation of NMe_2Ph, generated in the activation process, with **43*** (See section 4.6).

Activation of **42*** with $B(C_6F_5)_3$ leads to clean hydride abstraction and formation of [(MesNpy)Hf(*i-Bu)][$HB(C_6F_5)_3$] (**48***) as well as $^{13}CH_2=C(CH_3)_2$ (eq 4.3).

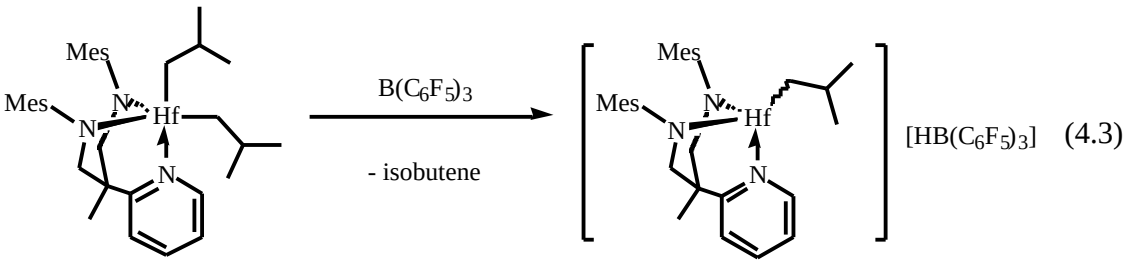

42 **48** (4.3)

The ^1H and $^{13}C\{^1H\}$ NMR spectra (0 ˚C, C_6D_5Br) of **48*** show resonances for the Hf-CH_2 protons and carbon at 0.4 and 94.0 ppm, respectively, which are very close to those reported for **43***. The ^1H NMR resonance for $[HB(C_6F_5)_3]^-$ is very broad and could not be observed. The only by-product of the reaction is isobutene, which is not polymerized over a period of at least 24 h. In contrast, activation of diisobutyl complexes with $[Ph_3C][B(C_6F_5)_4]$ results in the polymerization of the isobutene by-product, which is catalyzed by a slight excess of $[Ph_3C]^+$.

The initiator generated in this system, **48**, is sparingly soluble in toluene, whereas the initiator with the $[B(C_6F_5)_4]^-$ anion, **43**, is relatively insoluble in toluene. Polymerization of 1-hexene with **48** was well-behaved. Figure 4.9 shows a comparison of polymerization rates with different anions and solvents at 0 ˚C.

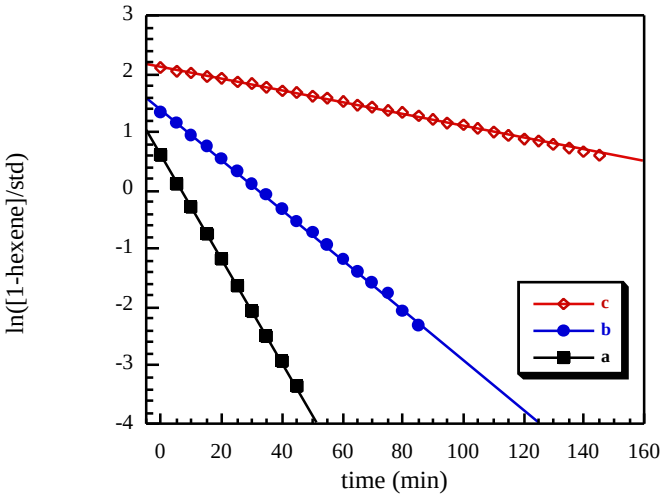

Figure 4.9. Plots of ln([1-hexene]/Ph_2CH_2) vs. time (min) for addition of 1-hexene to [(MesNpy)Hf(i-Bu)][A] (~15 mM) (0 ˚C, S); **a**) (A = $[B(C_6F_5)_4]^-$, S = C_6D_5Br), **b**) (A = $[HB(C_6F_5)_3]^-$, S = C_6D_5Br), **c**) (A = $[HB(C_6F_5)_3]^-$, S = $C_6D_5CD_3$).

Plot **a** in Figure 4.9 is a representative polymerization with the $[B(C_6F_5)_4]^-$ anion, carried out in C_6D_5Br (k_p = 6.0(6) M^{-1} min^{-1}, 0.10(1) M^{-1} s^{-1}). If the counter ion is changed to $[HB(C_6F_5)_3]^-$, plot **b**, the k_p is decreased to 2.87(7) M^{-1} min^{-1} (0.048(1) M^{-1} s^{-1}), indicating a significant anion effect. This may be due to closer interaction of the anion with the cation. Finally, retaining the $[HB(C_6F_5)_3]^-$ anion and changing the solvent to $C_6D_5CD_3$, plot **c**, reduces k_p further to 0.67(15) M^{-1} min^{-1} (0.0111(3) M^{-1} s^{-1}), which is one order of magnitude less than **a**. This decrease may also be a result of closer cation-anion interaction in a less polar solvent.

These rates are comparable to those reported in Chapter 3 for the primary alkyl cation $[(MesNpy)Hf(CH_2CH(CH_3)CH(CH_3)_2)][HB(C_6F_5)_3]$, which indicates that there is indeed an

anion effect in these systems. In light of these results and the importance of the cation-anion interaction in the polymerization process, attempts were made to better understand the role of the anion in solution.

Complex **42*** was activated with $B(C_6F_5)_3$ to yield **48***, and the solution was monitored by $^{13}C\{^1H\}$ NMR spectroscopy ($C_6D_5CD_3$) at temperatures from 0 to –100 ˚C (Figure 4.10). These spectra show no significant change in the Hf-*C*H_2 resonance over the temperature range studied. The reason for the signal broadening observed at –100 ˚C is unknown.

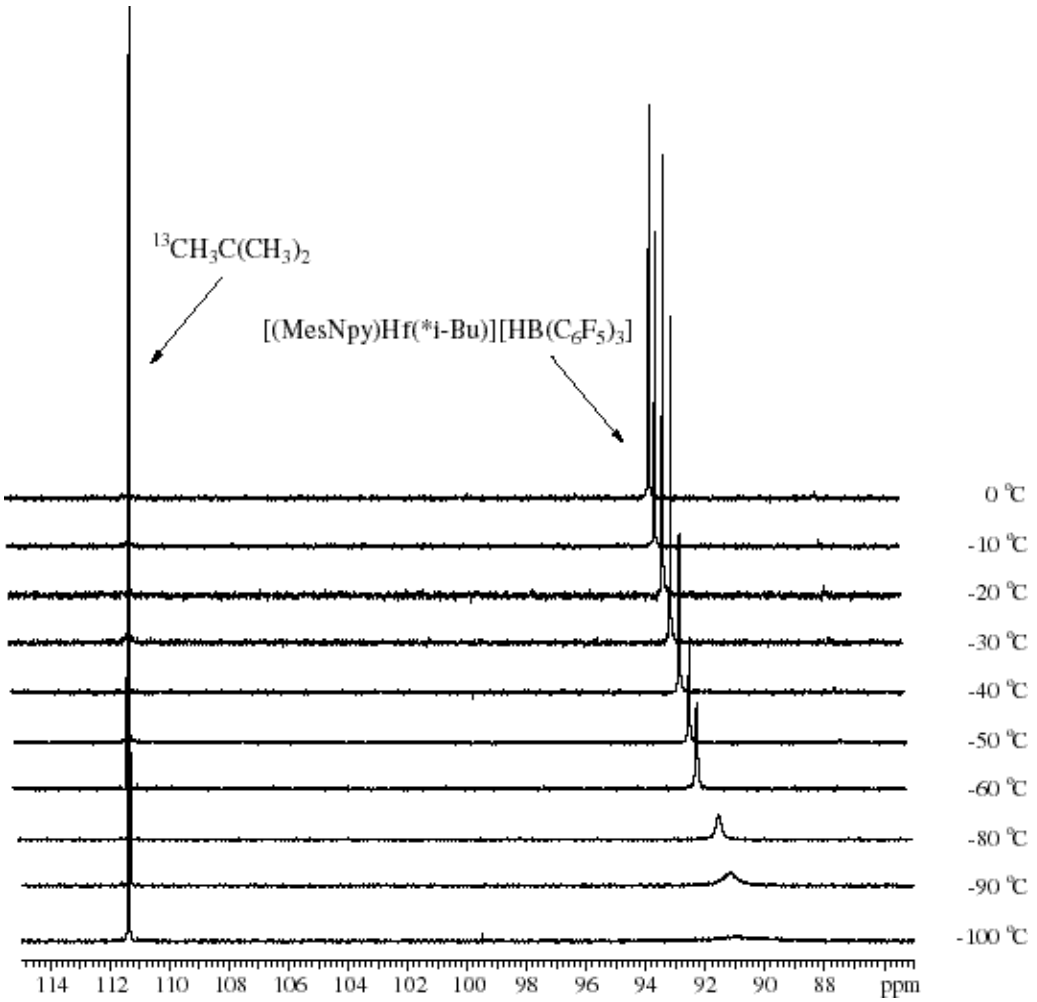

Figure 4.10. $^{13}C\{^1H\}$ NMR spectra (–100 - 0 ˚C, $C_6D_5CD_3$) for Hf-*C*H_2 carbons of **48***.

In order to determine the effect of anion on polymerization rate, $\{[(MesNpy)Hf]_2(CH_3)_3\}\{MeB(C_6F_5)_3\}$ (**18**) was used a source of the $[MeB(C_6F_5)_3]^-$ anion. Compound **18** can by synthesized and isolated as an analytically pure powder and is unreactive towards 1-hexene at 0 ˚C or at room temperature. In a series of experiments, **42** was activated with $[Ph_3C][B(C_6F_5)_4]$ to yield **43**, and to this solution were added various equivalents of **18** followed by 1-hexene. The polymerization reactions were monitored at 0 ˚C (eq 4.4).

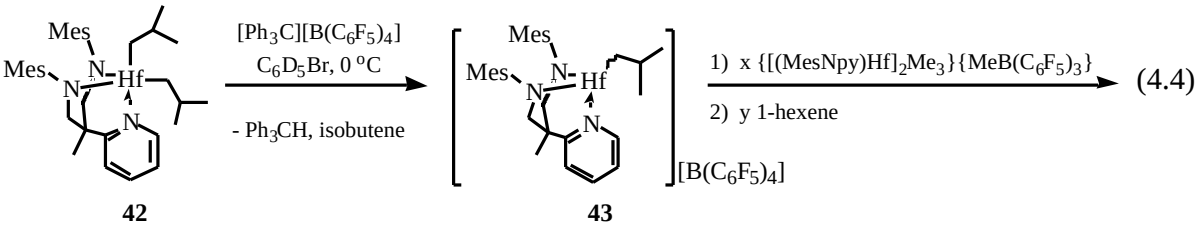

42 **43**

Up to 2 equiv of **18** were added in various runs, however, the plot of equiv $[MeB(C_6F_5)_3]^-$ vs. k_p does not show a significant anion effect (Figure 4.11).

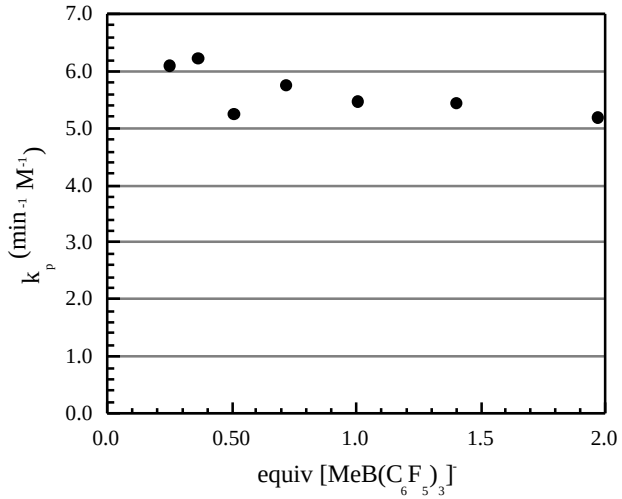

Figure 4.11. Plot of k_p ($min^{-1}M^{-1}$) vs. equiv $[MeB(C_6F_5)_3]^-$ for polymerization of 1-hexene with **43** (0 ˚C, C_6D_5Br).

Variable temperature $^{13}C\{^1H\}$ NMR spectroscopy (–60 - 20 ˚C, 1:1 C_6D_5Br : $C_6D_5CD_3$) of $\{[(MesNpy)Hf]_2(^{13}Me)_3\}\{^{13}MeB(C_6F_5)_3\}$ (**18***) shows no significant change in the resonance for the $^{13}CH_3$-B carbon, indicating that there is no significant interaction of the anion with the metal center (Figure 4.12). In the ^{13}C NMR spectra of systems where the $[MeB(C_6F_5)_3]^-$ anion is coordinated to the metal, the CH_3-B signal is usually reported at ~ 30 ppm.[36]

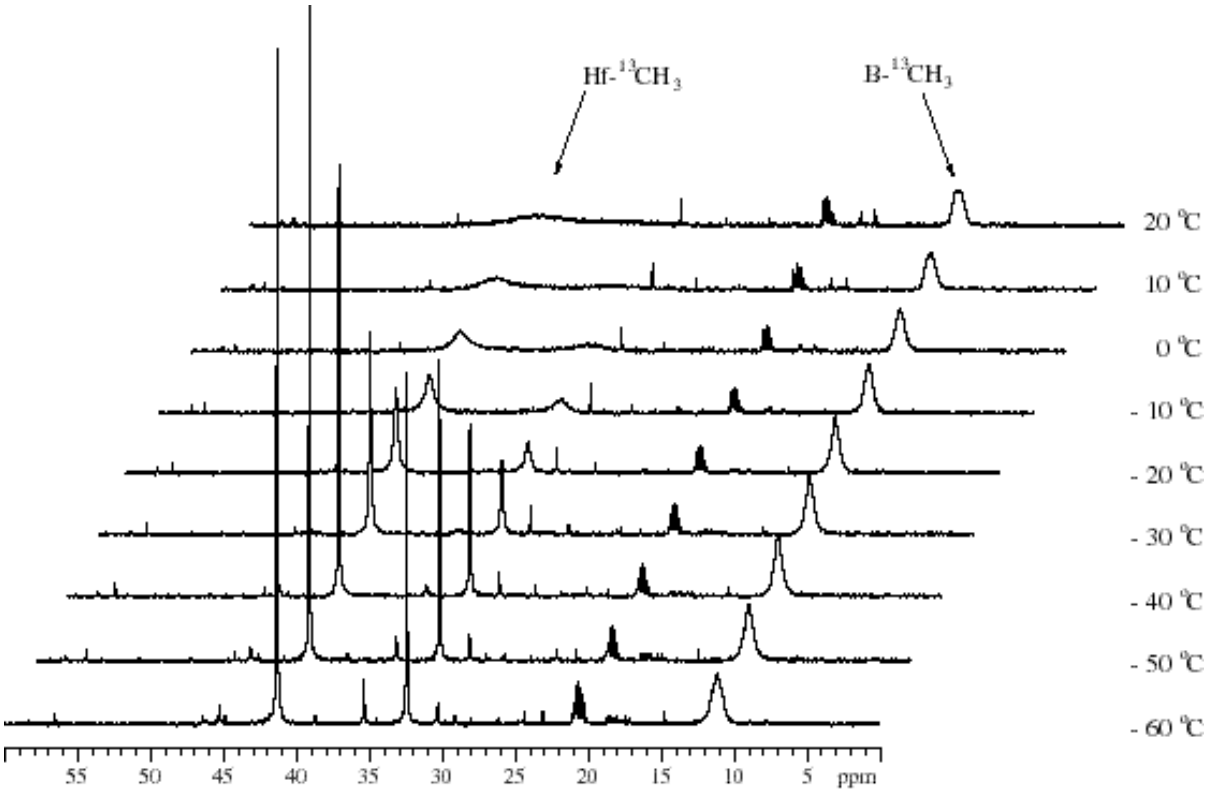

Figure 4.12. $^{13}C\{^1H\}$ NMR spectra (–60 - 20 ˚C, 1:1 C_6D_5Br : $C_6D_5CD_3$) of a mixture of **43** and **18***.

The reverse labeling experiment, *i.e.* addition of **18** to **43***, was carried out to further study the interaction of the anion with the cation. The $^{13}C\{^1H\}$ NMR spectrum of the solution mixture at the beginning of this experiment shows a signal at 93.4 ppm belonging to the Hf-$^{13}CH_2$ of **43*** as well as a new broad signal at 39.5 ppm, belonging to compound **A**. After 95 min

the new signal doubles in intensity. Signals corresponding to the backbone and pyridyl protons of a new complex, presumably **A**, are also observed in the ^{1}H NMR spectrum.

A possible explanation for this new signal may involve interaction of **43*** with the {[(MesNpy)Hf]$_2$Me$_3$} cation instead of interaction with the [MeB(C$_6$F$_5$)$_3$] anion. In order to rule out this interaction, it was important to have a source of the [MeB(C$_6$F$_5$)$_3$] anion with an innocent cation. To this end, [(n-Bu)$_4$N][MeB(C$_6$F$_5$)$_3$] (**49**) was prepared similarly to a method reported by Jordan *et al.*[104]

Two equiv of **49** were added to **43*** and the resulting solution was monitored by NMR spectroscopy. The ^{1}H NMR spectrum (0 ˚C, C$_6$D$_5$Br) of the mixture shows signals for **43*** as well as a set of signals that correspond closely to compound **A**. The ^{13}C{^{1}H} NMR spectrum shows a signal for the Hf-^{13}*C*H$_2$ carbon of **43*** as well as a signal at 39.5 ppm, corresponding to **A**. The signals attributed to **A** increase in intensity after 2 h at 0 ˚C. Polymerization of 94 equiv of 1-hexene with the resulting solution proceeds in a first order manner, with a k_p value of 2.8(1) M^{-1} min^{-1} (0.046(2) M^{-1} s^{-1}). It should be noted that this rate is obtained using the initial [**43***] and is thus expected to be less than the expected value of 6.0(6) M^{-1} min^{-1} (0.10(1) M^{-1} s^{-1}).

Although the nature of the new product **A** is unknown, it can be concluded that there is an interaction of **43** with the [MeB(C$_6$F$_5$)$_3$] anion. This species is not observed in control reactions without addition of the anion, while in both sets of experiments where **18** or **49** is used as the anion source, product **A** is observed. Scheme 4.3 summarizes the above experiments. From these studies one can conclude that the [MeB(C$_6$F$_5$)$_3$] anion is not suitable for polymerization reactions.

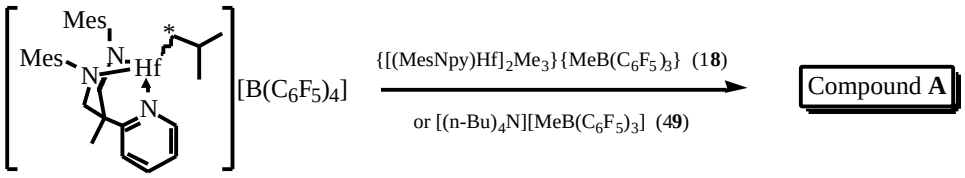

42*

Scheme 4.3. Addition of $[MeB(C_6F_5)_3]^-$ to $[(MesNpy)Hf(i\text{-}Bu)][B(C_6F_5)_4]$ (**43***).

4.6 Inhibition studies with $[(MesNpy)Hf(i\text{-}Bu)][B(C_6F_5)_4]$

One of the aims of this project is the controlled block copolymerization of α-olefins. When the block copolymerization of two olefins with significantly different polymerization rates, such as 1-hexene and ethylene, is attempted it is important to control the rate of ethylene polymerization in order to achieve a homogeneous solution and a uniform polymerization process. This can be done by rapid mechanical stirring or by slowing the rate of ethylene polymerization using an inhibitor. Initial studies in this area include inhibition of 1-hexene polymerization by a variety of bases including Et_2O, NMe_2Ph, Ph_2O, $(i\text{-}Pr)_2O$, NEt_3, NBu_3, and $N(i\text{-}Pr)_2Et$.

Et_2O. Past studies have shown that Et_2O is an inhibitor for various diamido-donor systems.[29] In a control experiment, 4 equiv of Et_2O were added to a 22 mM solution of **43** and to this mixture was added 72 equiv of 1-hexene. Polymerization was not observed at 0 ˚C after 2 h, confirming that diethyl ether inhibits the polymerization process completely.

NMe_2Ph. Dimethylaniline is a byproduct of activation with $[HNMe_2Ph][B(C_6F_5)_4]$ and has been studied in our group previously.[5,15,16,29,30,32,33,35,36,38,39] NMR scale kinetics experiments (0 ˚C, C_6D_5Br) with this inhibitor were carried out according to eq 4.5.

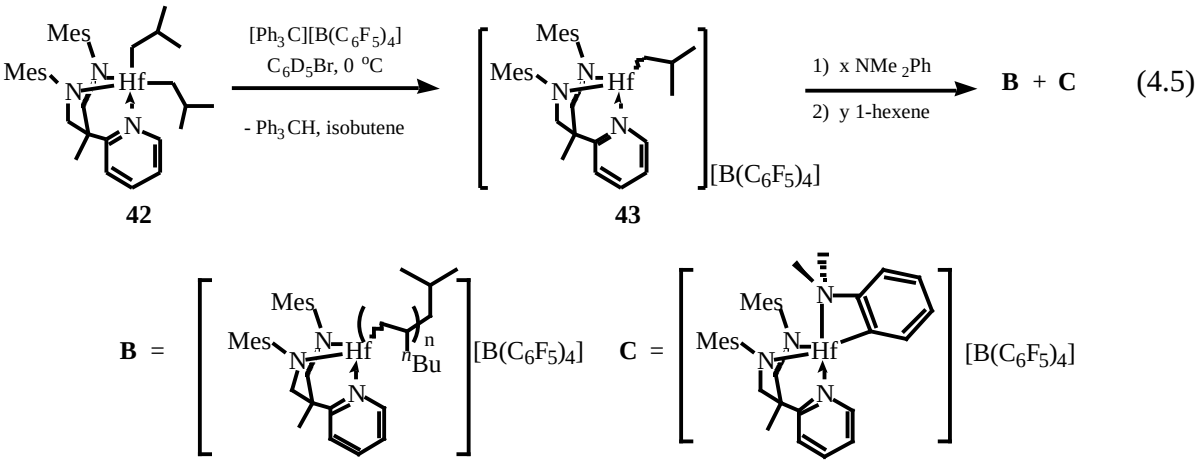

When x = 18 and y = 120, the ^{1}H NMR spectrum of the reaction mixture shows two distinct signals for the *ortho* pyridyl protons of the ligand. A broad signal at 8.72 ppm is attributed to the complex bound to the propagating chain, **B**. A sharp doublet at 9.03 ppm is also observed and is tentatively assigned to **C**, the product of C-H activation of NMe_2Ph by the Hf complex. After 2 h, the signal at 8.72 ppm has completely disappeared and the ^{1}H NMR spectrum, including the backbone region, shows signals for one distinct species, **C** (Figure 4.13).

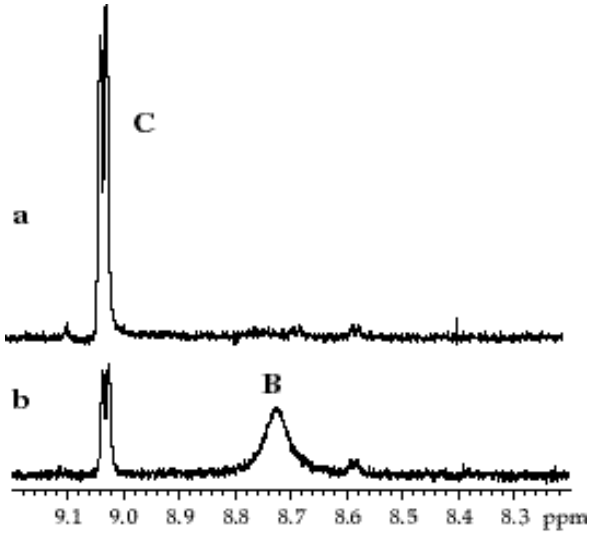

Figure 4.13. ^{1}H NMR spectra (0 ˚C, C_6D_5Br) for the *ortho* pyridyl region after addition of 18 equiv NMe_2Ph and 1-hexene to **43** a) after 2 h; b) initially.

Signals corresponding to vinylidene protons are not observed, which indicates that chain termination did not occur via β-hydride elimination. Figure 4.14 shows that the plot of ln([1-hexene]/std) vs. time for this system is slightly convex, resulting in a k_p value of 0.30(15) M^{-1} min^{-1} (0.036(2) M^{-1} s^{-1}) which is approximately 1/20 of the value obtained for the base-free system (6.0(6) M^{-1} min^{-1}, 0.10(6) M^{-1} s^{-1}). When a smaller amount of base is added, x = 5, y = 110, k_p is 2.2(1) M^{-1} min^{-1} (0.0050(3) M^{-1} s^{-1}) or 1/3 the expected value.

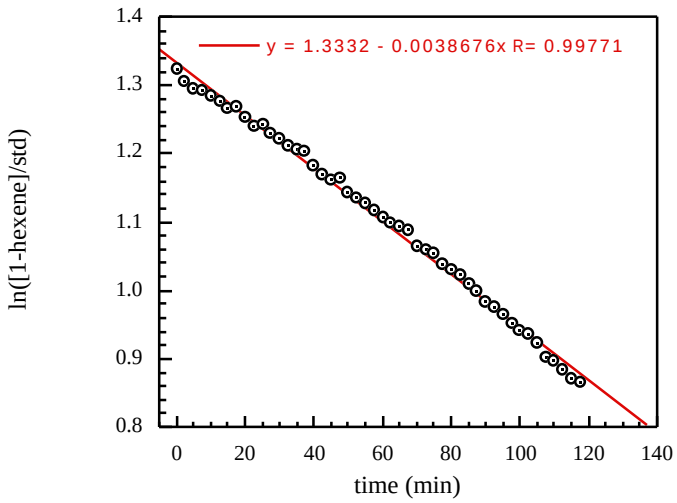

Figure 4.14. Plot of ln([1-hexene]/Ph_3CH) vs. time (min) for addition of 120 equiv of 1-hexene to **43** (0.013 M) in the presence of 18 equiv NMe_2Ph (0 ˚C, C_6D_5Br).

In order to further investigate this system, decomposition of **43*** in the presence of excess NMe_2Ph was observed by ^1H and $^{13}C\{^1H\}$ NMR spectroscopy (0 ˚C, C_6D_5Br) (eq 4.6).

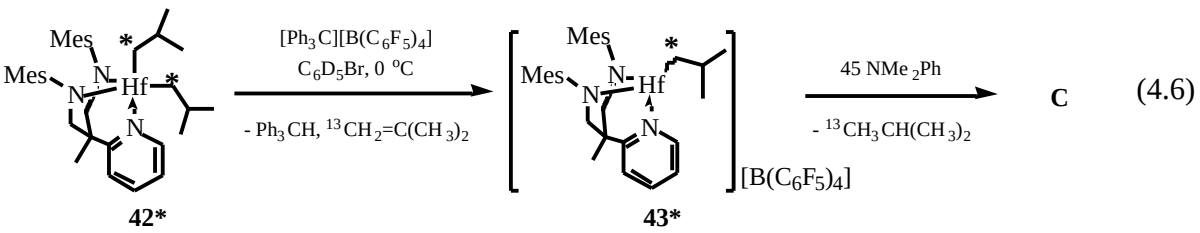

(4.6)

After 10 min two sharp doublets corresponding to the *ortho* pyridyl protons are observed at 8.76 and 9.01 ppm (6:1 ratio) in the ^{1}H NMR spectrum. The $^{13}C\{^{1}H\}$ NMR spectrum shows signals for $^{13}CH_2=C(CH_3)_2$ (111.14 ppm), **43*** (94.22 ppm, *cf*. base free 93.3 ppm) and $^{13}CH_3CH(CH_3)_2$ (24.82 ppm). After 125 min at 0 ˚C, the ^{1}H NMR spectrum shows a 1:1 ratio of the *ortho* pyridyl signals. The $^{13}C\{^{1}H\}$ NMR spectrum shows an increase in the isobutane signal and a corresponding decrease in the cation signal (Figure 4.15).

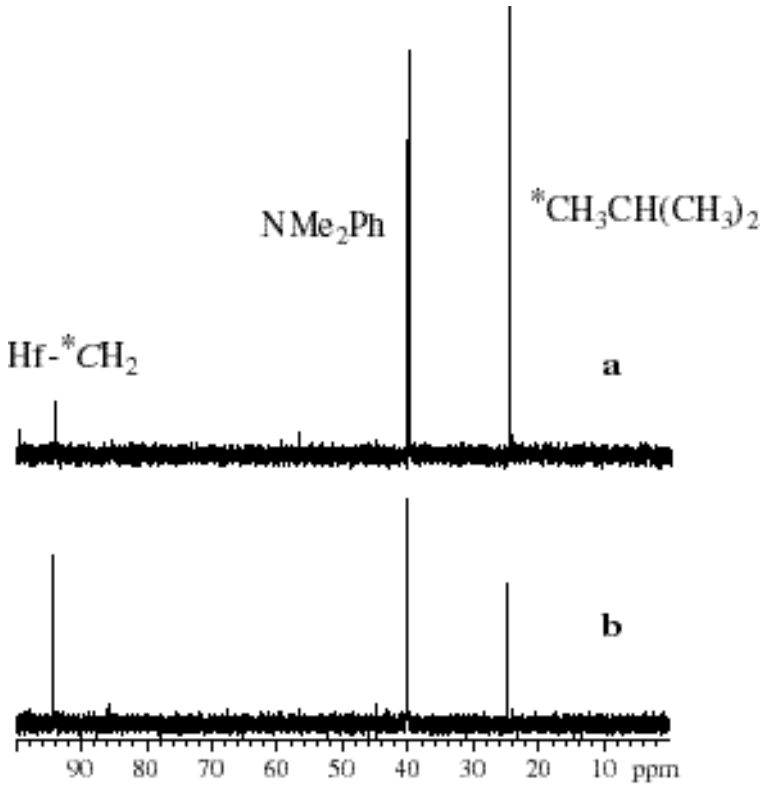

Figure 4.15. $^{13}C\{^{1}H\}$ NMR spectra (0 ˚C, C_6D_5Br) of addition of NMe_2Ph to **43**. a) after 2 h; b) initially.

It was possible to follow the decomposition process quantitatively by monitoring the disappearance of the backbone signal for the cation (4.4 ppm) in the ^{1}H NMR spectrum (Figure 4.16). The decomposition process is strictly first order with k_d of 0.00664(4) min^{-1} (1.11(2) × 10^{-4} s^{-1}).

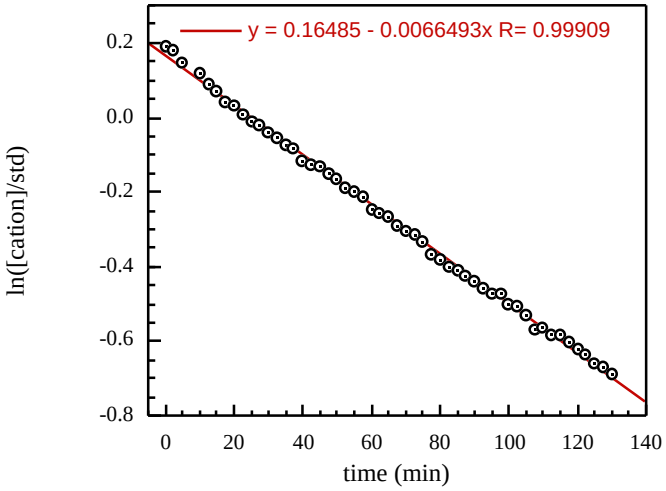

Figure 4.16. Plot of ln([cation]/Ph_3CH) vs. time (min) for addition of 45 equiv of NMe_2Ph to **43*** (0.019 M) (0 ˚C, C_6D_5Br).

The C-H activated product, [(MesNpy)Hf($C_6H_4NMe_2$)][$B(C_6F_5)_4$] (**50**), can by synthesized by adding 1 equiv of NMe_2Ph to [(MesNpy)Hf(i-Bu)][$HB(C_6F_5)_3$] (**48**) and stirring the mixture at 0 ˚C for 24 h (eq 4.7). The product was isolated as a yellow powder in 72% yield,

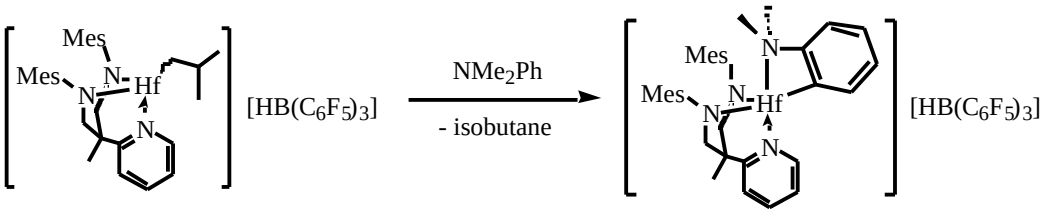

48 **50** (4.7)

and has been characterized by elemental analysis as well as various NMR spectroscopic methods. The ^{1}H NMR spectrum (20 ˚C, C_6D_5Br) is very similar to those obtained for **C** in the above experiments. The resonance for the *ortho* pyridyl proton is at 9.02 ppm and in the aliphatic region four resonances, each corresponding to six protons, are observed. A gCOSY experiment allowed a full assignment of the spectrum. Three of these signals were attributed to methyl groups of the mesityl ring. The fourth signal at 2.13 ppm is assigned to the N-CH_3 groups of a C-H activated dimethylaniline. Resonances for the 4 protons of the N-C_6H_4 ring were also observed and clearly assigned. The ^{13}C{^{1}H} NMR spectrum shows a signal at 47.9 ppm for the N-CH_3 carbons. Although no X-ray crystal structure has been obtained, all the experimental evidence gathered points toward the structure of this complex as shown in eq 4.7.

Ph_2O. The use of Ph_2O as an inhibitor was also complicated by catalyst decomposition (eq 4.8).

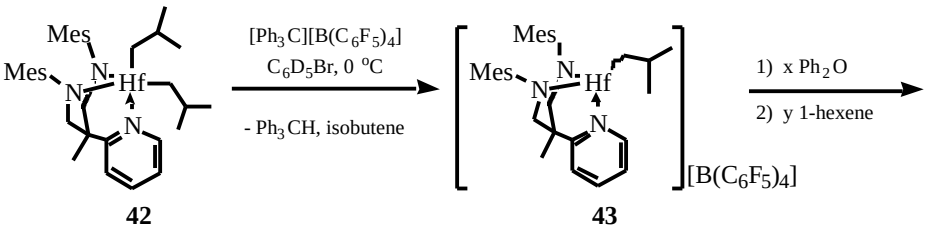

42 **43** (4.8)

Monitoring the *ortho* pyridyl region of a given experiment, x = 17, y = 89, shows that in addition to the broad signal for the polymer-bound hafnium complex, **B**, two sets of sharp doublets are observed at 8.70 and 8.74 ppm, indicating the generation of two unidentified species during the polymerization process, **D** and **E**.

The consumption of 1-hexene by this solution was also monitored (Figure 4.17). The plot in Figure 4.17 is clearly curved, indicative of catalyst decomposition. This decomposition may be attributed to C-H activation of the aryl rings of Ph_2O, analogous to the NMe_2Ph case, to yield two possible products. The identity of these products remains unclear.

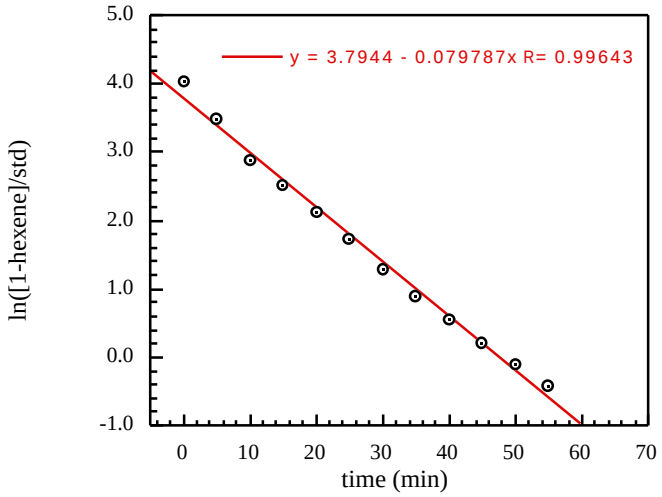

Figure 4.17. Plot of ln([1-hexene]/Ph_3CH) vs. time (min) for addition of 89 equiv of 1-hexene to **43** in the presence of 17 equiv Ph_2O (0 ˚C, C_6D_5Br).

$(i\text{-}Pr)_2O$. As bases with aryl rings were found to be unstable towards C-H activation, and more donating bases such as diethyl ether stopped polymerization, $(i\text{-}Pr)_2O$ was chosen as an inhibitor (eq 4.9).

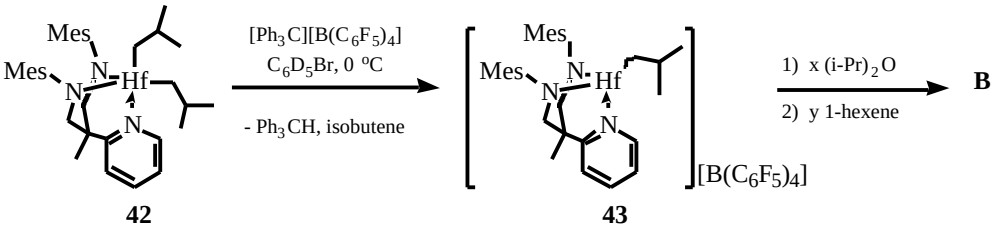

42 **43** (4.9)

This base proved to be very well-behaved. Figure 4.18 shows kinetics runs with varying equivalents of $(i\text{-}Pr)_2O$.

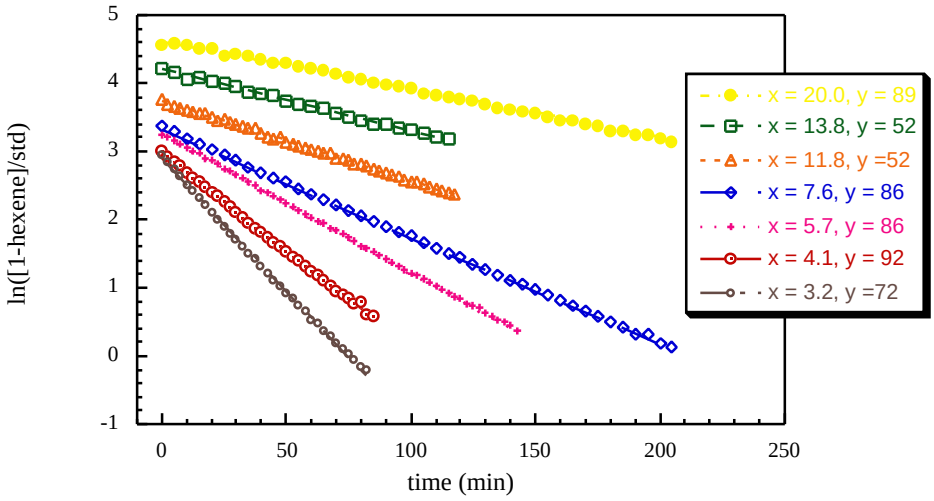

Figure 4.18. Plot of ln([1-hexene]/Ph_3CH) vs. time (min) for addition of y equiv of 1-hexene to **43** (~ 10 mM) in the presence of x equiv $(i\text{-}Pr)_2O$ (0 ˚C, C_6D_5Br).

The above polymerization studies are first order in olefin and show a corresponding decrease in propagation rate with an increase in equivalents of $(i\text{-}Pr)_2O$. A simple kinetics relationship can be derived to relate the observed first order rate constant to equivalents of base (eq 4.10 - 4.15). In the derivation, it is assumed that there is a fast equilibrium between the active catalyst (cat) and the inactive base (B) adduct (cat·B).

$$\text{cat} + \text{B} \underset{k_{-1}}{\overset{k_1}{\rightleftharpoons}} \text{cat}\cdot\text{B} \tag{4.10}$$

$$K = \frac{[\text{cat B}]}{[\text{cat}][\text{B}]} \tag{4.11}$$

$$[\text{cat}] = [\text{cat}]_o - [\text{cat B}] \tag{4.12}$$

$$\frac{-d[\text{ol}]}{dt} = k_p[\text{cat}][\text{ol}] + k_{obs}[\text{ol}] \tag{4.13}$$

$$k_{obs} = \frac{k_p[\text{cat}]_o}{1 + K[\text{B}]} \tag{4.14}$$

$$\frac{[\text{cat}]_o}{k_{obs}} = \frac{K}{k_p}[\text{B}] + \frac{1}{k_p} \tag{4.15}$$

The equilibrium constant (K) for the coordination of a given base (B) to a catalyst (cat) is defined by eq 4.11, where cat·B is a base adduct of the catalyst. An expression for the concentration of catalyst in solution at any given time, [cat], can be derived from eq 4.11 and 4.12. Thus the observed rate constant (k_{obs}) for olefin (ol) polymerization as defined in eq 4.13 can be defined in terms of the rate of propagation (k_p) and K (eq 4.14). Rearrangement of eq 4.14 yields the desired relationship between k_{obs} and [B] (eq 4.15).

A plot of $[Hf]_o/k_{obs}$ vs. [B] (Figure 4.19) gives a value for k_p of 6.3 (27) $min^{-1}M^{-1}$ and for K of 41(5) M^{-1}. The derived value for k_p agrees roughly with the experimental value of 6.0(6) M^{-1} min^{-1} (0.10(1) M^{-1} s^{-1}) derived from base-free polymerizations. From the equilibrium constant, K, one can determine the rate with the appropriate concentration of base.

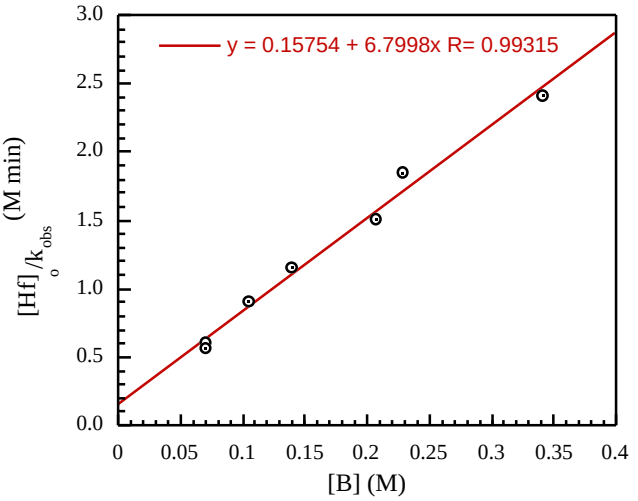

[i-Pr $_2$O] (M)	[Hf] $_o$ / k_{obs} (M min)
0.433	2.61
0.341	2.41
0.229	1.85
0.207	1.51
0.139	1.16
0.104	0.906
0.0703	0.601
0.0703	0.567

Figure 4.19. Plot of $[Hf]_o/k_{obs}$ (M min) vs. [B] for addition of 1-hexene to **43** (~ 15 mM) in the presence of $(i\text{-}Pr)_2O$ (0 ˚C, C_6D_5Br).

The efficiency of $(i\text{-}Pr)_2O$ as inhibitor can be demonstrated in a simple experiment (eq 4.16). In this experiment 52 equiv of 1-hexene are polymerized by **43**, then 14 equiv $(i\text{-}Pr)_2O$ are added to the same solution and after mixing, a further 52 equiv of 1-hexene are added (Figure 4.20).

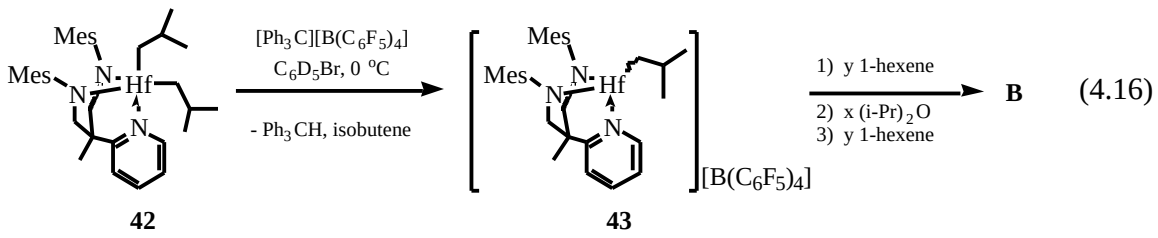

42 **43** (4.16)

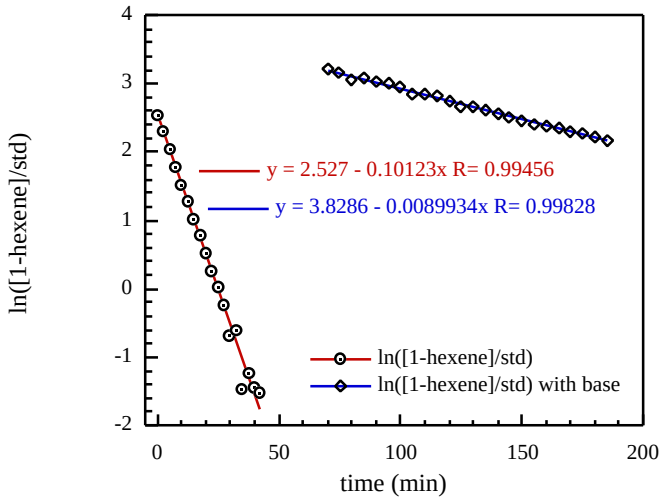

Figure 4.20. Plot of ln([1-hexene]/Ph_3CH) vs. time (min) for addition of 52 equiv of 1-hexene to **43** (0.017 M) followed by addition of a further 52 equiv in the presence of 14 equiv $(i\text{-}Pr)_2O$ (0 ˚C, C_6D_5Br).

Figure 4.20 shows that the observed rate constant for the inhibited reaction is about an order of magnitude less than the base-free reaction. A sample bulk polymerization reaction (141 equiv 1-hexene) with 13 equiv of $(i\text{-}Pr)_2O$ gives polymer samples with PDI = 1.05 and M_n = 11900 (expected M_n = 11866).

Tertiary amines: NEt_3, NBu_3, and $N(i\text{-}Pr)_2Et$. The success of $(i\text{-}Pr)_2O$ as an inhibitor prompted us to investigate non-arylated tertiary amines as bases.

Polymerization of 1-hexene with **43** in the presence of up to 13 equiv of NEt_3 proceeded with first order kinetics and no observable initiation period. The plot of $[Hf]_o/k_{obs}$ vs. [B] (Figure

4.21) is linear and shows a K value of 73(7) M^{-1}. Triethylamine proved well behaved in a bulk polymerization reaction as well. Polymerization of 247 equiv 1-hexene with a 10 mM solution of **43** (0 ˚C, C_6H_5Cl) with 9 equiv NEt_3 resulted in a polymer sample with M_n = 22900 (M_n expected = 20800) and PDI = 1.08.

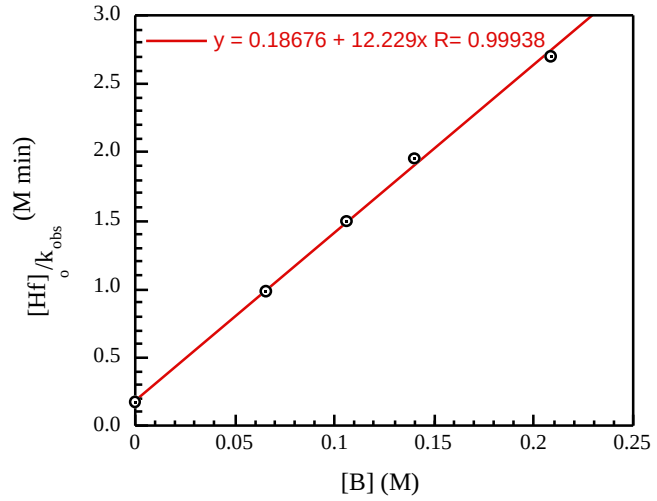

[NEt 3] (M)	[Hf] o / k obs (M min)
0.209	2.70
0.140	1.95
0.106	1.49
0.0658	0.985
0	0.170

Figure 4.21. Plot of $[Hf]_o/k_{obs}$ (M min) vs. [B] for addition of 1-hexene to **43** (~ 17 mM) in the presence of NEt_3 (0 ˚C, C_6D_5Br).

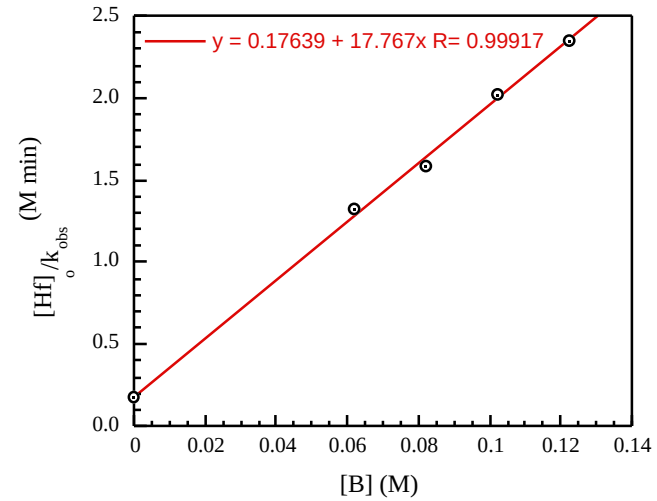

[NBu 3] (M)	[Hf] o / k obs (M min)
0.122	2.35
0.102	2.02
0.082	1.59
0.062	1.32
0	0.170

Figure 4.22. Plot of $[Hf]_o/k_{obs}$ (M min) vs. [B] for addition of 1-hexene to **43** (~ 17 mM) in the presence of NBu_3 (0 ˚C, C_6D_5Br).

In order to determine the importance of amine steric bulk, NBu_3 was utilized. The plot of $[Hf]_o/k_{obs}$ vs. [B] (Figure 4.22) is linear and shows a K value of 107(11) M^{-1}. It should be noted that kinetics data were reliable for up to only 7 equiv of base. At higher base concentrations, not enough data could be obtained in a reasonable time.

A more bulky amine, $N(i\text{-}Pr)_2Et$, was also investigated. Addition of 7, 13, and 32 equiv of base to a solution of **43** did not cause inhibition of 1-hexene polymerization. However, two resonances at 4.84 and 4.86 ppm were observed in the ^1H NMR spectrum (0 ˚C, C_6D_5Br) after consumption of all the 1-hexene. These signals correspond to vinylidene protons at 4.8 ppm resulting from β-hydride elimination of the 1,2-insertion product. One hypothesis for the appearance of these signals is a base-mediated decrease in cation-anion interaction resulting in destabilization of the cation. Further studies in this area are required to ascertain the likelihood of this possibility.

A number of inhibitors were investigated, and general trends for a successful inhibitor were observed (Table 4.3). Activators with aryl groups were prone to C-H activation and were thus unsuccessful. Bulky ethers and amines were successful, however, and it was possible to obtain equilibrium constants for base association, while very bulky amines were not good inhibitors. With the use of these successful inhibitors, it is possible to have a greater degree of control over the polymerization process.

Table 4.3. Summary of inhibitor studies with $[(MesNpy)Zr(i\text{-}Bu)][B(C_6F_5)_4]$ (**43**).

Inhibitor	Inhibition activity or K
Et_2O	Inhibits completely
NMe_2Ph	C-H activation
Ph_2O	C-H activation
$(i\text{-}Pr)_2O$	K = 41(5) M^{-1}
NEt_3	K = 73(7) M^{-1}
NBu_3	K = 107(11) M^{-1}
$N(i\text{-}Pr)_2Et$	No inhibition

4.7 Different monomers / block copolymerization

The successful generation and study of a controlled living polymerization system opens the way to the study of a variety of monomers in block copolymerization reactions. Results in this area are preliminary, but prove encouraging for future studies.

Styrene and vinylcyclohexane (VCH). Attempts to carry out styrene polymerization were not successful. Forty eight equiv of styrene were added to a 29 mM solution of **43** and the polymerization activity was monitored. The ^{1}H NMR spectrum (0 ˚C, C_6D_5Br) of the reaction mixture remains essentially unchanged in a nearly 3 h time period and shows signals for excess styrene as well as broad signals at ~ 2.4 and 1.9 ppm, which may be traces of polystyrene. The remaining signals are attributed to a single complex (only one ortho pyridyl proton is observed at 8.5 ppm) where the backbone signals are split into four sets of sharp doublets, indicative of a loss of C_s symmetry. These signals may belong to a styrene coordinated species; further studies will be needed to determine the nature of this species.

In light of studies carried out by Sita *et al.*[19], vinylcyclohexane (VCH) was also investigated. Addition of 41 equiv of VCH to a 20 mM solution of **43** at 20 ˚C showed very slow polymerization. Under similar conditions, 1-hexene polymerization is complete within less than 5 min. These data show that the [MesNpy] system is not appropriate for the polymerization of VCH, however other, more active systems being studied in this group may show promise for this monomer.[16]

1-Hexene/ethylene block copolymers. First attempts at block copolymerization were carried out by polymerizing 1-hexene with a solution of **43**, freezing the solution in liquid nitrogen, and condensing ethylene into the reaction vessel. These reactions resulted in biphasic polymer samples composed of a soluble layer, poly(1-hexene), and an insoluble, brittle crust. This crust is likely composed of a hexene-ethylene block copolymer with a very long polyethylene segment

generated as a result of poor diffusion of ethylene in solution and rapid polymerization on surface of the reaction mixture. The addition of an inhibitor solved this problem to some extent.

In one experiment 364 equiv of 1-hexene were polymerized by a 7 mM solution of **43** (0 ˚C, C_6H_5Cl) for 4 h. Only 0.005% of the 1-hexene remained after this time. Then 43 equiv (i-Pr)$_2$O was added to the solution and mixed thoroughly. Ethylene (137 equiv) was then condensed into this reaction mixture, the mixture was warmed to 0 ˚C, and the polymerization resumed at this temperature with vigorous stirring.

The resulting polymer is a homogeneous gelatinous substance which had absorbed the C_6H_5Cl. When a sample of this material is taken up in a solvent such as methanol or pentane, it slowly loses the trapped chlorobenzene to yield a solid material that has much greater structural cohesiveness than poly(1-hexene) and yet is not brittle. A GPC trace of this material, after passing it through a plug of silica, shows two distinct peaks: one with a very short retention time, *i.e.* high M_n (1×10^7), and the other with a retention closer to the value expected for approximately a 400-mer. It was very difficult to obtain accurate values for the molecular weights. It is possible that the polymer samples are forming aggregates or micelles in THF at room temperature, thus leading to the obtained results. Further work is required in this area to obtain pure polymer samples and characterize them by high temperature GPC measurements.

4.8 Conclusions

Chapter 4 described the study of activated [ArNpy]Hf(i-Bu)$_2$ systems and showed that some of these systems are capable of catalyzing the living polymerization of α-olefins.

In particular, [(MesNpy)Hf(i-Bu)][B(C_6F_5)$_4$] showed great promise as a very well-behaved system, as it met all of the criteria listed in the introduction. An important benefit of this system was its viability under various conditions. Catalyst concentration, temperature, counterion and inhibitors have all been varied and result in living systems.

The interaction of cations with neutral dialkyl species, with other cations, and with the counterion was discussed. Rapid alkyl transfer from [(MesNpy)Hf(*i-Bu)][$B(C_6F_5)_4$] to [TripNpy]Hf(i-$Bu)_2$ showed that trace amounts of unactivated dialkyl complex may catalyze alkyl transfer between two cationic centers. In a living system this should not be a problem as all metal-bound polymer chains are of the same length and thus chain transfer should have no effect on polymer properties. However, in systems where chain termination is rapid, this phenomenon may be of importance in explaining polymer defects.

The role of anion in the polymerization process was also discussed in this chapter. A significant reduction in polymerization rate was observed when the anion was changed from [$B(C_6F_5)_4$] to [$HB(C_6F_5)_3$]. Also, some evidence for cation interaction with [$MeB(C_6F_5)_3$] was presented. These observations highlight the importance of the cation-anion pair.

Inhibitors proved successful in controlling polymerization rate. Inhibitors with aryl groups, such as NMe_2Ph and Ph_2O, resulted in C-H activation of aryl protons leading to catalyst decomposition. Bulky ethers and amines, however, led to very well-behaved systems. If the amine used is very bulky, such as N(i-$Pr)_2$Et, the polymerization rate is not hindered. This may prove advantageous if olefins with TMS-protected functional groups are to be used in co-polymerization processes. Preliminary block polymerization reactions of 1-hexene and ethylene were successful, and promised further interesting results with this system.

This thesis has explored a variety of systems bearing the $[ArNpy]^{-2}$ ligand and has made it possible to directly compare the rates of 1-hexene polymerization with these catalysts under a variety of conditions. Table 4.4 highlights some of the most important findings. Rates obtained for precatalysts bearing methyl groups are significantly lower than other catalyst systems due to formation of unreactive dinuclear monocations which drastically reduce catalyst efficiency.

Zirconium cations have similar polymerization rates to their hafnium counterparts, however the polymer samples that were obtained have molecular weights significantly higher than expected. Attempts to increase catalyst activity by increasing cation steric bulk had the

opposite effect; systems bearing the $[TripNpy]^{2-}$ ligand had significantly lower polymerization rates than those bearing the $[MesNpy]^{2-}$ ligand. The effects of different activator, anion, solvent and inhibitors were also explored, and each of these factors was found to be significant in designing a well-behaved living polymerization catalyst.

Table 4.4. A comparison of different catalyst systems bearing $[ArNpy]^{2-}$ ligands.

Precatalyst	Activator	Solvent / T (°C)	k_p (M^{-1} min^{-1})	k_p (M^{-1} s^{-1})	$\Delta H^{\ddagger}$ (kcal mol^{-1})	$\Delta S^{\ddagger}$ (cal mol^{-1} K^{-1})
[MesNpy]Hf(i-Bu)$_2$	$[Ph_3C][B(C_6F_5)_4]$	C_6D_5Br / 0	6.0(6)	0.10(1)	10.86(46)	–28.6(28)
	$B(C_6F_5)_3$	C_6D_5Br / 0	2.87(7)	0.048(1)		
	$B(C_6F_5)_3$	$C_6D_5CD_3$ / 0	0.67(15)	0.0111(3)		
[MesNpy]Hf(i-Pr)$_2$ [a]	$[HNMe_2Ph][B(C_6F_5)_4]$	C_6D_5Br / 0	4.5(2)	0.075(3)		
[MesNpy]Hf(i-Pr)$_2$	$B(C_6F_5)_3$	C_6D_5Br / 0	2.75(6)	0.046(1)		
[TripNpy]Hf(i-Bu)$_2$	$[Ph_3C][B(C_6F_5)_4]$	C_6D_5Br / 0	1.71(8)	0.029(1)		
[MesNpy]Zr(i-Bu)$_2$	$[Ph_3C][B(C_6F_5)_4]$	C_6D_5Br / 0	4.8(1)	0.079(2)	8.09(65)	–33.3(26)
[TripNpy]Zr(i-Bu)$_2$	$[Ph_3C][B(C_6F_5)_4]$	C_6D_5Br / 0	2.7(1)	0.044(2)		
[MesNpy]ZrMe$_2$ [b]	$[Ph_3C][B(C_6F_5)_4]$	C_6D_5Br / 25	0.016(1) min^{-1}	2.7(2) × 10^{-4} s^{-1}	14.40(49)	–23.1(19)
[TripNpy]ZrMe$_2$ [b]	$[Ph_3C][B(C_6F_5)_4]$	C_6D_5Br / 25	0.025(1) min^{-1}	4.2(2) × 10^{-4} s^{-1}		

[a] The rate may be affected by aniline coordination and C-H activation.
[b] The rates vary with reaction conditions.

4.9 Experimental

General Procedures. All manipulations, with the exception of the synthesis of ligand precursors, were performed under N_2 in a glove-box or using standard Schlenk procedures. Solvents were dried using conventional procedures.[60] Chlorobenzene (HPLC grade) and deuterated solvents were degassed, stored over and distilled from CaH_2. Commercial reagents were used without further purification. NMR spectra were recorded on a Varian INOVA 500 spectrometer. ^1H NMR chemical shifts are given in ppm versus residual protons in the deuterated solvents as follows: δ 7.16 C_6D_6, δ 2.09 toluene-d_8 (methyl), δ 7.29 C_6D_5Br (most downfield resonance). $^{13}C\{^1H\}$ NMR chemical shifts are given in ppm versus residual ^{13}C in the solvents as follows: δ 128.39 C_6D_6, δ 20.4 toluene-d_8 (methyl), δ 122.25 C_6D_5Br (most upfield resonance). Some aryl resonances in ^1H and $^{13}C\{^1H\}$ spectra are not given.

Elemental analyses were performed by H. Kolbe, Mikroanalytisches Laboratorium (Mülheim an der Ruhr, Germany). GPC analyses were carried out on a system equipped with two Jordi-Gel DVB mixed bed columns (250 mm length × 10 mm inner diameter) in series. HPLC grade THF was supplied at a flow rate of 1.0 mL/min with a Knauer 64 HPLC pump. A Wyatt Technology mini Dawn light scattering detector coupled with a Knauer differential refractometer was employed. Data analysis was carried out using Astrette 1.2 software (Whatt Technology). M_n and M_w values for poly(1-hexene) were obtained using dn/dc = 0.076 mL/gr (Wyatt Technology) and the auxiliary constant of the apparatus (5.9×10^{-4}) calibrated using a polystyrene standard ($M_n = 2.2 \times 10^5$).

Grignard reagents $^{13}CH_3MgI$ and $(CH_3)_2CH^{13}CH_2MgBr$ were prepared from $^{13}CH_3I$ and $(CH_3)_2CH^{13}CH_2Br$[105,106] respectively, and Mg turnings in diethyl ether according to standard procedures, all others were purchased from Aldrich. All Grignard reagents were carefully titrated with 2-butanol in the presence of 1,10-phenanthroline prior to use. $[MesNpy]H_2$[26] and $Hf(NMe_2)_4$[61] have been prepared according to previously reported methods. The anion source

$[Bu_4N][MeB(C_6F_5)_3]$ was prepared according to similar methods reported by Jordan *et al.*[104] Syntheses of $[MesNpy]Hf(NMe_2)_2$ and $[MesNpy]HfCl_2$ are described in Chapter 1.

$[MesNpy]Hf(i\text{-}Bu)_2$ (42). A suspension of $[MesNpy]HfCl_2$ (1.70 g, 2.62 mmol) in diethyl ether (50 mL) was cooled to -30 ˚C. To the cold solution was added (i-Bu)MgBr (2.0 M in diethyl ether, 2.88 mL, 5.76 mmol) and the resulting mixture was stirred at room temperature for 10 min until the cloudy suspension became clear. Dioxane (0.670 mL, 0.786 mmol) was added to the solution and the resulting white solid was filtered through Celite. The solvent was removed *in vacuo* to yield a white powder, which was redissolved in 5 mL diethyl ether and crystallized at -30 ˚C to yield the product as white crystals. Yield: 1.5 g, 83%. $[MesNpy]Hf(^{13}CH_2CHMe_2)_2$ (**42***) was prepared in a similar fashion from $Me_2CH^{13}CH_2MgBr$. ^{1}H NMR (500 MHz, C_6D_6, 295 K) δ 0.82 (m, 2H, Hf-CH_2CH$(CH_3)_2$), 0.85 (m, 4H, Hf-CH_2CH$(CH_3)_2$), 0.92 (s, 3H, CH_3), 0.95 (d, 6H, Hf-CH_2CH(C$H_3)_2$), 1.27 (d, 6H, Hf-CH_2CH(C$H_3)_2$), 2.17 (s, 6H, *p*-CH_3), 2.3 (broad s, 12H, *o*-CH_3), 2.41 (m, 1H, Hf-CH_2C*H*$(CH_3)_2$), 2.54 (m, 1H, Hf-CH_2C*H*$(CH_3)_2$), 2.84 (d, 2H, CH_2), 4.12 (d, 2H, CH_2), 6.62 (m, 1H, py-C*H*), 6.78 (m, 1H, py-C*H*), 6.90 (s, 4H, C*H*), 7.04 (m, 1H, py-C*H*), 8.96 (m, 1H, py-*o*-C*H*). ^{13}C{^{1}H} NMR (125 MHz, C_6D_6, 295 K) δ 19.23 (s, *o*-*C*H_3), 21.29 (s, *p*-*C*H_3), 25.38 (s, *C*H_3), 29.85 (s, Hf-CH_2CH(*C*$H_3)_2$), 30.41 (s, Hf-CH_2CH(*C*$H_3)_2$), 30.77 (s, Hf-CH_2*C*H$(CH_3)_2$), 32.80 (s, Hf-CH_2*C*H$(CH_3)_2$), 45.84 (s, *C*R_4), 66.29 (s, *C*H_2), 82.36 (s, Hf-*C*H_2CH$(CH_3)_2$), 83.88 (s, Hf-*C*H_2CH$(CH_3)_2$), 120.80 (s, Ar-*C*), 122.83 (s, Ar-*C*), 130.15 (s, Ar-*C*), 134.13 (s, Ar-*C*), 135.70 (s, Ar-*C*), 139.27 (s, Ar-*C*), 146.92 (s, Ar-*C*), 147.40 (s, Ar-*C*), 163.40 (s, Ar-*C*). Anal. Calcd for $C_{35}H_{51}N_3Hf$: C, 60.72; H, 7.43; N, 6.07. Found: C, 60.65; H, 7.51; N, 6.12.

$[TripNpy]Hf(NMe_2)_2$ (44). $Hf(NMe_2)_4$ (0.66 g, 1.85 mmol) and H_2[TripNpy] (1.06 g, 1.86 mmol) were dissolved in pentane (60 mL). The reaction mixture was stirred at room temperature for 16 h, residual insoluble precipitate filtered, and the solution stirred at room

temperature for a further 16 h. The solution was filtered to remove small amounts of solid residue, and the solvent was reduced to yield a red solution which was cooled to -30 ˚C for 12 h to yield a yellow precipitate. Yield: 0.70 g, 45%. ^{1}H NMR (500 MHz, C_6D_6, 295 K) δ 0.66 (d, 6H, C*H*$_3$), 1.03 (s, 3H, C*H*$_3$), 1.28 (d, 12H, C*H*$_3$), 1.33 (d, 6H, C*H*$_3$), 1.58 (d, 6H, C*H*$_3$), 1.59 (d, 6H, C*H*$_3$), 2.86 (m, 2H, C*H*), 2.93 (s, 6H, N(C*H*$_3$)$_2$), 3.02 (m, 2H, C*H*), 3.07 (d, 2H, C*H*$_2$), 3.10 (s, 6H, N(C*H*$_3$)$_2$), 4.12 (m, 2H, C*H*), 4.27 (d, 2H, C*H*$_2$), 6.69 (m, 1H, py-C*H*), 6.78 (m, 1H, py-C*H*), 7.05 (m, 1H, py-C*H*), 7.10 (d, 2H, C*H*), 7.27 (d, 2H, C*H*), 8.79 (m, 1H, py-*o*-C*H*). Anal. Calcd for $C_{43}H_{69}N_5Hf$: C, 61.89; H, 8.33; N, 8.39. Found: C, 62.01; H, 8.36; N, 8.31.

[TripNpy]HfCl$_2$ (45). To a solution of [TripNpy]Hf(NMe$_2$)$_2$ (0.465 g, 0.567 mmol) in diethyl ether (15 mL) was added TMSCl (0.2 mL, 1.67 mmol) and the reaction mixture was stirred at room temperature for 4 h. The resulting white solid was filtered, washed with pentane (3 × 10 mL) and dried *in vacuo* for 4 h. Yield: 0.375 g, 82%. ^{1}H NMR (300 MHz, C_6D_6, 295 K) δ 0.67 (d, 6H, C*H*$_3$), 0.91 (s, 3H, C*H*$_3$), 1.12 (br d, 6H, C*H*$_3$), 1.30 (d, 6H, C*H*$_3$), 1.32 (d, 6H, C*H*$_3$), 1.59 (d, 6H, C*H*$_3$), 1.86 (d, 6H, C*H*$_3$), 2.43 (br m, 2H, C*H*), 2.88 (m, 2H, C*H*), 3.16 (d, 2H, C*H*$_2$), 4.28 (d, 2H, C*H*$_2$), 4.37 (br m, 2H, C*H*), 6.68 (m, 2H, py-C*H*), 6.95 (m, 1H, py-C*H*), 7.00 (s, 2H, C*H*), 7.28 (d, 2H, C*H*), 10.17 (m, 1H, py-*o*-C*H*).

[TripNpy]Hf(i-Bu)$_2$ (46). A suspension of [TripNpy]HfCl$_2$ (0.600 g, 0.734 mmol) in diethyl ether (20 mL) was cooled to –30 ˚C. To the cold solution was added (i-Bu)MgBr (2.0 M in diethyl ether, 0.92 mL, 1.83 mmol) and the resulting mixture was stirred at room temperature for 1 hr until the cloudy suspension became clear. Dioxane (0.20 mL, 2.2 mmol) was added to the solution and the resulting white solid was filtered through Celite. The solvent was removed *in vacuo* to yield a white powder, which was redissolved in 5 mL diethyl ether and crystallized at –30 ˚C to yield the product as white crystals. Yield: 0.44 g, 70%. [TripNpy]Hf(^{13}CH$_2$CHMe$_2$)$_2$ (**46***) was prepared in a similar fashion from Me$_2$CH^{13}CH$_2$MgBr. ^{1}H NMR (500 MHz, C_6D_5Br,

295 K) δ 0.51 (d, 6H, Hf-$CH_2CH(CH_3)_2$), 0.55 (d, 2H, Hf-$CH_2CH(CH_3)_2$), 0.60 (d, 6H, Hf-$CH_2CH(CH_3)_2$), 0.72 (d, 2H, Hf-$CH_2CH(CH_3)_2$), 1.11 (d, 6H, *o*-CH_3), 1.20 (s, 3H, CH_3), 1.21 (d, 12H, *p*-CH_3), 1.32 (d, 6H, *o*-CH_3), 1.47 (d, 6H, *o*-CH_3), 1.61 (d, 6H, *o*-CH_3), 2.17 (m, 1H, Hf-$CH_2CH(CH_3)_2$), 2.36 (m, 1H, Hf-$CH_2CH(CH_3)_2$), 2.83 (m, 1H, CH), 3.05 (d, 2H, CH_2), 3.09 (m, 1H, CH), 3.90 (d, 1H, CH), 4.20 (d, 2H, CH_2), 7.01 (s, 2H, CH), 7.11 (m, 1H, py-CH), 7.12 (m, 1H, py-CH), 7.16 (s, 2H, CH), 7.46 (m, 1H, py-CH), 9.07 (m, 1H, py-*o*-CH). $^{13}C\{^1H\}$ NMR (125 MHz, C_6D_5Br, 295 K) δ 23.47 (s, CH_3), 24.38 (s, CH_3), 24.08 (s, CH_3), 25.42 (s, CH), 25.82 (s, CH_3), 27.47 (s, CH_3), 27.90(s, CH), 28.42 (s, CH_3), 28.72 (s, CH), 29.84 (s, CH), 29.46 (s, CH_3), 32.21 (s, CH), 34.15 (s, CH_3), 45.50 (s, CR_4), 68.44 (s, CH_2), 81.68 (s, Hf-$CH_2CH(CH_3)_2$), 83.04 (s, Hf-$CH_2CH(CH_3)_2$), (some aryl signals omitted here). Anal. Calcd for $C_{47}H_{75}N_3Hf$: C, 65.59; H, 8.78; N, 4.88. Found: C, 65.43; H, 8.71; N, 4.95.

Activation of dialkyl complexes. The dialkyl complexes were activated in a similar fashion. Some NMR signals are not included as overlapping signals make assignment difficult.

Observation of [(MesNpy)Hf(i-Bu)][B(C_6F_5)$_4$] (43). Solutions of [MesNpy]Hf(i-Bu)$_2$ (0.0091 g, 0.013 mmol) and [Ph_3C][B(C_6F_5)$_4$] (0.0122 g, 0.0132 mmol), each in C_6D_5Br (0.5 mL) were prepared and cooled to –30 ˚C. The solutions were mixed while still cold and the resulting yellow solution was transferred to an NMR tube and frozen in N_2(l) within 2 min of the preparation of the sample. 1H NMR (500 MHz, C_6D_5Br, 273 K) δ 0.44 (d, 2H, Hf-$CH_2CH(CH_3)_2$), 0.55 (d, 3H, Hf-$CH_2CH(CH_3)_2$), 1.28 (s, 3H, CH_3), 1.57 (broad s, 6H, *o*-CH_3), 1.62 (s, 6H, $CH_2C(CH_3)_2$), 1.73 (m, 1H, Hf-$CH_2CH(CH_3)_2$), 2.18 (s, 6H, *p*-CH_3), 2.35 (broad s, 6H, *o*-CH_3), 2.95 (d, 2H, CH_2), 4.22 (d, 2H, CH_2), 4.73 (s, 2H, $CH_2C(CH_3)_2$), 5.45 (s, 1H, Ph_3CH), 6.77 (broad s, 2H, CH), 6.85 (broad s, 2H, CH), (some aryl peaks omitted here), 7.23 (m, 1H, py-CH), 7.38 (m, 1H, py-CH), 7.69 (m, 1H, py-CH), 8.54 (m, 1H, py-*o*-CH). $^{13}C\{^1H\}$ NMR (125 MHz, C_6D_5Br, 273 K) δ 18.57 (s, *o*-CH_3), 20.73 (s, *p*-CH_3), 24.20 (s, $CH_2C(CH_3)_2$),

24.91 (s, *C*CH_3), 27.58 (s, Hf-CH_2CH(*C*H_3)$_2$), 28.75 (s, Hf-CH_2*C*H(CH_3)$_2$), 42.79 (s, *C*R_4), 56.79 (s, Ph_3*C*H), 64.25 (s, *C*H_2), 93.34 (s, Hf-*C*H_2CH(CH_3)$_2$), 111.23 (s, *C*H_2C(CH_3)$_2$), (some aryl peaks omitted here).

Reactions of [(MesNpy)Hf(i-Bu)][B(C_6F_5)$_4$] (43) with 1-hexene: kinetics studies. Solutions of [MesNpy]Hf(i-Bu)$_2$ (0.0091 g, 0.013 mmol) and [Ph_3C][B(C_6F_5)$_4$] (0.0122 g, 0.013 mmol), each in C_6D_5Br (0.5 mL) were prepared and cooled to –30 ˚C. The solutions were mixed while still cold and 1-hexene (0.100 mL, 0.80 mmol) was added to the mixture. The NMR samples were obtained directly from this solution, and frozen with $N_{2(l)}$ prior to experimentation.

Reactions of [(MesNpy)Hf(i-Bu)][B(C_6F_5)$_4$] (43) with 1-hexene: bulk polymerization. Solutions of [MesNpy]Hf(i-Bu)$_2$ (0.0131 g, 0.0189 mmol) and [Ph_3C][B(C_6F_5)$_4$] (0.0177 g, 0.0192 mmol), each in C_6H_5Cl (1.5 mL) were prepared and cooled to –30 ˚C. The solutions were mixed while still cold and 1-hexene (0.700 mL, 5.60 mmol) was added to the mixture. The samples stirred at 0 ˚C for 2 hrs, quenched with methanol, and the solvent removed *in vacuo*. The sample was then redissolved in pentane, passed through silica, and dried *in vacuo* for 16 h.

Observation of [(TripNpy)Hf(i-Bu)][B(C_6F_5)$_4$] (47). Solutions of [TripNpy]Hf(i-Bu)$_2$ (0.0114 g, 0.0132 mmol) and [Ph_3C][B(C_6F_5)$_4$] (0.0122 g, 0.0132 mmol), each in C_6D_5Br (0.4 mL) were prepared and cooled to –30 ˚C. The solutions were mixed while still cold and the resulting yellow solution was transferred to an NMR tube and frozen in $N_{2(l)}$ within 2 min of the preparation of the sample. ^{1}H NMR (500 MHz, C_6D_5Br, 273 K) δ 0.56 (d, 6H, Hf-CH_2CH(C*H*$_3$)$_2$), 0.59 (d, 2H, Hf-C*H*$_2$CH(CH_3)$_2$), 0.63 (d, 6H, *o*-C*H*$_3$), 1.06 (d, 6H, *o*-C*H*$_3$), 1.22 (d, 12H, *p*-C*H*$_3$), 1.26 (s, 3H, C*H*$_3$), 1.36 (d, 12H, *o*-C*H*$_3$), 1.62(s, 6H, CH_2C(C*H*$_3$)$_2$), 1.64 (m, 1H, Hf-CH_2C*H*(CH_3)$_2$), 1.90 (m, 1H, C*H*), 2.83 (m, 1H, C*H*), 3.19 (d, 2H, C*H*$_2$), 3.37 (d, 1H, C*H*), 4.35 (d, 2H, C*H*$_2$), 4.73 (s, 2H, C*H*$_2$C(CH_3)$_2$), 5.45 (s, 1H, Ph_3C*H*), (some peaks omitted here),

7.37 (m, 1H, py-C*H*), 7.72 (m, 1H, py-C*H*), 8.40 (m, 1H, py-*o*-C*H*). $^{13}C\{^1H\}$ NMR (125 MHz, C_6D_5Br, 273 K) δ 23.42 (s, *C*H_3), 24.16 (s, *C*H_3), 24.19 (s, $CH_2C(CH_3)_2$), 24.65 (s, *C*H_3), 25.01 (s, *C*H), 25.55 (s, *C*H), 26.44 (s, *C*H_3), 27.00 (s, *C*H_3), 28.94 (s, *C*H), 29.76 (s, *C*H), 34.21 (s, *C*H_3), 43.5 (s, *C*R_4), 56.79 (s, Ph_3CH), 67.49 (s, *C*H_2), 89.21 (s, Hf-*C*$H_2CH(CH_3)_2$), (some aryl signals omitted here).

[(MesNpy)Hf($C_6H_4NMe_2$)][$HB(C_6F_5)_3$] (50). Solutions of [MesNpy]Hf(i-Bu)$_2$ (0.324 g, 0.468 mmol) and $B(C_6F_5)_3$ (0.240 g, 0.468 mmol), in C_6H_5Cl and toluene respectively, (total volume = 3.0 mL) were prepared and cooled to –30 ˚C for 30 min. The solutions were mixed while still cold and the yellow mixture was stirred at 0 ˚C for 24 h. The solvent was removed *in vacuo* and the residue was triturated with pentane to yield yellow powder. Yield: 0.410 g, 72%. ^1H NMR (500 MHz, C_6D_5Br, 293 K) δ 1.36 (s, 3H, C*H*$_3$), 1.50 (s, 6H, *o*-C*H*$_3$), 2.03 (s, 6H, *p*-C*H*$_3$), 2.13 (s, 6H, N-C*H*$_3$), 2.32 (s, 6H, *p*-C*H*$_3$), 2.94 (d, 2H, C*H*$_2$), 4.42 (d, 2H, C*H*$_2$), 6.71 (m, 1H, anil-C*H*), 6.43 (s, 2H, mes-C*H*), 6.73 (s, 2H, mes-C*H*), 6.99 (m, 1H, anil-C*H*), 7.21 (m, 1H, py-C*H*), 7.43 (m, 1H, py-C*H*), 7.47 (m, 1H, anil-C*H*), 7.83 (m, 1H, py-C*H*), 7.85 (m, 1H, anil-C*H*), 9.02 (m, 1H, py-*o*-C*H*). $^{13}C\{^1H\}$ NMR (125 MHz, C_6D_5Br, 293 K) δ 18.13 (s, *o*-*C*H_3), 19.82 (s, *o*-*C*H_3), 20.82 (s, *p*-*C*H_3), 22.72 (s, *C*H_3), 43.17 (s, *C*R_4), 47.89 (s, N-*C*H_3), 64.48 (s, *C*H_2), 99.74 (s, Ar-*C*), (some aryl peaks omitted here), 186.06 (s, Ar-*C*). Anal. Calcd for $C_{53}H_{44}N_4BF_{15}Hf$: C, 52.56; H, 3.66; N, 4.63. Found: C, 52.63; H, 3.61; N, 4.57.

Inhibition studies. The following is an example of the inhibition studies presented. All analogous inhibition studies were carried out in a similar manner.

Polymerization of 1-hexene with [(MesNpy)Hf(i-Bu)][$B(C_6F_5)_4$] (43) in the presence of (i-Pr)$_2$O. Solutions of [MesNpy]Hf(i-Bu)$_2$ (0.0129 g, 0.0186 mmol) and [Ph_3C][$B(C_6F_5)_4$] (0.0178 g, 0.0193 mmol), each in C_6D_5Br (0.4 mL) were prepared and cooled to –30 ˚C. The

solutions were mixed while still cold and $(i\text{-}Pr)_2O$ (0.015 mL, 0.11 mmol) was added and the mixture stirred vigorously. 1-hexene (0.200 mL, 1.60 mmol) was then added to the mixture. The NMR samples were obtained directly from this solution, and frozen with $N_{2(l)}$ prior to experimentation.

Appendix 1

Tantalum complexes of the arylated diamidopyridine ligands

A.1 Introduction

Trimethyl tantalum complexes bearing diamidophosphine ligands have been reported by Fryzuk *et al.* and have shown interesting reactivity in a variety of systems.[107-109] In order to investigate the viability of diamidopyridine ligands for tantalum chemistry, preliminary reactions towards synthesis and reactivity of [ArNpy] complexes of tantalum were carried out.

A.2 Synthesis and activation of [ArNpy]$TaMe_3$ complexes

Complexes [MesNpy]$TaMe_3$ (**51**) and [TripNpy]$TaMe_3$ (**52**) were prepared by treating a solution of $TaMe_3Cl_2$ with 1 equiv of Li_2[ArNpy] at -78 ˚C and allowing the reaction to warm to room temperature over a 24 h period. The compounds were isolated as yellow crystals in ~25% yield (eq A.1).

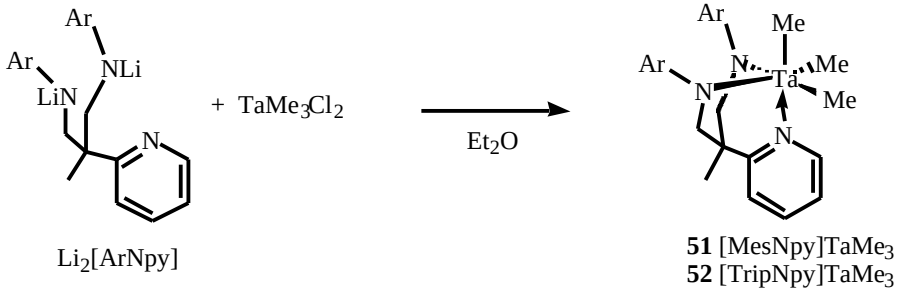

Li_2[ArNpy]

51 [MesNpy]$TaMe_3$
52 [TripNpy]$TaMe_3$

(A.1)

The ^{1}H NMR spectrum (20 ˚C, C_6D_6) of **51** shows a singlet (9H) at 1.05 ppm corresponding to three methyl groups, and the *ortho* pyridyl proton is found at 9.15 ppm. The crystal structure of this complex shows *pseudo*-octahedral geometry and C_s symmetry (Figure A.1). The three methyl groups are facially coordinated at nearly 90˚ angles to one another (C(1)-Ta-C(2) = 84.2(2)˚, C(1)-Ta-C(3) = 93.6(3)˚, and C(2)-Ta-C(3) = 88.3(3)˚); the Ta-C bond lengths are all approximately 2.2 Å.

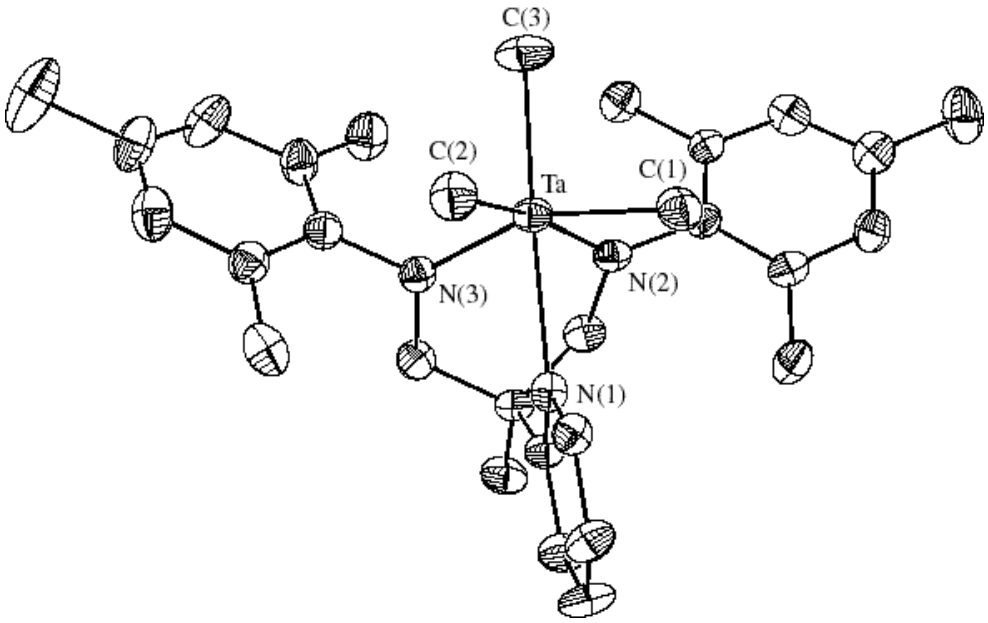

Figure A.1. Thermal ellipsoid diagram (35% probability level) of [MesNpy]$TaMe_3$ (**51**).

Table A.1. Selected bond lengths (Å) and angles (˚) for [MesNpy]$TaMe_3$ (**51**).

Bond Lengths

Ta-N(1)	2.394(5)	Ta-C(1)	2.225(6)
Ta-N(2)	2.044(4)	Ta-C(2)	2.246(6)
Ta-N(3)	1.999(5)	Ta-C(3)	2.175(6)

Bond Angles

N(2)-Ta-N(3)	87.69(19)	C(3)-Ta-C(1)	93.6(3)
N(2)-Ta-C(3)	102.9(2)	C(3)-Ta-C(2)	88.3(3)
N(3)-Ta-C(3)	108.7(3)	C(1)-Ta-N(1)	81.2(2)
N(1)-Ta-C(3)	173.6(2)	C(2)-Ta-N(1)	87.5(2)

The ^{1}H NMR spectrum (20 ˚C, C_6D_6) of the analogous compound [TripNpy]$TaMe_3$ (**52**) showed a singlet (9H) for the methyl groups at 1.25 ppm. In both **51** and **52** restricted rotation of the aryl rings was observed in solution multiple signals for substituents on the aryl rings.

During early attempts to synthesize these complexes, a complication was observed. When the reaction for the synthesis of **51** was carried out at room temperature for only 20 min, a mixture of two compounds was isolated. One was later identified as **51**; the other showed an asymmetric pattern in the backbone signals and those for the aryl rings (6 signals were observed for the mesityl methyl groups indicating loss of C_s symmetry in the molecule). A similar pattern was observed when attempts were made to synthesize **52** in a similar manner; in this case the asymmetric species was the sole product and was isolated as yellow crystals in ~20% yield. The ^{1}H NMR spectrum (20 ˚C, C_6D_6) of this compound (**53**) showed 6 isopropyl groups and the backbone consisted of signals at 3.32, 3.02, and 2.38 ppm, each corresponding to a single proton. The *ortho* pyridyl proton was observed at 9.2 ppm.

The crystal structure of this complex showed an asymmetric, six coordinate tantalum center bound to a pyridine nitrogen and one amido group, as well as two methyl groups and a chloride. The final coordination position is occupied by a backbone methylene carbon (Figure A.2).

A list of selected bond lengths and angles is presented in Table A.2. Although tantalum is six coordinate, N(3) of the free amine points towards the metal center; the Ta-N(3) distance is 3.3 Å and the C(1)-Ta-N(3) angle is 177˚. This decomposition product and the related compound bearing the [MesNpy] ligand may be the cause of the poor yields obtained during the synthesis of **51** and **52**.

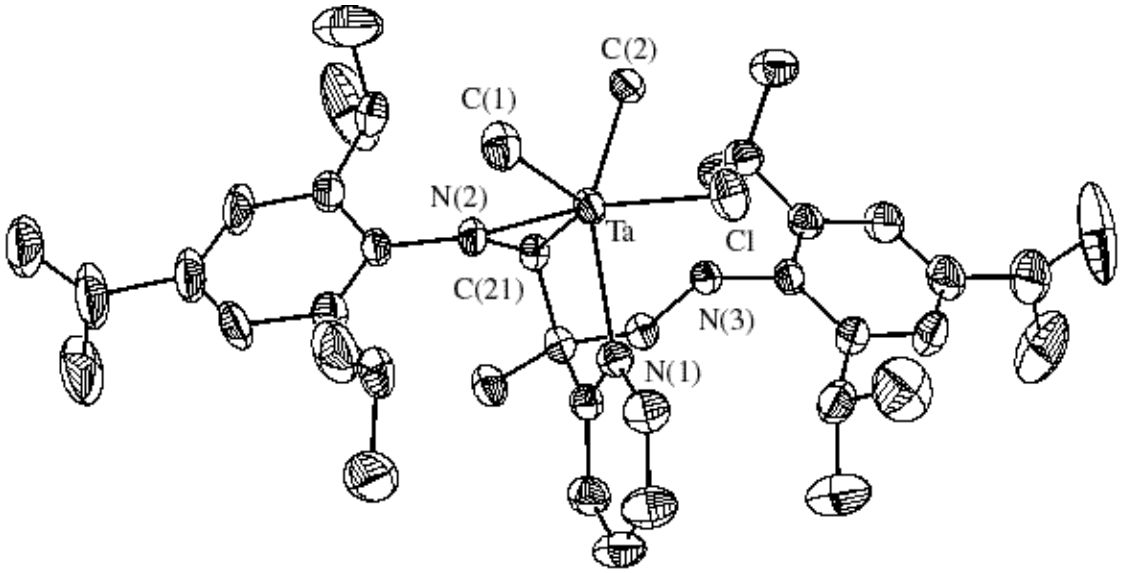

Figure A.2. Thermal ellipsoid diagram (35% probability level) of **53**.

Table A.2. Selected bond lengths (Å) and angles (˚) for decomposition product **53**.

Bond Lengths

Ta-N(1)	2.234(4)	Ta-C(1)	2.177(7)
Ta-N(2)	1.949(4)	Ta-C(2)	2.172(5)
Ta-Cl	2.4126(14)	Ta-C(21)	2.146(5)

Bond Angles

C(1)-Ta-N(1)	118.2(3)	Cl-Ta-N(1)	86.10(12)
C(2)-Ta-N(1)	140.15(17)	Cl-Ta-C(1)	90.3(2)
N(2)-Ta-N(1)	85.47(16)	Cl-Ta-C(2)	91.82(15)
C(21)-Ta-N(1)	75.10(18)	Cl-Ta-C(21)	146.95(13)
C(1)-Ta-C(2)	101.6(3)	Cl-Ta-N(2)	165.40(13)

Activation of [MesNpy]TaMe$_3$ with [Ph$_3$C][B(C$_6$F$_5$)$_4$]. Activation of [MesNpy]TaMe$_3$ (**51**) with 1 equiv of [Ph$_3$C][B(C$_6$F$_5$)$_4$] yields [(MesNpy)TaMe$_2$][B(C$_6$F$_5$)$_4$] (**54**) and 1 equiv of Ph$_3$CCH$_3$ (eq A.2).

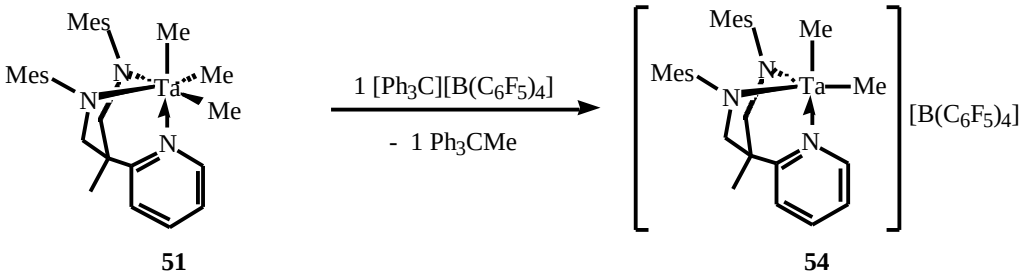

51 **54** (A.2)

Two distinct methyl groups were observed at 0.75 and 1.05 ppm in the ^{1}H NMR spectrum (–20 ˚C, C$_6$D$_5$Br) of **54**. One can ascertain that this compound is not a dinuclear monocation, analogous to those obtained upon activation of dimethyl zirconium and hafnium complexes, from the integration of Ph$_3$CC*H*$_3$ (3H vs. 6H for the Ta-C*H*$_3$ groups). Variable temperature NMR studies showed this cation to be stable to 60 ˚C. Exchange between the methyl groups was not observed even at elevated temperatures; only the signals for the aryl rings were affected (they broaden and merge with increasing temperature, as expected due to rotation).

Further experiments in this area will include determination of the activity of these cationic compounds in olefins polymerization. Other projects could involve the synthesis and study of hydride complexes as well as the synthesis and activation of triethyl tantalum complexes.[110]

A.3 Experimental section

General Procedures. All manipulations, with the exception of the synthesis of ligand precursors, were performed under N$_2$ in a glove-box or using standard Schlenk procedures.

Solvents were dried using conventional procedures.[60] Chlorobenzene (HPLC grade) and deuterated solvents were degassed, stored over and distilled from CaH_2. Commercial reagents were used without further purification. NMR spectra were recorded on a Varian INOVA 500 spectrometer. ^1H NMR chemical shifts are given in ppm versus residual protons in the deuterated solvents as follows: δ 7.16 C_6D_6, δ 2.09 toluene-d_8 (methyl), δ 7.29 C_6D_5Br (most downfield resonance). $^{13}C\{^1H\}$ NMR chemical shifts are given in ppm versus residual ^{13}C in the solvents as follows: δ 128.39 C_6D_6, δ 20.4 toluene-d_8 (methyl), δ 122.25 C_6D_5Br (most upfield resonance). Some aryl resonances in ^1H and $^{13}C\{^1H\}$ spectra are not given.

Elemental analyses were performed by H. Kolbe, Mikroanalytisches Laboratorium (Mülheim an der Ruhr, Germany). X-ray data were collected on a Siemens SMART/CCD diffractometer with λ(MoKα) = 0.71073 Å and solved using a full-matrix least squares refinement on F^2.

All Grignard reagents were carefully titrated with 2-butanol in the presence of 1,10-phenanthroline prior to use. [MesNpy]H_2[26] and $TaMe_3Cl_2$[111,112] have been prepared according to previously reported methods.

Lithium salts of both H_2[MesNpy] and H_2[TripNpy] were prepared in the following manner:

Li_2[MesNpy]. To a solution of H_2[MesNpy] (2.073 g, 5.16 mmol) at –30 ˚C in diethyl ether was added (n-Bu)Li (1.6 M in hexanes, 6.5 mL, 10.4 mmol) and the yellow solution was stirred at room temperature for 2 h. The resulting insoluble yellow precipitate was filtered, washed with pentane and dried *in vacuo*. Yield: 1.9 g, 89%. Anal. Calcd for $C_{27}H_{33}N_3Li_2$: C, 78.43; H, 8.04; N, 10.16. Found: C, 78.53; H, 7.91; N, 10.04.

[MesNpy]$TaMe_3$ (51). Solutions of $TaMe_3Cl_2$ (0.820 g, 2.76 mmol) and Li_2[MesNpy] (1.14 g, 2.76 mmol) in diethyl ether (60 mL) were cooled to –20 ˚C. The cold slurry of ligand was added to the tantalum solution over a period of 5 min. The dark brown mixture reaction

mixture was stirred at room temperature for 16 h. The diethyl ether was removed *in vacuo*, the solution taken up in benzene and the salts filtered through Celite. The benzene was removed *in vacuo* and the resulting brown solid dissolved in minimal toluene, and recrystallized twice from a toluene pentane mixture. Yield: 0.39 g, 23%. ^{1}H NMR (500 MHz, C_6D_6, 295 K) δ 0.86 (s, 3H, CH_3), 1.02 (s, 9H, Ta-CH_3), 1.42 (s, 6H, *o*-CH_3), 2.15 (s, 6H, *p*-CH_3), 2.68 (s, 6H, *o*-CH_3), 3.08 (d, 2H, CH_2), 3.87 (d, 2H, CH_2), 6.55 (m, 1H, py-C*H*), 6.77 (s, 2H, C*H*), 6.83 (m, 1H, py-C*H*), 6.95 (s, 2H, C*H*), 7.00 (m, 1H, py-C*H*), 9.15 (m, 1H, py-*o*-C*H*).

[TripNpy]TaMe$_3$ (52). Solutions of $TaMe_3Cl_2$ (0.183 g, 6.19 mmol) and Li_2[TripNpy] (0.360 g, 6.19 mmol) in diethyl ether (20 mL) were cooled to –20 ˚C. The cold slurry of ligand was added to the tantalum solution over a period of 5 min. The dark brown mixture reaction mixture was stirred at room temperature for 16 h. The diethyl ether was removed *in vacuo*, the solution taken up in benzene and the salts filtered through Celite. The benzene was removed *in vacuo* and the resulting brown solid dissolved in minimal toluene, and recrystallized twice from a toluene pentane mixture. Yield: 0.136 g, 28%. ^{1}H NMR (500 MHz, C_6D_6, 295 K) δ 0.77 (d, 6H, CH_3), 0.91 (s, 3H, CH_3), 1.25 (s, 9H, Ta-CH_3), 1.28 (d, 18H, CH_3), 1.49 (d, 6H, CH_3), 1.70 (d, 6H, CH_3), 2.41 (m, 2H, C*H*), 2.88 (m, 2H, C*H*), 3.18 (d, 2H, CH_2), 3.88 (d, 2H, CH_2), 4.08 (m, 2H, C*H*), 6.55 (m, 1H, py-C*H*), 6.67 (m, 1H, py-C*H*), 6.97 (m, 1H, py-C*H*), 7.12 (d, 2H, C*H*), 7.28 (d, 2H, C*H*), 9.07 (m, 1H, py-*o*-C*H*).

Solutions of [(MesNpy)TaMe$_2$][B(C$_6$F$_5$)$_4$] (54). Solutions of [MesNpy]$TaMe_3$ (0.0172 g, 0.0275 mmol) and [Ph_3C][B(C_6F_5)$_4$] (0.0248 g, 0.00275 mmol), each in C_6D_5Br (0.5 mL) were prepared and cooled to –20 ˚C. The solutions were mixed while still cold and the resulting yellow solution was transferred to an NMR tube and frozen in $N_{2(l)}$ within 2 min of the preparation of the sample. ^{1}H NMR (500 MHz, C_6D_5Br, 253 K) δ 0.68 (s, 3H, Ta-CH_3), 1.03 (s, 3H, Ta-CH_3), 1.23 (s, 3H, CH_3), 1.38 (s, 6H, *o*-CH_3), 2.02 (s, 3H, Ph_3CCH_3), 2.13 (s, 6H, *p*-CH_3),

2.23 (s, 6H, *o*-CH_3), 3.07 (d, 2H, CH_2), 4.67 (d, 2H, CH_2), 6.68 (s, 2H, C*H*), 6.83 (s, 2H, C*H*), some aryl peaks omitted here, 7.22 (m, 1H, py-C*H*), 7.68 (m, 1H, py-C*H*), 8.39 (m, 1H, py-*o*-C*H*).

Appendix 2

Crystallographic parameters and tables

Table A.3. Crystal data and structure refinement for [MesNpy]Zr(THF)Me_2 (**2**).

Identification code	99083	
Empirical formula	C33 H47 N3 O Zr	
Formula weight	592.96	
Temperature	180(2) K	
Wavelength	0.71073 Å	
Crystal system	Monoclinic	
Space group	C2/c	
Unit cell dimensions	a = 32.739(2) Å	α= 90˚
	b = 12.6838(7) Å	β= 92.890(2)˚
	c = 15.1138(9) Å	γ = 90˚
Volume	6268.0(6) $Å^3$	
Z	8	
Density (calculated)	1.257 Mg/m^3	
Absorption coefficient	0.379 mm^{-1}	
F(000)	2512	
Crystal size	0.32 x 0.25 x 0.18 mm^3	
Theta range for data collection	1.25 to 23.28˚	
Index ranges	-36<=h<=36, -14<=k<=9, -15<=l<=16	
Reflections collected	12617	
Independent reflections	4502 [R(int) = 0.0528]	
Completeness to theta = 23.28˚	99.9%	
Absorption correction	None	
Max. and min. transmission	0.9349 and 0.8883	
Refinement method	Full-matrix least-squares on F^2	
Data / restraints / parameters	4502 / 0 / 363	
Goodness-of-fit on F^2	1.263	
Final R indices [I>2σ(I)]	R1 = 0.0616, wR2 = 0.1346	
R indices (all data)	R1 = 0.0718, wR2 = 0.1395	
Extinction coefficient	0.00008(8)	
Largest diff. peak and hole	0.461 and -0.444 e.$Å^{-3}$	

Table A.4. Crystal data and structure refinement for $[Li{\cdot}OEt_2][(MesNpy)ZrMe_3]$ (**3**).

Identification code	01009	
Empirical formula	C34 H52 Li1 O1 N3 Zr1	
Formula weight	617.15	
Temperature	183 K	
Wavelength	0.71073 Å	
Crystal system	Orthorhombic, P2(1)2(1)2(1)	
Space group	P2(1)2(1)2(1)	
Unit cell dimensions	a = 14.540(6) Å	α = 90˚
	b = 15.451(6) Å	β = 90˚
	c = 15.504(5) Å	γ = 90˚
Volume	3483(2) A^3	
Z	3	
Density (calculated)	1.176 Mg/m^3	
Absorption coefficient	0.343 mm^{-1}	
F(000)	1312	
Crystal size	0.3 x 0.3 x 0.3 mm^3	
Theta range for data collection	2.33 to 23.39 °	
Index ranges	-16<=h<=11, -17<=k<=12, -12<=l<=13	
Reflections collected	6715	
Independent reflections	4175 [R(int) = 0.0478]	
Completeness to theta = 23.39˚	85.5%	
Absorption correction	Empirical	
Max. and min. transmission	0.2731 and 0.2158	
Refinement method	Full-matrix least-squares on F^2	
Data / restraints / parameters	4175 / 0 / 361	
Goodness-of-fit on F^2	0.941	
Final R indices [I>2σ(I)]	R1 = 0.0426, wR2 = 0.0842	
R indices (all data)	R1 = 0.0745, wR2 = 0.0924	
Extinction coefficient	-0.04(6)	
Largest diff. peak and hole	0.248 and -0.298 $e.A^{-3}$	

Table A.5. Crystal data and structure refinement for [MesNpy]$ZrMe_2$ (**1**).

Identification code	99199	
Empirical formula	C33 H49 N3 O Zr	
Formula weight	594.97	
Temperature	183(2) K	
Wavelength	0.71073 Å	
Crystal system	Orthorhombic	
Space group	P2(1)2(1)2(1)	
Unit cell dimensions	a = 11.4721(2) Å	α= 90°
	b = 16.3643(3) Å	β= 90°
	c = 17.5024(2) Å	γ = 90°
Volume	3285.78(9) $Å^3$	
Z	4	
Density (calculated)	1.203 g/cm^3	
Absorption coefficient	0.362 mm^{-1}	
F(000)	1264	
Crystal size	0.5 x 0.5 x 0.5 mm^3	
2θ range for data collection	4.24 to 46.50°	
Index ranges	-12<=h<=8, -18<=k<=18, -19<=l<=19	
Reflections collected	13544	
Independent reflections	4674 [R(int) = 0.0361]	
Completeness to theta = 23.25°	99.9%	
Absorption correction	Empirical	
Max. and min. transmission	0.2617 and 0.2347	
Refinement method	Full-matrix least-squares on F^2	
Data / restraints / parameters	4674 / 0 / 344	
Goodness-of-fit on F^2	1.129	
Final R indices [I>2σ(I)]	R1 = 0.0410, wR2 = 0.0990	
R indices (all data)	R1 = 0.0462, wR2 = 0.1030	
Absolute structure parameter	-0.02(5)	
Extinction coefficient	0.0028(5)	
Largest diff. peak and hole	0.462 and -0.436 e.$Å^{-3}$	

Table A.6. Crystal data and structure refinement for [TripNpy]Zr(i-Bu)$_2$ (**26**).

Identification code	00084	
Empirical formula	C47 H75 N3 Zr	
Formula weight	773.32	
Temperature	293(2) K	
Wavelength	0.71073 Å	
Crystal system	Triclinic	
Space group	$P\bar{1}$	
Unit cell dimensions	a = 12.592(4) Å	α = 69.662(5)°
	b = 12.601(4) Å	β = 86.747(5)°
	c = 17.403(6) Å	γ = 64.631(5)°
Volume	2325.6(13) Å^3	
Z	2	
Density (calculated)	1.104 g/cm^3	
Absorption coefficient	0.268 mm^{-1}	
F(000)	836	
Crystal size	0.2 x 0.2 x 0.1 mm^3	
2θ range for data collection	5.08 to 23.31°.	
Index ranges	-8<=h<=13, -13<=k<=10, -19<=l<=13	
Reflections collected	4637	
Independent reflections	4249 [R(int) = 0.0330]	
Completeness to theta = 23.31	63.4%	
Absorption correction	Empirical	
Max. and min. transmission	0.9291 and 0.6462	
Refinement method	Full-matrix least-squares on F^2	
Data / restraints / parameters	4249 / 0 / 460	
Goodness-of-fit on F^2	1.020	
Final R indices [I>2σ(I)]	R1 = 0.0452, wR2 = 0.1125	
R indices (all data)	R1 = 0.0608, wR2 = 0.1217	
Largest diff. peak and hole	0.421 and -0.309 e.Å^{-3}	

Table A.7. Crystal data and structure refinement for [MesNpy]Hf(i-Pr)Cl (**36**).

Identification code	01065	
Empirical formula	C30 H40 Cl Hf N3	
Formula weight	656.59	
Temperature	183(2) K	
Wavelength	0.71073 Å	
Crystal system	Orthorhombic	
Space group	Pbca	
Unit cell dimensions	a = 15.4981(9) Å	α= 90°
	b = 18.3136(11) Å	β= 90°
	c = 21.0590(13) Å	γ = 90°
Volume	5977.1(6) $Å^3$	
Z	8	
Density (calculated)	1.459 Mg/m^3	
Absorption coefficient	3.601 mm-1	
F(000)	2640	
Crystal size	0.26 x 0.20 x 0.10 mm^3	
Theta range for data collection	2.34 to 23.27°	
Index ranges	-16<=h<=17, -18<=k<=20, -23<=l<=21	
Reflections collected	22824	
Independent reflections	4288 [R(int) = 0.0499]	
Completeness to theta = 23.27°	99.8%	
Absorption correction	Empirical	
Max. and min. transmission	0.7147 and 0.4545	
Refinement method	Full-matrix least-squares on F^2	
Data / restraints / parameters	4288 / 0 / 453	
Goodness-of-fit on F^2	1.125	
Final R indices [I>2σ(I)]	R1 = 0.0375, wR2 = 0.0727	
R indices (all data)	R1 = 0.0461, wR2 = 0.0758	
Extinction coefficient	0.000000(13)	
Largest diff. peak and hole	0.652 and -0.983 $e.Å^{-3}$	

Table A.8. Crystal data and structure refinement for [MesNpy]Hf(i-Pr)$_2$ (**37**).

Identification code	01029	
Empirical formula	C33 H47 Hf N3	
Formula weight	664.23	
Temperature	293(2) K	
Wavelength	0.71073 Å	
Crystal system	Orthorhombic	
Space group	Pbca	
Unit cell dimensions	a = 15.926(4) Å	α= 90°
	b = 18.600(5) Å	β= 90°
	c = 20.937(6) Å	γ = 90°
Volume	6202(3) Å^3	
Z	8	
Density (calculated)	1.423 Mg/m^3	
Absorption coefficient	3.388 mm^{-1}	
F(000)	2704	
Crystal size	0.16 x 0.14 x 0.10 mm^3	
Theta range for data collection	1.94 to 23.27°.	
Index ranges	-17<=h<=17, -20<=k<=15, -23<=l<=21	
Reflections collected	24072	
Independent reflections	4450 [R(int) = 0.0468]	
Completeness to theta = 23.27°	99.9%	
Absorption correction	Empirical	
Max. and min. transmission	0.9848 and 0.6827	
Refinement method	Full-matrix least-squares on F^2	
Data / restraints / parameters	4450 / 0 / 346	
Goodness-of-fit on F^2	1.082	
Final R indices [I>2σ(I)]	R1 = 0.0292, wR2 = 0.0603	
R indices (all data)	R1 = 0.0380, wR2 = 0.0634	
Extinction coefficient	0.000024(16)	
Largest diff. peak and hole	0.825 and -0.667 e.Å^{-3}	

Table A.9. Crystal data and structure refinement for [MesNpy]$TaMe_3$ (**52**).

Identification code	01089	
Empirical formula	C35 H54 N3 Ta	
Formula weight	697.76	
Temperature	183(2) K	
Wavelength	0.71073 Å	
Crystal system	Orthorhombic	
Space group	P2(1)2(1)2(1)	
Unit cell dimensions	a = 13.5751(15) Å	α= 90°
	b = 15.5983(17) Å	β= 90°
	c = 15.8230(17) Å	γ = 90°
Volume	3350.5(6) $Å^3$	
Z	4	
Density (calculated)	1.383 Mg/m^3	
Absorption coefficient	3.306 mm^{-1}	
F(000)	1432	
Crystal size	0.17 x 0.10 x 0.09 mm^3	
Theta range for data collection	2.37 to 23.30˚	
Index ranges	-15<=h<=11, -17<=k<=15, -14<=l<=17	
Reflections collected	13573	
Independent reflections	4798 [R(int) = 0.0468]	
Completeness to Theta = 23.30°	99.5%	
Absorption correction	None	
Max. and min. transmission	0.7551 and 0.6033	
Refinement method	Full-matrix least-squares on F^2	
Data / restraints / parameters	4798 / 0 / 352	
Goodness-of-fit on F^2	1.058	
Final R indices [I>2σ(I)]	R1 = 0.0290, wR2 = 0.0628	
R indices (all data)	R1 = 0.0312, wR2 = 0.0638	
Absolute structure parameter	-0.017(12)	
Largest diff. peak and hole	0.519 and -0.549 e.$Å^{-3}$	

Table A.10. Crystal data and structure refinement for Assymetric TripTaMe_2Cl (**53**).

Identification code	01083	
Empirical formula	C43 H66 Cl N3 Ta	
Formula weight	847.39	
Temperature	183(2) K	
Wavelength	0.71073 Å	
Crystal system	Triclinic	
Space group	$P\bar{1}$	
Unit cell dimensions	a = 10.0483(6) Å	α= 96.8030(10)°
	b = 13.3129(8) Å	β= 98.1510(10)°
	c = 16.8821(10) Å	γ = 90.3450(10)°
Volume	2219.2(2) $Å^3$	
Z	2	
Density (calculated)	1.268 Mg/m^3	
Absorption coefficient	2.567 mm^{-1}	
F(000)	876	
Crystal size	0.20 x 0.18 x 0.14 mm^3	
Theta range for data collection	2.08 to 23.27°.	
Index ranges	-10<=h<=11, -11<=k<=14, -18<=l<=18	
Reflections collected	9000	
Independent reflections	6249 [R(int) = 0.0213]	
Completeness to theta = 23.27°	97.9%	
Absorption correction	Empirical	
Max. and min. transmission	0.7152 and 0.6278	
Refinement method	Full-matrix least-squares on F^2	
Data / restraints / parameters	6249 / 0 / 549	
Goodness-of-fit on F^2	1.129	
Final R indices [I>2σ(I)]	R1 = 0.0320, wR2 = 0.0806	
R indices (all data)	R1 = 0.0347, wR2 = 0.0820	
Largest diff. peak and hole	1.374 and -0.556 e.$Å^{-3}$	

(1) For recent reviews see: *Chem. Rev.* **2000**, *100*.
(2) Coates, G. W.; Hustad, P. D.; Reinartz, S. *Angew. Chem. Int. Ed.* **2002**, *41*, 2236.
(3) Grubbs, R. H.; Coates, G. W. *Acc. Chem. Res.* **1996**, *29*, 85.
(4) Resconi, L.; Cavalo, L.; Fait, A.; Piemontesi, F. *Chem. Rev.* **2000**, *100*.
(5) Schrodi, Y.; Schrock, R. R.; Bonitatebus, P. J., Jr. *Organometallics* **2001**, *20*, 3560.
(6) Kawamura-Kuribayashi, H.; Koga, N.; Morokuma, K. *J. Am. Chem. Soc.* **1992**, *114*, 8687.
(7) Kawamura-Kuribayashi, H.; Koga, N.; Morokuma, K. *J. Am. Chem. Soc.* **1992**, *114*, 2359.
(8) Resconi, L.; Camurati, I.; Sudmeijer, O. *Top. Catal.* **1999**, *7*, 145.
(9) Scollard, J. D.; McConville, D. H. *J. Am. Chem. Soc.* **1996**, *118*, 10008.
(10) Scollard, J. D.; McConville, D. H.; Vittal, J. J.; Payne, N. C. *J. Mol. Catal. A Chem.* **1998**, *128*, 201.
(11) Scollard, J. D.; McConville, D. H.; Rettig, S. J. *Organometallics* **1997**, *16*, 1810.
(12) Kempe, R. *Angew. Chem. Int. Ed.* **2000**, *39*, 468.
(13) Britovsek, G. J. P.; Gibson, V. C.; Wass, D. F. *Angew. Chem. Int. Ed.* **1999**, *38*, 428.
(14) Gade, L. H. *Chem. Commun.* **2000**, 173.
(15) Baumann, R.; Davis, W. M.; Schrock, R. R. *J. Am. Chem. Soc.* **1997**, *119*, 3830.
(16) Schrock, R. R.; Bonitatebus, P. J., Jr.; Schrodi, Y. *Organometallics* **2001**, *20*, 1056.
(17) Jayaratne, K. C.; Sita, L. R. *J. Am. Chem. Soc.* **2000**, *122*, 958.
(18) Jayaratne, K. C.; Keaton, R. J.; Henningsen, D. A.; Sita, L. R. *J. Am. Chem. Soc.* **2000**, *122*, 10490.
(19) Keaton, R. J.; Jayaratne, K. C.; Henningsen, D. A.; Koterwas, L. A.; Sita, L. R. *J. Am. Chem. Soc.* **2001**, *123*, 6197.
(20) Tshuva, E. Y.; Goldberg, I.; Kol, M. *J. Am. Chem. Soc.* **2000**, *122*, 10706.
(21) Tshuva, E. Y.; Goldberg, I.; Kol, M.; Goldschmidt, Z. *Chem. Commun.* **2001**, 2120.
(22) Tshuva, E. Y.; Groysman, S.; Goldberg, I.; Kol, M.; Goldschmidt, Z. *Organometallics* **2002**, *2002*, 662.
(23) Tian, J.; Hustad, P. D.; Coates, G. W. *J. Am. Chem. Soc.* **2001**, *123*, 5134.
(24) Keaton, R. J.; Sita, L. R. *J. Am. Chem. Soc.* **2002**, *ASAP article*.
(25) Darling, T. R.; Davis, T. P.; Fryd, M.; Gridnev, A. A.; Haddleton, D. M.; Ittel, S. D.; Mathieson, R. R., Jr.; Moad, G.; Rizzardo, E. *J. Polym. Sci.: Part A: Polym Chem.* **2000**, *38*, 1706.
(26) Mehrkhodavandi, P.; Bonitatebus, P. J.; Schrock, R. R. *J. Am. Chem. Soc.* **2000**, *122*, 7841.
(27) Mehrkhodavandi, P.; Schrock, R. R. *J. Am. Chem. Soc.* **2001**, *123*, 10746.
(28) Warren, T. H.; Schrock, R. R.; Davis, W. M. *Organometallics* **1996**, *15*, 562.
(29) Aizenberg, M.; Turculet, L.; Schattenmann, F.; Davis, W. M.; Schrock, R. R. *Organometallics* **1998**, *17*, 4795.
(30) Baumann, R.; Stumpf, R.; Davis, W. M.; Liang, L.-C.; Schrock, R. R. *J. Am. Chem. Soc.* **1999**, *121*, 7822.
(31) Baumann, R.; Schrock, R. R. *J. Organomet. Chem* **1998**, *557*, 69.
(32) Flores, M. A.; Manzoni, M. R.; Baumann, R.; Davis, W. M.; Schrock, R. R. *Organometallics* **1999**, *18*, 3220.
(33) Goodman, J. T.; Schrock, R. R. *Organometallics* **2001**, *20*, 5205.

(34) Liang, L.-C.; Schrock, R. R.; Davis, W. M.; McConville, D. H. *J. Am. Chem. Soc.* **1999**, *121*, 5797.
(35) Schrock, R. R.; Schattenmann, F.; Aizenberg, M.; Davis, W. M. *Chem. Commun.* **1998**, 199.
(36) Schrock, R. R.; Baumann, R.; Reid, S. M.; Goodman, J. T.; Stumpf, R.; Davis, W. M. *Organometallics* **1999**, *18*, 3649.
(37) Schrock, R. R.; Seidel, S. W.; Schrodi, Y.; Davis, W. M. *Organometallics* **1999**, *18*, 428.
(38) Schrock, R. R.; Casado, A. L.; Goodman, J. T.; Liang, L.-C.; Bonitatebus, P. J., Jr.; Davis, W. M. *Organometallics* **2000**, *19*, 5325.
(39) Warren, T. H.; Schrock, R. R.; Davis, W. M. *Organometallics* **1998**, *17*, 308.
(40) Friedrich, S.; Schubart, M.; Gade, L. H.; Scowen, I. J.; Edwards, A. J.; McPartlin, M. *Chem. Ber./ Recueil* **1997**, *130*, 1751.
(41) Blake, A. J.; Collier, P. E.; Gade, L. H.; McPartlin, M.; Mountford, P.; Schubart, M.; Scowen, I. J. *Chem. Commun.* **1997**, 1555.
(42) Schrock, R. R.; Seidel, S. W.; Mosch-Zanetti, N. C.; Shih, K.-Y.; O'Donoghue, M. B.; Davis, W. M.; Reiff, W. M. *J. Am. Chem. Soc.* **1997**, *119*, 11876.
(43) Bochmann, M.; Lancaster, S. J. *Angew. Chem. Int. Ed. Engl.* **1994**, *33*, 1634.
(44) Beck, S.; Prosenc, M. H.; Brintzinger, H. H.; Goretzki, R.; Herfert, N.; Fink, G. *J. Molec. Catal. A* **1996**, *111*, 67.
(45) Koehler, K.; Piers, W. E.; Jarvis, A. P.; Xin, S.; Feng, Y.; Bravakis, A. M.; Collins, S.; Clegg, W.; Yap, G. P. A.; Marder, T. B. *Organometallics* **1998**, *17*, 3557.
(46) Bochmann, M.; Lancaster, S. J.; Hursthouse, M. B.; Malik, K. M. A. *Organometallics* **1994**, *13*, 2235.
(47) Jia, L.; Yang, X.; Stern, C. L.; Marks, T. J. *Organometallics* **1997**, *16*, 842.
(48) Buchwald, S. L.; Lucas, E. A.; Davis, W. M. *J. Am. Chem. Soc.* **1989**, *111*, 397.
(49) Watson, P. L.; Parshall, G. W. *Acc. Chem. Res.* **1985**, *18*, 51.
(50) Watson, P. L. *J. Am. Chem. Soc.* **1983**, *105*, 6491.
(51) Waymouth, R. M.; Santarsiero, B. D.; Grubbs, R. H. *J. Am. Chem. Soc.* **1984**, *106*, 4050.
(52) Chen, E. Y.-X.; Marks, T. J. *Chem. Rev.* **2000**, *100*, 1391.
(53) Chen, E. Y.-X.; Stern, C. L.; Yang, S.; Marks, T. J. *J. Am. Chem. Soc.* **1996**, *118*, 12451.
(54) Wolfe, J. P.; Wagaw, S.; Buchwald, S. L. *J. Am. Chem. Soc.* **1996**, *118*, 7215.
(55) Wolfe, J. P.; Wagaw, S.; Marcoux, J.-F.; Buchwald, S. L. *Acc. Chem. Res.* **1998**, *31*, 805.
(56) Morse, P. M.; Girolami, G. S. *J. Am. Chem. Soc.* **1989**, *111*, 4114.
(57) Guérin, F.; McConville, D. H.; Payne, N. C. *Organometallics* **1996**, *15*, 5085.
(58) Ozawa, F.; Park, J. W.; Mackenzie, P. B.; Schaefer, W. P.; Henling, L. M.; Grubbs, R. H. *J. Am. Chem. Soc.* **1989**, *111*, 1319.
(59) Waymouth, R. M.; Santarsiero, B. D.; Grubbs, R. H. *J. Am. Chem. Soc.* **1984**, *106*, 4050.
(60) Pangborn, A. B.; Giardello, M. A.; Grubbs, R. H.; Rosen, R. K.; Tinners, F. J. *Organometallics* **1996**, *15*, 1518.
(61) Diamond, G. M.; Jordan, R. F. *Organometallics* **1996**, *15*, 4030.
(62) Coates, G. W. *J. Chem. Soc., Dalton Trans.* **2002**, 467.
(63) Fink, G.; Zoller, W. *Makromol. Chem.* **1981**, *182*, 3265.
(64) Fink, G.; Schnell, D. *Angew. Makromol. Chem.* **1982**, *105*, 31.
(65) Mynott, R.; Fink, G.; W., F. *Angew. Makromol. Chem.* **1987**, *154*, 1.
(66) Fink, G.; Fenzl, W.; Mynott, R. Z. *Naturforsch., B: Chem. Sci.* **1985**, *40b*, 158.

(67) Zhou, J.; Lancanster, S. J.; Walker, D. A.; Beck, S.; Thornton-Pett, M.; Bochmann, M. *J. Am. Chem. Soc.* **2001**, *123*, 223.
(68) Beswick, C. L.; Marks, T. J. *Organometallics* **1999**, *18*, 2410.
(69) Schattenmann, F.; Schrock, R. R.; Davis, W. M. *Organometallics* **1998**, *17*, 989.
(70) Gold, L. *J. Chem. Phys.* **1958**, *28*, 91.
(71) Guérin, F.; McConville, D. H.; Jagadese, J. V.; Yap, G. A. P. *Organometallics* **1998**, *17*, 5172.
(72) Negishi, E.; Takahashi, T. *Acc. Chem. Res.* **1994**, *27*, 124.
(73) Keaton, R. J.; Koterwas, L. A.; Fettinger, J. C.; Sita, L. R. *J. Am. Chem. Soc.* **2002**, *124*, 5932.
(74) Amor, F.; Spaniol, T. P.; Okuda, J. *Organometallics* **1997**, *16*, 4765.
(75) Amor, J. I.; Cuenca, T.; Galakhov, M.; Gomez-Sal, P.; Manzanero, A.; Royo, P. *J. Organomet. Chem.* **1997**, *535*, 155.
(76) Amor, F.; Butt, A.; duPlooy, K. E.; Spaniol, T. P.; Okuda, J. *Organometallics* **1998**, *17*, 5836.
(77) Paolucci, G.; Pojana, G.; Zanon, J.; Lucchini, V.; Avtomonov, E. *Organometallics* **1997**, *16*, 5312.
(78) Buchwald, S. L.; Kreutzer, K. A.; Fisher, R. A. *J. Am. Chem. Soc.* **1990**, *112*, 4600.
(79) Jordan, R. F. *Adv. Organomet. Chem.* **1991**, *32*, 325.
(80) Chisholm, M. H.; Haitko, D. A.; Folting, K.; Huffman, J. C. *J. Am. Chem. Soc.* **1981**, *103*, 4046.
(81) Jaffart, J.; Mathieu, R.; Etienne, M.; McGrady, J. E.; Eisenstein, O.; Maseras, F. *Chem. Commun.* **1998**, 2011.
(82) Jones, W. D.; Wick, D. D. *Inorg. Chem.* **1997**, *36*, 2723.
(83) Pahor, N. B.; Dreos-Garlatti, R.; Geremia, S.; Randaccio, L.; Tauzher, G.; Zangrando, E. *Inorg. Chem.* **1990**, *29*, 3437.
(84) Randaccio, L.; Bresciani-Pahor, N.; Toscano, P. J.; Marzilli, L. G. *J. Am. Chem. Soc.* **1980**, *102*, 7372.
(85) Reger, D. L.; Garza, D. G.; Lebioda, L. *Organometallics* **1991**, *10*, 902.
(86) Liu, Z.; Somsook, E.; Landis, C. R. *J. Am. Chem. Soc.* **2001**, *123*, 2915.
(87) Liu, Z.; Somsook, E.; White, C. B.; Rosaaen, K. A.; Landis, C. R. *J. Am. Chem. Soc.* **2001**, *123*, 11193.
(88) Bochmann, M. *Angew. Chem., Int. Ed. Engl.* **1992**, *31*, 1181.
(89) Vanka, K.; Chan, M. S. W.; Pye, C. C.; Ziegler, T. *Organometallics* **2000**, *19*, 1841.
(90) Vanka, K.; Ziegler, T. *Organometallics* **2001**, *20*, 905.
(91) Beck, W.; Sunkel, K. *Chem. Rev.* **1988**, *88*, 1405.
(92) Beck, S.; Lieber, S.; Schaper, F.; Geyer, A.; Brintzinger, H.-H. *J. Am. Chem. Soc.* **2001**, *123*, 1483.
(93) Chien, J. C. W.; Iwamoto, Y.; Rausch, M. D.; Wedler, W.; Winter, H. H. *Macromolecules* **1997**, *30*, 3447.
(94) Song, W.; Zhengtian, Y.; Chien, J. C. W. *J. Organomet. Chem.* **1996**, *512*, 131.
(95) Lieber, S.; Brintzinger, H. H. *Macromolecules* **2000**, *33*, 9192.
(96) Keaton, R. J.; Jayaratne, K. C.; Fettinger, J. C.; Sita, L. R. *J. Am. Chem. Soc.* **2000**, *122*, 12909.
(97) Jayaratne, K. C.; Sita, L. R. *J. Am. Chem. Soc.* **2001**, *123*, 10754.
(98) Asakura, T.; Demura, M.; Nishiyama, Y. *Macromolecules* **1991**, *24*, 2334.

(99) Babu, G. N.; Newmark, R. A.; Chien, J. C. *Macromolecules* **1994**, *27*, 3383.
(100) Moscardi, G.; Resconi, L.; Cavallo, L. *Organometallics* **2001**, *20*, 1918.
(101) Resconi, L.; Piemontesi, F.; Camurati, I.; Sudmeijer, O.; Nifant'ev, I. E.; Ivchenko, P. V.; Kuz'mina, L. G. *J. Am. Chem. Soc.* **1998**, *120*, 2308.
(102) Molecular weights were determined by light scattering in THF with a Wyatt Minidawn system using a d*n*/dc value of 0.076. The d*n*/dc value was determined by Wyatt on poly(1-hexene) samples prepared with the hafnium catalysts.
(103) Shapiro, P. J.; Cotter, W. D.; Schaefer, W. P.; Labinger, J. A.; Bercaw, J. E. *J. Am. Chem. Soc.* **1994**, *116*, 4623.
(104) Carpentier, J.-F.; Wu, Z. L., C. W.; Stromberg, S.; Christopher, J. N.; Jordan, R. F. *J. Am. Chem. Soc.* **2000**, *122*, 7750.
(105) The reaction of $^{13}CO_2$ with i-PrMgBr in diethyl ether followed by *in situ* reduction with $LiAlH_4$ and quenching of the reaction mixture with water resulted in ^{13}C-labeled isobutanol. The alcohol was separated from diethyl ether by careful and repeated distillations. It was treated with PBr_3 at 0 ˚C, followed by refluxing at 90 ˚C for 2 h, to yield the ^{13}C-labeled isobutyl bromide which was diltilled (80 - 84 ˚C, 30 mtorr) and dried over $MgSO_4$.
(106) Furniss, B. S.; Hannaford, A. J.; Smith, P. W. G.; Tatchell, A. R. *Textbook of Practical Organic Chemistry*; 5 ed.; Longman: London, 1989.
(107) Fryzuk, M. D.; Johnson, S. A.; Rettig, S. J. *J. Am. Chem. Soc.* **1998**, *120*, 11024.
(108) Fryzuk, M. D.; Johnson, S. A.; Rettig, S. J. *Organometallics* **1999**, *18*, 4059.
(109) Fryzuk, M. D.; Johnson, S. A.; Patrick, B. O.; Albinati, A.; Mason, S. A.; Koetzle, T. F. *J. Am. Chem. Soc.* **2001**, *123*, 3960.
(110) L. P. H. Lopez, unpublished observations.
(111) Fowles, G. W. A.; Rice, D. A.; Wilkins, J. D. *J. Chem. Soc., Dalton Trans.* **1973**, 961.
(112) Juvinall, G. L. *J. Am. Chem. Soc.* **1964**, *86*, 4202.

PARISA MEHKHODAVANDI

Massachusetts Institute of Technology
Department of Chemistry 6-428
Cambridge, MA 02139
Tel. (617) 253-1795
Fax (617) 253-7670

305 Memorial Dr. #308B
Cambridge, MA 02139
Tel. (617) 225-9719
email meparisa@mit.edu

EDUCATION

Doctor of Philosophy, Chemistry *September 2002*
Massachusetts Institute of Technology, Cambridge, MA, USA
Advisor: Professor Richard R. Schrock
Thesis: "Mechanistic studies of amide-supported living Ziegler-Natta catalysts"

Bachelor of Science, Chemistry, with Honors *June 1998*
University of British Columbia, Vancouver, BC, Canada
Advisor: Professor Chris Orvig
Thesis: "Determination of the stability constants for diaminopropyl D-glucopyranoside complexes of divalent nickel, copper and zinc ions"

RESEARCH EXPERIENCE

Massachusetts Institute of Technology *August 1998-present*
Design and synthesis new amide supported group IV organometallic complexes and assessed their properties as catalysts for the living polymerization of α-olefins. Determination of relative rates of olefin polymerization *via* kinetic studies. Discovery of an "alkyl initiator effect" between methyl and isobutyl initiators. Study of the first insertion products of α-olefins by activation of various dialkyl compounds and utilization of ^{13}C-labeling experiments and various NMR techniques.

University of British Columbia (Advisor: Professor Michael D. Fryzuk) *May-Sept 1997*
Study of group IV complexes that bind and activate dinitrogen. Isolation and characterization of a dinuclear, arene-bridged zirconium complex.

University of British Columbia (Advisor: Professor Chris Orvig) *May-Sept 1996*
Synthesis and characterization of a series of chelate supported lanthanide complexes for use as possible imaging agents. Determination of stability constants for sugar-linked diamine complexes of nickel, copper and zinc.

University of British Columbia (Advisor: Professor Colin C. Fyfe) *May-Sept 1995*
Synthesis and characterization of ^{13}C-labeled organic substrates for use in solid state NMR experiments to determine the cavity structure of various zeolites.

TEACHING EXPERIENCE

Massachusetts Institute of Technology *September 1998-May 1999*
(Professors Robert J. Silbey and Daniel J. Nocera)
Recitation teaching assistant for Chemistry 5.11, General Chemistry.
Teaching assistant for Chemistry 5.110, Introductory Laboratory Course.

University of British Columbia *September 1997-May 1998*

Teaching assistant for the First Nations Student Access Program. Responsible for teaching introductory mathematics and chemistry to university transfer students.

University of British Columbia *September 1996-May 1997*

Teaching assistant responsible for grading assignments for second year calculus and linear algebra courses.

PUBLICATIONS

Fryzuk, M. D.; Kozak, C. M.; Mehrkhodavandi, P.; Morello, L.; Patrick, B. O. "Phosphorus phenyl-group activation by reduced zirconium and niobium complexes stabilized by the [P_2N_2] macrocycle" *J. Am. Chem. Soc.* **2002**, *124*, 516-517.

Mehrkhodavandi, P.; Schrock, R. R. "Cationic hafnium alkyl complexes that are stable towards β-hydride elimination below 10 ˚C and active as initiators for the living polymerization of 1-hexene" *J. Am. Chem. Soc.* **2001**, *123*, 10746-10747.

Mehrkhodavandi, P.; Bonitatebus, P. J.; Schrock, R. R. "A comparison of cationic zirconium methyl and isobutyl initiators that contain an arylated diamido-pyridine ligand for polymerization of 1-hexene. Elucidation of a dramatic "initiator effect"" *J. Am. Chem. Soc.* **2000**, *122*, 7841-7842.

Song, B.; Mehrkhodavandi, P.; Buglyo, P.; Mikata, Y.; Shinohara, Y.; Yoneda, K.; Yano, S.; Orvig, C. "Acid-base and metal ion-binding properties of diaminopropyl D-glucopyranoside and diaminopropyl D-mannopyranoside compounds in aqueous solution" *J. Chem. Soc., Dalton Trans.* **2000**, *8*, 1325-1333.

Yano, S.; Shinohara, Y.; Mogami, K.; Yokoyama, M.; Tanase, T.; Sakakibara, T.; Nishida, F.; Mochida, K.; Kinoshita, I.; Doe, M.; Ichihara, K.; Naruta, Y.; Mehrkhodavandi, P.; Buglyo, P.; Song, B.; Orvig, C.; Mikata, Y. "General synthesis of useful chelating reagents having a sugar unit, 1,3-diamino-2-propyl β-D-glucopyranoside and 1,3-diamino-2-propyl α-D-mannopyranoside" *Chem. Lett.* **1999**, *3*, 255-256.

Caravan, P.; Mehrkhodavandi, P.; Orvig, C. "Cationic lanthanide complexes of N,N'-bis(2-methylpyridyl)ethylenediamine-N,N'-diacetic acid (H_2bped)" *Inorg. Chem.* **1997**, *36*, 1306-1315.

PRESENTATIONS

Mehrkhodavandi, P.; Schrock, R. R. "Control of factors affecting living α-olefin polymerization by cationic hafnium complexes" 224th ACS National Meeting, Boston, MA; August, **2002**, oral presentation in preparation.

Mehrkhodavandi, P.; Schrock, R. R. "Living polymerization of 1-hexene by cationic hafnium alkyl complexes" 222nd ACS National Meeting, Chicago, Il; August, **2001**, INOR 244, oral presentation.

Mehrkhodavandi, P.; Schrock, R. R. "Observation of first insertion products of ethylene and propylene: Cationic hafnium alkyl complexes that catalyze the living polymerization of 1-hexene " XIVth International Symposium on Olefin Metathesis, Boston, MA; August, **2001**, poster presentation.

Mehrkhodavandi, P.; Schrock, R. R.; Bonitatebus, P. J. "Polymerization of 1-hexene by zirconium initiators that contain an arylated diamido-pyridine ligand" 220th ACS National Meeting, Washington, DC; August, **2000**, INOR 57, oral presentation.

HONORS AND PROFESSIONAL AFFILIATIONS

NSERC Postgraduate Scholarship (PGS B)	MIT	*2001-2003*
NSERC Postgraduate Scholarship (PGS A)	Declined	*1997-1998*
NSERC Undergraduate Student Research Award	AnorMED, Inc.	*1997-1998*
Agnes and Gilbert Hooley Scholarship	UBC	*1997-1998*
Molson Scholarship in Chemistry	UBC	*1996-1997*
Charles and Jane Banks Scholarship	UBC	*1995-1996*
NSERC Summer Research Fellowship	UBC	*1995-1996*
UBC Chancellor's Entrance Scholarship	UBC	*1994-1998*
Canada Scholarship	UBC	*1994-1998*
UBC Outstanding Student Initiative Scholarship	UBC	*1994-1995*
UBC University Women's Scholarship	UBC	*1994-1995*
BC Provincial Scholarship	UBC	*1994-1995*
Bill Stewart Memorial Scholarship	UBC	*1994-1995*

Dean's Honor list for each year of study at UBC
American Chemical Society, Member
The Canadian Society for Chemistry, Member

Acknowledgments

"Hi, do you have a minute?"
"Yeees… Come on down."

These must be the most commonly repeated phrases between Richard Schrock and I. He likes to complain that in one week I saw him EVERY day about some new result. I have to say that this was mostly his own fault! I would like to thank him for always being available, and for being willing to listen to chemistry as well as to personal problems. His praise when things went well, his criticism when it was warranted, and his boundless enthusiasm and love for science, have made these past four years a very enriching time. I think the most important lesson that I learned from Dick during this time was to let mother nature do her thing and look at an unexpected result as an interesting mystery to be solved instead of as a failure. I learned to ski (in a fashion) thanks to wonderful ski trips sponsored by Dick, and I had an absolutely fabulous time skiing with Nancy Schrock. I would like to thank her for her kindness and for Sherlock Holmes!

Paula Diaconescu and I started graduate school together, and I consider her a very nice and normal friend! Thank you, Paula, for teaching me all about my subconscious and also for the dream. Thanks must also go to Vlad Iluc for his marvelous cheese cakes and his glamorous curls!

The Schrock group is an ever-evolving entity, and I have had the pleasure of working with a number of great people during my four year membership. I would like to thank Sarah Aeilts for teaching me a lot about tools, ham and life in general! I will always have fond memories of your delicious fresh baked crapple. Kai Hultzsch, a.k.a. Dr. Evil, was my very own literature search engine and a fountain of knowledge for all things Ziegler-Natta. I thoroughly enjoyed our romp through Germany and Austria, and will take to heart his advice in München: "Order the 1L stein, the small glasses are for tourists!" Steve Miller has been one of the best labmates one can wish for. His valuable insights into chemistry, his advice and guidance, and his ability to tolerate unlimited amounts of Sarah Brightman made him an invaluable resource and a great friend. Kai and Steve, as well as Eric Liang, Arturo Casado, Klaus Ruhland and Dima Yandulov are former and current group members who have given me invaluable counsel on my project.

Other group members with whom I've spent many a Happy Hour are Jennifer Jamieson, Frank Cochran, Peter Tsang, James Araujo, George Greco, Connie Lu, Yann Schrodi, Vincent Ritleng, Frederic Pezet, Pia Lopez, Denyce Wicht, Elisa Calimano, Daniel Kramer (the honorary Schrock group member) and Sarah Dolman. I will always remember Sarah for introducing me to Bi Bim Bap, for "just holding the catalyst", and for doing her "… group job"! I wish the best of luck for the new graduate students in our group: Jennifer Adamchuk, Adam Hock, Lara Pryor, Amrit Sinha, Nathan Smythe and Walter Weare. Lara and Jen have been my labmates during some of the most stressful times of my Ph.D. and I thank them for their patience and resilience. Thanks must go to Paula, SarahD, Daniel and Dima for proofreading my thesis. I thank Nathan for coming to my rescue at an hour of need, *i.e.* right before my thesis was due, and fixing my temperamental word program with the wonder of patches!

The crystal structures in this thesis were solved by Pete Bonitatebus, Jr., Paula Diaconescu and Bill Davis. The instrumental facilities were a great asset to me and I would like to thank Jeff Simpson, Mark Wall, David Bray and Li Li for all their help. I also thank Ed of James Glass, “glassblower to the stars”, for many great conversations.

Gretchen Kappelmann has been an absolutely invaluable resource and a friend. I thoroughly enjoyed our chats and wish her all the best in future endeavors. I would also like to thank Susan Brighton and Kitty Valleli for their continued help throughout the years.

I would like to thank Prof. Kit Cummins for fruitful and stimulating discussions and Prof. Daniel Nocera and Prof. Joseph Sadighi for helpful comments on my thesis.

My undergraduate advisors Prof. Mike Gerry, Prof. Colin Fyfe, Prof. Chris Orvig and Prof. Mike Fryzuk had an enormous impact on my decision to enter and pursue chemistry and I thank them for their continual encouragement.

I thank my grandparents for their love and support. Bamas Jahangir, especially, encouraged me to continue my education. His passion for life and for learning have been a constant source of inspiration for me. I thank my brother, Farhad, for his amazing stamina in putting up with my moods, and for being proud of me.

Finally, I want to thank my parents. Their love for me, and the hard decisions they have made in their life because of that love, is the only reason I have been able to write this thesis. Maman and Baba, this is for you.